

# Technische Universität München

## Lehrstuhl für Entwicklungsgenetik

### Loss of the caretaker function of the *Rb1* tumour suppressor gene triggers radiation-induced cancer

Iria Maria Gonzalez Vasconcellos

Vollständiger Abdruck der von der Fakultät Wissenschaftszentrum Weihenstephan für Ernährung, Landnutzung und Umwelt der Technischen Universität München zur Erlangung des akademischen Grades eines

Doktors der Naturwissenschaften

genehmigten Dissertation.

Vorsitzender:

Univ.- Prof. Dr. S. Scherer

Prüfer der Dissertation:

1. apl. Prof. Dr. J. Graw
2. Univ.- Prof. A. Schnieke, Ph.D.
3. Univ.- Prof. Dr. M. J. Atkinson

Die Dissertation wurde am 23.08.2011 bei der Technischen Universität München eingereicht und durch die Fakultät Wissenschaftszentrum Weihenstephan für Ernährung, Landnutzung und Umwelt am 20.12.2011 angenommen.

*To my beloveds for making this work possible*

<b>INDEX:</b>	<b>Page</b>
<b>SUMMARY</b>	<b>1</b>
<b>ZUSAMMENFASSUNG</b>	<b>2</b>
<b>ABREVIATIONS</b>	<b>3</b>
<b>I INTRODUCTION</b>	<b>5</b>
1.1. What is the mechanism of radiation induced cancer?	5
1.2. Hallmarks of cancer	5
1.3. <i>Rb1</i> and cell cycle regulation	6
1.4. Osteosarcomagenesis	11
1.5. Carcinogenesis	13
1.6. <i>Rb1</i> and telomeres	19
1.7. The alternative telomere lengthening (ALT) pathway and cancer	22
1.8. CIN and telomeres	25
1.9. <i>Rb1</i> , telomeres and osteosarcomagenesis	26
1.10. Genetic instability, radiation and cancer	27
<b>II MATERIALS</b>	<b>29</b>
<b>III METHODS</b>	<b>41</b>
3.1. Transgenic mice	41
3.2. Mice maintenance	43
3.3. DNA isolation for analysis	43
3.4. PCR based genotyping	44
3.5. Agarose gel electrophoresis	45
3.6. Isolation of primary osteoblasts and their culture	45
3.7. Alkaline Phosphatase staining	46
3.8. Cell cycle analysis	47
3.9. Micronuclei assay	47
3.10. Anaphase bridges assay	48
3.11. Protein analysis	49
3.12. <i>LacZ</i> Histochemistry	51
3.13. RT-(q)PCR	51
3.14. Real time PCR	53
3.15. Telomeric repeats fragments (TRFs) determination	54
3.16. Immunofluorescence	55
3.17. Senescence-associated $\beta$ -galactosidase assay	56
3.18. FISH with PNA probe on cultures seeded on slides	56
3.19. Telomere length measurement by flow-cytometry	58
3.20. Irradiation protocol	59
3.21. RNA interference	59
3.22. Viral infections	62
3.23. Cytofluorimetric analysis (FACS) of infected cells	62
3.24. Transient transfection	62
3.25. <i>RB1</i> cloning strategy for phenotype rescue	63
<b>IV RESULTS</b>	<b>67</b>
<b>Chapter 1: <i>Rb1</i>, CIN and telomere stability (<i>in vitro</i> study)</b>	<b>67</b>
4.1. Lineage specific deletion of <i>Rb1</i> in mouse osteogenic tissue	67
4.2. Conditional deletion of <i>Rb1</i>	69
4.3. Exon 19 deletion detected when sequencing <i>Rb1</i> <sup>+/<math>\Delta</math>19</sup> osteoblasts	71
4.4. RNA and protein levels of <i>Rb1</i> <sup>+/<math>\Delta</math>19</sup> osteoblasts confirm <i>Rb1</i> haploinsufficiency	72
4.5. Cell cycle is impaired in <i>Rb1</i> <sup>+/<math>\Delta</math>19</sup> osteoblasts after radiation	74
4.6. Failure senescence induction in <i>Rb1</i> <sup>+/<math>\Delta</math>19</sup> primary osteoblasts	76
4.7. pRb1 localises in close proximity to the DNA on metaphases suggesting a role of pRb1 during cell division different from E2F modulator	77

4.8.	Increased genomic instability in the <i>Rb1</i> <sup>+/<math>\Delta</math>19</sup> osteoblasts with the effect amplified after radiation	78
4.9.	<i>Rb1</i> <sup>+/<math>\Delta</math>19</sup> harbour shorter telomeres compared to its wild-type counterpart	82
4.10.	Heterogeneous telomeric loss in <i>Rb1</i> <sup>+/<math>\Delta</math>19</sup>	83
4.11.	Reduced telomeric signal numbers in <i>Rb1</i> <sup>+/<math>\Delta</math>19</sup> osteoblasts	83
4.12.	Telomere length differences between <i>Rb1</i> <sup>+/<math>\Delta</math>19</sup> and <i>Rb1</i> <sup>+/+</sup> increase with aging	84
4.13.	Telomeric shortening is independent of radiation exposure	85
4.14.	Telomeric measurements using RealTime-qPCR show telomeric reduction in <i>Rb1</i> <sup>+/<math>\Delta</math>19</sup> compared to <i>Rb1</i> <sup>+/+</sup>	86
4.15.	sh <i>RB1</i> ablation in both <i>Rb1</i> <sup>+/+</sup> and <i>Rb1</i> <sup>+/<math>\Delta</math>19</sup> in murine osteoblasts in vitro leads to shorter telomeres	86
4.16.	Cloning and expression of <i>RB1</i> into osteoblasts for recovery of the <i>Rb1</i> status	87
4.17.	Rescue of <i>Rb1</i> <sup>+/<math>\Delta</math>19</sup> phenotype by <i>RB1</i> expression prevents loss of telomere length	91
4.18.	Rescue of <i>Rb1</i> haploinsufficiency leads to a reduction of segregational defects	91
4.19.	Telophase bridges present in <i>Rb1</i> <sup>+/<math>\Delta</math>19</sup> as well as in osteosarcoma cell lines present several telomeric sequences along the bridge	92
4.20.	Telomere shortening in <i>Rb1</i> <sup>+/<math>\Delta</math>19</sup> cells and activation of ALT pathway	93
4.21.	ALT activated osteoblasts lost p53 via point mutation in vitro and induced fast tumourigenesis	94
4.22.	PML-NBS body numbers, a marker of ALT activation is elevated in <i>Rb1</i> <sup>+/<math>\Delta</math>19</sup> Cells and is further increased after in vitro transformation	96
4.23.	PML-NBS body numbers are not decreased by expression of <i>RB1</i> that rescues decline in telomere length, suggesting that <i>Rb1</i> replenishment is not enough to reverse ALT activation	97
4.24.	Epigenetic markers known to be crucial for telomere maintenance are reduced in <i>Rb1</i> <sup>+/<math>\Delta</math>19</sup> osteoblasts and show a further decrease after irradiation	98
4.25.	<i>Rb1</i> influence on the H4 K20 tri-met fluorescence intensity is not mediated by transcriptional regulation of the enzyme that catalysis H4 K20 tri-methylation	100
<b>V</b>	<b>Chapter 2: <i>Rb1</i> and Tumourigenesis (<i>in-vivo</i> study)</b>	<b>101</b>
<b>VI</b>	<b>Chapter 3: <i>Rb1</i> and Tumour development (LOH study)</b>	<b>102</b>
<b>VII</b>	<b>DISCUSSION</b>	<b>104</b>
7.1	<i>Rb1</i> cell cycle and senescence regulation	106
7.2	<i>Rb1</i> and CIN	108
7.3	<i>Rb1</i> and telomeres	109
7.4	p <i>Rb1</i> and epigenetics	113
7.5	<i>Rb1</i> and the ALT mechanism	114
7.6	<i>Rb1</i> haploinsufficiency in an <i>in-vivo</i> model	115
7.7	<i>Rb1</i> mutator phenotype, a model of osteosarcoma development	116
7.8	Conclusions	117
<b>VIII</b>	<b>REFERENCES</b>	<b>118</b>
<b>IX</b>	<b>ANNEX I</b>	<b>135</b>
<b>X</b>	<b>ACKNOWLEDGEMENTS</b>	<b>139</b>
<b>IX</b>	<b>CV</b>	<b>140</b>

## SUMMARY

Genomic instability is a hallmark of malignant progression; uncapping of the telomeres and associated chromosomal damage are contributing factors in this process.

Mutation of the retinoblastoma tumour suppressor gene is strongly linked to osteosarcoma formation. Such tumours are characterised by ALT (Alternative lengthening of the telomeres) activation and high rates of genomic instability.

Our analysis of *Rb1*<sup>+/ $\Delta$ 19</sup> primary osteoblasts showed a faster and prominent reduction on telomere length as compared to their wild-type counterparts.

When exposed to radiotherapy comparable doses of  $\gamma$ -radiation, *Rb1* haploinsufficient cells showed not only depleted cell cycle control and failure to induce senescence, but also an increase in typical genomic instability features, including micronucleus formation and segregating defects such as anaphase bridges and late telophase persistent bridges. A reduction in the telomeric length of up to 50% was observed in *Rb1*<sup>+/ $\Delta$ 19</sup> primary osteoblasts when compared to their *Rb1*<sup>+/+</sup> counterparts.

*Rb1*<sup>+/ $\Delta$ 19</sup> cells showed an increase in PML-NBs (Promyelocytic Leukemia nuclear bodies), typical marker of ALT activation, as well as epigenetically, a reduction of the trimethylation of the lysine 20 of histone 4 (H4K20-3met), known to be important for the heterochromatin packaging.

Conditional somatic deletion of a floxed-*Rb1* allele in the osteoblastic lineage produces an increased sensitivity to the osteosarcomagenic effects of radiation and further loss of the wild-type allele has been proved when studying osteosarcomas arising from *Rb1*<sup>+/ $\Delta$ 19</sup> mice after irradiation.

These studies suggest that the tumour suppressor gene *Rb1* functions, not only as a gatekeeper, but also as a caretaker of the genome controlling the telomere dynamics and genomic stability. Therefore, partial germline depletions of the *Rb1* can be a mayor feature towards osteosarcoma initiation and progression via an increase in genomic instability of the primary osteoblasts, defect enhanced by radiation exposure.

## ZUSAMMENFASSUNG

Genomische Instabilität ist ein typisches Merkmal von Zellen während ihrer bösartigen Transformation. Einer der Faktoren, die zu dieser progressiven Instabilität beitragen, ist der Verlust der schützenden Funktion der Telomere und daraus resultierende Chromosomen-Instabilität.

Osteosarkome, die bösartigen Weichteil-Tumoren des Knochens, zeigen sehr charakteristische Merkmale einer alternativen Telomer-Verlängerung (ALT) und gleichzeitig ein hohes Mass an genomischer Instabilität. Für das Tumor-Suppressor-Gen *Rb1*, dessen primäre Funktion die Kontrolle des Zellzykluses ist und welches häufig in Osteosarkomen einen Defekt aufweist, konnte hier eine neue Rolle bei der Regulation des Telomer-Erhaltes gezeigt werden. Es konnte nachgewiesen werden, dass der Expressions-Verlust von *Rb1* sowohl zu einer beschleunigten Telomer-Erosion als auch zu chromosomaler Instabilität führen kann.

Parallel mit der Telomer-Verkürzung in *Rb1*<sup>+/ $\Delta$ 19</sup> Zellen zeigen sich epigenetische Veränderungen in der Histon-Methylierung. Dabei zeigte sich am Histon 4 ein dramatischer Rückgang der Methylierung des Lysin 20.

Mit zunehmender Zell-Passage kommt es dabei zu einer um bis zu 50% reduzierten Telomer-Verkürzung. Die Mutanten-Zellen zeigen dabei eine stärkere Tendenz zur Polyploidie und chromosomaler Miss-Segregation nach Bestrahlung.

In einem Maus-Model mit einer *Cre-Lox* vermittelten, knochenspezifischen *Rb1* Deletion wurde darüber hinaus gezeigt, dass dadurch die strahleninduzierte Knochentumour-Inzidenz signifikant ansteigt, wobei es in den dabei gefundenen Osteosarkomen zu einem zusätzlichen Verlust des verbliebenen *Rb1* wild-type Alleles kommt.

Durch *In-vitro* Bestrahlung der aus den *Rb1-Cre-LoxP* Mäusen etablierten heterozygoten Osteoblasten konnte gezeigt werden, dass es in diesen im Vergleich zu Wildtyp-Zellen zu einer drastisch reduzierten Induktion der zellulären Senescence kommt.

Diese Untersuchungen lassen vermuten, dass das Tumour-Suppressor-Gen *Rb1* nicht nur eine Funktion in der Zell-Zyklus-Regulation hat (sogenannter „Torwächter“ an bestimmten Zell-Zyklus Kontroll-Punkten), sondern dass es ebenfalls eine Rolle für den Erhalt der durch die Telomer-Struktur bedingten chromosomalen Integrität spielt.

**ABREVIATIONS:**

Ab:	Antibody
AI:	Allelic Imbalance
AP:	Alkaline phosphatase
ALT:	Alternative lengthening of the telomeres
AUF:	Arbitrary units of fluorescence
BFB cycle:	Breakage fusion breakage cycles
bp:	Base pair
CIN:	Chromosomal instability
CDK:	Cyclin-dependent kinase
cDNA:	Complementary deoxyribonucleic acid
CDS:	Coding sequence
Ct:	Cycle threshold
Cp:	Crossing point
Cy3:	Cyanine 3 fluorescent dye
DAPI:	4',6-diamidino-2-phenylindole
DDR:	DNA damage response
DMEM:	Dulbecco's Modified Eagle's Medium
DMSO:	Dimethyl sulfoxide
E. coli:	Escherichia coli
EDTA:	Ethylenediaminetetraacetic Acid
E2F:	E2 Transcription Factor
E2F <sup>TD</sup> :	E2F transactivation domain
FISH:	Fluorescence <i>in-situ</i> hybridization
FITC:	Fluorescein isothiocyanate
GFP:	Green fluorescent protein
Gy:	Gray (radiation unit)
Het:	Heterozygous
HR:	Homologous recombination
3metK20H4:	Trimethylation in the residue Lysin 20 of the Histone 4
LOH:	Loss of heterozygosity
LoxP:	Locus of crossover from P1 bacteriophage
LV:	Lentivirus
kDa:	Kilodalton
MN:	Micronuclei
MOS cell lines	Mouse osteosarcoma cell lines
Napthol AS-MX:	4-Chloro-2-methylbenzenediazonium/3-Hydroxy-2-naphthoic acid 2,4-dimethylanilide phosphate
PI:	Propidium Iodide
PML-NBs:	Promyelocytic Leukemia nuclear bodies
PNA:	Peptide nucleic acid
pRb1:	Phosphorylated form of Rb1
<i>RB1</i> :	Retinoblastoma gene human
<i>Rb1</i> :	Retinoblastoma gene mouse
Rb1:	Retinoblastoma protein mouse
RPEs:	Retinal Pigment Epithelium cells
RT:	Reverse transcription
<i>R26R</i> :	Rosa26 reporter

PCR:	Polymerase chain reaction
PNA	Peptide nucleic Acid
PFEF:	Pulse field electrophoresis
RT-PCR:	Real time polymerase chain reaction
SDS-PAGE:	Sodium dodecyl sulfate poly-acrylamide gel electrophoresis
shRNA:	Short hairpin RNA
TERT:	Telomerase reverse transcriptase
TERC:	Telomerase RNA component
Tg:	Transgene
TSG:	Tumour suppressor gene
X-gal:	5-bromo-4-chloro-3-indolyl- $\beta$ -D-galactopyranoside
WB:	Western blot
Wt:	Wild-type



## I. INTRODUCTION

### 1.1 What is the mechanism of radiation induced cancer?

The malignant transformation of cells following radiation exposure has long been recognised (Beebe et al 1962) and the causes remain under investigation today (Grant et al 2011, Ozasa et al 2011). However, little is known about the mechanisms of the process that follow radiation exposure and which lead to cancer development.

The *Rb1* gene, the first identified tumour suppressor gene, is known to play a role in both radiation sensitivity and in susceptibility to cancer (Wilson et al 2008), as well as in the process of transformation itself (Rosemann et al 2002, Rosemann et al 2003). Again the mechanisms by which mutations in *Rb1* lead to radiation-induced cancer are not yet understood.

*Rb1* is a known gatekeeper of the genome due to its ability to regulate the cell cycle, but it has also been implicated in epigenetic regulation (Gonzalo et al 2005) as well as telomere biology (Blasco 2007). In this thesis, the relationship between these different functions of the *Rb1* gene and the mechanisms of radiation induced cancer has been studied, using osteosarcoma as a model system.

### 1.2 Hallmarks of cancer

In the last decade great efforts have been made towards understanding the 6 hallmarks of cancer, presented in 2000, (Hanahan & Weinberg 2000) and revised in 2011 (Hanahan & Weinberg 2011) to be the main elements constituting the framework of the great diversity of neoplasias (Figure 1). Cells acquire either a set, or all of these hallmarks towards transformation progression and metastasis (Brabletz et al 2005).

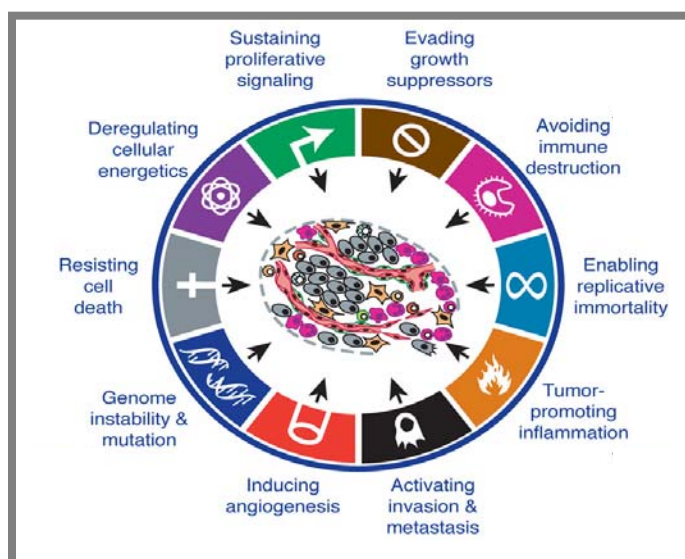


**Figure 1: The 6 hallmarks of cancer as presented in 2011 by Hanahan and Weinberg.** In their view, cancer arises from these set, or subset, of newly acquired capabilities. After Hanahan & Weinberg 2011.

Underlying such hallmarks (summarized in the picture above), is genomic instability, as the compendium of events generating genetic diversity that expedite the acquisition of these

hallmarks during carcinogenesis. This suggests genomic instability, as an enabling tool towards malignant transformation, via mutational gains, as the outcome of an unstable genome (Hanahan & Weinberg 2011).

Certain mutant genotypes confere a selective advantage on a clonal subset of cells that can eventually outgrow the local tissue environment. Accordingly, multistep tumour progression can be described as a succession of clonal expansions, each triggered by an enabling mutant genotype. These genotypes can be heritable, suggesting the importance of germline mutations in driving unstable genomes (Bois & Jeffreys 1999, Boyle et al 1998, Deng & Scott 2000, Goel et al 2010, Yin & Shen 2008).

Several defects, present in the germline or aquired de novo, can affect various components of the DNA-maintenance machinery, often referred to as the “caretakers” of the genome. (Kinzler & Vogelstein 1997). Mutations in caretaker genes have been introduced into the mouse germline and result, predictably, in increased cancer incidence, supporting their potential involvement in human cancer predisposition and development (Clark-Knowles et al 2009, Yin & Shen 2008).

The loss of telomeric DNA in many tumours generates karyotypic instability and associated amplification and deletion of chromosomal segments (Artandi & DePinho 2010), therefore instability of telomeres are also an enabler of the hallmark capability for unlimited replicative potential and must also be added to the list of critical points responsible for maintaining genome integrity. This leads the conclusion that the defects in genome maintenance are selectively advantageous and therefore instrumental for tumour progression, accelerating the rate at which evolving premalignant cells can accumulate favorable genotypes. As such, genome instability is clearly an enabling characteristic that is causally associated with the acquisition of hallmark capabilities.

In this work, the main character under study will be the *Rb1* gene, its germline mutations and its possible diverse functions

### **1.3 *Rb1* and cell cycle**

#### **1.3.1 Retinoblastoma, *Rb1***

The *Rb1* gene is found in man on chromosome 13, at position 13q14.3. In mouse, *Rb1* is found on chromosome 14, at location 71,929,657-72,059,946 MB with the 5' end and promoter heading towards the telomere (source: [www.ensembl.org](http://www.ensembl.org)) (see Figure 2).

The Rb1 protein belongs to the RB1 inducible coiled coil 1 family. The members of this family are: pRb, pRb2/p130 and p107 (Cao et al 2010).

*Rb1* in mouse has 6 splicing forms, but only one (4656 bp, 27 exons) codes for the Rb1 protein. The protein has 928 aa, and a binding pocket (see Figure 3) that binds to E2F<sup>TD</sup> transactivating domain. The C-terminus binds to the E2F and DP (dimerization partner)

transcription factors. Phosphorylation of the pocket linker (S608/S612) avoids the binding of the E2F<sup>TD</sup> since the phosphor group binds the pocket domain at the E2F<sup>TD</sup> binding site (Burke et al 2010).

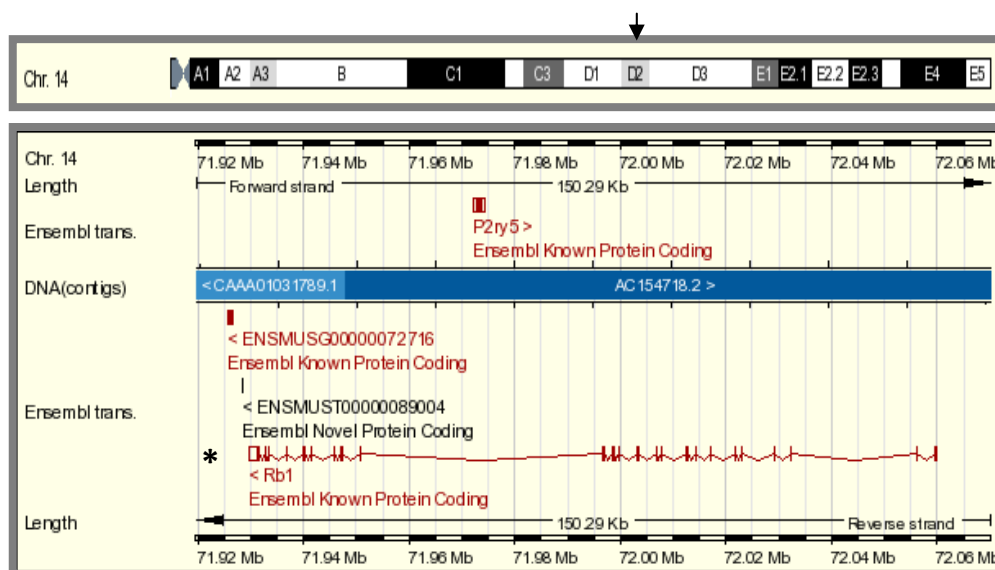


**Figure 2: Mouse (*Mus musculus*) chromosome 14.** The location of the *Rb1* gene (arrow) and its sequence in chromosome 14. As shown by contigs from shotgun and BACs overlapping sequencing, it occupies approx 0.15 Mb in the D2 region of chromosome 14. Here the splicing transcript coding for the Rb1 protein is shown with its 27 exons (marker with \*). Source ENSEMBL.

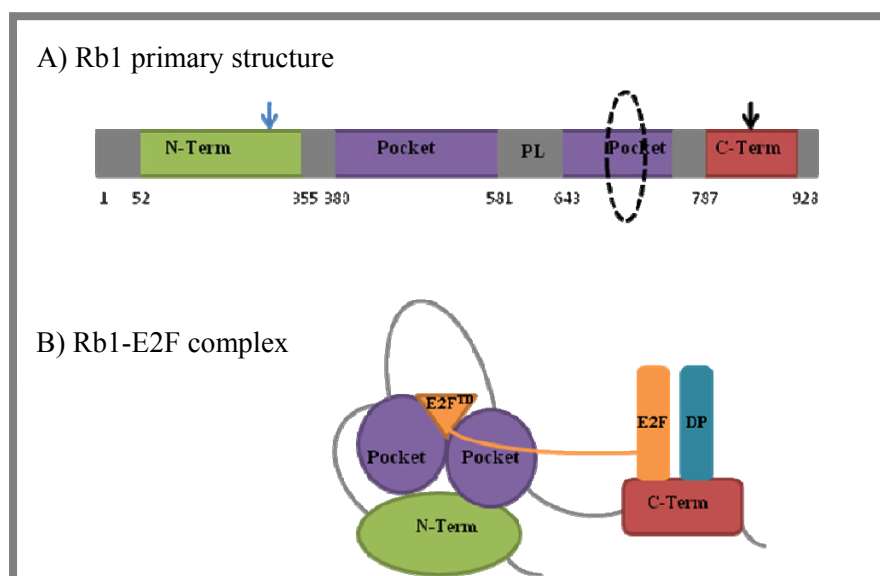


**Figure 3: Domain structure of Rb1 and interactions with E2F-DP.** A) Rb1 consists of a structured N-terminal domain (N-Term) and central pocket domain. Its C-terminal domain (C-Term) is disordered except for a short sequence that adopts a structure upon E2F binding. Two other unstructured sequences are the interdomain linker between N-Term and pocket domain, and pocket linker (PL). Structured regions are colored, and amino acid numbers stated. B) Rb1 makes two distinct contacts with E2F. The pocket domain binds the E2F transactivation domain (E2F<sup>TD</sup>), and C-Term binds the E2F-DP (dimerization partner) transcription factor dimer (Burke et al 2010). Blue arrow marks the location of the epitope of the antibody against Rb1 used in this thesis (Becton & Dickinson), and the black arrow the epitope of the antibody used against the pRb1. The dashed circle marked the location of the sequence coded by exon 19, deleted in our animal model. Modified from Burke et al 2010.

Rb1 phosphorylation at different sites controls the binding of different proteins, as for binding c-Abl (Ser807 Ser 811) or for binding LXCXE proteins (Thr821, Thr826) (Knudsen & Wang 1996) but for binding E2F which is the transcription factor needed for starting the S phase, the phosphorylation pattern is more complex and appears to be regulated by multiple phosphorylation sites (Knudsen & Wang 1997). The functions of the Rb1 phosphorylated protein, once released from its bound to E2F are to be further investigated.

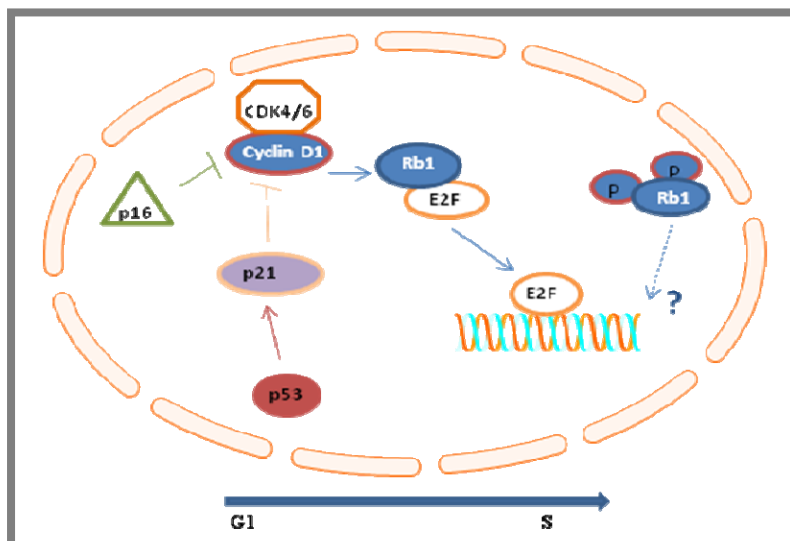


**Figure 4: Rb1 pathway and main partners.**

Unphosphorylated Rb1 is tightly bound to E2F and only the phosphorylation by one of the mentioned cyclin complexes can release the complex and lead the cell to the S phase. Note the question mark referring to the function of hyperphosphorylated Rb1.

### 1.3.2 Rb1 and cell cycle regulation

Rb1 has its main known function in the G1/S phase checkpoint, and therefore has been classified as a tumour suppressor gene (TSG), due to its cell cycle regulator function. To date, osteosarcoma development in man and mouse have been recognised as a cellular abnormality involving disregulated cell cycle control (Castillero-Trejo et al 2005, Yuan et al 2007)

LOH and molecular defects affecting both TSG and oncogenes that regulate cell cycle, control the fate of the osteoblasts being transformed (Sunters et al 1998). The cell cycle is controlled by a series of events, which help the cell to coordinate the duplication of its genetic material and subsequently divided into two identical daughters. The cell cycle is divided in: G1 (G0) S G2 and M phases (Figure 5).

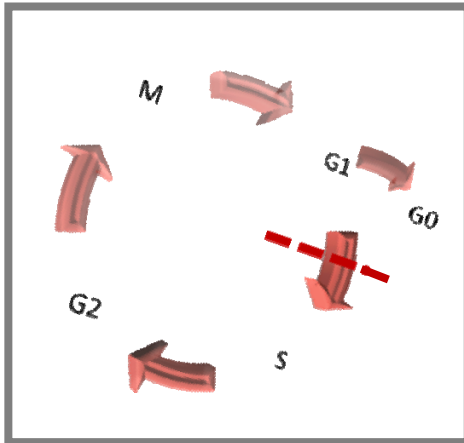


**Figure 5: Cell cycle scheme.** Dashed arrow showing the G1/S checkpoint where *Rb1* plays a major role.

During G1, cells prepare for division, and before leaving this phase the cells need to pass the so called G1/S phase checkpoint to initiate DNA replication.

In S phase, the initial DNA is replicated and undergoes a second checkpoint which signals stalled replication forks that can be caused by DNA breaks or cross-links. During G2 the cells synthesize two identical DNA daughter chromatids that until mitosis are held together by proteins of the cohesin family.

In mitosis, the two sister chromatids of each chromosome separate by the action of condensins, microtubuli bind to the centromeres and pulls them apart towards the spindle poles. This process normally

ensures the proper segregation of one entire set of chromosomes into the two daughter cells. The checkpoints control the timing of cell cycle transition and ensure that critical events such as DNA replication and chromosome segregation occur in a regulated order. They serve as a brake to pause the cycle in case of DNA damage or errors made in the process (Hartwell & Weinert 1989, Tessema et al 2004). In case that one particular requirement for progression to the next cell cycle phase is not met, checkpoints will delay the progression. In case of persisting DNA damages, checkpoints stall cell cycle progression until the lesion is repaired. If repair does not happen, normal cells will be driven into G0, heading to quiescence senescence and/or apoptosis (Golubnitschaja 2007, Nakanishi 2009).

The regulation of cycle progression through the different checkpoints is the responsibility of numerous proteins, including cyclin family members, the cyclin dependent kinases (CDKs), the CDK inhibitors (p27, p16, p53), as well as the family of E2F transcription factors and their antagonists of the pocket protein family of Rb1, p107 and p130. Failure of cell cycle checkpoints can result in non-viable cells or unstable, lacking key chromosomes, but in some circumstances cells with aberrant chromosomal complements are viable and some are even capable of replicating (Schvartzman et al 2010) generating instability. Failure of cell cycle checkpoints is potentially a key factor in allowing genomically unstable cells to traverse the cycle successfully and may lead to cancer as such unstable cells are believed to be precursors of malignant cells. Mutations in, for example, DNA repair genes, may predispose the carriers of these mutations to cancer by increasing the level of genomic instability. Mutations in checkpoint control genes might lead to cancer. A genomic instability associated with such defects might ultimately lead to uncontrolled growth and disrupting tissue homeostasis (Nojima 1997, Schvartzman et al 2010). It is then crucial for each cell to

maintain genomic stability ensuring proper function and survival, by having a complete unmutated genomic dotation.

The *Rb1* gene, the central player in the G1/S cell cycle transition was the first identified human tumour suppressor gene, and it has been shown to be involved in the genesis of a variety of human cancers (Lin et al 1996). It has been previously shown that Rb1 is a critical component of the cell cycle regulatory machinery (Riley et al 1994). Its best understood molecular function is its ability to sequester E2F-transcription factors and thereby switching off transcription of their target genes (Riley et al 1994). Rb1 activity, in particular through phosphorylation of several residues, is regulated by an intrinsic network of upstream Rb1 cell cycle regulatory proteins, some of which such as p16 are also been implicated as tumour suppressor genes and potential oncogenes (Burkhart et al 2010, Riley et al 1994, Schwartzman et al 2010).

Quiescent cells have hypophosphorylated (inert) Rb1 that sequesters E2F-proteins and keeps them in an inactive complex. As the cyclin / cdk complex become activated during progress through G1 the level of phosphorylation of Rb1 increases. Rb1 is maintained phosphorylated all through the G2 and M phases of the cell cycle. As the cell emerges from the M phase, Rb1 is dephosphorylated and the hypophosphorylated form becomes abundant again (Geng et al 1996). Upon phosphorylation by the Cyclin / CDK complexes the Rb1 is no longer able to bind to E2F and consequently the inactive Rb1/E2F complex is dissociated. The released E2F is now able to transcriptionally activate a set of genes that allow the cell to enter S phase.

Functional loss of Rb1 in G1 phase may be a universal mechanism underlying cellular transformation (Hatakeyama & Weinberg 1995, Ma et al 2003). The Rb1 pathway appears to be disrupted in nearly all cancers (Hatakeyama & Weinberg 1995), with either Rb1 itself or any of its upstream regulators losing function or becoming dysregulated, thereby rendering the cell incapable of blocking cell cycle transition from G1 into S phase. Moreover, it was shown that some tumour suppressors, like *p16* which is lost from a variety of human tumours and human cell lines, have its main function as tumour suppressor through inhibiting the CDK/cyclin mediated phosphorylation and functional inactivation of the retinoblastoma protein (Medema et al 1995).

The retinoblastoma protein was shown to be involved in other cellular functions besides cell cycle such as differentiation, senescence and apoptosis (Ma et al 2003).

## 1.4 Osteosarcomagenesis

### 1.4.1 Osteogenesis and bone formation

Bone is a dense, semirigid, porous, calcified connective tissue forming the major portion of the skeleton of most vertebrates (Figure 6). Osteogenesis (bone formation) involves 3 steps – the synthesis and secretion of an extracellular organic matrix (osteoid) by mature osteoblast cells, followed by the passive mineralisation of this matrix to form the bone, and subsequently remodelling of the formed bone structure by local osteoclast-mediated resorption and resynthesis. These processes (except mineralization) are governed by a temporally and spatially orchestrated multistage pathway of cell proliferation and differentiation, leading to the formation of mature bone with its mechanical and biochemical properties (Zou et al 2011).

At the origin of bone formation are the mesenchymal stem cells (MSCs). These pluripotent stem cells have the ability to differentiate into multiple lineages forming cartilage, fibroblasts, tendons, adipocytes and osteoblasts. To give rise to bone forming cells, MSCs first give rise to osteoprogenitors, which are still immature but can further differentiate into osteoblasts by expressing the transcription factor Cbfa1/Runx2 (Schroeder et al 2005). Runx2 regulates osteoblast differentiation.

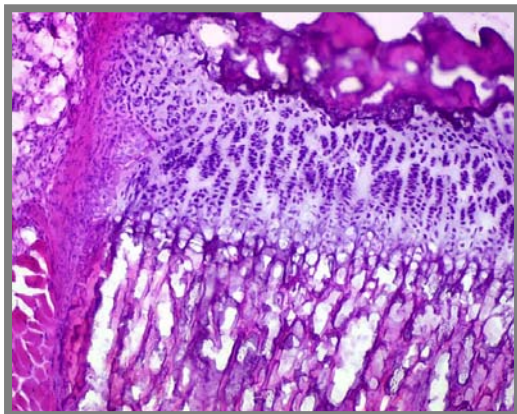


**Figure 6: Knee section.** H&E staining of a 6 month old murine knee (10x). Figure shows mineralised epyphysis and methapysis.

The differentiation of osteoblasts from osteoprogenitors has been shown to depend upon bone morphogenic proteins (BMPs) as well as other growth factors such as fibroblast growth factor (FGF), transforming growth factor  $\beta$  (TGF- $\beta$ ) and platelet derived growth factor (PDGF).

They are responsible for secreting osteoid – the organic compound of bone tissue that when mineralised form the new bone tissue together with the bone cells.

Osteoid is mainly composed of Type-I collagen, and also consists of chondroitin sulphate and osteocalcin (the non-collagenous protein of the bone matrix). After maturation osteoblasts either become embedded in the bone to form osteocytes, become inactive as bone-lining cells, undergo apoptosis or transdifferentiating into other mesenchymal lineages (Manolagas 2000).

### 1.4.2 Osteosarcomagenesis

Osteosarcoma (arising from MSC lineage cells) are rare spontaneous bone malignancies occurring both in man and mouse (Luz et al 1991). The induction of osteosarcoma is significantly increased following ionising radiation in both species (Gossner & Luz 1994, Koshurnikova et al 2000). Understanding the biological and pathogenical characteristics of osteosarcoma has been an important aspect of cancer research specially due to the nature of the disease and its poor prognostics. As the most common primary malignant tumour in children and adolescents, it accounts for 5% of all childhood cancers and 20% of all paediatric bone malignancies. Despite efforts made in the last 30 years in developing methods combining chemotherapy and surgery, the probability of metastasis remains high and long-term survival is limited (Kaste et al 2008, Navid et al 2008, Rosenthal et al 2008).

Incidence of osteosarcoma has a bimodal age distribution, with peaks occurring during early adolescence and after 50 years of age (Ottaviani & Jaffe 2009a, Ottaviani & Jaffe 2009b). The peak at adolescence is thought to be related to the rapid osteoblast proliferation growth spurt during puberty, and the pattern of a higher incidence in the most active regions of bone growth is evidence that suggest osteoblast proliferation is playing a major role in tumourigenesis.

Osteosarcoma cases can be characterised by the production of osteoid or bony matrix that can potentially result in a malignant neoplasm of the bone (Unni 1998). The most common sites of disease are the long bones of the leg, followed by the long bones of the arms, the axial skeleton and the small bones epyphysis (Mertens & Bramwell 1994).

So far it is unclear what exactly causes osteosarcomagenesis; however there is evidence that suggests that the inactivation of the tumour suppressor genes such as *p53*, *RB1* and *MDM2* initiates tumour development. The study and screening of such candidate tumour suppressor genes and oncogenes plays a large role in the study of osteosarcoma in current research.



## 1.5 Carcinogenesis

### 1.5.1 Mechanism of carcinogenesis

Since the first two-stage theory publication, already in 1957, cancer has been considered a multistage disease, arising, according to the multistep model, from a single mutational event that is followed by the accumulation of additional chromosomal and epigenetic alterations in the transformed cell(s). All of these events, both at the initiation step as well as during tumour promotion are passed on through cell division (Armitage & Doll 1957, Gorgojo & Little 1989, Hagemann et al 1996).

The first event “the initiating mutation” is to occur through an oncogene activation or tumour suppressor loss (Bowden et al 1994). Oncogenes are those genes that normally positively regulate cell division, whose mutation leads to the acquisition of functional over-activity and hence uncontrolled growth. Since they act in a dominant manner only one copy of an oncogene requires to acquire a mutation either sporadically or inherited (Weinstein 1988) Normally mutations of oncogenes are the result of point mutations, translocations or copy number amplifications.

Tumour suppressor genes, in their native form negatively regulate the processes of cell growth and cell death. They can prevent uncontrolled growth and hence tumour development by antagonizing signals that would initiate cell proliferation. When a tumour suppressor gene is inactivated by mutation, this may lead to uncontrolled growth and subsequent cellular transformation. Until recently it has always been thought that both alleles need to be inactivated to cause the phenotype (Knudson 1986); now such statements are being reviewed and partial loss of gene function by haploinsufficiency are discussed as being sufficient in some cases to impair their tumour-suppressor function. However, a rapidly growing number of tumour suppressor genes show a haploinsufficient phenotype, where loss of only one allele is sufficient to predispose to cancer without showing loss of the remaining wild-type allele in the tumour cells. A mutation in a tumour suppressor gene may be acquired through the parental germline. When this happens, a mutation in one of the alleles will already be present in all the cells of the body, for the required total functional loss of this gene a second hit in any somatic cell is sufficient.

As shown in Figure 7, a series of mutations are needed, to generate malignant cells from normally functioning ones. Each stage of tumour progression corresponds to a different genetic state of the cell. Two alternative models of carcinogenesis are currently discussed: In contrast to the classic “2 hit model” of Knudson (Knudson 1971, Knudson 1986) another

assumption proposes further promoting events (such as genomic instability for example, see 1.2.4) are required for a tumour to develop (Fodde & Smits 2002).

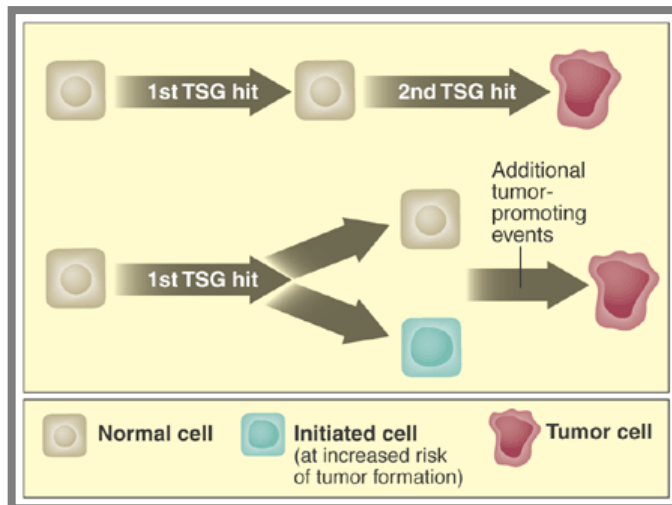


**Figure 7: Illustration of the two alternative models of carcinogenesis.** Either a two hit model where both hits on a TSG are needed or the one hit model, where one hit in a TSG followed by promoting events are enough to cause a cancer initiation. After Fodde & Smits 2002.

### 1.5.2 Loss of heterozygosity (LOH) and allelic imbalance

LOH is the loss of the wild-type function of one allele of a gene in a tissue where the other allele was already inactivated. LOH can occur in cancer, where it indicates a somatic change during tumour formation, usually associated with a loss of function of a tumour suppressor gene in the affected region. Occurrence of LOH can facilitate tumour development and progression by allowing or promoting uncontrolled cell division. Analysis of LOH has been employed to assess the status of particular genes or to identify new loci that can be involved in the initiation of progression of cancer (Chang et al 2010, Levine & Burger 1993, Zhang et al 2010).

Previous studies showed that LOH can substantially occur in osteosarcoma with great affinity for the TSG *Rb1* region (Chang et al 2010, Eisenberg et al 1997, Feugeas et al 1996, Rosemann et al 2003, Sasaki & Toguchida 1989, Sztan et al 1997, Zhang et al 2010) relating this phenomenon to the genetic predisposition of such tumours (See chapter 1.5.5).

### 1.5.3 Radiation Carcinogenesis

The impact of ionising radiation on cancer induction has always been an area of interest. It is nowadays accepted that exposure of tissues to ionizing radiation increases the risk of many types of cancer (Sowby 2008).

The largest population available for epidemiological studies on cancer induction after high dose and high dose rate radiation exposure are the A-bomb survivors from Hiroshima and Nagasaki (Little 1997, Pierce et al 1996). In this cohort, a large population was exposed to a relatively uniform radiation field composed mainly of highly penetrant gamma- and neutron-radiation with an intermediate (50mSv) to high dose exposure (3Sv) and at a very high (acute exposure) dose-rate. The life-time span study on these A-bomb survivors has established the reference for dose versus risk of developing tumours after radiation exposure. (Mabuchi et al 1994, Thompson et al 1994) .Due to the prolonged follow-up time, large number of exposed individuals, and sophisticated retrospective dosimetry, this data set serves as the reference for risk estimations. These data are limited in their relevance since such exposure situations similar to those of the A-bomb, namely acute, high-dose irradiation, uniform radiation field throughout the body, are rare.

Exposure conditions such as these are nowadays the absolute exception. The total population dose in the modern society is lower and is often protracted over extended periods and is delivered under quite different conditions.

Radiation exposure from medical applications involves mainly diagnostic X-rays and high-voltage  $\gamma$  and  $\beta$  rays delivered at high doses for radiotherapy. These exposures are usually extremely non-uniform, but organ specific instead. In some individuals repeated imaging can lead to significant cumulative doses.

Radiation exposure is also unavoidable in some occupational conditions such as for health personnel, aircrew and nuclear workers. It is usually characterized by low-dose rate, but can be with “exotic” types of radiation like in high-altitude air-planes or space-flights.

The total average annual radiation dose to a European is estimated to be in the range of 5 mSv . If the excess relative risk (risk imposed by exposures as an increment to the excess disease risk above the background rate of the disease) for all solid tumours as derived from the A-Bomb life time study are applied for a straight extrapolation to the European population, it would erroneously predict that this very small dose would cause some 240.000 tumours each year directly attributable to ionizing-radiation. The difficulty lies in extrapolating from the A-bomb data to other doses, dose-rates, radiation-types or radiation fields.

Whereas no excess was seen in the exposed A-bomb survivors, non-uniform exposure conditions with incorporated alpha emitters have a clinically established and a dramatic effect for bone tumour induction (Huvos & Woodard 1988, Huvos et al 1985, Pitcher et al 1994).

Therefore, to better understand the individual radiation risk further studies are urgent regarding the cellular mechanisms of radiation tumourigenesis and genetic predisposition.

#### 1.5.4 Radiation induced osteosarcoma

Osteosarcoma are prominent late effects following incorporation of bone-seeking radionucleotides, such as the  $\beta$ -emitter  $^{90}\text{Sr}$  or the  $\alpha$ -emitters  $^{239}\text{Pu}$ ,  $^{238}\text{U}$ ,  $^{224}\text{Ra}$  or  $^{227}\text{Th}$ . Since these isotopes specifically accumulate in bone by mimicking Calcium in mature mineralisation, they can deliver a localised radiation dose to the proliferating bone forming osteoblasts by *in-situ* decay of the radionucleotide sitting in mineralised bone, while sparing the remaining organism from acute radiation effects.

The consequences of this highly localised radiation exposure led to one of the first cases of a clear increase of tumour incidence due to occupational radiation exposure. Increase tumour incidence was found among female radium dial painters in the US, who ingested different doses of  $^{226}\text{Ra}$  and  $^{228}\text{Ra}$  developing osteosarcoma. In that cohort, the rate of osteosarcoma increased by a factor of more than 1000 fold (Polednak 1978a, Polednak 1978b, Polednak et al 1978). The radionuclides, ingested by the dial painters when licking the brushes for further painting, were deposited in the newly formed bone matrix, causing continuous short term and long term  $\alpha$ -irradiation with high doses to the skeleton. Among a total of 1391 workers, 46 of the 154 women with doses greater than 10Gy developed osteosarcomas. Such higher doses applied so close to the bone cells suggested a threshold dose for osteosarcoma induction

Despite the signs of a long-term detrimental effect certain osteotropic  $\alpha$ -emitters were applied for medical use. These include drugs such as Petheostor containing  $^{224}\text{Ra}$  (Spiess & Gerspach 1978) or Thorotrast containing  $^{227}\text{Th}$  (Mays & Spiess 1979) drugs. In particular, young patients that were treated in post war Germany with Petheostor for ankylosing spondylitis and/or bone tuberculosis developed significantly more osteosarcoma later in life as compared to non-exposed people (Spiess 2002). Osteosarcoma can also arise as secondary malignancy following conventional radiotherapy. This was most obvious after a study on the mortality of secondary tumours after childhood retinoblastoma (Eng et al 1993) (As shown in Figure 8).

An increased risk for sarcomas in the radiation field after treatment of retinoblastoma was also shown by Wong et al (Wong et al 1997) at local doses above 5 Gy, with the incidence rate rising to 10.7 fold compared to the sporadic rate when doses exceed 60 Gy.

Mouse-models were developed to elucidate the pathobiological and molecular genetic factors that govern osteosarcoma development after alpha-irradiation. These animal studies lead to the discovery of activated endogenous retroviruses (tumour-viruses) from radiogenic osteosarcomas (Erflle et al 1979) and to the discovery of congenital factors that control individual tumour susceptibility in different mouse strains (Rosemann et al 2002). The observation that some mouse strains have a higher susceptibility for  $\alpha$ -induced osteosarcoma was shown to be caused by inherited gene variations (Rosemann et al 2006).

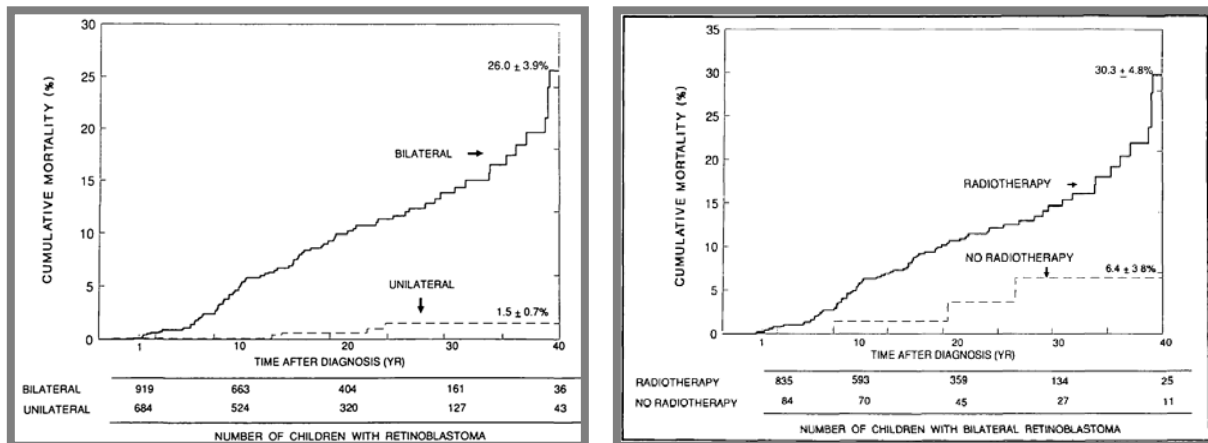


**Figure 8: Cumulative mortality from osteosarcoma of survivors of Retinoblastoma patients after RT treatment and the comparison between bilateral and unilateral retinoblastoma.** First panel shows the induction of osteosarcoma depending on the genetic predisposition (bilateral) of spontaneous occurrence (unilateral). The second panel shows the increase in induction after treatment with radiotherapy. From Eng et al 1993.

### 1.5.5 Genetic predisposition to radiation induced osteosarcoma

The majority of osteosarcoma occurs sporadically, without radiation exposure, but there is evidence that some inherited genetic conditions may result in a predisposition to sporadic osteosarcoma (Strong et al 1989). These include hereditary Retinoblastoma, Rothmund-Thomson syndrome, Werner syndrome and Li-Fraumeni syndrome. These syndromes all share a common characteristic, which is the association of germline gene mutations that show unbalanced karyotypes and alterations of certain genes that play a key role in cell cycle control or DNA metabolism (Brenton et al 1980, Ghule et al 2006).

As shown in Figure 8, first panel, secondary (metastatic tumour arising from a first one in a different organ) radiotherapy-induced osteosarcoma have a higher incidence in patients with primary bilateral (germline mutation) compared to unilateral (sporadic somatic mutation) Retinoblastoma, highlighting the importance of genetic predisposition by a germline mutation of the Retinoblastoma tumour suppressor gene, *RB1*. In fact the strongest predisposition to osteosarcoma is found in patients who suffer first from bilateral Retinoblastoma in childhood, for whom secondary neoplasias in the radiation field are a common late complication. The majority of these secondary malignancies are sarcomas, of which 50% are osteosarcomas (Eilber et al 2003).

The relative risk of developing a non radiogenic secondary osteosarcoma in patients with a germline mutation of the *RB1* is estimated to be 230 (Matsunaga 1980) whilst it increases up to 446 in the radiation field when the tumour of the eye had been previously treated with radiation (Wong et al 1997).

A promoter polymorphism in the *Rb1* allele, resulting in a reduced *Rb1* gene expression by about 50% was found to be linked to the increased osteosarcoma susceptibility in *BALB/c* strain mice (unpublished data). In addition to the tumour predisposing effect of this germline *Rb1* polymorphism, later in the process of osteosarcoma formation somatic losses of the second *Rb1* allele could be detected (Belchis et al 1996, Feugeas et al 1996, Miller et al 1996, Rosemann et al 2003, Wadayama et al 1994).

More indications for the direct involvement of the Retinoblastoma tumour suppressor in the formation of radiogenic tumours were found by the observation that, complementary to cases with somatic LOH at the *Rb1* locus were tumours with LOH at the *p15/p16* locus that harbours the gene *CDKN2A* that is functionally directly upstream of *Rb1* (Rosemann et al 2002). Unlike the established link between germline mutations of *Rb1* and osteosarcoma predisposition, clear relationship between mutations in this TSG and the increase on osteosarcoma incidence, no such link was found for either the *p15* or *p16* genes, where no polymorphisms nor mutations increased the osteosarcoma incidence. Mutations in *p16* led to melanomas (Harland et al 2008).

All this premises has led to formulate the hypothesis that there may be an additional tumour provoking function of *Rb1* that is distinct from the classical action as a component of the *p16/Rb1/E2F* pathway, which normally serves as a gatekeeper and is frequently the target of disruption by somatic allelic loss. This novel function of the *Rb1* gene may be independent of the cell cycle regulator network and more related to maintenance of genomic stability (caretaker function).

#### 1.5.6 Heritable forms of cancer and TSG

As previously stated, Retinoblastoma patients show an increase risk of osteosarcoma development (Fearon 1997, Meadows et al 1980) and family history has been recognized as an important component of cancer risk (Fearon 1997). For some yet unknown reasons, genetic predisposition to cancer is more often conferred by defects in tumour suppressor genes rather than by mutations in proto-oncogenes (Haber & Harlow 1997).

Type I TSG (gate keeper) have to be inactive for a permanent tumour growth. Their restoration can stop tumourigenesis, and cause tumour regression. The type I TSG, such as *p53*, pathways are thus promising targets for cancer therapy (Aranda-Anzaldo & Dent 2007, Saito et al 2004).

Type II TSG (caretaker) frequently plays an important role in genomic stability. Usually, their disruption promotes already early steps in tumour formation. Their restoration cannot inhibit tumour growth anymore; hence they are no targets for therapeutic intervention. There are

however, TSGs whose function might overlap between types I and II. Such could be the case for *Rb1*. Here, although the canonical function as TSG Type I is obvious during cell cycle progression, *Rb1* restoration in cancer cells does not render them less malignant. Therefore, one might suggest in addition a type II TSG function that could be involved in the maintenance of the telomeres and genomic stability.

In the case of *Rb1* mutations, tumour development occurs several years after the initial radiotherapy (Weichselbaum et al 1988, Weichselbaum et al 1989, Wong et al 1997), suggesting a relatively slow progress of tumourigenesis induction (Figure 8) that might be governed by additional promoting events rather than second mutation hit.

## 1.6 *Rb1* and telomeres

### 1.6.1 Mammalian telomeres

Telomeres are specialized structures at the ends of linear chromosomes of eukaryotic cells. They are composed of tandem repeats of the TTAGGG DNA sequence, typically 10 to 15 Kb long in human cells and from 12 to 80 Kb in the mouse. These sequence motifs bind specific proteins such as POT, TRF1, TRF2, TIN2, RAP1 (He et al 2006, Martinez et al 2010, Martinez et al 2009) that form stable DNA-protein complexes. During normal DNA replication, telomeric DNA cannot be completely replicated because binding of the DNA polymerase to the DNA template strand is not possible from the distal end. The 5' → 3' synthesis of the new strand starts always several base pairs distally of the binding site, what in the case of the lagging strand causes loss of several tens of base-pairs in each cell cycle (Bertuch et al 2003). As a result, telomeric DNA is shortened with every cell division. A specialized enzyme, telomerase, (Chan & Blackburn 2004) is capable of synthesising telomere repeats *de novo* using an RNA template binding to the telomere, but is only expressed at low levels in adult tissues and does not completely compensate this telomere length reduction. Thus, the telomeres can be seen as a biological clock of the cell, as cell division stops when telomeres are too short. Healthy cells can only divide, a limited amount of times, Hayflick limit, (Hayflick & Moorhead 1961) until they reach critical telomeric length and are driven into quiescence, senescence and apoptosis. In this phenomenon, the telomeric length is critical and is attributed to the end-replication problem. Cancer cells avoid this programming death, by finding ways of elongating the telomeres, via activation of Tert or ALT (Aragona et al 2000, Cong et al 2002, De Lange 2005).

Tumour cells that undergo a large number of cell divisions need to bypass the telomere mediated limitation of cell proliferation. Most tumour cells achieve this by activating or expressing higher levels of telomerase (Kim et al 1994) but a subset of about 10 to 15 % of

tumour cells (sarcomas and solid tumours) bypass the end replication problem in a telomerase-independent manner, the process of which is called alternative lengthening of telomeres (ALT) (Bryan et al 1995), among them, osteosarcomas (Muntoni & Reddel 2005).

### 1.6.2 Structure of the telomeres

Telomere repeats are associated to binding factors such as TRF1 and TRF2 and other proteins that form a specific nucleoprotein complex with telomeric DNA, known as the telosome. The function of the telosome is to prevent the end-to-end fusion of chromosomes by hiding the open end at the end of the chromosome and to prevent telomeres from the DNA double strand breaks repair machinery by forming the so called loop of the telomere: T-loop (Bertuch & Lundblad 2006).

The particularity of eukaryotic telomeres is the protrusion of a single stranded G-rich fragment of 150-200 nucleotides in length at the 3' end of the chromosome. This fragment plays a central role in the telomere structure as it leads to the formation of the T-loop which is formed by the invasion of the terminal single-stranded DNA into the duplex region of the telomere, thereby creating a solution for the telomere end protection (Griffith et al 1999). The single stranded overhang also serves as substrate for the telomerase, the enzyme responsible for the elongation of the telomeres because telomerase *in vitro* acts exclusively on single-stranded substrates with a free 3' end, (Bianchi & Shore 2008) it is well poised to act on chromosome ends, due to fact that telomeres terminate in 3' single stranded overhangs of the G-rich strand. The formation of these long overhangs in S phase is independent of telomerase activity (Dionne & Wellinger 1996) suggesting that it is instead due to processing of the ends, possibly by incomplete replication of the lagging strand or by exonucleolytic activity (Dai et al 2010).

### 1.6.3 Telomere constitutive heterochromatin and its epigenetic regulation

A challenge to nuclear organization is achieving is packaging two meter long linear DNA string in a ~10  $\mu\text{m}$  diameter sphere in a manner that preserves its integrity as well as its accessibility to the transcription and replication machinery. This is achieved by the association of DNA with histones and other chromosomal proteins in different levels of packaging. At the first level 147 DNA base pairs are wrapped 1.67 times around the core histone, forming the nucleosome, the basic subunit of chromatin (Kornberg & Thomas 1974). The histone protein core is a cylinder-shaped structure formed by an octamer made of pairs of the four histones H2A, H2B, H3 and H4.



In contrast to yeast, the mammalian telomeres contain histones, and therefore, telomeres, as well as sub-telomeric regions display epigenetic markers of constitutive heterochromatin (Blasco 2007). The constitutive heterochromatin is normally found in inactive regions of repetitive DNA such as pericentric satellites repeats or telomeres and is characterized by an enrichment in heterochromatin protein 1 (HP1) isoforms, H3 K9 3met and H4 K20 3met (Figure 9). Mammalian telomere repeats, (TTAGGG) $_n$ , lack the CpG sequence that is usual the substrate of DNA methyltransferases (DNMTs) and can therefore not be methylated. In contrast, the sub-telomeric sequences are heavily methylated.

Interestingly, the methylation status of the sub-telomeric regions seems to play an important role in the regulation of telomere repeat length as DNMT1 deficient mouse embryonic stem cells (ES) show dramatically elongated telomeres as compared to control (Gonzalo et al 2005, Gonzalo et al 2006).

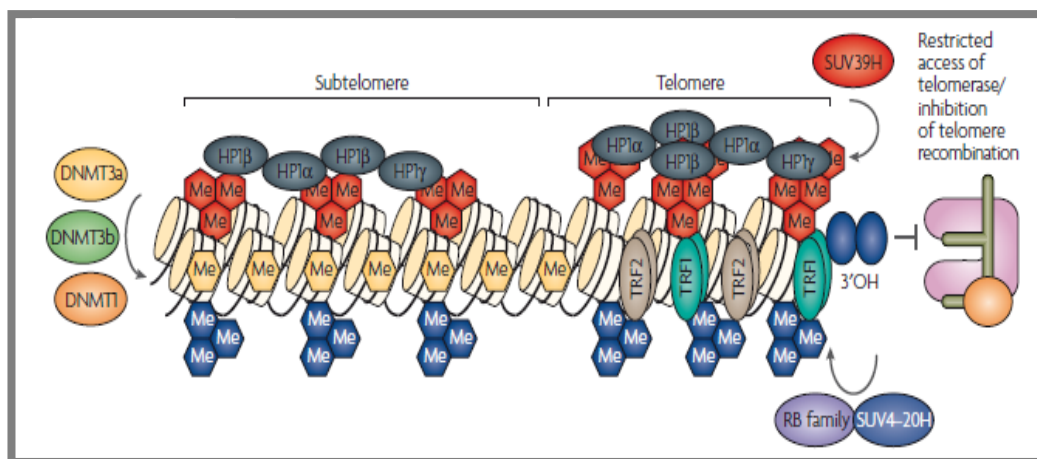


**Figure 9: Epigenetic modifications at mammalian telomeres:** Telomeric structure showing the different epigenetic markers. Both telomeric and sub-telomeric chromatin regions are enriched in trimethylated H3K9 and H4K20, and HP1 isoforms. In addition subtelomeric DNA is heavily methylated. The constituted telosome shelters the telomere from the telomerase and the recombination machinery. From Blasco et al 2007.

In contrast, in telomerase deficient mice, with short telomeres, the level of constitutive heterochromatin markers (Histones H3 and H4 trimethylations) as well as methylation of the sub-telomeric regions appear to decrease (Benetti et al 2007). This suggests that telomere repeats length influences also the sub-telomeric chromatin status (Figure 10). From a functional point of view the telomere displays the ability to silence genes that are located in neighbouring sub-telomeric regions. This phenomenon known as “telomere positioning effect” (TPE) occurs in mammals as well as in yeast with profound effects on gene expression patterns. It seems that the induction of a more compact chromatin at the telomeres also affects the nearby regions (Baur et al 2001) to telomerase and represses recombination between telomeric repeats.

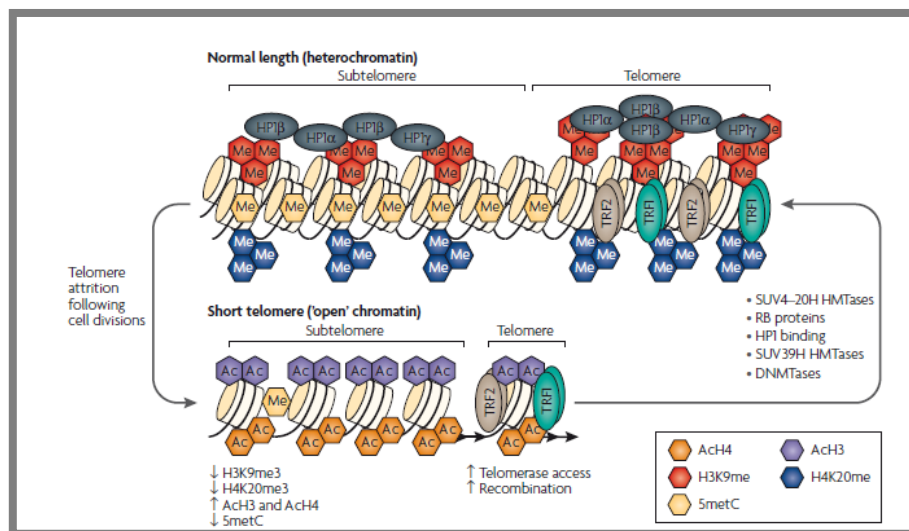


**Figure 10: A model for the role of epigenetic modifications in telomere-length control.** Normal-length telomeres have features of constitutive heterochromatin, such as subtelomeric DNA hypermethylation, hypermethylation of histone H3 at lysine 9 (H3K9) and histone H4 at lysine 20 (H4K20), hypoacetylation of histones H3 and H4, and heterochromatin protein HP1 binding at both telomeres and subtelomeres. With cell divisions and telomere shortening, the epigenetics of the telomeres change to a pattern of acetylation (AcH4, AcH3) and loss of methylation. From Blasco et al 2007.

As telomeres become shorter with increasing cell divisions, these heterochromatic marks are decreased from telomeres and sub-telomeres, coupled to an increased histone acetylation (Figure 10). This raises the possibility that loss of DNA methylation is an important additional mechanism for telomere-length control, as cells with defective H3K9 and H4K20 trimethylation also show DNA-methylation defects (Gonzalo et al 2005, Peters et al 2001, Schotta et al 2004).

Loss of methylation leads to a more “open” chromatin state, which allows a greater accessibility of telomere-elongating activities (by telomerase and proteins that are involved in telomere recombination, which can lead to elongation by alternative lengthening of telomeres (ALT). Rb1 has previously been suggested to play a role in these processes (Blasco 2007).

## 1.7 The alternative telomere lengthening (ALT) pathway and cancer

### 1.7.1 ALT pathway

Telomerase independent replenishment of the telomeres can be achieved by the cells of some tumour types, among them osteosarcomas by homologous recombination. The ALT pathway (alternative lengthening of the telomeres) is activated when telomeres reach critical length and using the sister chromatid strand, the telomere can be replenished (see Figure 11).

Unique features are found in ALT cells compared with telomerase-positive tumour cells (Reddel 2003). It appears that ALT is more often present in cell lines and tumours of mesenchymal origin, such as osteosarcomas (Muntoni & Reddel 2005) and *in-vitro* transformed human fibroblasts, than in those of epithelial origin. The reason for this difference is completely unclear. Telomere length of ALT cells is characterized by heterogeneity: some telomeres are extremely long; at the same time, others are very short or even undetectable in a single cell. Asymmetrical telomeres can even be observed at some chromosome ends. ALT cells are, moreover characterized by a pronounced chromosomal instability (Ulaner et al 2004). Interestingly, in ALT cells some promyelocytic leukaemia nuclear bodies (PML-NBs) nuclear bodies form specific structures with telomeres that are called APBs for ALT-associated PML-NBs (Yeager et al 1999).

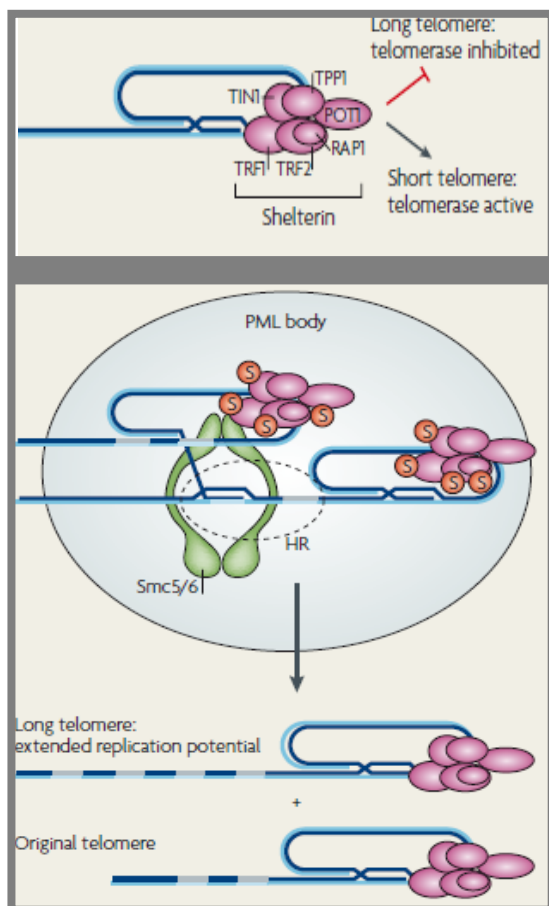


**Figure 11: ALT pathway main features.** Upper panel; Telosome, showing telomere with its sheltering complex (in mammals). In the absence of telomerase, telomeres shorten because the last few nucleotides of a chromosome cannot be synthesized by DNA replication. The resulting telomere shortening leads to cellular senescence. Normal somatic cells repress telomerase activity to limit the proliferative potential. In contrast, telomerase is upregulated in many cancer cells, which enables unlimited proliferation. In telomerase negative cancer cells, homologous recombination (HR) is used to increase telomere length through the alternative lengthening of telomeres (ALT) pathway. Lower panel; in cells undergoing ALT, telomeres associate with promyelocytic leukaemia (PML-NBS) bodies, known as ALT-associated PML-NBS bodies (APBs). In ALT cells, the Smc5/6 complex and HR proteins associate with PML-NBS bodies in G2phase (when sister chromatids are available for HR). Sister chromatids recombine (dashed circle) and the shorter telomere gets replenished with great level of heterogeneity between different telomeres. Sumorilation of sheltering complex, activates the Smc complex that promotes the recombination process and replenishment of the telomere. From Murray & Carr 2008.

Although observation in model system suggest that ALT tumour may be relatively benign, they appear to be sometimes lethal in patients (Reddel & Bryan 2003) but the prognostic significance of ALT seem to vary among tumour type. However, ALT tumours may be less likely to metastasize than telomerase-positive tumours (Henson et al 2005).

### 1.7.2 ALT and PML-NBs

Promyelocytic leukaemia nuclear bodies (PML-NBs) fall in the category of protein “bodies” that were so far identified in the mammalian nucleus. They were first seen in Promyelocytic leukaemia, where the PML-NBs protein was over expressed (Ascoli & Maul 1991, Boublikova et al 2006, Gambacorta et al 1996). PML-NBs are dynamic nuclear structures that are involved in numerous cellular processes and have several isoforms. The PML-NBs are heterogeneous structures. They facilitate post-translational modification and can localize proteins to their sites of action. PML-NBs are shown to be involved in processes as different as apoptosis, senescence, cell proliferation, chromatin remodelling, DNA damage repair, transcription or telomere lengthening (Weidtkamp-Peters et al 2008). Interestingly, PML-NBs are known to be involved in the telomere lengthening of telomerase negative tumour cells through, as previously mentioned, the alternative telomere lengthening (ALT) pathway.

PML-NBs are also reported to be involved in premature senescence (Ferbeyre et al 2000). This phenomenon appears to be mediated by the PML-NBs IV isoform that stabilize and activates p53 phosphorylation and acetylation (Bischof et al., 2002; Salomoni and Pandolfi, 2002). PML-NBs have also been shown to physically interact with phospho-Rb1 which suggests PML-NBs may be involved in the control of cell cycle entry and cellular senescence (Alcalay et al., 1998) as well as possibly act as a tumour suppressor (Salomoni & Pandolfi 2002).

Together with Daxx, the PML-NBs protein plays a central role in p53-mediated apoptosis. For example PML<sup>-/-</sup> cells are resistant to the lethal effects of  $\gamma$  irradiation and CD95-induced apoptosis (Chen et al 1997, Guo et al 2000, Wang et al 1998) by control of apoptosis, cell proliferation, and senescence, since tumourigenesis is enhanced in PML mutants.

Altogether, these results suggest that PML-NBs are also involved in genomic stability. PML-NBs are moreover found to co-localize with unscheduled DNA synthesis loci in damaged cells suggesting they play a direct role in DNA repair (Dellaire & Bazett-Jones 2004).

PML-NBs have been shown to associate tightly with chromatin (Eskiw & Bazett-Jones 2002, Eskiw et al 2003, Muratani et al 2002) at least transiently and their functional interactions appear to be very complex. On the one hand chromatin modifying proteins such as acetyltransferases (Boisvert et al 2001) and de-acetylases (Wu et al 2000) as well as the heterochromatin protein 1 (HP1) (Hayakawa et al 2003) accumulate in PML-NBs, implying a role in chromatin structure regulation. PML-NBs are in addition suspected to play a central role in the establishment of the constitutive heterochromatin at DNA satellites (Luciani et al 2006). On the other hand chromatin itself has been shown to play a direct role in PML bodies structural integrity as for example DNase treatments of the nucleus or apoptosis induction leads to their destabilization (Eskiw et al 2004). Moreover a study has shown that PML-NBs

number is increasing in early S phase by a fission process suggesting that PML-NBs, tightly bound to several chromatin domains are torn apart by the replication machinery (Dellaire et al., 2006).

One remarkable feature of the PML-NBs is the role that they play in the alternative telomere lengthening pathway. A fraction of cells in a given ALT population possess enlarged PML-NBs called ALT associated PML-NBs or APBs (Eskiw et al 2004). APBs display the unique feature to enclose a large amount of telomeric repeats as revealed by fluorescence *in-situ* hybridization (FISH) or the immunological detection of telomeric DNA-binding proteins TRF1 and TRF2. APBs contain PML protein variants along with Sp100, Rad50, and BLM that exist in PML-NBs. In addition, APBs contain the telomere associating protein Rap1 and the recombination proteins Rad51, Rad52, and BRCA1, which are not present in PML-NBs, as well as many proteins involved in double strand break detection and reparation machinery such as hRad9, hHus1, hRad1 and hRad17 (Nabetani et al 2004, Wu et al 2000, Wu et al 2003). Furthermore, 5-bromo-2'-deoxyuridine (BrdU) incorporation was detected in U2OS (human osteosarcoma cell line) cells at foci where the APB marker hRad9 and telomere DNA co-localize indicating that DNA is repaired and synthesized at APBs.

## 1.8 CIN and telomeres

In the context of chromosomal instability, the telomeres the end of the chromosomes can be considered an open DNA double strand break. Only their association with the telosome protein cap prevents them from being recognised as an unrepaired DNA lesion. With each cell division, however telomeres get shorter, and under non proper packaging as seen before they will erode even faster, thereby losing its ability to bind the telosome caps and consequently being exposed in the nucleus like an open DNA break. Following association to another open chromosomal end the short range integrity of the DNA will be restored and cell-cycle progression re-initiated, but only at the expense of global chromosomal rearrangements such as gene amplification, deletion or as described by McClintock (Mc 1951) already in 1951 a so-called breakage-fusion-breakage cycle (Figure 12).

Dysfunctional telomeres, either owing to critically short telomeres or to uncapping, elicit a DNA damage response by activation of upstream kinases, DNA-dependent protein kinase catalytic subunit (DNA-PKcs), ataxia-telangiectasia mutated (ATM) and ataxia telangiectasia and Rad3-related (ATR). DNA damage response activation may drive cells towards two opposing outcomes depending on the p53 and p21 status. Consequent activation of the tumour suppressor p53 induces cell cycle arrest, apoptosis or senescence, negatively

affecting stem cell functionality and causing tissue degeneration and ultimately organ failure (Ghule et al 2006).

When such systems fails, tetraploidisation can readily initiate genomic instability owing to the presence of multiple centrosomes that will give rise to the random distribution of chromosomes originating aneuploid daughter cells in mitosis. Activation of either the classic or the alternative non-homologous end joining (NHEJ) pathways results in end-to-end fusions that initiate successive cycles of breakage–fusion–breakage cycles.

On telomere healing, either by telomerase reactivation or by homologous recombination-based mechanisms, such as the alternative lengthening of the telomere (ALT), stable malignant clones will be generated, giving rise to metastatic tumours (Martinez & Blasco 2011).

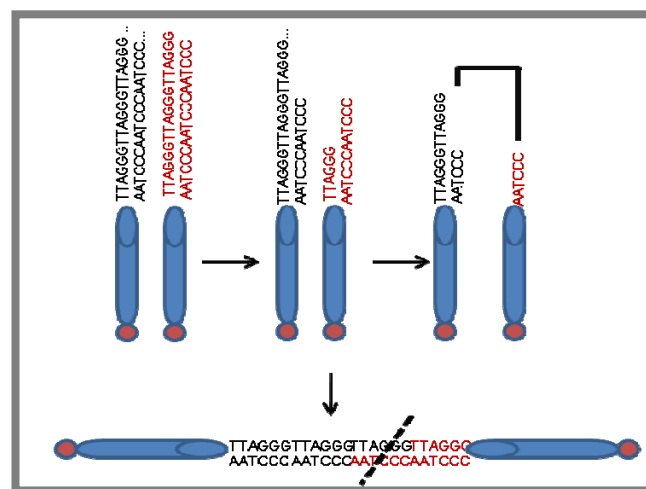


**Figure 12: Schematic representation of anaphase bridges due to telomere defects.** A double strand break arises from a critically short telomere that fuses to another DSB from a neighbouring telomere forming a bridge and creating a dicentric. During cell division, in anaphase, the two daughter cells that will separate and break randomly along the chromosome creating a new break and therefore restarting the cycle (Diagonal lines mark a random break).

### 1.9 *Rb1*, telomeres and osteosarcomagenesis

Cells lacking telomerase are subject to telomere attrition with each round of replication, eventually leading to loss of telomere capping chromosome ends (Smogorzewska & de Lange 2002). One of the proposed *Rb1* functions, brings it in relation to cell immortalization of the cells, a mechanism only in part associated with its tumour suppressor activity (Kiyono et al 1998).

One possibility would be a novel *Rb1* function involving telomere maintenance as previously proposed (Garcia-Cao et al 2002, Seger et al 2002). They postulated a connection between the members of the retinoblastoma family of proteins, *Rb1* (retinoblastoma 1), *Rb1-1*

(retinoblastoma-like 1) and Rbl-2 (retinoblastoma-like 2), and the mechanisms that regulate telomere length.

Osteosarcomas without telomere maintenance mechanisms such as telomerase or alternative lengthening of telomeres (ALT) have a better prognosis than those with this mechanism active (Ulaner et al 2003). This suggests that there might be a relation between the malignant properties of osteosarcomas and their molecular features such as telomere maintenance, increased chromosomal instability and the carcinogenic process.

### **1.10 Genetic instability, radiation and cancer**

An unstable karyotype is a feature of nearly all adult-onset solid tumours and a characteristic of osteosarcoma (Maire et al 2009). Such instability is known to appear in the early stages of cancer progression, but can also manifest itself as the non-clonal alterations such as segregational defects, inversions, deletions etc in different cells within one and the same tumour. The list of gene mutations generating genomic instability in sporadic cancers is not complete (Anderson et al 2001a, Dominguez-Brauer et al 2009). Instability may prompt the cumulative generation of additional somatic changes to a genetically heterogeneous population of cells.

A number of rare genetic disorders are characterised by increase levels of genomic instability detectable already in somatic cells, among those well known: Ataxia telangiectasia (*ATM* gene), Nijmegen breakage syndrome (*NBS1* gene), Fanconi's anaemia (*FA* gene) or Blooms syndrome (Blm-helicase gene) (Little 2003).

Genomic instability or chromosomal instability (CIN) is known to be a hallmark of cancer transformation and progression (Tang et al 2005). The term refers to a range of genetic alterations from point mutations to chromosome rearrangements and can be divided into classes according to the affected genomic structure. Nothing is known yet about such a relation to the Retinoblastoma familial syndrome, and whether genomic instability is involved in cancer predisposition. It would depend on the question whether, in addition to its gate keeper function at the G1/S checkpoint Rb1 also confers a caretaker function towards genome stability.

Among others, two element types play a key role in instability leading to rearrangements: those acting to prevent instability (replication, repair and S-phase checkpoint factors) and those chromosomal hotspots of instability such as fragile sites (among them the telomeres) or highly transcribed sequences (Little 2003).

An interesting feature of such phenotype is that it can be transmissible from a cell exposed to genotoxic agents to its progeny. When exposed to ionising radiation, the induced genetic instability can remain in the progeny for several cell divisions and generations (Belyakov et al 1999, Jamali & Trott 1996, Marder & Morgan 1993, Trott et al 1998). This implies that the initial carcinogenic event may not always be a rare mutation occurring in a specific gene or set of genes, rather, radiation may induce a process of instability in many cells in a population, enhancing the rate at which multiple gene mutations will be acquired for a further cancer development of cancer in a given cell lineage.

Radiation could act at any stage in the development of cancer by facilitating the accumulation of the remaining genetic events required to produce a fully malignant tumour. This can also occur if the first mutation triggers a so called “mutator phenotype” being this the result from mutations in genes that function in the maintenance of genetic stability. It is manifested by increases in mutation rates and in genetic evolution of cancer cells that drives tumour progression (Loeb 2001) which in case of *Rb1* could accelerate a fully malignant transformation by promoting the rapid generation of additional genetic defects. This statement could imply that the initial event in radiation carcinogenesis does not have to be a mutation occurring in a gene or set of genes that end up gaining a selective growth advantage but radiation might induce a process of instability that could enhance the set of mutations in a given cell lineage (Lorimore et al 2003).

The aim of this study is to find the causality in the relationship between haploinsufficient germline mutations in the *Rb1* gene, and the increase in radiation induced osteosarcoma (Rosemann et al 2006). This work insights into the cellular complications arising from germline mutations in the retinoblastoma gene and their relationship to radiation induced osteosarcomagenesis. Does *Rb1* function impairment lead to radiation induced cancer? Does *Rb1* have a secondary function controlling the stability of the genome?



## II. MATERIALS

### 2.1 Equipment

Applied Biosystems Real Time PCR,	Applera GmbH, Darmstadt (Germany)
Centrifuge Biofuge fresco,	Heraeus Instruments, Osterode (Germany)
Centrifuge Biofuge pico	Heraeus Instruments, Osterode (Germany)
Centrifuge Eppendorf 5415R	Eppendorf, Hamburg (Germany)
Centrifuge Fisherbrand Mini	Fisher Scientific, Schwerte (Germany)
Centrifuge Rotanta 460R	Andreas Hettich, Tuttlingen (Germany)
Centrifuge Rotina 420R Andreas	Andreas Hettich, Tuttlingen (Germany)
Centrifuge Variofuge 3.0R	Heraeus Sepatech, Osterode (Germany)
Cell counter	Coulter (Germany)
Dispenser Multipette® plus	Eppendorf, Hamburg (Germany)
Electrophoresis Cell GT	Bio-Rad Laboratories, Munich (Germany)
Electrophoresis Transfer Blot	Bio-Rad Laboratories, Munich (Germany)
Pipettes 10, 20, 100, 200, 1000 µl,	Eppendorf, Hamburg (Germany)
Freezer -20°C ,	Liebherr (Germany)
Freezer -80 °C	New Brunswick, Nürtingen (Germany)
Frigocut (microtome) 2800	Leica, Heidelberg (Germany)
Fluor Chem HD2, High dynamic range imaging	Biozym Hessisch Oldendorf (Germany)
Heating block Thermomixer comfort 1.5 ml	Eppendorf, Hamburg (Germany)
Heating block Thermomixer confort 1.5 ml	Eppendorf, Hamburg (Germany)
HWM-2000 machine	Siemens, Erlangen (Germany)
Incubator 37°C	Sanyo, Bad Nenndorf (Germany)
LSR II flow cytometer	BD, San Jose, CA (USA)
Light cycler	Roche Diagnostics, Mannheim (Germany)
Microplate Reader Model 680	Bio-Rad Laboratories, Munich (Germany)
Microscope LSM	Carl Zeiss, Jena (Germany)
Microscope Axiovert 135	Carl Zeiss, Jena (Germany)
Microscope Axioplan2	Carl Zeiss, Jena (Germany)
Microwave Privileg 1034HGD	Otto, Hamburg (Germany)
Neubauer chamber,	Marienfeld (Germany)
PCR cycler	Veriti (Germany)
pH meter	Schott instruments (Germany)

Power supply Model 200/2.0	Bio-Rad Laboratories, Munich (Germany)
Spectrophotometer NanoDrop® ND-1000	Thermo Scientific, Rhein (Germany)
SpeedVac Concentrator, Univapo 100H,	UniEquip, München (Germany)
Shaker	GFL, Segnitz (Germany)
Sonicator, Sonifier B12	Branson Ultrasonic (USA)
StepOne	Applied biosystems, Darmstadt, (Germany)
Infinite M200 plate reader	Tecan, Crailsheim (Germany)
Tank Blot	Bio-Rad Laboratories, Dreieich (Germany)
Tweezers No.5	Biolab, München (Germany)
Vacuum Concentrator plus	Eppendorf, Hamburg (Germany)
Vi- cell counter	Beckman Coulter (Germany)
Vortexer Reax top	Heidolph Instr., Schwabach (Germany)
Water Bath 37°C	GFL, Segnitz (Germany)
X-cell sure lock Western blot system	Invitrogene, Darmstadt (Germany)

## 2.2 Consumables

6 well plates	Nunc, Rhein (Germany)
96 tube PCR plate	AB gene, Rhein (Germany)
Blotting paper	Biometra, Gottingen (Germany)
Capillaries for light cyclers	Roche Diagnostics, Mannheim (Germany)
Cell culture flasks,	Nunc and CellStar (Germany)
Cover slips	VWR, Darmstadt (Germany)
Cryogenic vials sterile	VWR, Darmstadt (Germany)
Gel cassettes 1.5 mm	Invitrogene, Darmstadt (Germany)
Glass slides SuperFrost® 76 x 26 mm	Carl Roth, Karlsruhe (Germany)
Membrane Western Amersham™ Hybond™	GE Healthcare, Munich (Germany)
Needles Sterican® Ø 0.60 x 60 mm 23G x 2 3/8"	B. Braun, Melsungen (Germany)
Parafilm®	Carl Roth, Karlsruhe (Germany)
PCR tubes	Eppendorf, Hamburg (Germany)
Petri dishes	Greiner, Frickenhausen (Germany)
Potassium Ferricyanide Crystalline	Merck, Darmstadt (Germany)
Potassium Ferricyanide Trihydrate	Merck, Darmstadt (Germany)
Photographic film, Hyperfilm 18x24cm	GE Healthcare, Munich (Germany)
Pipettes, Pasteur glass 3.2 ml	Carl Roth, Karlsruhe (Germany)

Pipette tips Graduated Filter Tips TipOne	Starlab, Ahrensburg (Germany)
PNA probes with FITC and Cy3	Panagene, Tokio (Japan)
Reacion tubes 1.5 ml	Eppendorf, Hamburg (Germany)
Reaction tubes Falcon™ Blue Max	BD Biosciences, Heidelberg (Germany)
Scalpel, sterile, disposable	Paragon (Germany)
Syringe, single-use 50 ml (60 ml)	Henke-Sass-Wolf, Tuttlingen (Germany)
Tissue culture flasks, filter cap Nunclon™ Δ	Nunc, Rhein (Germany)
Tissue culture 6 well plates	Greiner, Frickenhausen (Germany)

### 2.3 Chemicals and reagents

β-mercaptoethanol	Sigma-Aldrich, Steinheim (Germany)
Acetic Acid	Merck, Darmstadt (Germany)
Acrylamide/ Bisacrylamide gel	Invitrogene, Darmstadt (Germany)
Agarose	Biozym Hessisch Oldendorf (Germany)
Agarose LE for gel electrophoresis	Biozym, Hessisch Oldendorf (Germany)
Albumin from bovine serum (BSA)	Sigma-Aldrich, Steinheim (Germany)
Ampuwa® water	Fresenius (Germany)
APS	Sigma-Aldrich, Steinheim (Germany)
Big Dye 3.1	Applied biosystems, Darmstadt, Germany
Bis-acrylamide ProtoGel 30 % (w/v)	National diagnostics, Atlanta (GA, USA)
Complete mini	Roche Diagnostics, Mannheim (Germany)
Chemiluminescent substrate	GE Healthcare, Munich (Germany)
Chloroform	Merck, Darmstadt (Germany)
Cresol red	AppliChem, Darmstadt (Germany)
Cytochalasin B, 0.5 µg/ml,	AppliChem, Darmstadt (Germany)
DAPI nuclei staining, 150ng/ml	Merck, Darmstadt (Germany)
Dil	Invitrogene, Darmstadt (Germany)
DMEM	Gibco/Invitrogen, Karlsruhe (Germany)
DMSO	Sigma-Aldrich, Steinheim (Germany)
NaCl	Merck, Darmstadt (Germany)
Ethanol	Merck, Darmstadt (Germany)
Ethidium bromide	Merck, Darmstadt (Germany)
Fast blue	Serva, Heidelberg (Germany)
FCS (Fetal Calf Serum)	PAA Laboratories GmbH, Cölbe (Germany)

---

Formalin deionised	Applichem, Darmstadt (Germany)
HCl, 1 mol/l (1 N)	Merck, Darmstadt (Germany)
Hoechst 33342	Merck, Darmstadt (Germany)
Isopropanol	Merck, Darmstadt (Germany)
LB broth base	Invitrogene, Darmstadt (Germany)
Magnesium Chloride	Sigma-Aldrich, Steinheim (Germany)
Methanol	Merck, Darmstadt (Germany)
MOPS	Merck, Darmstadt (Germany)
NP-40 Tergitol	Sigma-Aldrich, Steinheim (Germany)
Naphtol AS-MX	Sigma-Aldrich, Steinheim (Germany)
Opti-MEM	Gibco Darmstadt (Germany)
Paraformaldehyde	Merck, Darmstadt (Germany)
PBS	Invitrogene, Darmstadt (Germany)
Phosphatase inhibitors	Sigma-Aldrich, Steinheim (Germany)
Polybrene	Sigma-Aldrich, Steinheim (Germany)
Ponceau	Sigma-Aldrich, Steinheim (Germany)
Potassium hexacyanoferratell	Sigma-Aldrich, Steinheim (Germany)
Potassium hexacyanoferratelll	Sigma-Aldrich, Steinheim (Germany)
Proteinase K	Roche Diagnostics, Mannheim (Germany)
Protease inhibitor cocktail tablets complete mini	Roche Diagnostics, Mannheim (Germany)
Reverse transcriptase SuperScript® II	Invitrogene, Darmstadt (Germany)
RIPA buffer	Thermo Scientific, Rhein (Germany)
RNase OUT	Invitrogene (Germany)
Random primers	Promega. Mannheim (Germany)
Roth 10x running buffer	Roth (Germany)
Sequencing Kit'	Appelera GmbH, Darmstadt, (Germany)
SDS 10 % (w/v) solution	Bio-Rad Laboratories, Munich (Germany)
SDS-PAGE running buffer Rotiphorese, 10x	Carl Roth, Karlsruhe (Germany)
Taq DNA polymerase	Fermentas, St. Leon-Rot (Germany)
Taq man master mix	Applied life technologies, Darmstadt (Germany)
Trypsin	Invitrogene, Darmstadt (Germany)
Tween 20	Sigma-Aldrich, Steinheim (Germany)
Stripping buffer Restore™ PLUS	Pierce/ Thermo Scientific, Rhein (Germany)

Vecta shield;

Linaris, Wertheim (Germany)

X-gal

Boehringer, Mannheim (Germany)

## 2.4 Length standards:

DNA molecular weight marker VIII, Roche, Mannheim. Germany

Long fragment marker, kindly given by R. Cadwell, Helmholtz Center, Munich, Germany

## 2.5 Buffers and Solutions

### 1x Transfer buffer for Western Blot

10% (v/v) 10x transfer buffer

20% (v/v) MeOH

### LB media (pH 7.5)

10g Bacto-Tryptone

5g Yeast extract

10g NaCl

### Separating gel (12 %) for SDS-PAGE (10 ml) (5ml)

4ml 30 % (w/v) acrylamide/bis

2.5ml 1.5 M Tris (pH 8.8)-HCl

100µl 10% (w/v) SDS

50µl 10 % (w/v) APS

5µl TEMED

3.35ml H<sub>2</sub>O bidest.

### FACS Sol I: lysis solution: 584mg/L NaCl 15g/L citric acid

1000 mg/L Na-citrate (Tri-sodium citrate)

10 mg/L RNase A from bovine pancreas

0.3 ml/L Nonidet P-40

EtBr

Filter sterilized

### 5x TBE buffer (pH 8.3)

89 mM Tris base

89 mM Boric Acid

2 mM EDTA

### LB Agar (pH 7.0)

10g Tryptone

5g Yeast extract

5g NaCl

15g bacterial Agar

### Stacking gel (4%) for SDS-PAGE

670µl 30 % (w/v) acrylamide/bis

1.26ml 0.5M Tris (pH 6.8)

50µl 10% (w/v) SDS

25µl 10% (w/v) APS

5µl TEMED

3ml H<sub>2</sub>O bidest.

### FACS Sol II: stabilizing solution

0.25M sucrose

15g/L citric acid

Filter sterilised

EtBr

**LacZ fix buffer**

4% PFA  
0.005 M EGTA  
0.001 M MgCl<sub>2</sub>  
0.01% Deoxycholate  
0.02% NP40  
PBS, pH 7.4 (adjust with HCl/NaOH)

**LacZ staining**

0.1% X-Gal in PBS

**Tissue lysis buffer**

100ml 1M Tris  
40ml 0.5M EDTA  
4ml 5M NaCl  
proteinase K(50µg/ml)  
10ml 20% SDS  
0.01M EDTA

**Hybridisation buffer for Flow-FISH**

70% formamide deionised  
20mM Tris pH 7.1  
1% BSA  
0.3µg/ml probe

**LacZ wash buffer**

0.002M MgCl<sub>2</sub>  
0.005M Ferrocyanide  
0.005M Ferricyanide  
Diluted in *LacZ* wash buffer

**Eosin stock solution**

10gr Eosin yellow  
180ml distilled water  
2-5 drops of acetic acid.

**TBE Buffer**

0.4M Boric Acid  
0.4M Tris  
pH 8.0

**Hybridisation buffer for FISH PNA**

70% formamide deionised  
10mM Tris pH 7.2  
0.3µg/ml probe

**Wasing buffer for FISH PNA**

70% formamide deionised  
10mM Tris pH 7.2  
0.15M NaCl (pH=7.5)  
0.05% Tween20

**Wash I buffer for flow-FISH**

70% formamide deionised  
10mM Tris pH 7.1  
0.1% BSA  
0.1% Tween20

**Wash II buffer for flow-FISH**

PBS  
0.1% BSA  
0.1% Tween20

**Blocking solution for immunofluorescence**

100 ml PBS  
1g BSA  
0.15g Glycin

**PCR buffer**

100mM Tris-HCl, pH 8.3  
500mM KCl  
15mM MgCl<sub>2</sub>  
15mM MgCl<sub>2</sub>  
0.01% Gelatine

**Loading buffer for agarose gel**

50% Glycerine  
1mM EDTA, pH 8.0  
0.2% Bromphenol blue  
0.2% Xylencyanol

**T-TBS**

7.26g Trizma base  
24g NaCl  
Dissolve in 2750ml dH<sub>2</sub>O (pH 7.6 with HCl)  
3ml Tween  
HCl/NaOH (pH adjustment)

**Staining buffer for Flow-FISH**

500µl PBS  
0.1% BSA  
10µg/ml RNase  
0.1µg/ml PI

**Antibody solution**

1.5ml PBS  
2% BSA  
0.01 Tween20  
Antibody depending on concentration

**Protein lysis buffer**

1ml 1x RIPA  
1 tablet of complete mini  
10µl cocktail 1  
10µl cocktail 2

**Laemmli buffer**

20ml 10% SDS  
5 ml 2-mercaptoethanol  
10ml Glycerol  
10ml dH<sub>2</sub>O  
0.005g Bromophenol blue(0.01%)

**Carnoy fixative**

10ml Acetic Acid glacial  
30ml Methanol

**Freezing media**

10% DMSO

90% DMEM (10% FCS)

**Eosin working solution**

20 ml stock solution

1000ml distilled water

**2.6 Commercially available kits**

BCA Protein Assay Pierce®

GenElute™ Miniprep Kit

PureYield™ Midiprep Kit

QuiaAmp<sup>R</sup> DNA extraction kit,RNeasy<sup>R</sup> RNA extraction Kit,QuiaQuick<sup>R</sup>, gel extraction kit

Senescence kit

TTAGGG telomere kit

Light cycler PLUS mix

Thermo Scientific, Rhein (Germany)

Sigma-Aldrich, Steinheim, (Germany)

Promega, Mannheim (Germany)

Qiagen, Hilden (Germany)

Qiagen, Hilden (Germany)

Qiagen, Hilden (Germany)

Sigma-Aldrich, Steinheim (Germany)

Roche Diagnostics, Mannheim (Germany)

Roche Diagnostics, Mannheim (Germany)

**2.7 Plasmids**IRAT SPORT6 *RB1* plasmid, Invitrogene, Darmstadt (Germany)

pCDH-EF1-T2A-GFP, courtesy of Dr Anastasov, Helmholtz Center Munich

Packaging system for virus production commercially available, Biocat, Heidelberg (Germany)

pSUPER, courtesy of Dr Anastasov, Helmholtz Center Munich

pFUGW, courtesy of Dr Anastasov, Helmholtz Center Munich

pF-sh*RB1*, courtesy of Dr Anastasov, Helmholtz Center Munich**2.8 Antibodies**

Antibody	Concentration	Secondary antibody
<b>Rb1 clone G3-245, from BD</b>	1:250 mouse	α- mouse from Calbiochem
<b>Epitope: DARLFLDHDKTLQ<sub>(641-653)</sub></b>	1:1000 human	
<b>pRb Ser 807/811 from cell signaling</b>	1:1000mouse	α- rabbit from Calbiochem
<b>SPLKS<sub>(807-811)</sub></b>	/human	



<b>3met H4 Lys20 from from millipore</b>	1:1000	$\alpha$ - rabbit from Calbiochem
<b>H1 clone AE-4 from millipore</b>	1:1000	$\alpha$ - mouse from Calbiochem
<b>H3 Lys9 courtesy of LMU Munich</b>	1:1000	$\alpha$ - mouse from Calbiochem
<b><math>\alpha</math> -Tubulin clone B-5-1-2 from Sigma</b>	1:60000	$\alpha$ - mouse from Calbiochem
<b>PML clone 36.1-104 from upstate</b>	1:1000	$\alpha$ - mouse from Calbiochem

## 2.9 Mice and Cell lines

Promoter *col-1a1* driven *cre* expressing mice from MMRRC, University of California

*R26R LacZ* reporter mice: courtesy of Dr Lickart, HMGU

*FLoxP-Rb1* mice from MMHC, NCI, USA

MC3T3 cells: CRL-2593™ available in our laboratory

HEK293T cells: CRL-11268™ courtesy of Dr Anastasov

RPE cells: CRL-2302™ Courtesy of Dr Mortl

MOS cells: Mouse osteosarcoma cell lines established in our laboratory.

## 2.10 Software

AxioVision 4.6	Carl Zeiss, Jena (Germany)
MS Office 2003	Microsoft, Unterschleißheim (Germany)
GraphPad	GraphPad software Inc, California (USA)
ImageQuant	GE healthcare, Freiburg (Germany)
Zeiss LSM	Carl Zeiss, Jena (Germany)
Chromas Lite	Open Access, Technelysium Ltd (Australia)
WinMDI software	Open access, Scripps Research Institute (USA)
FACS DIVA™	Becton and Dickinson, Heidelberg (Germany)
EMBOSS needle-Alignment	Open access, EMBL-EBI Hinxton (UK)
BLASTN 2.2.25	<a href="http://blast.ncbi.nlm.nih.gov/Blast.cgi">http://blast.ncbi.nlm.nih.gov/Blast.cgi</a>

## 2.11 Primers

- *Cre-col 1a1* PCR primers (727 bp)

<b>Cre1</b>	<b>(5'ACCAGCCAGCTATCAACTC 3')</b>
<b>Cre2</b>	<b>(5'TATACGCGTGCTAGCGAAGATCTCCATCTTCCAGCAG 3')</b>

- *Rb1* PCR primers (wild-type: 650 bp)

<b>Rb1-18</b>	<b>(5'GGCGTGTGCCATCAATG 3')</b>
<b>Rb1-212</b>	<b>(5'GAAAGGAAAGTCAGGGACATTGGG 3')</b>

- *R26R* primers (wildtype: 500bp)

<b>R26R forward:</b>	<b>5'AAAGTCGCTCTGAGTTGTTAT-3'</b>
<b>R26R reverse 1:</b>	<b>5'-GCGAAGAGTTTGTCTCAACC-3'</b>
<b>R26R reverse 2:</b>	<b>5'-GGAGCGGGAGAAATGGATATG-3'</b>

- *Cre* Real time PCR expression primers

<b>Cre-694f</b>	<b>5'-TCCATATTGGCAGAACGAAA-3'</b>
<b>Cre-804r</b>	<b>5'-CAGCTACACCAGAGACGGAA-3'</b>
<b>Cre-379f</b>	<b>5'-AACATTTGGGCCAGCTAAAC-3'</b>
<b>Cre-446r</b>	<b>5'-AGCATTGCTGTCACTTGGTC-3'</b>
<b>Cre-642f</b>	<b>5'-GCCAGGATCAGGGTTAAAGA-3'</b>
<b>Cre-713r</b>	<b>5'-TTTCGTTCTGCCAATATGGA-3'</b>

- *RB1* PCR cloning

<b>RB1-IRAT-f-long</b>	<b>5'GGATCCTTATTTTTGTAACGGGAGTCGGGAGAGGACG</b>
<b>RB1-IRAT-r1-long</b>	<b>5'GCGGCCGCGTGGCCATAAACAGAACCTGGGAAAG</b>

- *Rb1* sequencing primers (cDNA)

<b><i>RB1</i>-cDNAf1</b>	<b>5'-GGAAGATGATCTGGTGATTTC</b>
<b><i>RB1</i>-cDNAf2</b>	5'-CTGCAGCAGATATGTATCTTTC
<b><i>RB1</i>-cDNAf3</b>	5'-GTGCTGAAGGAAGCAACCCTC
<b><i>RB1</i>-cDNAr1</b>	5'-CTCCCAATACTCCATCCACAG
<b><i>RB1</i>-cDNAr2</b>	5'-GTATCGCTGTGATCCAATTTC

- *Suv4-20h1* expression in mouse cells

<b>mSUV4-20h1 forward</b>	<b>5'-AGAGTGGAACGAAATGACAAA -3'</b>
<b>mSUV4-20h1 reverse</b>	5'-GCATGTTCTCCTCAATTTTGA -3'

- LOH *Rb1* quantification primers

<b><i>Rb1-Ex19-f</i></b>	<b>5'-CACGTGTAAATTCTGCTGCAA-3'</b>
<b><i>Rb1-Ex19-r</i></b>	<b>5'-AGGGCAAGGGAGGTAGATTT-3'</b>
<b><i>Rb1-Ex17-f1</i></b>	<b>5'-TGAGCATCGAATCATGGAAT-3'</b>
<b><i>Rb1-Ex17-r1</i></b>	<b>5'-TGCTCGCTAACAGGTCACCTT-3'</b>
<b><i>Rb1-Ex19-f</i></b>	<b>5'-CACGTGTAAATTCTGCTGCAA-3'</b>
<b><i>Rb1-Ex19-r</i></b>	<b>5'-AGGGCAAGGGAGGTAGATTT-3'</b>

## 2.12 Restriction enzymes

<i>EcoR1</i>	Roche Diagnostics, Mannheim (Germany)
<i>BamHI</i>	Roche Diagnostics, Mannheim (Germany)
<i>NotI</i>	Roche Diagnostics, Mannheim (Germany)
<i>Bgl2</i>	Roche Diagnostics, Mannheim (Germany)
<i>HindIII</i>	Roche Diagnostics, Mannheim (Germany)
<i>PacI</i>	Roche Diagnostics, Mannheim (Germany)

## 2.13 Polymerases

Roche high fidelity Taq	Roche Diagnostics, Mannheim (Germany)
Phusion flash Taq	Thermo Scientific, Rhein (Germany)

Go Taq® hot start polymerase      Genecraft, Lüdinghausen (Germany)

#### 2.14 *RB1* oligos for sh*RB1*

5'-GCTTAAATCAGAAGAAGAA-3'

3'-GCTTAAATCAGAAGAAGAA-5'

Scrambled<sup>™</sup> siRNA

Dharmacon Research, Chicago, IL (USA)

5'-GCCGCUUUGUAGGAUAGAG-3'

#### 2.15 Taqman probes

Comercially available taqman probes from Applied biosystems for pan *Rb1* in exon 5, exon 19 to check expression of the wild-type allele, and designed primers for the junction between exón 18 and 20 for the mutated allele:

- Primers for junction between exon 18 and 20:

<b>Forward primer</b>	GCCTCTCCAGGGTAACCATACT
<b>Reverse primer</b>	TCCGACTAAATACACTCTGTGC
<b>Quencher</b>	CTAGACGGTACAATATCTG

#### 2.16 Blocking peptide for Rb1

Rb-G3-245-block

GenScript Corporation, NJ, USA

Sequence: DARLFDHDKTLQ

### III. METHODS

3.1 Transgenic mice: Purchased externally and mated as indicated at HMGU (Helmholtz Center Munich).

Three strains of transgenic mice were used in order to establish a model system to further study the consequences of germline mutations of *Rb1*. The characteristics of each purchased mouse strain are shown below.

#### 3.1.1 FVB; 129-Rb1<sup>tm2Brn</sup>

The mouse strain was obtained as an FVB background. Using somatic recombination in an ES-cell line, two *LoxP* sites flanking exon 19 of the endogenous *Rb1* gene were knocked into this strain permitting the deletion of this exon by conditional expression of the enzyme *Cre* recombinase (Marino et al 2000).

Location of rearrangement in *Rb1* gene in this strain is as shown below (Figure 13).

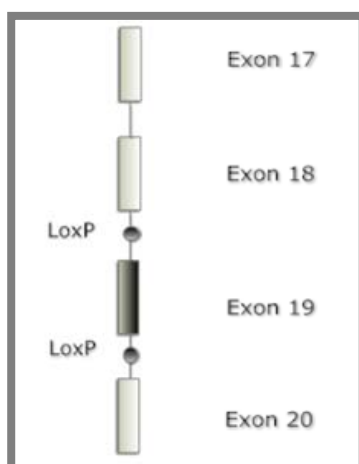


**Figure 13: Scheme of rearrangements in *Rb1* gene in FVB-*Rb1*-*LoxP***: Location of the *LoxP* sites in the introns between exon 18 and 19 as well as another one between exon 19 and exon 20 to enable the shedding of exon 19 by *Cre* recombinase.

#### 3.1.2 FVB-Tg (col 1a1-cre) 1Kry/Ucd

This mouse line is of pure FVB background and contains an inserted transgene of the phage *Cre*-recombinase gene, fused to a rat collagenase 1 $\alpha$ 1 promoter that allows expression of the *Cre* only in cells of the osteoblastic lineage.

This transgenic line was generated by injection of a linearized *Cre*-expression vector into oocyte pro-nuclei. The vector contained the *Cre*-cDNA under control of a 2.3 kb fragment of the endogenous alpha1(I) collagenase promoter (Dacquin et al 2002). Since genome integration is not targeted but random, neither the locus nor the copy number of the transgene is known.

### 3.1.3 Cre-LoxP system, and animal mating

Crossbreeding of our two transgenic mice FVB-*col-1a1-Cre-Tg* x FVB-*Rb1-LoxP* (Figure 14) led to progeny that are heterozygous for the *Rb1-LoxP* allele and that express Cre recombinase in osteoblast cells. The Cre recombinase expression is driven by a collagen 1a1 promoter which results in a heterozygous *Rb1* defect in all bone cells.

This conditional deletion allows the progeny to be born with normal *Rb1* expression in all tissue, but lead to an *Rb1* haploinsufficiency in the differentiated bone cells. We suspect that complete knockout might be lethal *in utero*. As shown in the diagram below, the crossbred between these animals allows us to delete an exon in the *Rb1*, generating animals with haploinsufficiency for this gene, since the rest of the coding sequence 3' of exon 19 is affected by frame-shift.

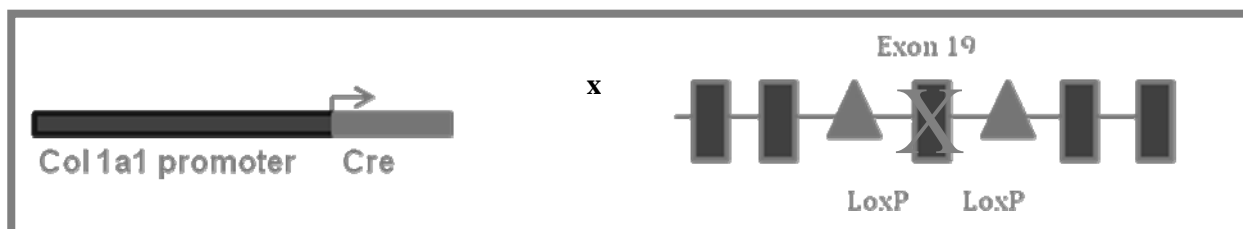


**Figure 14: Crossing of the two transgenic mice to generate progeny harvesting *Rb1* haploinsufficiency in bone.** The conditional expression of Cre driven by its collagen 1a1 (*col 1a1*) promoter, leads to conditional partial deletion of *Rb1* in bone cells of the progeny by deleting exon 19 leading to an out of frame sequence towards the 3' end of the transcript. The transcript is reduced to the first 18 exons only.

### 3.1.4 R26R-LacZ reporter mice

Mouse strains expressing the Cre recombinase facilitate conditional ablation of gene function when a critical region of the gene of interest is flanked by *LoxP* sites. If the expression of *Cre* can be rendered tissue specific then deletion can be restricted only to that tissue. *Cre* was engineered under a 2.3kb fragment of the collagenal promoter, known to be active during bone development.

*ROSA-R26R* mouse is a knock-in line (Soriano 1999) in which a conditional *lacZ* reporter construct was inserted into the *ROSA26* locus. Expression of the galactosidase-protein depends on the Cre-mediated removal of an intervening neo expression cassette flanked by *LoxP* sites. Only in those cells with sufficient *Cre* expression the *LoxP* sites will be targeted for somatic recombination, thus removing the neo cassette and allowing the *LacZ* to be expressed and the galactosidase activity detected by X-Gal staining in tissues or cells (Figure 15)

This mouse strain was used to monitor tissue specificity of *Cre* expression, in our case in bone cells.

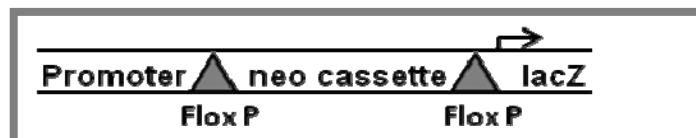


**Figure 15:** Shows the main features of the locus reporter gene of *R26R* mice. This locus carries a neo cassette flanked by *LoxP* sites between the *LacZ* reporter gene and its promoter. Such reporter gene is only active when cre recombinase removes the neo cassette via *LoxP* recognition and recombination.

### 3.2 Mice maintainance

Mice were maintained and treated according to the *German Tierschutzgesetz*. Groups of up to 4 male or female mice were kept in standard cages, performing their identification by ear clipping. Water and food were provided *ad libidum*. Mouse facilities are maintained at 22°C in 55% relative humidity and under 12 hour day/night rhythm.

### Molecular biology techniques

#### 3.3 DNA isolation for analysis

3.3.1 DNA for genotyping the animals for *Cre* and *Rb1* was extracted from mouse tail tips: 1 cm tail tip was cut off of the animals to be genotyped, and digested overnight at 55°C in lysis buffer; the following day, 250 µl of 6M NaCl was added, centrifuged at 1000 rpm (4°C) in a rotor centrifuge and DNA further precipitated from the supernatant by adding 100% ethanol. Later the DNA pellet was washed with 70% EtOH, dried and resuspend in distilled H<sub>2</sub>O.

3.3.2 DNA from cells: cells were collected using Trypsin as digestion agent washed in PBS and DNA was extracted as follows: Cells were collected in PBS, centrifuged for 5 minutes at 1200 rpm, and pellets resuspended in 500 µl of lysis buffer with proteinase k (lysis buffer, materials), the following day, 250 µl of 6M NaCl was added, centrifuged at 1000 rpm (4°C) in a rotor centrifuge and DNA further precipitated from the supernatant by adding 100% ethanol. Later the DNA pellet was washed with 70% EtOH, dried and resuspend in distilled H<sub>2</sub>O.

3.3.3 From paraffin sections: Tissue was scrapped from the slide using an scalpel, and immersed in Xylol for at least 4 hours (up to overnight) then remove xylol and add 100% EtOH, 85% EtOH and 50% EtOH washed. Once deparafinised, using the Qiagen DNA extraction kit and its buffers, tissue was lysed in 500 µl buffer ATL with proteinase K at 55°C overnight. The following day, 300 µl of 100% EtOH was added to the mixture and this was decanted in the Qiagen DNA extraction kit column and centrifuged for 1 minute at 800 rpm. Column was

subsequently washed with buffer AW1, centrifuged for 1 minute at 800 rpm and buffer AW2 was then added to the column, centrifuged and DNA was eluted with buffer AE (1:6).

3.3.4 From agarose gels, fragments were purified using QuiaQuick<sup>R</sup>, gel extraction kit under its standard protocol, in brief, dissolving the agarose plug by adding 3 volumes of buffer QG to 1 volume of gel, incubate for 10 minutes at 50°C to later add 1 volume of isopropanol. Apply mixture to the column, washed and eluted.

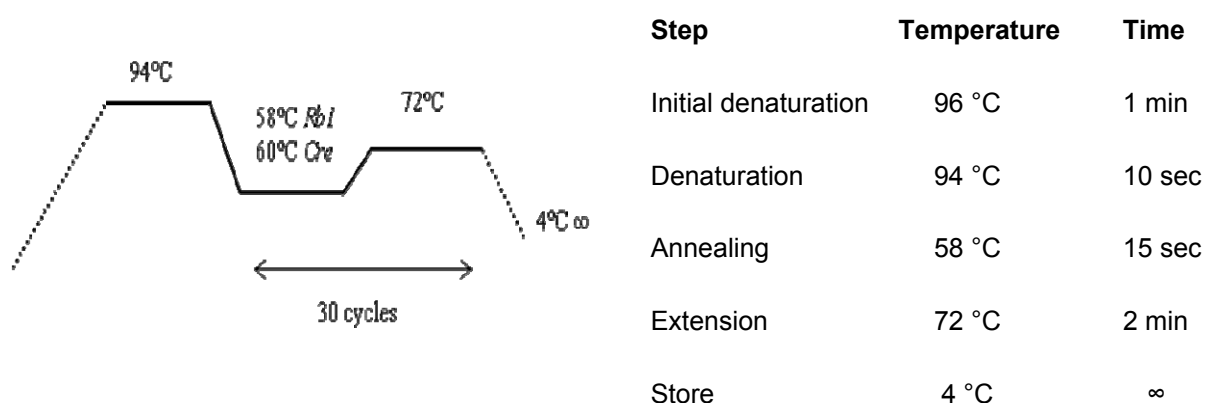
Concentrations of DNA and its purity were measured by UV-spectrophotometry at 260nm and 280 nm using the Tecan plate reader with a special NanoAmp plate called black flat for 16 samples (Tecan).

### 3.4 PCR based genotyping

As well established, PCR can be used for amplification of DNA fragments *in vitro* (Saiki et al 1988) using a double stranded DNA (dsDNA) as a template. Using tail tip DNA from F1-F3 mice, genotyping was performed using the following (standard for all PCR) reaction mixture:

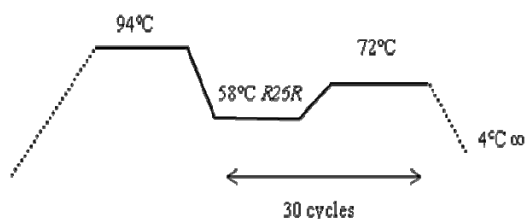
Master mix	17µl
Forward primer	1µl
Reverse primer	1µl
Template	1 µl
Taq Polymerase	0.2µl

***Rb1* and *Cre* genotyping:** Amplification was performed using the PCR primers described in the materials, using this protocol:



***R26R* reporter genotyping:** To screen for positivity of the *R26R*-allele, F1 *Cre-col-1a1* x *R26R*/+ mice were genotyped using a combination of three primers: *R26f*, *R26R1* and *R26R2*, described in materials using the following protocol:





Step	Temperature	Time
Initial denaturation	96 °C	1 min
Denaturation	94 °C	10 sec
Annealing	58 °C	15 sec
Extension	72 °C	2 min
Store	4 °C	∞

### 3.5 Agarose gel electrophoresis:

To detect and separate DNA fragments, electrophoresis in 1-3% agarose in TBE gels was used for PCR products as well as for RE digested plasmids. Electrophoresis was done at 90V in a 20cm long chamber for about 60 minutes. Ethidium bromide was used for detection. Sensitivity: visualization of at least 100 ng of DNA.

### 3.6 Isolation of primary osteoblasts and their culture

3.6.1 Explantation: *Rb1*<sup>+/+</sup> as well as *Rb1*<sup>+/ $\Delta$ 19</sup> mice (previously genotyped using tail tips) were sacrificed between the second and fourth week of life using a CO<sub>2</sub> chamber.

Long bones such as femour or humerous, as well as knees and elbows were dissected under sterile conditions and washed 2-3 times with PBS. Under a sterile work-bench, all adherent non-bone tissue was removed and the bone marrow aspirated by flushing the marrow channel with 1ml PBS. Cleaned bones were dissected into small pieces using a scalpel. These pieces of bone were placed into 6 well plates and fed with 1 ml DMEM supplemented with 10% FCS. Explants started growing osteoblasts in 4-6 days and after a week they were passaged for the first time following subsequent passaging.

3.6.2 Culture of osteoblast: DMEM Medium supplemented with 10% FCS was used to feed and maintain the osteoblasts *in vitro*. Cells were handled inside a sterile bench and incubated at 37 °C in an atmosphere of 6 % CO<sub>2</sub>.

When reached confluence of about 70%, the cells were washed in sterile PBS, incubated at room temperature with 0.5-1ml of trypsin no longer than 5 minutes, then 5 ml of media were added to the cell suspension to stop the action of trypsin. Cells were counted using a coulter counter and plated in 75 cm<sup>2</sup> flasks for subsequent passaging. Viability was checked sporadically using Vi-cell counter.

3.6.3 Freezing Osteoblasts: Cells were centrifuged and pellets resuspended in freezing media containing 10% DMSO. Vials were placed into cryo freezing chambers and left overnight at  $-80^{\circ}\text{C}$  to be later moved to liquid nitrogen for long time storage.

### 3.7 Alkaline Phosphatase staining

Alkaline phosphatase is known to be a good marker for early osteoblastic lineage differentiation (Arosarena et al 2011) and therefore this analysis was set to probe the lineage of our culture cells.

*Rb1*<sup>+/+</sup> and *Rb1*<sup>+/ $\Delta$ 19</sup> primary cells explanted from bone were grown under standard protocols until passage 5 to later carry on with the assay by supplementing the medium with 50  $\mu\text{g}/\text{ml}$  ascorbic acid and 8 mM  $\beta$ -glycerophosphate for 24 hours for differentiation.

As positive controls ROS17/2.8, a rat osteosarcoma cell line, were used and RPE (retinal pigment epithelium) cells as negative controls, both cell lines grown in supplemented differentiating medium as well.

Once differentiating medium was removed, cells were twice washed with PBS and fixed in Formalin-Calcium for about 20 minutes.

After washing once with PBS staining was performed by adding to the cells:

<b>300 ml Tris buffer 0. 1 M pH=8.3 using HCl (pH critical for staining)</b>
<b>30 mg naphthol AS-MX (dissolved in 3 ml dimethyl formaldehyde)</b>
<b>30 mg of fast blue salt dissolved in Tris buffer.</b>

Staining was performed overnight. The following morning, cells were rinsed with tap water and analysed with Axiovert microscope.

### 3.8 Cell cycle analysis

Cultured cells were harvested at different time points after irradiation, washed with PBS and spun down at 1000 rpm for 5 minutes to be then analysed by FACS using a well established protocol (Nusse et al 1994) which is suitable for micronuclei measurement as well as cell cycle distribution. It is a two step protocol including a treatment of cells with a salt solution (sol I, see materials), which contains a detergent in order to destroy the cell membrane and the cytoplasm releasing the nuclei in suspension. In a second step, a buffer containing citric

acid and sucrose (sol II, see materials) is added to stabilize the nuclei. Both solutions contain 0.025mg/ml Ethidium Bromide (EB) as a DNA specific fluorescent dye.

Flow cytometry analysis was performed using a Becton Dickinson LSR II. The instrument is equipped with two lasers (488nm, blue laser, and a 633nm, red laser). Excitation of the EtBr was provided by the 488nm beam, and the fluorescence was detected with a combination of filters. 50 000 cells were counted for each sample. Data recording was performed with a HP work station using FACSDiva, software (BD). This method distinguishes cells with different DNA content, since EtBr incorporation is quantitative and therefore discriminates between cells in different stages of their cell cycle.

### 3.9 Micronuclei assay

To assess the induction of unstable chromosome aberrations in the osteoblast cell lines 50.000 cells per slide of both *Rb1* wild-type and haploinsufficient cells were seeded, and irradiated with 2 and 4 Gy 24 hours after seeding using an X-ray source operating at 230 kVp and 20mA, with 1mm Al and 0.5mm Cu-filter (Isovolt 200).

To block the cells at the cytokinesis stage, cytochalasin B was added after radiation at a concentration of 0.5µg/ml for 18 hours. After incubation with the drug, and a short PBS wash, cells were fixed in ethanol, by soaking the slides in 80% ethanol for 15 to 20 minutes.

Nuclear staining was performed using DAPI (150 ng/ml). Slides were covered with DAPI solution for 5 minutes, washed in distilled H<sub>2</sub>O, and air dried. Once dry, slides were covered with Vecta Shield and a cover slip, for further microscope analysis.

Micronuclei were counted using the Axioplan2 fluorescence microscope. 200 binucleated cells were scored following the directions of the HUMN (Human micronuclei) project (Fenech et al 2003), which establishes the scoring criteria.

To obtain an objective scoring (Fenech et al 2003) cells with the following features were excluded from the analysis as artifacts: multinucleated cells, micronuclei on monucleated cells, cells with nucleoplasmic bridges or structures reassembling micronuclei.

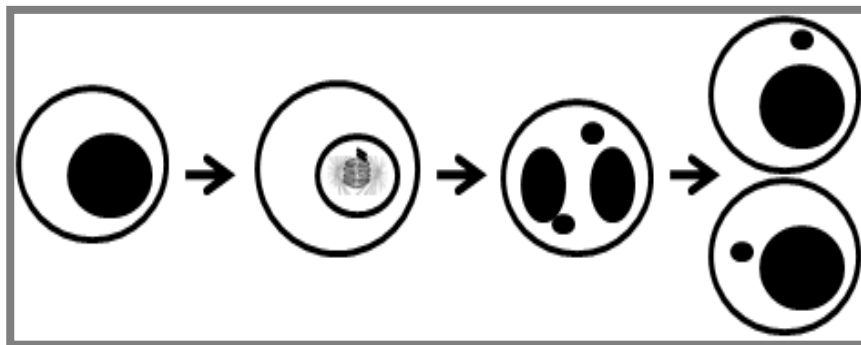


**Figure 16: Micronuclei formation:** arise from lagging acentric chromosome fragments in a dividing cell at anaphase following a chromosomal break. During the cytokinesis block (induced by cytochalasin-B, a microfilament assembly inhibitor) cells that have undergone one nuclear division and therefore, capable of exhibiting micronucleus, are identified by their binucleate appearance. Next to these binucleated cells, acentric fragments that will be independently segregated to the daughter cells can be found and quantified, as a measure of genomic instability (Fenech & Morley 1985, Fenech & Morley 1986).

### 3.10 Anaphase bridges assay

Both  $Rb1^{+/+}$  and  $Rb1^{+/Δ19}$  primary cells explanted from bone were seeded on slides at a density of 50.000 cells per slide in quadruplets irradiated 24 hours after seeding with an X-ray source (Isovolt 200) both at 2 and 4 Gy. Cells grew further for another 48 hours to allow at least 4 cell divisions. Subsequently fixation was performed in 80% MeOH for 15 minutes; afterwards slides were stained with Hoechst 33342 for 5 minutes, washed with PBS twice and cover slip mounted with one drop of Vectashield.

When an anaphase plate harboured more than one bridge (as in figure 36 upper right) they were counted as 1 defected cell.

### 3.11 Protein analysis

3.11.1 Protein collection: Cells were washed and extracted in 1ml PBS using a cell scrapper. After centrifugation at 1500 for 5 minutes, cell pellets were resuspended in RIPA extraction buffer (see table below). The volume of buffer used varied depending on cell amount, between 20  $\mu$ l and 200  $\mu$ l

<b>1ml RIPA buffer</b>
<b>1 tablet of complete mini (protease inhibitor)</b>
<b>10<math>\mu</math>l of cocktail 1      phosphatase inhibitors</b>
<b>10<math>\mu</math>l of cocktail 2      phosphatase inhibitors</b>

Cell lysate was then vortexed and left on ice for 20 minutes and sonicated for 10 seconds before measuring.

3.11.2 Protein measurements: Calculation of protein concentrations were performed using the well established BCA kit for protein quantification, in brief; first a standard curve was prepared using BSA at the concentrations shown below:

<b>BSA(1 mg/ ml) in <math>\mu</math>l</b>	<b>0</b>	<b>5</b>	<b>10</b>	<b>20</b>	<b>40</b>	<b>60</b>	<b>80</b>
<b>Extraction buffer in <math>\mu</math>l</b>	10	10	10	10	10	10	10
<b>H<sub>2</sub>O</b>	90	85	80	75	70	65	60

Samples:

<b>10 <math>\mu</math>l of cell lysate</b>
<b>90 <math>\mu</math>l of H<sub>2</sub>O</b>

After that in all the samples to be quantified, 2 ml of colorimetric reaction buffer provide by the kit was added. Samples were incubated at 60°C for 15 minutes and subsequently 200  $\mu$ l were transferred in quadruplets in a 96 well plate to be measured for absorption at 570 nm using a Tecan plate reader.

3.11.3 Western blot analysis: 30µg of protein samples plus one sample containing protein length marker were mixed with 2x Laemmli buffer (see materials), denaturized at 95 °C for 5 minutes and loaded on a 8-12% SDS polyacrylamide gels (PAGE), run for 1 to 2 hours at 120V with crushed-ice cooling.

Transfer was made using tank blotting system from biorad with 20 % MeOH transfer buffer for 2 hours at 100V. Membranes were then stained with PonceauS staining for 2 minutes to visualize the proteins transferred.

Blocking was performed at 37°C in 5% skimmed milk for 1 hour followed by immunoblotting using different antibodies (see table below) at 4°C overnight (primary AB), or 1 hour at 37°C (secondary AB) see page 36.

Unbound antibodies were removed by washing 3 times for 5 minutes with T-TBS. Secondary antibody against the IgG isotype of the primary AB were added to the membranes for 1 hour at room temperature, followed by 3 times washing for 5 minutes with T-TBS.

Blocking of the membrane, exposure to the AB and washing were all done on a rocking table at about 20/min.

After last washing step, 5 ml of GE Chemiluminescence substrate reagents mixed 1:1 were added to the blots for 5 minutes and the resulting chemiluminescence signal recorded using a FluorChemHD2 camera system from or a classical X-ray film.

#### 3.11.4 Histone extraction protocol (Acidic extraction)

In order to study epigenetics in the histones of the telomeres, a different protein extraction protocol was required in order to liberate the histone proteins from the surrounding DNA for further analysis.

For this propose, cells were harvested, washed twice with ice-cold PBS and resuspended in: Triton Extraction Buffer: PBS containing 0.5% Triton X 100 (v/v), protease and phosphatase inhibitors.

Cells were lysed on ice for 10 minutes with gentle stirring to then be centrifuged at 2000 rpm for 10 minutes at 4°C. Supernatant was discarded and pellets were resuspended in 0.2N HCl, which causes acidic degradation of the DNA and hence release of the histone proteins after overnight incubation at 4°C. Next morning, samples were centrifuged at 2000 rpm for 10 minutes at 4°C.

Supernatant was collected and its protein content determined using the BCA kit (Pierce).

Store samples at -20°C for further western blot analysis following standard protocols, but taking into account the usage of H1 as loading control.

### 3.12 LacZ Histochemistry

3.12.1 Bone frozen sections: *R26RxCre* reporter mice were sacrificed at 2 weeks of age. We dissected femur as example of enchondral ossificated bones, and calvaria, as an example of bone with intramembraneous ossification. The bones were snap frozen at -20°C until further handling the same day. Sections were cut using 2800 Frigocut (microtome).

3.12.2 Sectioning: The bones were embedded in tissue Tek to keep the tissues in place on the specimen holder for kryo- sectioning.

Sections were placed on microscope cover slips and kept frozen until staining, that was performed within the first hours after sectioning.

3.12.3 *LacZ* staining: The sections were fixed in cold formalin for 10 minutes, then washed in PBS and rinsed in distilled water. The slides were incubated in X-gal working solution (see materials) for 24h. For preventing the slides from drying, they were placed on a humid chamber and incubated for 24 hours at 37°C. The following day, the slides were rinsed twice for 5 minutes in PBS and briefly in distilled water. Sections were counterstained with nuclear fast red for another 5 minutes and covered with a resin and cover slips. The slides were checked for positive stain on an Axioplan2 microscope.

### 3.13 RT-(q)PCR

3.13.1 RNA was extracted from tissue or cultured cells using RNeasy extraction kit from Qiagen under standard protocols.

In brief, cells were collected in PBS (using a cell scrapper) centrifuge 5 minutes at 1200 rpm, and resuspend the pellet in 350 µl of RTL buffer with 35 µl of β-mercapto-ethanol. Incubate the mixture on ice for 3 minutes and centrifuge at 4°C at 12000 rpm. Supernatant was collected and add 350 µl of 70% EtOH and add it to the column. RNA was bound to the column membrane by spinning down for 15 seconds at 12000 rpm. 600 µl of buffer RW1 were then added to the column and centrifuge for 15 seconds at 12000 rpm. Wash the membrane with 600 µl of buffer RPE1 and centrifuge for 2 minutes at 12000 rpm. Elution was performed in 30 µl of RNase free H<sub>2</sub>O. Measurements of RNA concentration were performed by A260/A280 UV spectrophotometry using the Tecan plate reader.

3.13.2 Reverse transcription: was performed in 20  $\mu$ l total volume as follows:

<b>1 <math>\mu</math>g of RNA in a total volume of 8 <math>\mu</math>l</b>
<b>+ 1.5 <math>\mu</math>l Oligo dT</b>
<b>+ 1.5 <math>\mu</math>l of random primers</b>

Mixture incubated for 2 minutes at 70°C followed by 10 minutes at room temperature.

Subsequent addition of:

<b>+ 4 <math>\mu</math>l F-S buffer</b>
<b>+ 2 <math>\mu</math>l DTT</b>
<b>+ 1 <math>\mu</math>l RNase OUT</b>
<b>+ 1 <math>\mu</math>l Superscript II</b>

Further incubation for 1 hour at 42°C was performed, followed by 5 minutes at 95°C for RNA denaturation.

### 3.13.3 cDNA quantitative PCR

Using Taqman probes consisting of primer + quencher for desired genes, which are designed by Applied biosystems based on Taq Polymerase 5'–3' endonuclease activity. During the process of hybridization, the enzyme cleaves a dual-labeled probe to the complementary target sequence for a fluorophore-based detection. The qRT-PCR probe, which is labeled with two fluorescent dyes, is created within the amplicon defined by a gene-specific PCR primer pair. The 5' end is labeled with a reporter dye (usually 6-carboxy-fluorescein, FAM). 3' end is labeled with a second fluorescent dye (6-carboxy-tetramethyl-rhodamine, TAMRA). As long as the probe is intact, the emission of the reporter dye is quenched by the second fluorescence dye. With the beginning of the extension phase of PCR, the polymerase enzyme starts to cleave the TaqMan probe, which results in a release



of reporter dye. An automated sequence detector, equipped with specific software, is used to monitor the increasing amount of reporter fluorescent dye.

cDNA from RT was previously diluted 1:6 and reverse transcription was performed in 20  $\mu$ l total volume as follows:

<b>10 <math>\mu</math>l 2x master mix (applied biosystems)</b>
<b>1 <math>\mu</math>l 20x assay on demand</b>
<b>5 <math>\mu</math>l H<sub>2</sub>O</b>
<b>4 <math>\mu</math>l cDNA</b>

Samples were placed in 96 well plates always in doublets. As internal controls we used either microsatellites such as D14 mit 192 (for genomic DNA copy numbers) or expression of a housekeeping gene such as TBP (for cDNA expression analysis).

	<b>Step</b>	<b>Temperature</b>	<b>Time</b>
	Initial denaturation	95 °C	10 min
	Denaturation	94 °C	10 sec
	Annealing	60 °C	45 sec
	Extension	72 °C	1min
	Store	4 °C	$\infty$

This system quantifies PCR reaction products during each cycle by calculating the cycle threshold (Ct) value for each sample. Relative quantification was performed using the pre-recorded standard curve. The relative expression level in each sample was calculated using the comparative cycle threshold (Ct) method  $\Delta\Delta$ Ct compared to a reference cDNA that was produced from a pool of whole embryonic RNA.

### 3.14 Real time PCR

The light cycler from Roche was used for determination of genomic copy numbers of *Rb1*, *SUV4* and *Cre* expression following standard protocols by using Sybr green master mix. The Sybr green intercalates among the strands of the DNA in a quantitative manner, allowing us to quantify the copie numbers of our gene of interest. (See primers used in matherials)

<b>5 µl H<sub>2</sub>O</b>
<b>0.5 µl forward primer (5pmol/ µl)</b>
<b>0.5 µl reverse primer (5 pmol/ µl)</b>
<b>1 µl Roche light cycler mix with MgCl<sub>2</sub></b>
<b>1 µl DNA</b>

Both, crossing points (Cp) for quantification, as well as melting curves were analysed. As internal controls for quality standards we used: D13mit 262 (cDNA) and TBP (DNA).

For LOH studies, we used the melting peaks to determine the specificity of the primers and that they were only a single peak and that, in both, normal tissue and tumours arise at the same temperature, detecting the loss of the allele in some tumours when only a peak appeared at the primer dimer temperature suggesting no template for primer binding and therefore loss of the allele (see chapter 3).

### 3.15 Telomeric repeats fragments (TRFs) determination

The quantification of telomeric length in *Rb1<sup>+/+</sup>* and *Rb1<sup>+Δ19</sup>* was done following the protocol of the manufacturer (Roche diagnostics, Germany). In brief, DNA was isolated from bones or cell cultures as described before (see DNA isolation) and precipitated in 100% EtOH.

Digestion of 1µg of DNA was performed with *HinfI* and *RsaI* for 3 hours at 37°C followed by gel electrophoresis in 0, 8% agarose gel for about 6 hours at room temperature.

Southern blotting was performed after HCl treatment under standard protocols. DNA was cross-linked to the membrane using a UV chamber for 60 seconds.

Hybridization with a DIG-labelled telomeric probe provided by the manufacturer was performed for 1 hour at 42°C. Detection was done using a anti-DIG FaB fragment conjugated to HR-peroxydase. After washing the blot, the 1ml CSPD substrate (from the kit) was added and the resulting chemiluminescence detected by using the electronic FluorChemHD2 system.

### 3.16 Immunofluorescence

3.16.1 Cell collection: 50.000 cells were seeded on slides and incubated for 24 hours. Medium was discarded and cells washed with PBS to be fixed in 100% methanol for 15 minutes at room temperature. Following, cells were washed PBS with 0.15% Triton 3 times for 5 minutes.

3.16.2 Blocking and antibody reaction: Performed in 100ml PBS + 1g BSA + 0.15g Glycine for 1h at 37°C.

Primary antibody: In PBS + 2% BSA + 0.01% Tween 20 12h at 4°C (see table below for antibody concentration)

Antibody	Concentration	Secondary antibody
Rb1 clone G3-245, from BD	1:250	$\alpha$ - mouse from Calbiochem
3met H4 Lys20 from from Millipore	1:500	$\alpha$ - rabbit from Calbiochem
PML clone 36.1-104 from Upstate	1:500	$\alpha$ - mouse from Calbiochem
pRb Ser 807/811 from cell signaling (binds down stream of sequence coded by exon 19)	1:1000	$\alpha$ - rabbit from Calbiochem

The following day, slides were washed in PBS for 5 minutes in PBS + 0.15% Triton for 10 minutes and rinsed again in PBS for another 5 minutes.

Secondary antibody: PBS+ 2% BSA + 0.01% Tween 20 for 1 hour at room temperature using Alexa 488 anti mouse or anti rabbit at 1:500.

After the secondary antibody treatment, slides were washed in PBS with 0.15% Triton 2x5 minutes followed by nuclear counter-staining with Hoechst33342 or DAPI by adding 2  $\mu$ l (1mg/ml) in 20 ml for 2-3 minutes, to later rinse with PBS. Air dry slides and mount them with Vectashied. Pictures were taken using a Laser Scanning Microscope (LSM) provided by Zeiss. Pictures taking in about 8-10 stags/per picture (Cy3 was detected at 594nm; DAPI was detected at 450 nm). Image processing of the stained cells was carried out with Zeiss Axiovision computer software.

Immunofluorescence using blocking peptide: The protocol for staining was performed as a normal immunofluorescence (see above) but incubating the primary antibody with the blocking peptide 10 times in exceed for 15 minutes prior to applying the antibody solution to the slide.

### 3.16.3 Dil labeling for immunofluorescence:

Dil is a lipophilic dye used for tracing cells, *in-vivo* and *in vitro*. In our case., we used it as a tracer of a cell population in a population pool. We labeled one of the genotypes of *Rb1* (e.g. wt) and then mixed with the other population (ex. haploinsufficient) to see the pool of cells on the same slide, and performed the immunofluorescence together (for better control of fluorescence differences. 500.000 cells were collected and washed in PBS. Pellets were resuspended in 500  $\mu$ l of PBS containing 8  $\mu$ l of Dil stock solution. Cells were incubated in Dil solution for 15 minutes at 37°C. Cells were then centrifuged at 1500 rpm for 5 minutes and supernatant was discarded. Pellets were washed 3 times with PBS. Subsequently, cells labeled with Dil (of one population) were mixed with those unlabelled (other population) and seeded on slides for further immunofluorescence. Fixation was performed 24h after seeding.

### 3.17 Senescence-associated $\beta$ -galactosidase assay

The senescence-associated  $\beta$ -galactosidase ( $\beta$ -Gal) assay was performed using a  $\beta$ -gal staining kit according to the manufacturer's instructions. 24h after irradiation, cells were fixed in 1 $\times$ Fixative Solution for 10 min and washed in PBS twice. Cells were then stained in Staining solution at pH 6.0 for 14 h and the reaction, then plates were washed with tap water and check with the Axiovert microscope.

### 3.18 FISH with PNA probe on cultures seeded on slides

Cells were seeded on slides and metaphase spreads were prepared for collection Using colcemid block and hypotonic treatment with Na.citrate 0.01M at 37 degrees. 24 hours after seeding and wash slides with PBS for 5 minutes.

Fixation was performed for 2 minutes with 4% formaldehyde in PBS and washed using the same buffer 3 times followed by pepsin treatment: 1mg/ml in 0.1M HCl for 10 minutes at 37 °C and pH 2.0.

After rinsing with PBS, fixation was repeated with 4% formaldehyde in PBS for 2 minutes, followed by rinsing in PBS 3 times for 5 minutes.

Dehydration of the slides was performed with cold ethanol following the series: 70%, 85%, 100% EtOH, to later leave the slides to air dry.

10  $\mu$ l of Hybridization mixture containing (see table below)

<b>10mM Tris in HCl pH 7.2</b>
<b>70% formamide</b>
<b>0.3 <math>\mu</math>g/ml PNA probe</b>
<b>0.1% BSA</b>

Once the hybridization mixture was added, slides were covered with parafilm and a DNA denaturation step was performed at 80 °C for 5 minutes. Hybridization was performed at room temperature for 2 hours.

Subsequently, slides were washed 3 times for 5 minutes with:

<b>10mM Tris pH7.6</b>
<b>70% formamide</b>
<b>0.15M NaCl pH 7.5</b>
<b>0.05% Tween-20</b>

Followed by a PBS wash slides were stained using either PI or DAPI depending on the colour of the PNA probe used. Slides were then air dried and covered with 5-10  $\mu$ l of Vectashield antifade solution. Pictures were taken using a Laser Scanning Microscope (LSM) provided by Zeiss. Image processing of the stained cells was carried out with Zeiss Axiovision computer software.

### 3.19 Telomere length measurement by flow-cytometry

Using this technique we could determine the average telomere length of the entire cell population. About 500.000 cells were washed with PBS and centrifuged for 5 min at 1500 rpm. After discarding the supernatant, cell pellet was resuspended in 500µl of hybridization mixture containing:

<b>20mM Tris buffer, pH 7.1</b>
<b>70% formamide</b>
<b>0.3 µg/ml PNA probe (FitC )</b>
<b>1% BSA</b>

Denaturize DNA for 10 minutes at 80°C and leave to hybridise for 2 hours in the dark at room temperature (Use samples without PNA as a negative control). Cells were spun down for 5 min at 3000 rpms at room temperature. Subsequently cells were washed twice in wash solution containing:

<b>10mM Tris Buffer in HCl, pH 7</b>
<b>70% formamide</b>
<b>0.1% Tween 20</b>
<b>0.1% BSA</b>

Later cells were centrifuged for 5 minutes at 3000rpms at room temperature. Pellets were washed twice with PBS, 0.1% BSA and 0.1% tween-20. Subsequen centrifugation was performed for 5 minutes 2000rpms at room temperature.

Pellets were resuspended and further incubated in:

<b>500 µl PBS</b>
<b>10µg/ml RNase A</b>
<b>0.1µg/ml propidium iodide</b>

Incubation was performed for 1-2 h at 4 °C in darkness. Cells were then stored at 4°C until further analysis by flow cytometry. Telomeric length was determined by PNA fluorescence

intensity was detected using cytofluorimetric analysis (530nm filter whilst PI was detected with 630nm filter) using the BD FACSCalibur™ flow and analyzed with BD DIVA™ software (figure 17).

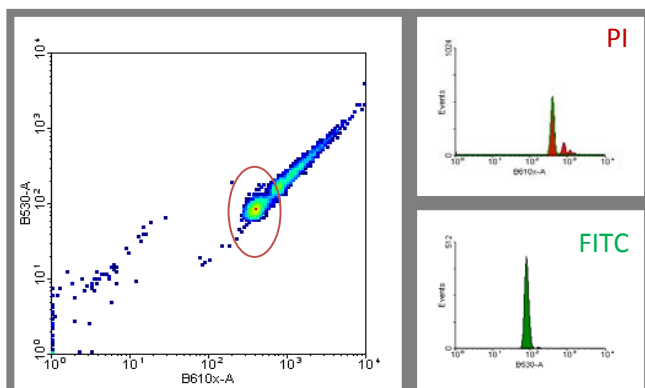


**Figure 17: Flow-FISH analysis.** Using the arbitrary units of fluorescence (AUF) as the length determinators. G1 population was gated using PI at 610nm (red circle), and AUFs were measured in the green channel (530nm) for the gated population.

### 3.20 Irradiation protocol

Irradiation was performed either using a X-ray source (Isovolt 200 operating at 200kVp and 20mA with 1mm Al and 0.5mm Cu filter) or a  $^{137}\text{Cs}$  source with a dose rate of 0,68 Gy/ min (HWM 2000). Doses used in this thesis ranged between 0.5 Gy and 4 Gy.

Cells were seeded into 25cm<sup>2</sup> flasks or glass slides for immunocytochemistry 24 hours before irradiation at 37degrees using preheated thermopacks. Irradiation was performed under current regulations and standards.

## Work with Lentivirus

### 3.21 RNA interference

Lentivirus: Viruses of the Retroviridae family, characterized by a long incubation period. Lentivirus deliver a significant amount of genetic information into the host cell's DNA and have the unique ability among retroviruses of being able to replicate in non-dividing cells, so they are one of the most efficient methods of a gene delivery vector. The one we used was a modified HIV virus.

Infectious viruses have 3 main genes coding for the viral proteins in the order: 5'-gag-pol-env-3'. There are additional genes depending on the virus (e.g., for HIV-1: vif, vpr, vpu, tat, rev, nef) whose products are involved in regulation of synthesis and processing viral RNA and other replicative functions. The Long terminal repeats (LTR) are about 600nt long, of which the U3 region is 450, the R sequence 100 and the U5 region some 70 nt long. Viral

proteins involved in early stages of replication include Reverse Transcriptase and Integrase. Design of shRNA constructs and cloning into pSuper vector (Anastasov et al 2009).

Specific shRNAs were designed by using bioinformatics tools publicly available from Invitrogen. We designed the sequence shown in materials targeting human *RB1* and tested it in mouse cells later. As a negative control, “scrambled” siRNA (Dharmacon Research, Chicago, IL, USA), with the sense sequence 5'-GCCGCUUUGUAGGAUAGAG-3' which lacks complementarity to any expressed human sequence was used.

Oligonucleotides were cloned into pSuper vector as described (Brummelkamp et al 2002). In brief, double-stranded DNA encoding siRNA oligonucleotides for *RB1* were synthesized (see below). The specific sequence contained a sense strand of 19 nucleotides followed by a short spacer (TTCAAGAGA) and the reverse complement of the sense strand. 5 thymidines were added at the end of synthesized oligonucleotide as RNA polymerase III transcriptional stop signal. Each pair of oligos was annealed at 20  $\mu$ M in annealing buffer (100 mM potassium acetate, 30 mM HEPES-KOH (pH 7.4), 2 mM magnesium acetate) for 4 min at 95°C, followed by incubation at 70°C for 10 min and slow cooling to room temperature. 40 picomolar of annealed oligos were phosphorylated by T4 polynucleotide kinase before they were ligated into pSuper vector digested by *Bgl*II and *Hind*III. All constructs were checked by *Eco*RI-*Hind*III digestion and by GAC sequencing.

- ***Rb1* Fw (sense-antisense) for pSuper**

GATCCCC GCTTAAATCAGAAGAAGAA tcaagaga TTCTTCTTCTGATTTAAGC  
TTTTTGGAAAGATCCCCGCTTAAATCAGAAGAAGAAAttcaagagaTTCTTCTTCTGATTTAAG  
CTTTTTGGAAA

- ***Rb1* Rev (sense-antisense) for pSuper**

AGCTTTTCCAAAAA GCTTAAATCAGAAGAAGAA tctcttgaa TTCTTCTTCTGATTTAAGC  
GGGAGCTTTTCCAAAAAGCTTAAATCAGAAGAAGAAAtctcttgaaTTCTTCTTCTGATTTAAGC  
GGG

#### Virus production and concentration

We used the pFUGW as transfer vector, the corresponding packaging plasmid, and the G-protein of vesicular stomatitis virus envelope plasmid were a kind gift of Dr. Baltimore (Lois et al 2002). The pFUGW lentiviral vector allows the expression of EGFP reporter gene driven by an internal ubiquitin-C promoter (Figure 18).



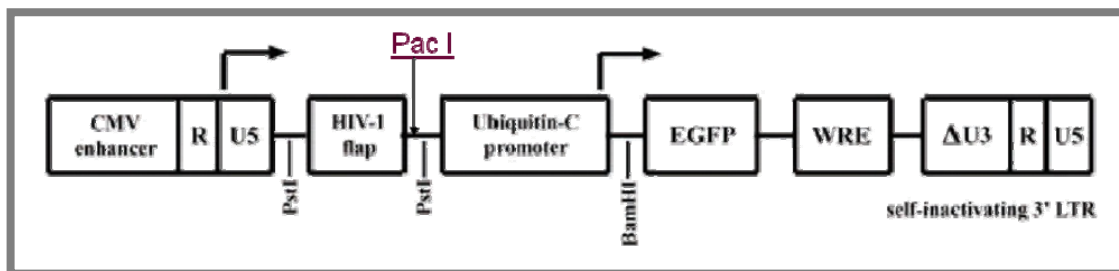


**Figure 18: FUGW lentiviral vector.** Map with main restriction site for *Pac I* (Lois et al 2002).

To insert a specific shRNA into the lentiviral vector, shRNA together with human H1 promoter from pSuper constructs was digested with *SmaI* and *HincII* and ligated into pFUGW digested with *PacI*, that had been blunt ended using T4 DNA polymerase. The orientations of the fragments were confirmed by *ClaI* and *EcoRI* digestion.

Replication-defective lentiviral virions were produced by transient co-transfection of:

7.5 µg pCMVdeltaR8.9
5 µg pHCMV-G
10 µg of the pFUGW

into HEK 293T cells using Lipofectamine 2000 transfection system.

250µl total volume of Opti-MEM medium containing 1000-3000ng of plasmid DNA were mixed with 250µl of opti-MEM medium containing 10µl of lipofectamine stock solution. Mixture was incubated at room temperature for 15 minutes (vesicle formation) and then 500µl were dropped on top of the cells to be transformed (growing in 5 ml of medium) /plate containing  $6 \times 10^6$  cells.

The media was changed 12 h after transfection and supernatant containing the virus was harvested 48 h after transfection, cleared of debris by low-speed centrifugation, and filtered through 0.45-µm Stericup filters. Yields were typically 80 to 120 ml from a ten to 15 10-cm dishes. The lentivirus was concentrated by ultrafiltration using Amicon-20 100-kDa-molecular-weight cut-off columns in accordance to the manufacturer's guidelines. The virus was subsequently aliquoted (100 µl) and supernatants were stored at  $-80^{\circ}\text{C}$ . Virus titers (multiplicity of infection—MOI) were determined by fluorescence-activated cell sorting (FACS) analysis of a known number of 293 T cells infected with serially diluted viral supernatant and GFP expression analysis.

### 3.22 Viral infections

500,000 primary *Rb1*<sup>+/+</sup> and *Rb1*<sup>+/ $\Delta$ 19</sup> osteoblasts were seeded in 6 well plates in 2 ml complete medium for 24 hours prior to infection. The following day, lentivirus-containing media (Opti-MEM, without FCS) with polybrene (8  $\mu$ g/ml) was decanted on top of the cells in the six well plates. Plates were centrifuged at 1,000 g for 90 min. After centrifugation, cells were incubated at 37°C in a CO<sub>2</sub> incubator for indicated time points to later collect RNA and protein for analysis as well as later passages for Flow-FISH telomere length determination.

### 3.23 Cytofluorimetric analysis (FACS) of infected cells

Three days after infection, cells were washed in phosphate-buffered saline (PBS) and resuspended in FACS buffer (PBS with 5% FCS and 1  $\mu$ g/ml of propidium iodide (PI)). PI was used to determine cell viability of infected cells and uninfected control. Gene transduction efficiency was determined by cytofluorimetric analysis using the BD FACSCalibur™ flow and analyzed with BD DIVA™ software. Infected cells were detected on the basis of GFP fluorescence relative to uninfected control.

### 3.24 Transient transfection

Asynchronously growing cells were transiently transfected with the different constructs when 70-80% confluent using Lipofectamine.

500ng-1 $\mu$ g of DNA diluted in 250  $\mu$ l of Opti-MEM was thoroughly mixed with 10  $\mu$ l transfection reagent Lipofectamine diluted in 250  $\mu$ l of Opti-MEM. The components incubated for 15 minutes at room temperature, to ensure interaction between carrier molecules of the transfection reagent and DNA molecules. After incubation, 500 $\mu$ l of transfection mix was added to each well with 5ml of medium and the plates carefully swirled to ensure even distribution. Cells were collected and lysed 24-120h later in protein lysis buffer.

### 3.25 RB1 cloning strategy for phenotype rescue

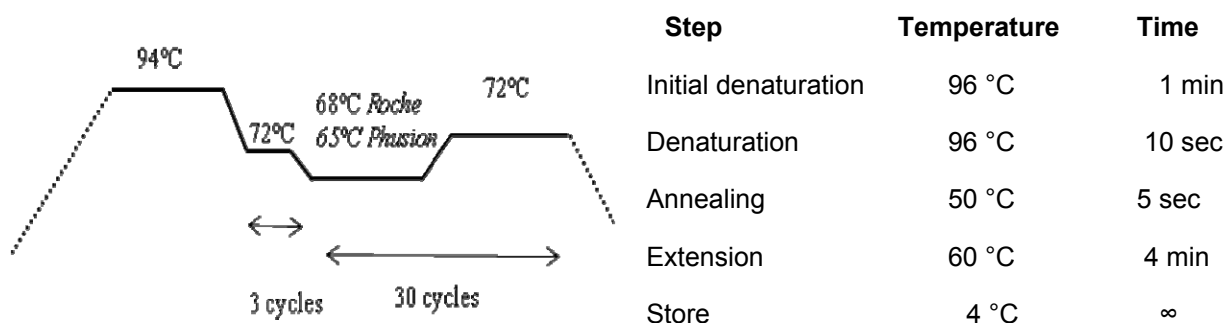
#### 3.25.1 Cloning strategy

The *RB1* fragment was extracted from pSPORT vector (see materials) by first linearising the plasmid with *XhoI* and then performing PCR amplification using the primers:

<b><i>RB1-IRAT-f1-long</i></b>	<b>5'NNNNGGATCCTTATTTTTGTAACGGGAGTCGGGAGAGGACG</b>
<b><i>RB1-IRAT-r1-long</i></b>	<b>5'NNGCGGCCGCGTGGCCATAAACAGAACCTGGGAAAG</b>

Those primers were designed to bind flanking the *RB1* coding sequence and adding a tail carrying the recognition sequence for *Bam*HI (forward) and *Not*I (reverse).

PCR was performed with *Rb1* protocol (see above). Such amplification protocol, lead to a small deletion in a histidine row coding sequence, which lead us to try different enzymes and protocols being the next one (see below) with either Roche high fidelity Taq enzyme as well as phusion flash Taq (Thermo scientific) those that remove the deletion from the insert (see 3.24.5 for sequences). Higher annealing temperature for the first cycles was crucial for the deletion removal.



Enzymatic digestion of the PCR product (following PCR purification using Qiagen Kit under standard protocol) and lentiviral vector (pCDH-EF1-MCS-T2A-copGFP) with *Bam*HI and *Not*I for 3 hours at 37°C was performed, following this protocol:

<b>1µg in 10µl of DNA</b>
<b>2 µl of <i>Bam</i>HI</b>
<b>4 µl of <i>Not</i>I</b>
<b>4 µl of <i>Bam</i>HI buffer</b>
<b>20 µl of H<sub>2</sub>O</b>

This was followed by gel purification and ligation using ligase IV.

<b>6.5µl of insert</b>
<b>1µg in 1.5 µl of vector</b>
<b>2 µl of dilution buffer</b>
<b>10 µl of ligation buffer</b>
<b>1 µl of ligase IV</b>

### 3.25.2 Transformation of competent *E. coli*:

Competent cells were thawed from -80°C and kept at 4°C, 10 µl of ligation mixture was added on top of the competent cells.

Incubation on ice for 5 minutes followed by 1 minute at 42°C and another 5 minutes of incubation on ice. Vial was then placed at 37°C with SOC medium for 1 hour and then seeded onto ampicillin LB agar plates and incubated overnight at 37°C.

Single colonies were picked (and streaked out on fresh plates or used to start 7ml miniprep liquid cultures.

Mini or Midi-prep kits (see materials) were used for DNA purification from colonies according to protocol recommended by manufacturer.

### 3.25.3 PCR and enzymatic screening

Using the primers: *RB1*-cDNAf1 and *RB1*-cDNAr2 primers we performed PCR screening for up to 50 colonies picked with a tooth pick from the plates, samples boiled for 5 minutes at 80°C (in 250 µl water) and 2 µl used as PCR template and place in PCR reaction tube for analysis, following standard *Rb1* protocol shown before.

Of those colonies with a positive signal on the gel, restriction pattern was analysed with *EcoR1*, *BamHI* and *NotI*. From all the positive clones, we chose 2, one per enzyme (Roche or Phusion) to validate the insert using sequencing.

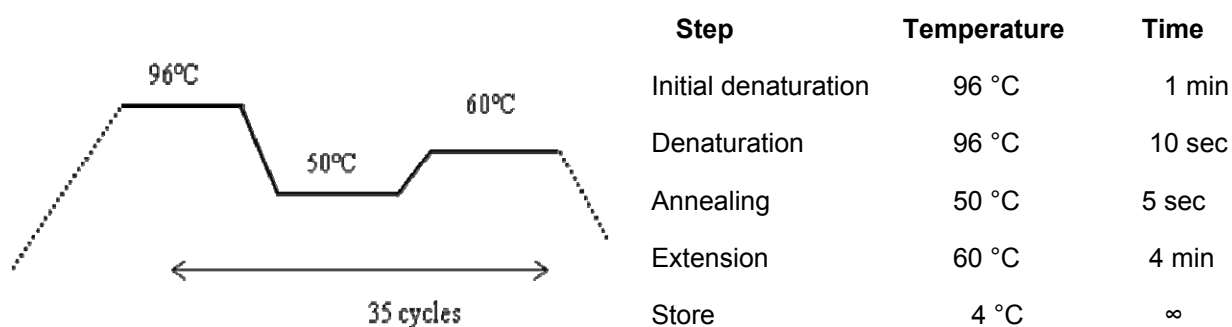
### 3.25.4 Sequencing

Using Dye terminator: by adding to the sequencing mixture ddNTPs, each chain reaction terminates when adding dideoxynucleotides (ddATP, ddGTP, ddCTP, or ddTTP). They lack the 3'-OH group that is required for the formation of a phosphodiester bond between two nucleotides and thus DNA strand extension terminates. This results in a number of DNA

fragments of diverse lengths. In our experiments, we used 'BigDye Terminator v3.1 Cycle Sequencing Kit' (Applied Biosystems, Darmstadt, Germany). The BigDye terminators are labelled with dRhodamine acceptor dyes. The primers were designed to detect *Rb1* coding sequence (see materials). The sequencing reaction was as follows:

1 $\mu$ l Terminator big dye 3.1
2 $\mu$ l of 5x buffer
1 $\mu$ l of DNA
1 $\mu$ l primer mix
5 $\mu$ l H <sub>2</sub> O

Cycle sequencing reaction followed this program:



Later, the sequencing reactions were in 30 $\mu$ l of 100% ethanol precipitated (15 minutes in the dark at room temperature), and plates were then centrifuged for 20 min at 10000 rpm. Pellets were then washed with 50 $\mu$ l of 70% ethanol and centrifuged another 20 minutes at 10000rpm. Supernatant was then removed and pellets were air dried to later be dissolved in 50 $\mu$ l of ampuva H<sub>2</sub>O. Sequence analysis was performed by the HMGU Genome Analysis Center on an ABI3730 capillary sequencer. Sequencing data (electropherograms of samples and sequence text files) were analyzed by using the computer program Chromas Lite.

#### 3.25.4 Change in PCR strategy led to proper cloning of *RB1*

Sequencing the first clone obtained by pcr amplification using a forward primer in the 5' end showed a persistent 32 bp deletion of the *RB1* sequence when amplified from pSport 6 downstream the ATG (as seeing below in figure 19) Such sequence coded for a arginine rich region with many cytosines and guanines, leading to a knot unresolved at the initial annealing temperature of 65°C.

PCR conditions were then changed to the first 2 cycles with an annealing temperature of 72°C, increasing the specificity and the rest of the cycles at 65°C, optimal temperature for the polymerase used, showed the resolution of the knot and proper amplification of the whole sequence. In figure 19 we can see the critical sequence points for unresolved knot (a) and the sequence for the wild-type Rb1 after PCR conditions changed (b) and below the alignment between the two sequences showing the 32bp missaligment corresponding to the deletion occurring in the PCR. For complete sequence see annex I.

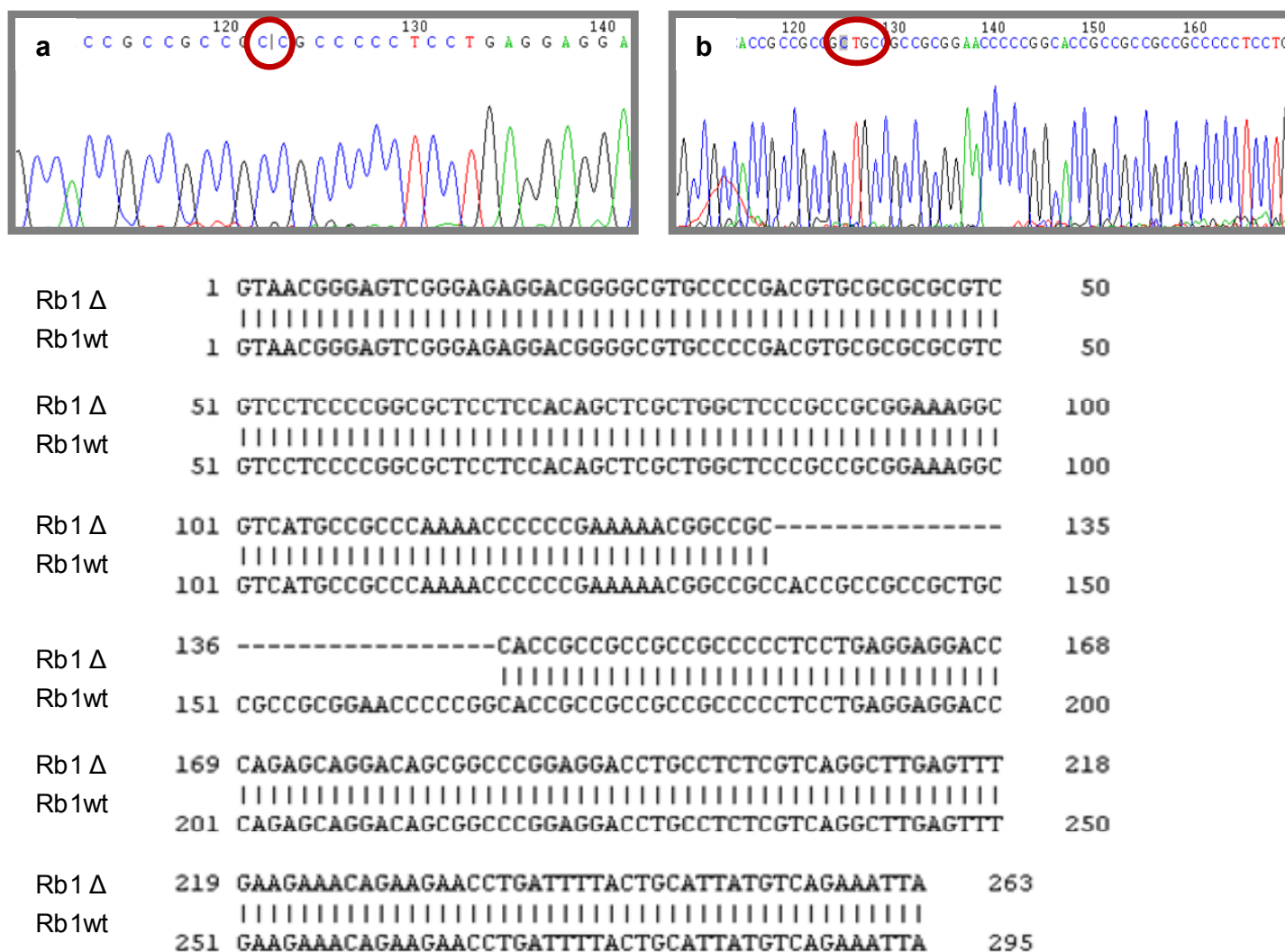


**Figure 19:** a) Sequencing of clone 18 showing the deletion of 32bp in the 5' end of the *RB1* sequence. Red circle marks the deletion location. b) Sequencing of clone 39 showing the complete sequence of the *RB1* gene cloned into our lentiviral plasmid. Red circle marks the location where the deletion used to be localized in clone 18. Lower panel: Alignment between the sequences of the two clones showing the resolution of the deletion of the G-C rich region by changing the PCR conditions.

## IV RESULTS

### 4 *Rb1* haploinsufficiency triggers genomic instability via telomere dysfunction

#### 4.1 Lineage deletion of *Rb1* in mouse osteogenic tissue

##### 4.1.1 Determining expression of *Coll1a1-Cre*

Aside other tissues already recorded in the MGI database, such as fibroblasts, head, inner ear or genital ridge and mesonephros we checked the expression of the *Coll1a1-Cre* by mating animals harbouring the *pROSA-R26R* reporter cassette with those harbouring the gene *Cre* recombinase under the promoter of *Coll1a1* were performed in our lab. Tail tip genotyping showed the deletion of the neo cassette when *Cre* transgene is present. 3 littermates for both *pROSA-R26R* (Figure 20 left panel) and *Cre* (Figure 20 right panel) genotypes are shown here. Under *Cre* expression (littermates 2 and 3) the neo cassette flanked by *loxP* sites of *R26R* is deleted (lower PCR band in left panel), whilst when lacking *Cre* expression (littermate 1) the *R26R* gene remains wild-type.

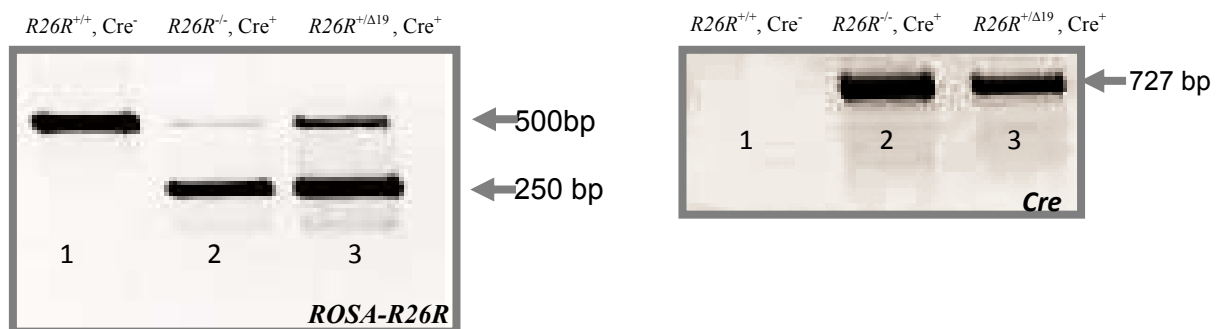


**Figure 20: Genotyping *R26R: Cre* litter mates:** Left panel: *R26R* genotype using the combination of the three primers *R26f*, *R26R1* and *R26R2*, resulting in the following fragments: 500-bp wild-type and 250-bp the mutant fragments. Lane 1:  $R26R^{+/+}$ , lanes 2:  $R26R^{-/-}$  and lane 3:  $R26R^{+/Δ19}$ . Right panel: *Cre* genotype for the same animals as in left panel using *Cre1* and *Cre2* primers (727 bp). Lane 1:  $Cre^{-}$  and lanes 2 and 3  $Cre^{+}$ .

These experiments show the deletion of the neo cassette when *Cre* is expressed in our mice, demonstrating the proper function of the *Cre* and *LoxP* system.

##### 4.1.2 *LacZ* staining shows *Coll1a1-Cre* activation in bone

To assess the *LacZ* production of the reporter mice by the *collagen1a1-Cre* driven recombination, we sacrificed a  $Cre^{+}:R26R$  animal as well as a wild-type  $Cre^{-}:R26R$  at 2 weeks of age and stained the fresh frozen femour and knee with X-gal. As can be seen in figure 21 and 22, positive staining for the *LacZ* reporter in cortical bone and in the epiphysis is seen in  $Cre^{+}$  animals.

This staining is absent in  $Cre^-$  mice and in tissue other than bone, like muscle, cartilage or bone marrow, demonstrating the high expression of Cre in bone cells.

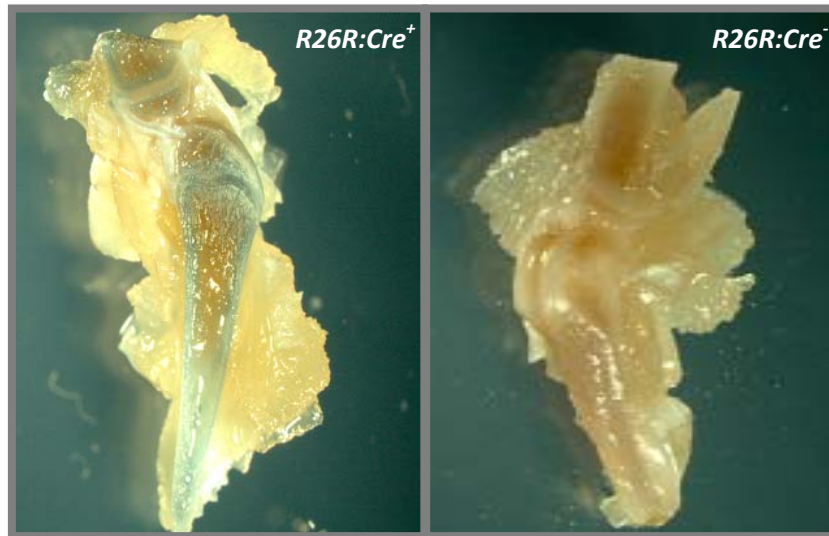


**Figure 21:** *LacZ* staining of  $R26R:Cre^+$  and  $R26R:Cre^-$  bones: X-gal derived blue staining is shown here to be restricted to the bone in the  $Cre^+$  animal in the tissues shown. 2 biological replicates for each genotype were performed.

#### 4.1.3 Osteoblasts report Cre-expression during differentiation to osteocytes

To assess the origin of the Cre-mediated *LacZ* signal within the bone tissue, histological sections of the  $R26R:Cre^+$  stained bones were performed. The strongest expression was found in the terminally differentiated osteocytes. Osteoblasts were found to express the *Cre* transgene as well as the later mineralised bone in  $R26R:Cre^+$  animals. Osteoblasts were positive for *LacZ* staining (arrow). Therefore, Cre recombinase is being expressed in the bone lineage already in the osteoblasts.

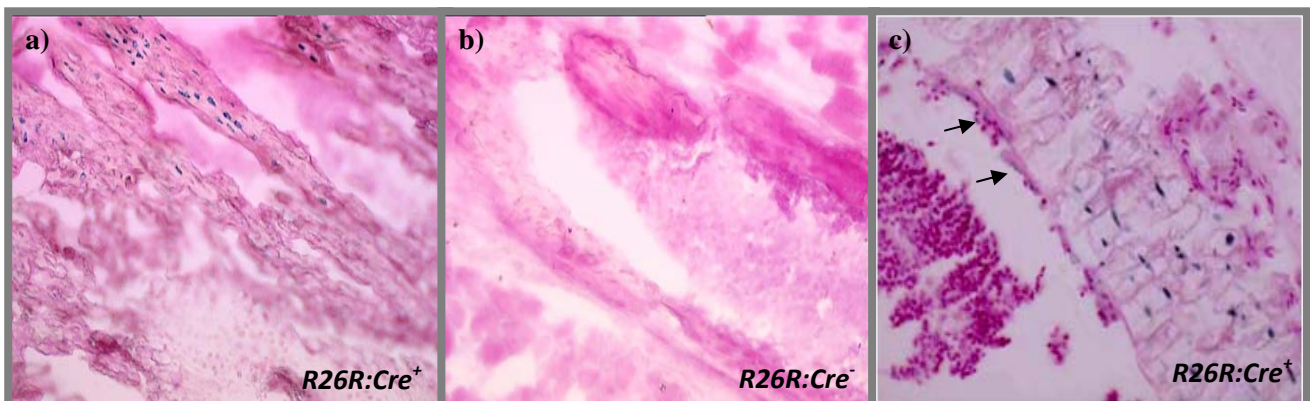


**Figure 22:** *LacZ* expression in  $R26R:Cre$  mice histological view. a) X-Gal staining of knee of  $R26R$  x *Colla1-Cre* heterozygous mice showing positive staining corresponding to bone cells (10x). b) Cre negative knee (10x). c) Positive *LacZ* staining of primary osteoblast line on top of mineralised bone. (arrow) (40x).



#### 4.1.4 Cre expression in other tissues

Using *Cre* specific PCR primers, real time PCR was performed using DNA from several tissues of the  $Rb1^{fl/+}; Cre^{-}$  and compared it to DNA from  $Rb1^{fl/+}; Cre^{+}$  to measure potential off-target expression of *Cre* transgene in other tissues. Other than in bone, we found expression in heart and kidney, demonstrating an off-target effect expression of the cre recombinase (Figure 23) to be added to the already existing in the MGI database.

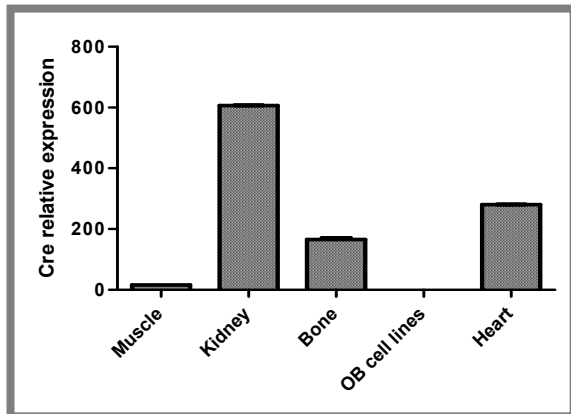


**Figure 23: Real time PCR results showing relative expression of *Cre* transgene in our animal system.** As well as bone, heart and kidney have high levels of *Cre* expression, demonstrating that expression of the transgene is not restricted to bone under the *col-1a1* promoter. Primary osteoblasts cell lines from  $Rb1^{fl/+}; Cre^{+}$  mice do not further express *Cre* recombinase *in vitro*. 2 biological replicates were used for these experiments with 2 technical replicates each.

## 4.2 Conditional deletion of *Rb1*

### 4.2.1 *Rb1* genotyping in tail tip

Mice harbouring transgenic *Cre* recombinase were mated with mice harbouring a floxed *Rb1-Δexon19*, and F1 progeny was genotyped using DNA extracted by PCR for *Rb1*. As seen in figure 24, *Cre* expression was detected by PCR (lane 1 left panel) when transgene present. *Rb1* genotyping showed that in presence of *Cre* (lane 1 of right panel) one allele of *Rb1* lost its exon 19 (reason for the smaller size of the band (235bp) as compared to the remaining wild-type band (650 bp). In the absence of *Cre* expression (lanes 2 and 3 of right panel) the wild-type or floxed alleles retained the exon 19 as shown. These experiments proved the *Cre* dependent deletion of *Rb1* exon 19 in our model system.

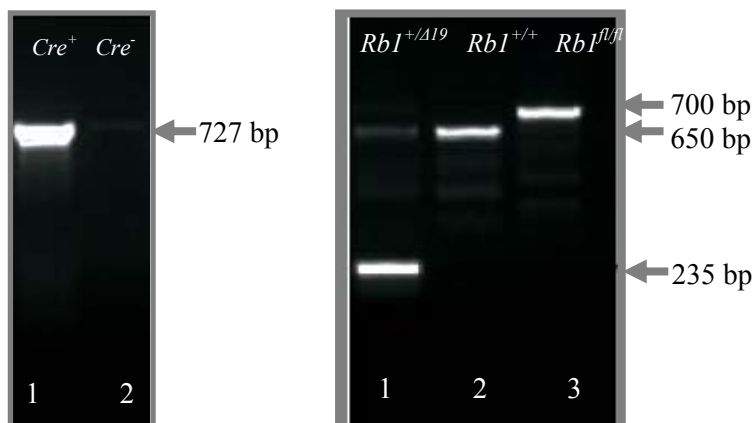


**Figure 24: *Rb1* genotyping in tail tips.** PCR products: Left panel: Lanes 1-2: *Cre* genotype. Lane 1: *Cre* positive (727 bp). Lane 2: *Cre* negative. Right panel: *Rb1* genotype. Lane 1: *Rb1-Δexon19* (235 bp) and remaining wt allele (650 bp), lane 2:  $Rb1^{+/+}$ , lane 3:  $Rb1^{fl/fl}$  (700 bp).

#### 4.2.2 Establishing of osteoblastic cell lines from explants cultures

Osteoblast explants from various types of the limb skeleton were derived from both *Rb1*<sup>+/+</sup> and *Rb1*<sup>+/ $\Delta$ 19</sup> mice to establish *in vitro*-models for mechanistic studies. Clean bones explanted osteoblastic cell lines obtaining monolayers in 7 up to 15 days, where the first passage was performed (Figure 25).

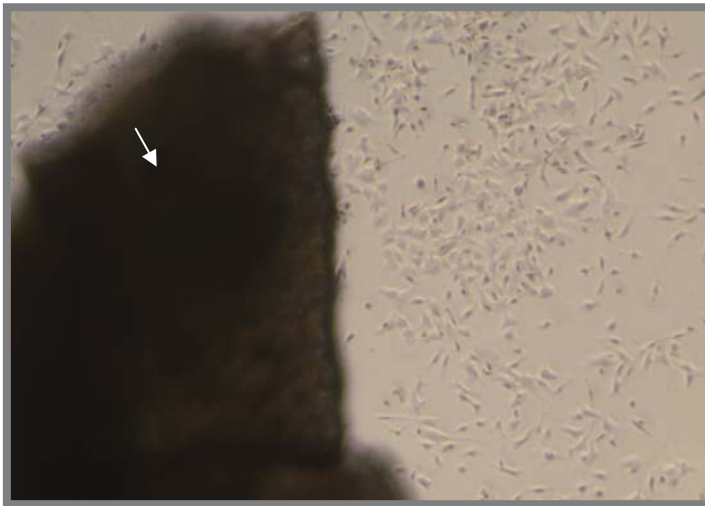


**Figure 25: Osteoblast explants from bone.** Picture shows the a piece of compact bone (arrow) in a Petri dish in DMEM medium with cells from the osteoblastic lineage seeding onto the culture vessel (six well plates). Picture taken at 10x one week after setting explants following animal sacrifice.

#### 4.2.3 Osteoblastic lineage of the cells was established by AP staining

To assess the osteogenic character of the explanted primary cells histochemical staining for alkaline phosphatase (AP) was performed. Both, primary osteoblasts explanting from bone and the positive control of the established osteosarcoma cell line (ROS17/2.8) exhibit AP positivity. No staining was found for a negative control cell line of retinal epithelial origin (RPE). In the primary osteoblasts, as observed in the ROS17/2.8 cells as well, the AP staining appears not homogeneous, but focally distributed throughout the cell culture (Figure 26).

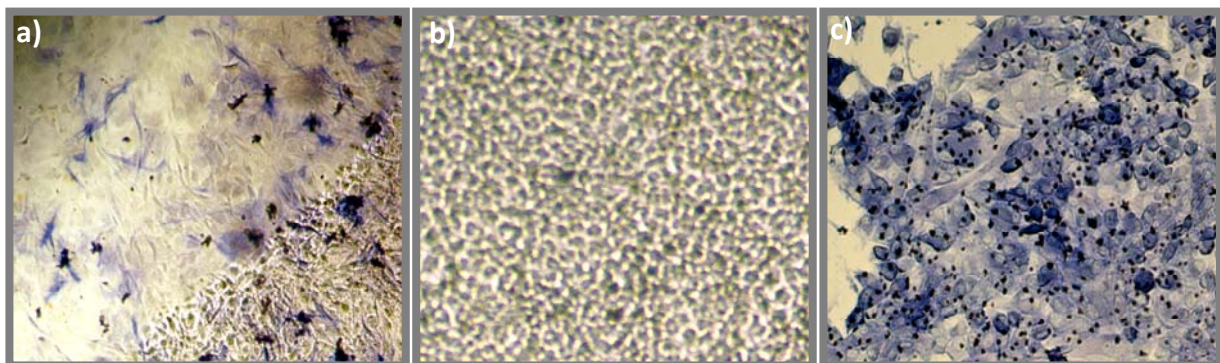


**Figure 26: AP staining results.** a) Primary osteoblasts after induction of differentiation for 24h staining positive for AP. b) RPE (retinal pigment epithelial cells) used as negative control. c) ROS (Rat Osteosarcoma) cells used as positive control. Determination was performed with 2 biological replicates.

#### 4.2.4 *Rb1* conditional deletion was confirmed in the explanted cell lines

Once primary cell lines were established from bones of mice with either the *Rb1*<sup>+/+</sup> or *Rb1*<sup>+/ $\Delta$ 19</sup> genotype, *in vitro* growing cells were genotyped to confirm the presence of the *Rb1* deletion. PCR of genomic DNA was performed using primers that flank the *LoxP*-*exon19* region to identify both the wild-type (Figure 27 lane 3) and the floxed *Rb1* allele (Figure 27, lane 2), but also the deleted exon 19 (*Rb1* $\Delta$  *exon19*) allele resulting from Cre mediated *LoxP* recombination (Figure 27, lane 4 lower band).

In figure 27 the 4 possible genotype outcomes of our model in cell culture are shown.

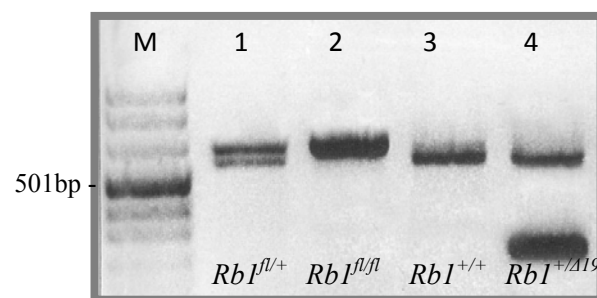


**Figure 27: Cell line genotypes for *Rb1*.** In this picture following the DNA marker, the genotypes of *Rb1*<sup>fl/+</sup>, *Rb1*<sup>fl/fl</sup> (700 bp), *Rb1*<sup>+/+</sup> (650 bp) and *Rb1*<sup>+/ $\Delta$ 19</sup> (650 bp, 235 bp) are shown for established primary cell lines. Lane 1: Marker, lane 2: *Rb1*<sup>fl/+</sup>, lane 3: *Rb1*<sup>fl/fl</sup>, lane 4: *Rb1*<sup>+/+</sup>, lane 5: *Rb1*<sup>+/ $\Delta$ 19</sup>.

We established osteoblast cell lines for the 4 possible genotypes of our model. We have not found *Rb1*<sup>-/-</sup> mutants, possibly due to early mortality or impaired development. For the functional assays further carried out in this work, *Rb1*<sup>+/+</sup> and *Rb1*<sup>+/ $\Delta$ 19</sup> were used.

Cell lines carrying a *LoxP* allele which were cultured *in vitro* did not lose the exon 19 even after many passages, suggesting (as shown in figure 27 where number 4 is Cre<sup>+</sup>) that Cre is not active once the cell lines are established.

#### 4.3 Exon 19 deletion detected when sequencing *Rb1*<sup>+/ $\Delta$ 19</sup> osteoblasts

After gel purification of the *Rb1* *exon19* deleted band the PCR products were sequenced using primer 18 (see materials for sequence) wild-type sequenced was sequence in parallel for control (data not shown). As shown in figure below (Figure 28), deletion of exon 19 was confirmed by sequencing showing the one *LoxP* site remaining after recombination between

intron 18 and intron 19. From 5' end: intron 18 was followed by the remaining *LoxP* site (italics) and this one followed by intron 19 of the *Rb1* gene (Blasted against ensembl data).

```

Sequence Rb1Δ exon19    1 GCATATTTTTCTGTTAAGCTAGATAACTTCGTATAGCATACATTATACG    50
                        | | | | | | | | | | | | | | | | | | | | | | | | | | | |
Intron 18              1 GCATATTTTTCTGTTAAGCTAG-----                          23

Sequence Rb1Δ exon19    51 AAGTTATATCTCTATGCCTTGGTTTCTTTGCTTATAAAATGAAAAAAAAA    100
                        | | | | | | | | | | | | | | | | | | | | | | | | | | | |
Intron 19              24 -----ATCTCTATGCCTTGGTTTCTTTGCTTATAAAATGAAAAAAAAA    66

Sequence Rb1Δ exon19    101 GATAATAATATACCT    116
                        | | | | | | | | | | | | | | | | | | | | | |
Intron 19              67 GATAATAATATACCT    82

```

**Figure 28: alignment of the sequence of the Cre-mediated *Rb1* deletion between intron 18 and intron 19.** 3 biological replicates of *Rb1*<sup>+/ $\Delta$ 19</sup> cells were shown to harbour the remaining *LoxP* site (after recombination) between intron 18 and intron 19. Exon 19 sequence was deleted and replaced by the remaining *LoxP* site (misalignment) after recombination.

#### 4.4 RNA and protein levels of *Rb1*<sup>+/ $\Delta$ 19</sup> osteoblasts confirm *Rb1* haploinsufficiency

##### 4.4.1 mRNA level shows *Rb1* haploinsufficiency

To assess whether the *Rb1*<sup>+/ $\Delta$ 19</sup> deletion translated into the expression level, or whether the remaining wild-type allele could be upregulated to compensate for the reduced gene, *Rb1* messenger RNA levels were studied in the *Rb1*<sup>+/ $\Delta$ 19</sup> and *Rb1*<sup>+/+</sup> cell lines (Figure 29). A Taqman<sup>R</sup> probe was used that detect both wild-type and *Rb1* $\Delta$  exon19 transcripts in exon 5. A second set detected only the *Rb1* wild-type allele binding exon 19 whilst a third set only binds to the *Rb1* $\Delta$ 19 induced junction between exons 18/20. We can see below that in *Rb1*<sup>+/ $\Delta$ 19</sup> osteoblasts the wild-type transcript is reduced by 50% (wild-type *Rb* allele bars) and the deficit is replaced by the *Rb1* $\Delta$ 19 transcript in the mutant cells (deleted *Rb* allele bar). Therefore, there is no dosage compensation arising from the wild-type allele.

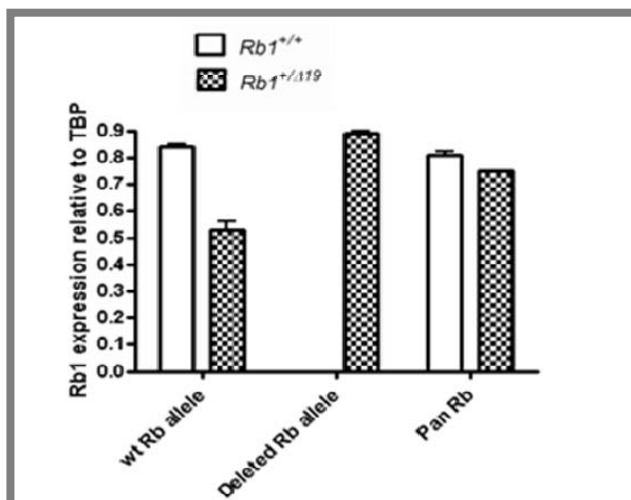


**Figure 29: RT-Q PCR of *Rb1*<sup>+/+</sup> and *Rb1*<sup>+/ $\Delta$ 19</sup> mRNA levels.** Figure shows the relative expression of *Rb1* wt allele (probe binding exon 19), *Rb1* $\Delta$ 19 allele (probe binding exon 18/20 junction) and pan *Rb1* (probe binding in exon 5) in established osteoblast cultures from *Rb1*<sup>+/+</sup> and *Rb1*<sup>+/ $\Delta$ 19</sup> mice. It demonstrates the haploinsufficiency of *Rb1*<sup>+/ $\Delta$ 19</sup> cells. Two biological replicates were used for this experiment.

No compensation of the wild-type allele was observed in the  $Rb1^{+/\Delta19}$  cultures, demonstrating the haploinsufficiency of the cultures.

#### 4.4.2 Analysis of the expressed Rb1 confirms the *Rb1* haploinsufficiency

Western blot analysis performed in both  $Rb1^{+/+}$  and  $Rb1^{+/\Delta19}$  cell lines confirmed the reduced levels of Rb1 protein in the mutant cell lines for both Rb1 and phosphoRb1 (pRb1). Lanes 1 and 2 show 2 biological replicates of  $Rb1^{+/+}$  and lanes 3 and 4 showing 2 biological replicates of  $Rb1^{+/\Delta19}$ , which demonstrate the haploinsufficiency of  $Rb1^{+/\Delta19}$  cultures on protein levels. Right panel shows the quantification of the western blots.

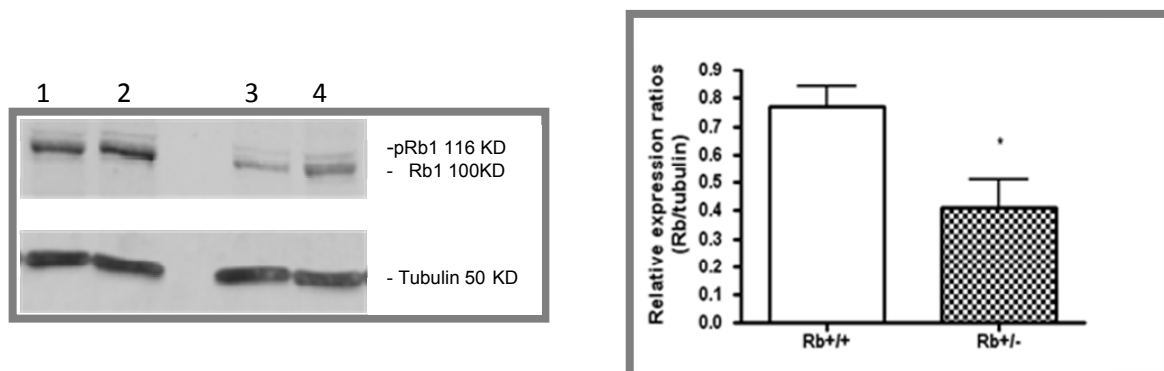


**Figure 30: Rb1 protein analysis.** **Left Panel:** upper blot Rb1 western blot analysis performed with anti Rb1 from BD. First 2 lines 2 biological replicates of  $Rb1^{+/+}$ , followed by empty slot and two biological replicates of  $Rb1^{+/\Delta19}$ . Lower blot tubulin used as loading control. 2 biological replicated shown in this figure. **Right panel** quantification of both Rb1 and pRb1 levels in the primary cells from 3 biological replicates with 2 technical replicated each, showing a reduction in Rb1 in  $Rb1^{+/\Delta19}$  cultures (t-test: \*  $p \leq 0.01$ ).

#### 4.5 Cell cycle is impaired in *Rb1*<sup>+Δ19</sup> osteoblasts after radiation

We performed cell cycle analysis of *Rb1*<sup>+/+</sup> and *Rb1*<sup>+Δ19</sup> cells to study the cell cycle control as well as the radiation effect on the check point control of *Rb1*<sup>+Δ19</sup> cells when compared to their wild-type counterparts.

Analysis was performed on cells at passage 4 (young osteoblasts) where cell cycle distribution was similar for both genotypes at 0 Gy. Six hours after radiation exposure to 4 Gy, *Rb1*<sup>+/+</sup> cells block the cell cycle, the S phase was reduced and cells accumulated in G1 and G2; whilst in *Rb1*<sup>+Δ19</sup> the S phase percentage did not change, suggesting the further entrance of cells into the S phase with unrepaired damage (Figure 31). Showing the impairment of haploinsufficient cells to block the cell cycle after radiation, and entering the S phase with potential DNA damage.

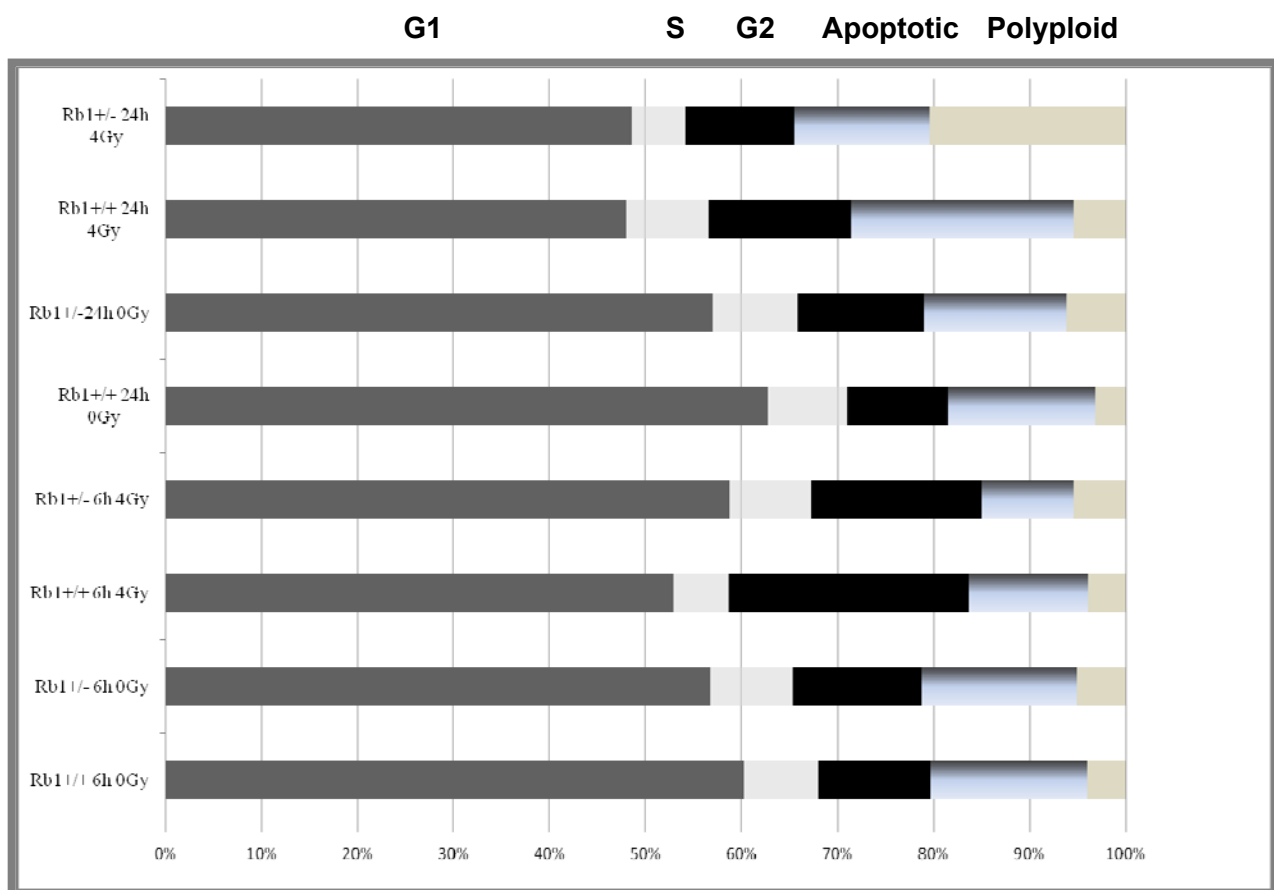


**Figure 31: Cell cycle analysis of *Rb1*<sup>+/+</sup> and *Rb1*<sup>+Δ19</sup> cells. Analysis performed at 0 and 4 Gy, samples taken 6 hours and 24 after radiation.** Impairment of *Rb1*<sup>+Δ19</sup> osteoblasts to block the cell cycle progression after exposure to radiation. No S phase changes were appreciated in *Rb1*<sup>+Δ19</sup> osteoblasts cultures 6 hours after exposure, whilst their wt counterparts accumulated in G1 and G2 phases. 24 hours after radiation exposure, apoptotic population was increased in wt cells, whilst polyploidy was increased in haploinsufficient cells.

24 hours after radiation exposure, *Rb1*<sup>+/+</sup> distribution showed an increase in the apoptotic fraction as outcome of radiation exposure and damage to the cells, whilst in *Rb1*<sup>+/ $\Delta$ 19</sup> cells the apoptotic fraction has not changed much, but instead the polyploid fraction has increased in the haploinsufficient cells, demonstrating a defect in the cell cycle, as well as an induction on polyploid fraction increase after radiation in *Rb1*<sup>+/ $\Delta$ 19</sup> osteoblasts (as further shown in figure 32).

It is interesting to note, as seen in figure 31, that the cell cycle distribution was very similar in unirradiated *Rb1*<sup>+/+</sup> and *Rb1*<sup>+/ $\Delta$ 19</sup> cells (Figure 31) at low passages. Cells were on passage 4 when exposed to radiation.

During culturing and especially at later passages, whilst *Rb1*<sup>+/+</sup> maintained a small tetraploid population, such population was further increased with passaging in *Rb1*<sup>+/ $\Delta$ 19</sup> cells as shown in figure 32. Haploinsufficient aging cells accumulated more and more cells with polyploid DNA dosage, avoiding apoptosis, and as shown on figure 34, avoiding senescence as well.

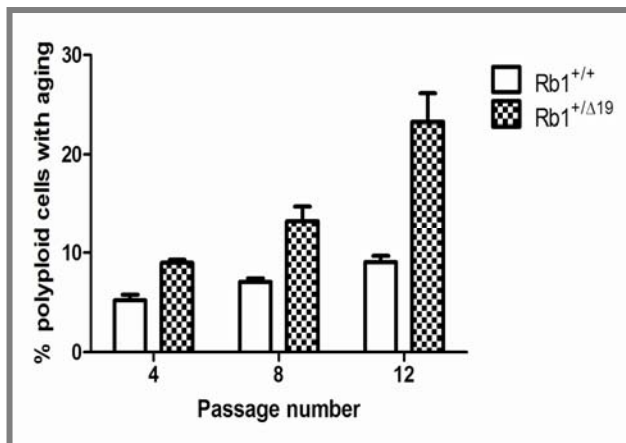


**Figure 32: Analysis of *Rb1*<sup>+/+</sup> and *Rb1*<sup>+/ $\Delta$ 19</sup> polyploid population with aging.** Induce of polyploidy population in *Rb1*<sup>+/ $\Delta$ 19</sup> osteoblasts with aging. Haploinsufficient cells were more prone to polyploidy with passages, suggesting a defect in the cell cycle already visible in haploinsufficiency of *Rb1* cells leading to instable genome (SD for 3 biological replicates).

As shown in figure 33, induction of polyploidy was greater in the *Rb1*<sup>+/ $\Delta$ 19</sup> cells 24 hours after irradiation exposure as compared to its wild-type counterpart. *Rb1*<sup>+/+</sup> after radiation showed an increase in apoptotic fraction (Figure 31), whilst *Rb1*<sup>+/ $\Delta$ 19</sup> cultures showed an increase in polyploid fraction after radiation exposure, demonstrating a further increase in aneuploidy by radiation exposure to *Rb1* haploinsufficient cells.

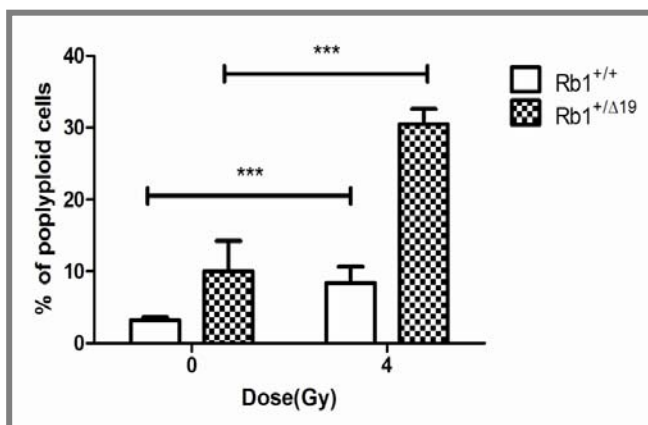


**Figure 33: Polyploidy induced by radiation exposure:** Remarkable increase in the polyploidy population in *Rb1*<sup>+/ $\Delta$ 19</sup> cultures (passage 4) 24 hours after radiation exposure (4 Gy), as compared to *Rb1*<sup>+/+</sup>.



These results demonstrate that *Rb1* haploinsufficiency causes cell cycle dysfunction in primary osteoblasts leading to aneuploidy. Radiation exposure has been shown to increase aneuploidy fraction in haploinsufficient cells.

#### 4.6 Failure of senescence induction in *Rb1*<sup>+/ $\Delta$ 19</sup> primary osteoblasts

Entering senescence is a common mechanism performed by damaged cells that cannot repair their DNA, or that have reached a critical telomere length. It is the phase of the cell cycle when cells even though they are metabolically active, they do not divide further. It can be detected by expression of senescence markers, and one well established is the expression of  $\beta$ -galactosidase in senescent cells.

At passage 5, primary *Rb1*<sup>+/+</sup> osteoblasts entered senescence 24h after radiation in a dose dependent manner, as expected an increase in the percentage of senescent cells is seen with increasing dose, in agreement with *Rb1*'s main function as a gate keeper of the genome (Figure 34). *Rb1*<sup>+/ $\Delta$ 19</sup> osteoblasts, show a discrete dose response but smaller amount of senescent cells (Figure 34). The basal level of senescent cells in non-irradiated cells was lower in the haploinsufficient cells. As control we used 4 mouse osteosarcoma cell lines (MOS) that do not enter senescence after radiation.

We can conclude that, in agreement with *Rb1* TSG function, *Rb1* haploinsufficient cells cease to neither enter senescence nor respond to radiation exposure in the same manner as their wild-type counterparts.

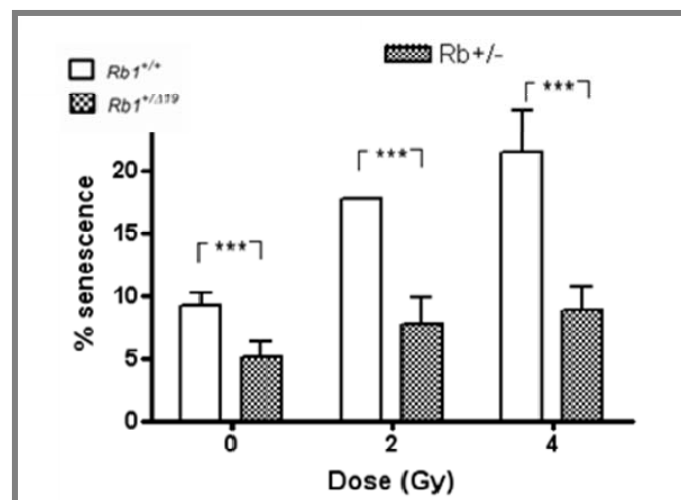


**Figure 34: Senescence studies.** Senescence determination of *Rb1*<sup>+/+</sup> (grey dotted) compared to the *Rb1*<sup>+/ $\Delta$ 19</sup> osteoblasts (blue squared pattern) at different radiation doses showing impairment in senescence induction on *Rb1*<sup>+/ $\Delta$ 19</sup> osteoblasts. Two biological replicates with 3 technical replicates each were used. 3 biological replicates (t-test \*\*\*  $p \leq 0,0001$ ).



#### 4.7 pRb1 localises in close proximity to the DNA on metaphases, suggesting a role of pRb1 during cell division different that is from E2F modulator

pRb1 immunofluorescence was performed in both *Rb1*<sup>+/+</sup> and *Rb1*<sup>+/ $\Delta$ 19</sup> osteoblasts in metaphase cells with condensed chromatin (Figure 35).

This close proximity of the phosphorylated form of Rb1 indicates a spatial relationship between the protein and DNA during mitosis. This is not consistent with the canonical function of *Rb1* during G1/S phase transition activation, suggesting a different function of the Rb1 protein during cell division.

In the *Rb1*<sup>+/+</sup> cells, where is easier to distinguish the protein, we can see pRb1 spots at the end of the chromosomes (arrows), suggesting a possible relation to telomeres or heterochromatin.

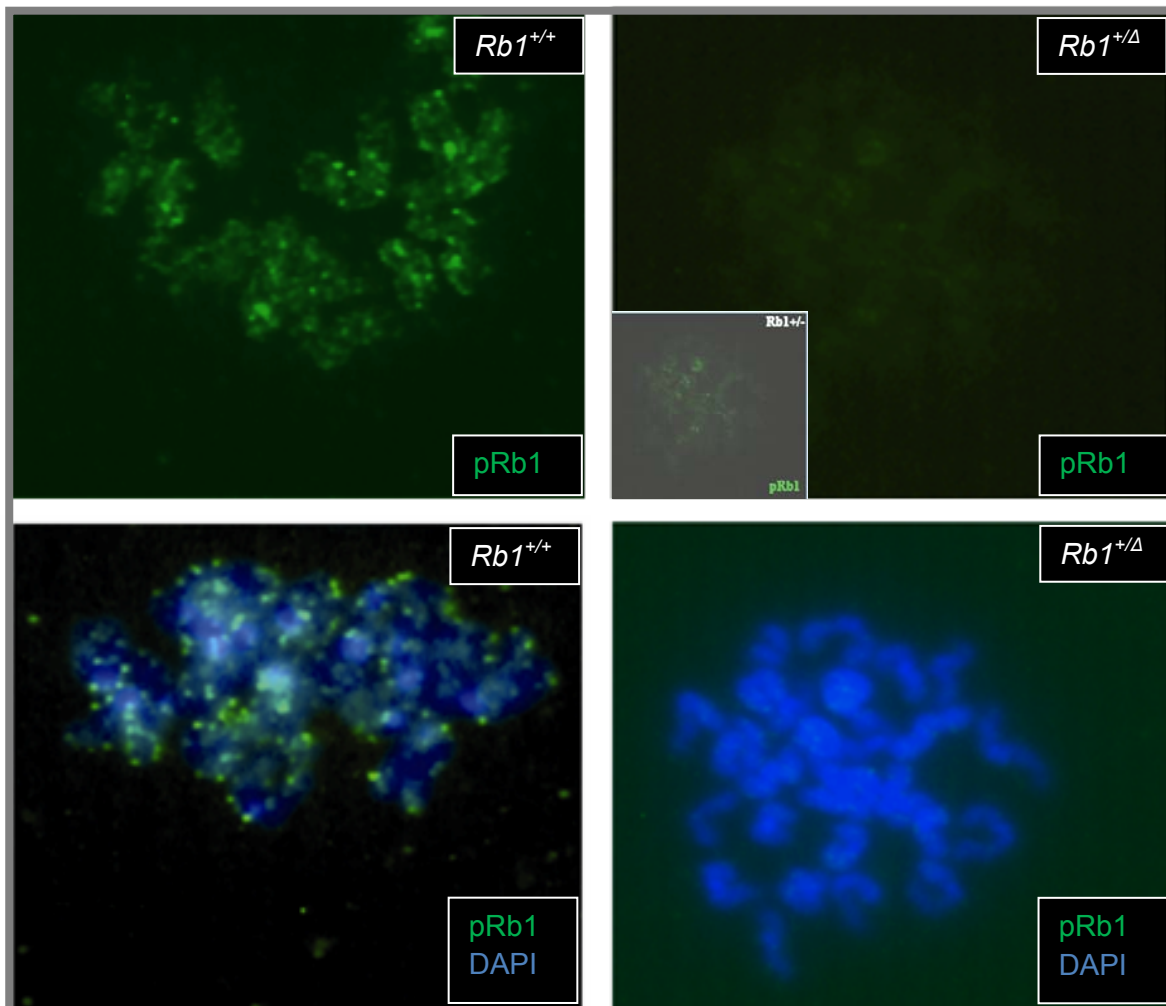


**Figure 35: pRb immunofluorescence in *Rb1*<sup>+/+</sup> and *Rb1*<sup>+/ $\Delta$ 19</sup>.** Left: shows pRb status in *Rb1*<sup>+/+</sup> cells, protein is present bound to the metaphase plate and in close proximity to heterochromatin. Right: *Rb1*<sup>+/ $\Delta$ 19</sup> haploinsufficient cells showing reduced amount of pRb1 protein present (In upper right panel see same figure overexposed) but in close proximity to the chromosomes as shown in their wt counterparts. Arrows point at pRb1 signals at the end of chromosomes, suggesting a close proximity of the phosphorylated protein to the telomeres. DNA was stained with DAPI.

#### 4.8 Increased genomic instability in the *Rb1*<sup>+/ $\Delta$ 19</sup> osteoblasts with the effect amplified after radiation

*Rb1*<sup>+/ $\Delta$ 19</sup> primary cells showed an increase in genomic instability, measured in both micronuclei induction as well as segregational defects such as anaphase bridges (Figure 36 upper panels) and persistent telophase bridges (Figure 36 lower panels). Such defects, though increased already in the baseline of the *Rb1*<sup>+/ $\Delta$ 19</sup> cultures, and absent in *Rb1*<sup>+/+</sup>, were prominently increased after radiation exposure (Figures 37, 38, 39, 40).

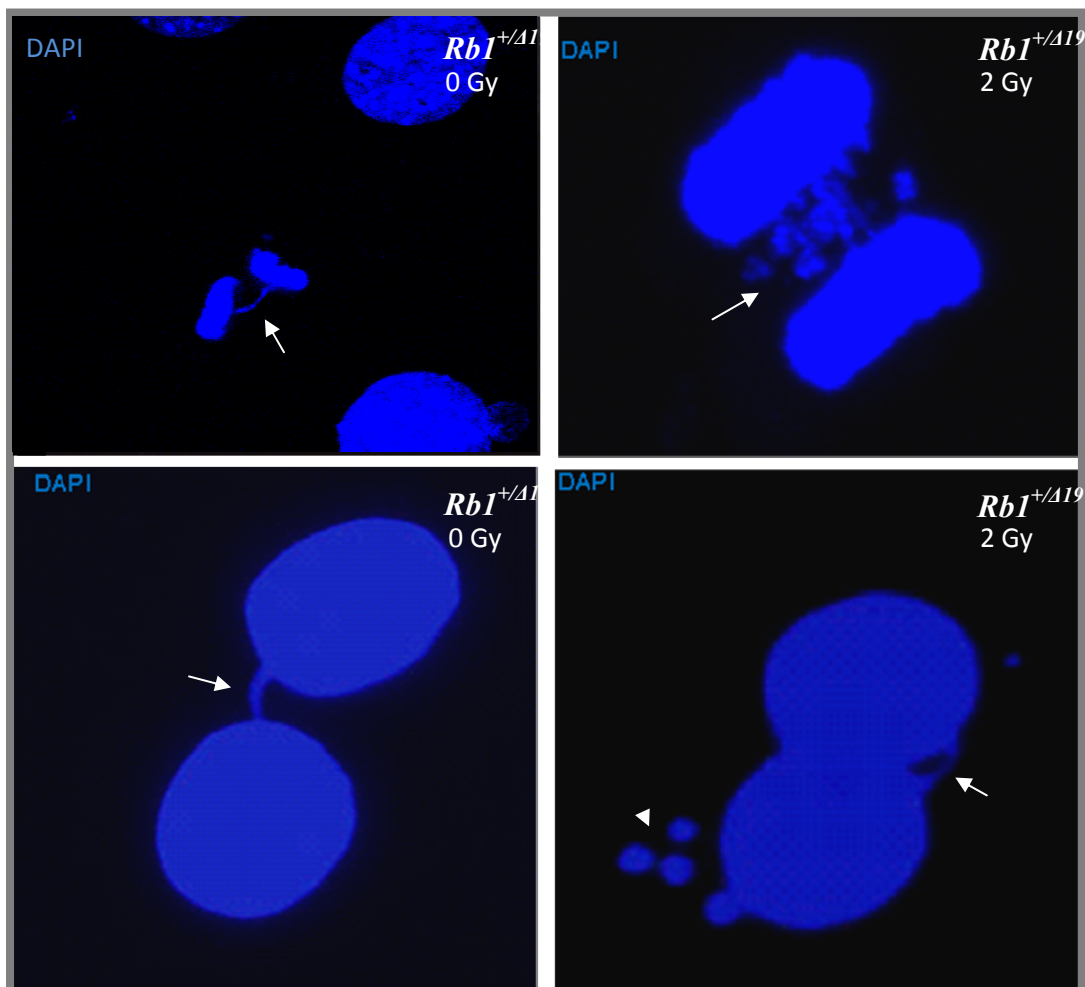


**Figure 36: Genomic instability measured as anaphase bridges and micronuclei in *Rb1*<sup>+/ $\Delta$ 19</sup> osteoblasts. Upper left:** Anaphase bridges present in unirradiated *Rb1*<sup>+/ $\Delta$ 19</sup> osteoblasts (40x). **Upper right:** Anaphase plates showing segregation defects in *Rb1*<sup>+/ $\Delta$ 19</sup> cells 1 week after 2 Gy irradiation (63x). **Lower left:** telophase persistent bridge in unirradiated *Rb1*<sup>+/ $\Delta$ 19</sup> osteoblasts (40x), **Lower right:** Anaphase bridge and radiation induced micronuclei in *Rb1*<sup>+/ $\Delta$ 19</sup> osteoblasts after 2 Gy (40x). White arrows point at segregational defects and arrow head in lower right point at micronuclei.

#### 4.8.1 Micronuclei (MN) frequency was increased in *Rb1*<sup>+/ $\Delta$ 19</sup> osteoblasts after 2 Gy of radiation

*Rb1*<sup>+/ $\Delta$ 19</sup> osteoblasts showed an increased baseline of MN (acentric fragments lost during cell division) in unirradiated cultures (passage 5) that significantly increased after radiation (passage 5) (Figure 37). 24 hours after radiation, the MN induction was shown increased in all cells but more prominent in *Rb1*<sup>+/ $\Delta$ 19</sup> cells, even though, as shown in Figure 38, the same amount of cells contained MN in both genotypes after radiation, demonstrating that the same amount of cells were damaged, but the damage was greater in *Rb1*<sup>+/ $\Delta$ 19</sup> osteoblasts.

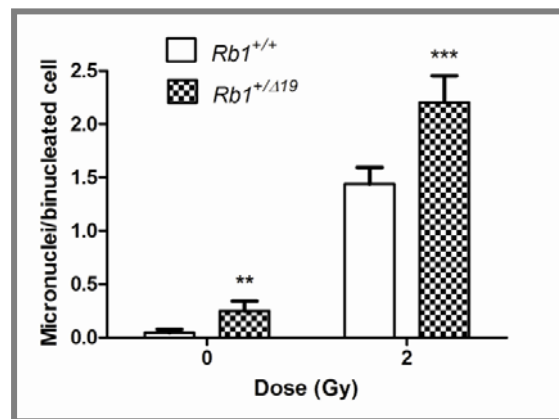


**Figure 37: Micronuclei induction quantification for both *Rb1*<sup>+/ $\Delta$ 19</sup> (squared) and *Rb1*<sup>+/+</sup> (dotted) osteoblasts.** Shows number of Micronuclei per cell before and 24 hours after radiation for *Rb1*<sup>+/ $\Delta$ 19</sup> (squared) and *Rb1*<sup>+/+</sup> (dotted) osteoblasts. 250 binucleated cells were counted showing the enhancement in instability after radiation and a remarkably effect in the haploinsufficient osteoblasts up to 1.7 fold increase. 250 binucleated cells were counted for 2 biological replicates (SD) (t-test  $p \leq 0,001$ ) at passage 5.

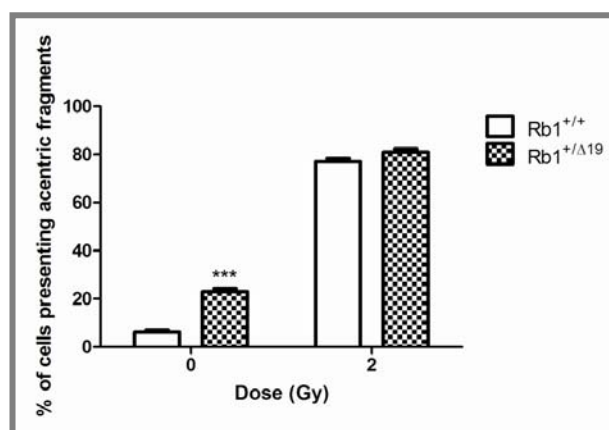


**Figure 38: Cells presenting MN for both *Rb1*<sup>+/ $\Delta$ 19</sup> (squared) and *Rb1*<sup>+/+</sup> (dotted) osteoblasts.** Shows number of cells presenting MN before and 24 hours after radiation for *Rb1*<sup>+/ $\Delta$ 19</sup> (squared) and *Rb1*<sup>+/+</sup> (dotted) osteoblasts. 250 binucleated cells were counted showing that the baseline of damage (at 0 Gy) is higher in the *Rb1*<sup>+/ $\Delta$ 19</sup> cells, but nearly the same number of cells were affected after radiation (2 Gy). 250 binucleated cells counted for 2 biological replicates (t-test  $p \leq 0,001$ ).

As well as the total number of MN, their distribution differs between  $Rb1^{+/+}$  and  $Rb1^{+/\Delta19}$  since most of the binucleated cells in the wild-type genotype harvest 1 or 2 MN after radiation, whilst in the haploinsufficient cells, cells seem to carry more acentric fragments in each division as compared to its wild-type counterpart which increases after radiation, suggesting a more instable genome in the  $Rb1^{+/\Delta19}$  cells (see summary in table below).

Dose	Binucleated cells with MN (affected)	MN/binucleated cells	% of binucleated cells with $\geq 4$ MN
0 GY	$Rb1^{+/+}$ 4%	0,045	0
	$Rb1^{+/\Delta19}$ 20%	0,25	10
2 GY	$Rb1^{+/+}$ 70%	1,44	12
	$Rb1^{+/\Delta19}$ 75%	2,3	52

**Table 4.8.1:** Shows the total MN analysis in  $Rb1^{+/+}$  and  $Rb1^{+/\Delta19}$  osteoblasts. The baseline increase of binucleated cells harvesting acentric fragments, and the increase in MN/binucleated cell after radiation shows  $Rb1^{+/\Delta19}$  osteoblasts to have a more unstable genome, feature that is enhanced by radiation exposure.

#### 4.8.2 Sporadic acentric fragments rate increased in $Rb1^{+/\Delta19}$ cultures

As shown before (Figure 39) unirradiated  $Rb1^{+/\Delta19}$  cells harvest more baseline damage than their wild-type counterparts. Such difference was found also in normal growing cultures where we found the existence of mononucleated cells (therefore non dividing cells, unlike those used for MN counts) harvesting MN. Though the MN assay is defined in dividing cells, these mononucleated cells with MN imply that there is a higher level of instability in  $Rb1^{+/\Delta19}$  cultures. To assess whether the instability was persistent with aging, we quantified the amount of sporadic DNA losses in  $Rb1^{+/+}$  and  $Rb1^{+/\Delta19}$  osteoblasts over several passages, as seen in figure 40.  $Rb1^{+/\Delta19}$  osteoblasts showed an increased instability (measured in acentric fragments per cell) which increased with aging, demonstrating that the damage of the cells harvesting the *Rb1* haploinsufficient mutation, is persistent and increases with aging.

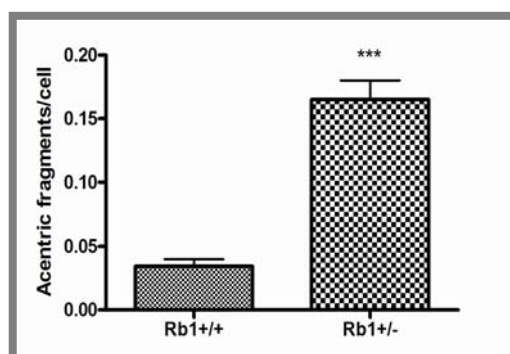


**Figure 39: Sporadic DNA acentric fragments (MN).** Shows the increase on acentric fragments that sporadically occur in  $Rb1^{+/\Delta19}$  cells in culture (passage 5). 250 mononucleated cells counted (SD of 3 biological replicates, t-test \*\*  $p \leq 0,001$ ).

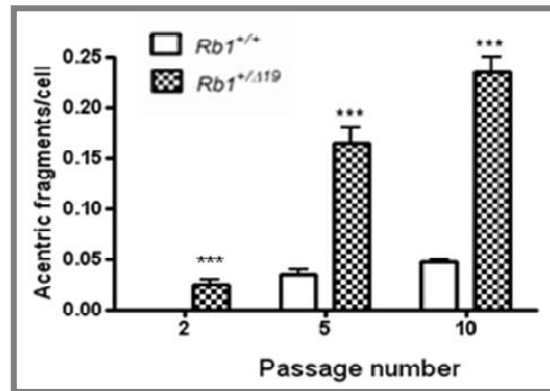


**Figure 40: Sporadic DNA acentric fragments (MN) increase with passages in *Rb1*<sup>+/Δ19</sup> osteoblasts.** Figure shows the increase on acentric fragments that sporadically occur in *Rb1*<sup>+/Δ19</sup> cells over several passages. 250 mononucleated cells counted (SD of 3 biological replicates, t-test \*\*\* p≤0,0001).

#### 4.8.3 Anaphase bridges counted per cell showed an increased instability in *Rb1*<sup>+/Δ19</sup> cells

Both, anaphase (condensed chromatin) and late persistent telophase bridges (separated nuclei of decondensed chromatin) were found in *Rb1*<sup>+/Δ19</sup> osteoblasts. Such defect, even though more persistent after radiation exposure, was found to be increased sporadically in unirradiated *Rb1*<sup>+/Δ19</sup> osteoblasts (Figure 41).

Bridges were counted in the whole cell population and as shown in figure 41, the number of bridges was increased in *Rb1*<sup>+/Δ19</sup> osteoblasts, sporadically as well as even further after radiation exposure. Such anaphase structures can be those leading to dicentric formation as the outcome of the anaphase bridges, and infact, dicentrics were found sporadically in metaphases of the *Rb1*<sup>+/Δ19</sup> cultures.

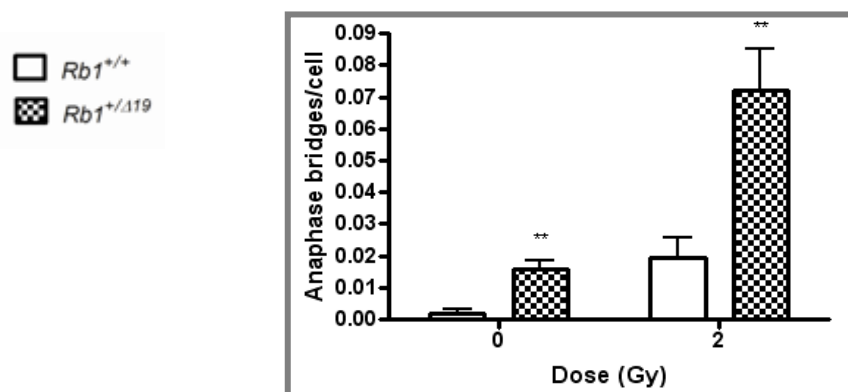


**Figure 41: Quantification of Anaphase bridges per cell, before and after radiation for both *Rb1*<sup>+/+</sup> and *Rb1*<sup>+/Δ19</sup> osteoblasts.** Anaphase bridges quantification showing an increased genomic instability in the *Rb1*<sup>+/Δ19</sup> osteoblasts as compared to its wt counterparts, 1.8 fold increase relative to wt. Such an effect was further enhanced by radiation (48 hours after radiation) and more pronounced in *Rb1*<sup>+/Δ19</sup> cells up to 3.7 fold increase. 500 cells counted per genotype, and dose of 3 biological replicates with 2 technical replicates each. Note that the bridges are giving here per cell (of a population of 500 cells). 2way ANOVA, column factor (genotype): \*\* p≤0,001 and Dose factor (radiation dose) \*\*\* p≤0,001).

#### 4.9 *Rb1*<sup>+/ $\Delta$ 19</sup> harbour shorter telomeres compared to its wild-type counterpart

The telomere length was analysed either on single chromosomes (Figure 42) or as the integral signal for the whole cells using different assays (Figure 42, and onwards). In both assays, a Cy3 labelled DNA probe that hybridise to telomeric sequences was used to label the telomeres in a quantitative manner. Decreased fluorescence intensity of PNA-Cy3 on *Rb1*<sup>+/ $\Delta$ 19</sup> osteoblasts implies reduced telomeric length in haploinsufficient cell lines.

As shown in figure 41 the strength of the PNA staining in passage 8 *Rb1*<sup>+/ $\Delta$ 19</sup> mutant cells was diminished to nearly absent compared to *Rb1*<sup>+/+</sup> cells grown under identical conditions. The labelling revealed a mixed cell population with different intensity levels for each cell (or group of cells) in each culture, showing this to be a continuous, dynamic process which continuously reduces with increasing passages (as shown in figure 45). We found that *Rb1*<sup>+/ $\Delta$ 19</sup> cells have a defect on telomere maintainance (Figure 42, 43, 44, 46), harvesting shorter telomeres as compared to their wild-type counterparts.

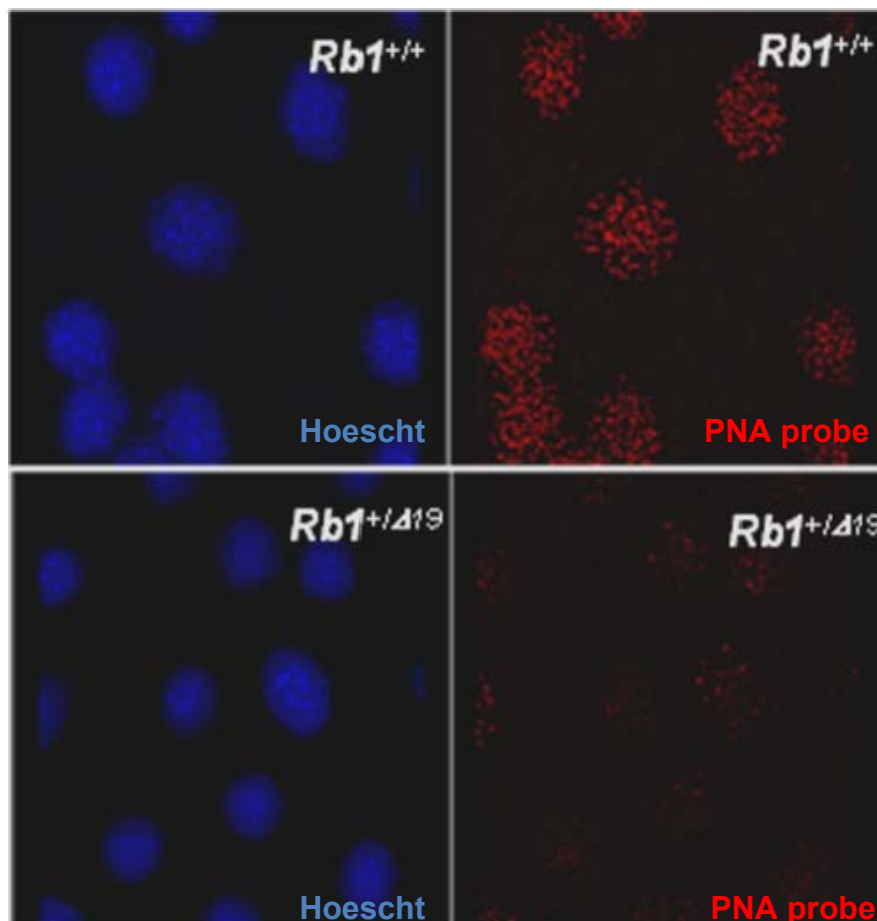


**Figure 42: FISH-PNA on osteoblasts.** Fluorescence *In-situ* hybridization was performed both in *Rb1*<sup>+/ $\Delta$ 19</sup> and *Rb1*<sup>+/+</sup> osteoblasts with PNA-Cy3 probe (40x). Two biological replicates with three technical replicates showed a reduction in telomere PNA staining in mutant *Rb1* when compared to the wt cells.



#### 4.10 Heterogeneous telomeric loss in *Rb1*<sup>+/ $\Delta$ 19</sup>

Using FISH (Figure 43a) we determined that the telomeric signals are heterogeneous in the *Rb1*<sup>+/ $\Delta$ 19</sup> cell lines, suggesting a heterogeneous maintenance of the telomeres. It is also substantial in interphase nuclei where whilst in *Rb1*<sup>+/+</sup> (Figure 43b) all the telomeric signal have similar intensities, in *Rb1*<sup>+/ $\Delta$ 19</sup> heterogeneity in the signals is seen and even undetected at times (Figure 43c).

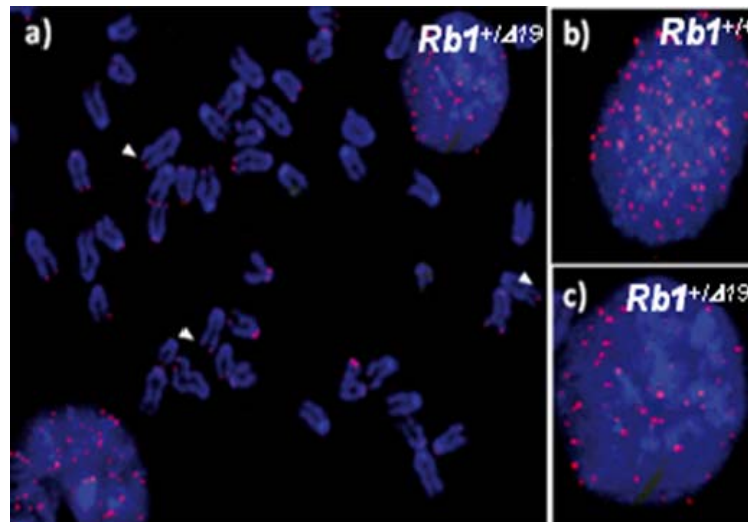


**Figure 43: Heterogeneous signals of *Rb1*<sup>+/ $\Delta$ 19</sup>.** a) Metaphase spread showing heterogeneous fluorescence intensity of the PNA-Cy3 probe on telomeres. b) *Rb1*<sup>+/+</sup> representative interphase nuclei with homogeneous telomeric signals. c) *Rb1*<sup>+/ $\Delta$ 19</sup> representative nuclei showing heterogeneous telomeric signals.

#### 4.11 Reduced telomeric signal numbers in *Rb1*<sup>+/ $\Delta$ 19</sup> osteoblasts

PNA speckles were visually counted in 35 interphase nuclei in passage 10. *Rb1*<sup>+/ $\Delta$ 19</sup> nuclei had less visual PNA speckles when compared to *Rb1*<sup>+/+</sup> osteoblasts suggesting not only telomeres with reduced length, but complete ablation of telomeres in certain chromosomes (as shown in figure 43c). As shown in figure 48, the average number of detectable individual telomere signals was 102 (+/- 5) in *Rb1*<sup>+/+</sup> cells, but only 43 (+/- 14) in *Rb1*<sup>+/ $\Delta$ 19</sup> cells. A normal mouse cell with 19+2 chromosomes should have 84 telomeres in G1/G0 phase, 168 telomeres in G2 phase and an intermediate number of signals during S-phase. Taking into account the cell-cycle distribution measured at 0 Gy (Figure 31) one can estimate that an intact, non-synchronized cell culture should have on average 108 telomeres (using the percentage of cells in each phase of the cell cycle on figure 31). The average of 102 telomere signals detected in *Rb1*<sup>+/+</sup> (Figure 44) interphase nuclei, at passage 8, suggests that our detection method is very well in line with this theoretical number.

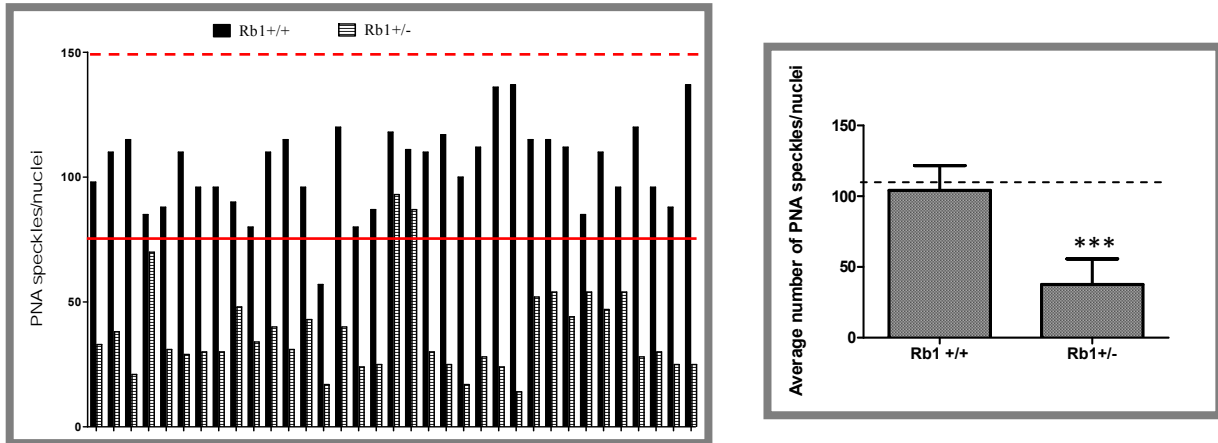


**Figure 44: Distribution and average of PNA speckles at passage 8.** **Left Panel:** shows distribution of the PNA signals in the 35 cells for both genotypes,  $Rb1^{+/+}$  (black bars) and  $Rb1^{+/\Delta 19}$  (dashed bars). The average signals at G1 (red line) and at G2 (dashed red line) are also shown. **Right panel:** Average of speckles signals counted per cell showing a significant decrease in the  $Rb1^{+/\Delta 19}$  cells, showing the average of 108 telomeric signals in a asynchronous population (dashed line) in wt cells.

#### 4.12 Telomere length differences between $Rb1^{+/\Delta 19}$ and $Rb1^{+/+}$ increase with aging

Using Flow FISH we determined the total telomeric signals per nuclei in a large number of cells (20.000 cells). Although the information about telomere length of individual chromosomes is lost, this method has the advantage of distinguishing cells. By gating only for G1 phase cells and recording their telomere signal a reduction on telomeric length could be seen in  $Rb1^{+/\Delta 19}$  osteoblasts as compared to  $Rb1^{+/+}$  cells.

In figure 45 we can see how the method detects telomeric shortening when analysing  $Rb1^{+/+}$  cells at different passages (aged) and how MC3T3, a known *tert* activated cell line, maintains telomeric length.

As shown in figure 46 the average telomeric length of  $Rb1^{+/\Delta 19}$  population had shorter telomeres (already by passage 5) than  $Rb1^{+/+}$  cells. With aging, the dynamics of shortening were found to be faster than in the  $Rb1^{+/+}$  and more prominent. By passage number 18,  $Rb1^{+/\Delta 19}$  cells had a telomere signal reduction by more than half relative to passage 1 and also relative to their wild-type counterparts.

These experiments demonstrate the faster dynamics and more prominent telomere attrition in  $Rb1^{+/\Delta 19}$  osteoblasts as compared to  $Rb1^{+/+}$  cells.



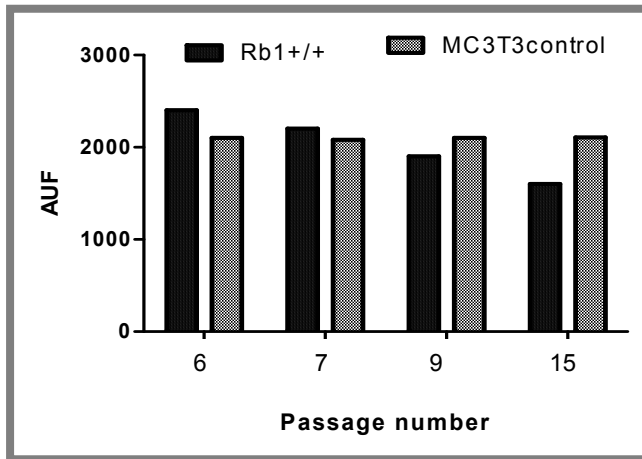


**Figure 45: *Rb1*<sup>+/+</sup> telomeric length decreases with increasing passage number:** aging osteoblasts (full black bars) lose telomeric length with aging whilst MC3T3 (*tert*<sup>+</sup>) (hatched) maintain telomeric length when aging.

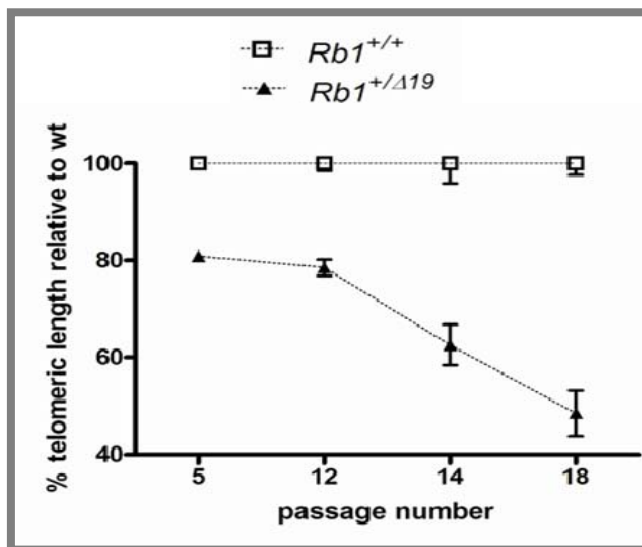


**Figure 46: Dynamics of telomeric shortening in both genotypes.** Shortening of the telomeres in *Rb1*<sup>+/Δ19</sup> osteoblasts was found increased relative to their wild-type counterparts. G1 cells were gated for analysis stained with PI, and the telomeric signals were detected with a PNA-FITC probe. Average fluorescence of a gated G1 population for both genotypes was used as telomeric length determinant. *Rb1*<sup>+/Δ19</sup> telomeric length relative to wild-type counterparts was accounted for each passage, showing the more pronounced loss of telomeric sequence in the *Rb1*<sup>+/Δ19</sup> haploinsufficient osteoblasts for each passage. Data are from two biological replicates.

#### 4.13 Telomeric shortening is independent of radiation exposure

The FACS FISH technique was also employed to assess telomeric length for both genotypes after X-ray exposure. Interestingly, radiation exposure did not cause a detectable reduction of the telomere length 48 hours after exposure, in either *Rb1*<sup>+/Δ19</sup> or *Rb1*<sup>+/+</sup> (Figure 47).

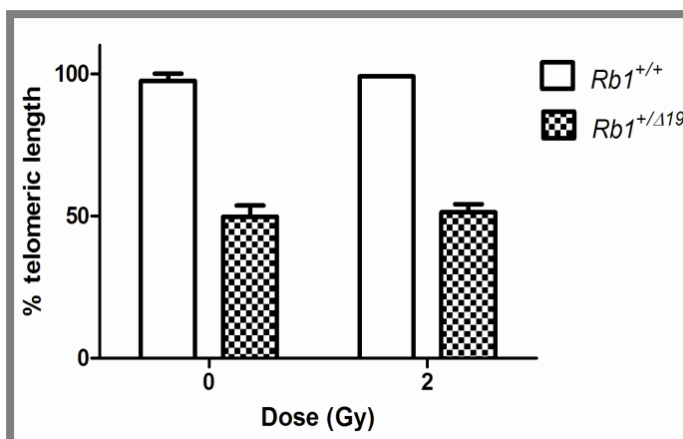


**Figure 47: Telomeric Flow-FISH.** Cells exposed to radiation showed the same length as the controls for both *Rb1*<sup>+/+</sup> and *Rb1*<sup>+/Δ19</sup>. Analysis performed 48 hours after radiation exposure. 3 biological replicates were used for this experiment at passage 8 (SD of 3 biological replicates).

#### 4.14 Telomeric measurements using RealTime-qPCR show telomeric reduction in *Rb1*<sup>+Δ19</sup> compared to *Rb1*<sup>+/+</sup>

Results showed, in agreement with Flow-FISH hybridizations that *Rb1*<sup>+Δ19</sup> harbours shorter telomeres when compared to its wild-type counterpart at the same passage, as seen in figure 48.

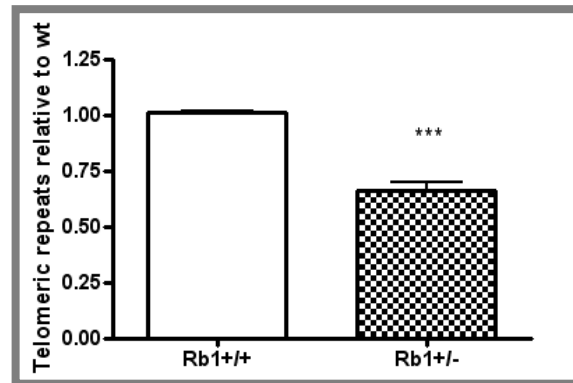


**Figure 48: Quantitative genomic PCR** for telomeric length was performed using (TTAGGG)<sub>n</sub> primers. D14-192 (microsatellite flanking region) was used as housekeeping gene. *Rb1*<sup>+Δ19</sup> cells showed an decrease of about 30% at passage 10 correlated to the results of the flow FISH. SD of 3 biological replicates with 2 technical replicates (t-test; p≤0.0001).

#### 4.15 sh*RB1* ablation in both *Rb1*<sup>+/+</sup> and *Rb1*<sup>+Δ19</sup> in murine osteoblasts *in vitro* leads to shorter telomeres

The stable knock down of *Rb1* with specific anti-*Rb1* shRNA transduced by lentiviral vector into *Rb1*<sup>+/+</sup> and *Rb1*<sup>+Δ19</sup> osteoblasts, resulted in a reduction of *Rb1* mRNA expression (Figure 49). In both *Rb1*<sup>+/+</sup> and *Rb1*<sup>+Δ19</sup> cells the expression level of the *Rb1* wild-type (wild-type *Rb1* taq-man probe Exon17) transcript dropped to about 20% of the original levels.

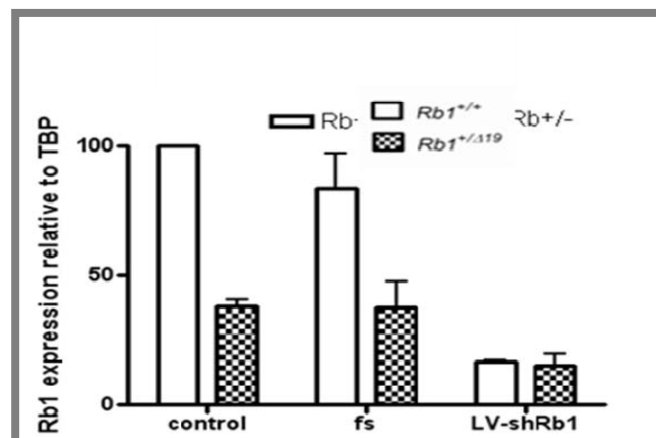


**Figure 49: Reduction of *Rb1* mRNA levels after infection with an antisense sh*RB1*.** Taqman assay shows how *Rb1*<sup>+/+</sup> present high levels of the *Rb1* until knock down by the lentivirus (LV-sh*RB1*). *Rb1*<sup>+Δ19</sup> controls show the expected reduction on messenger level that is further reduced after lentiviral infection with sh*RB1* sequence. Scramble was a second control infected with lentivirus with scramble RNA (SD of 2 biological replicates with 2 technical replicates each).

*Rb1*<sup>-/-</sup> cells had clear indications of telomere shortening as early as 3 passages after infection of *Rb1*<sup>+/+</sup> and *Rb1*<sup>+/ $\Delta$ 19</sup> cells with the LV-sh*RB1* (Figure 50). 3 passages after infection, *Rb1*<sup>-/-</sup> cells, both those arising from of *Rb1*<sup>+/+</sup> or *Rb1*<sup>+/ $\Delta$ 19</sup> cells, as shown in figure 55, harvest similar average telomeric length after the knock down of *Rb1*.

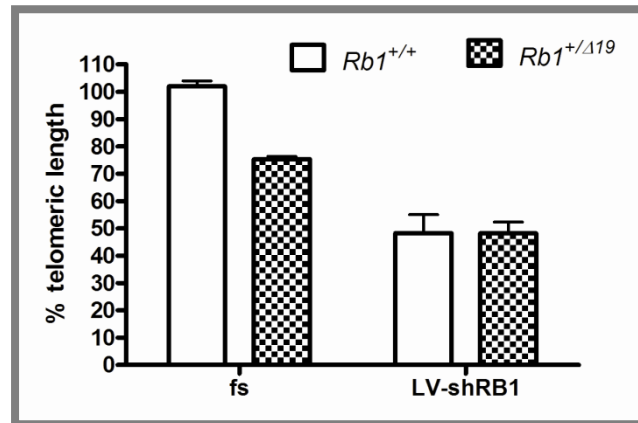


**Figure 50: Telomeric length 3 passages after LV infection using Flow-FISH.** Figure shows telomeric length changes in primary osteoblasts after infection with sh*RB1*. Reduction of *Rb1* mRNA led to shorter telomeres 3 passages after infection in genotypically *Rb1*<sup>+/+</sup> and *Rb1*<sup>+/ $\Delta$ 19</sup> cells. 2 biological replicates with 3 technical replicates were analysed (SD).

#### 4.16 Cloning and expression of *RB1* into osteoblasts for recovery of the *Rb1* status

For a stable expression of the *Rb1* gene in our system to rescue the mutant cells and study the telomeric dynamics, a lentiviral system was developed using human *RB1*. The cloning strategy is explained in methods.

##### 4.16.1 PCR screening

Initial screening of colonies for integration of *RB1* was carried out by PCR. Using the IRAT forward primer donor vector and the reverse1 designed for the *RB1* sequence we detected the positive clones out of 50 colonies sampled using the *Rb1* PCR conditions shown before (Figure 51).

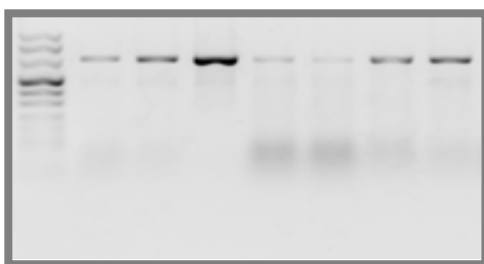


**Figure 51: PCR screening products.** Positive signal for those colonies carrying the *RB1* expression plasmid. For detection, primers previously designed for *RB1* sequencing, such as, IRAT *RB1* cloning forward long and cDNA rev1 were used. Showing in this picture 7 clones positive for the PCR screening. Lane 1: marker VIII, 7 subsequent lanes positive clones for PCR screening 750 bp).

##### 4.16.2 Enzymatic screening

To further verification of the expected sequence of the construct, enzymatic restriction screening to identify the right clone was performed:

Those colonies positive for the *RB1* PCR screening, underwent a restriction digestion with both *EcoRI* (present once both in insert and vector) as well as with the cloning enzymes *BamHI* and *NotI* to check replenishment of the restriction sites after ligation (Figure 52).

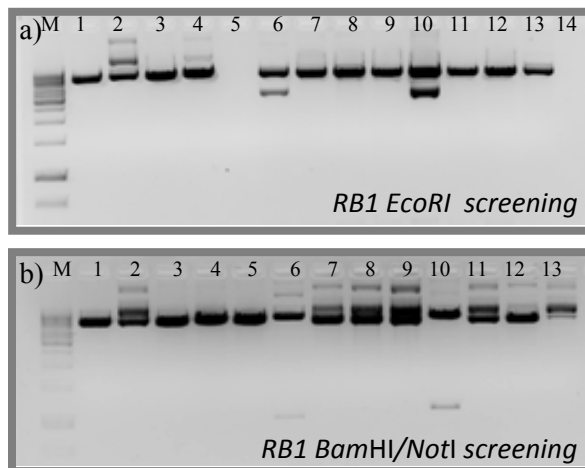


**Figure 52: Enzymatic restriction screening.** Panel a) shows screening of colonies with *BamHI* and *NotI*. Only two of the colonies shown here show a double band, being those the right ones, in the case of the 13 colonies that underwent restriction checking only number 6 and number 10 were positive for the right restriction pattern. Lane 1: marker VIII, 13 subsequent lines, clones under screening. Most colonies were negative for the right pattern except numbers 6 and 10 which maintained both recognition sites, for *BamHI* and *NotI* intact. Panel b) Same set of colonies screened with *EcoRI* showing the same two colonies, 6 and 10, to be the right ones, with two bands (one very small ~100bp), since the vector harvests one site and the insert another one for *EcoRI* recognition very close to each other. This experiments showed the two colonies 6 and 10, which were sequenced for *Rb1* completely, and then used for virus production.

Transient expression of the newly cloned *LV-RB1* lentiviral expression plasmid led to over expression of the *RB1* gene in HEK293T cells.

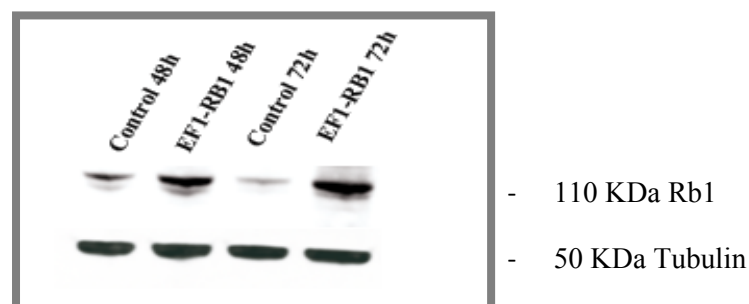


**Figure 53: Transient expression of the LV-*RB1* vector.** Transfection performed using lipofectamine showed an increase in *RB1* expression in HEK293T cells after 48 and 72 hours. Lanes 1 and 3 are the controls at 48 and 72 hours respectively, and lanes 2 and 4 the overexpressed *RB1* cells after 48 and 72 hours.

## 4.16.3 Primary osteoblast infections with lentivirus:

*Rb1*<sup>+/ $\Delta$ 19</sup> osteoblasts at passage 8 were infected with the *LV-RB1* virus using polybrene, and a light centrifugation to maximize the contact between cells and viral particles in order to increase transduction efficiency.

90 hours after infection GFP intensity was measured using FACS. As indicated in the titration table below (Table 4.16.1) we can see how the virus properly integrated in the cells in a concentration dependent manner and it was detectable up to 7 weeks after infection.

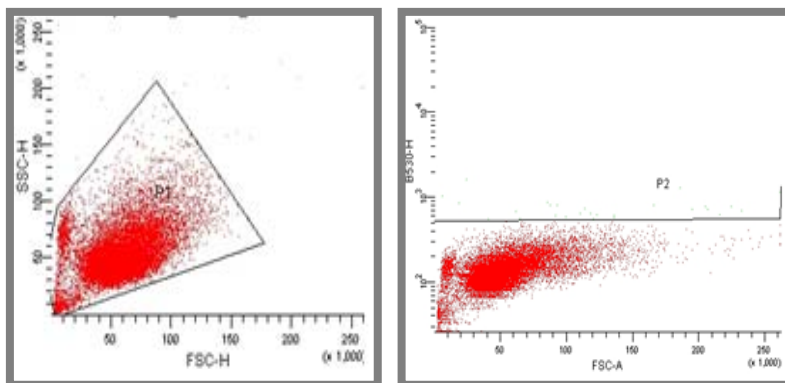


**Figure 54: Control cells.** Uninfected primary osteoblasts at passage 8 showing no GFP fluorescence. **Left panel:** Whole population in side (Y) and forward(x) scatter. **Right panel:** Whole population in red without fluorescent levels at 530 nm (green).

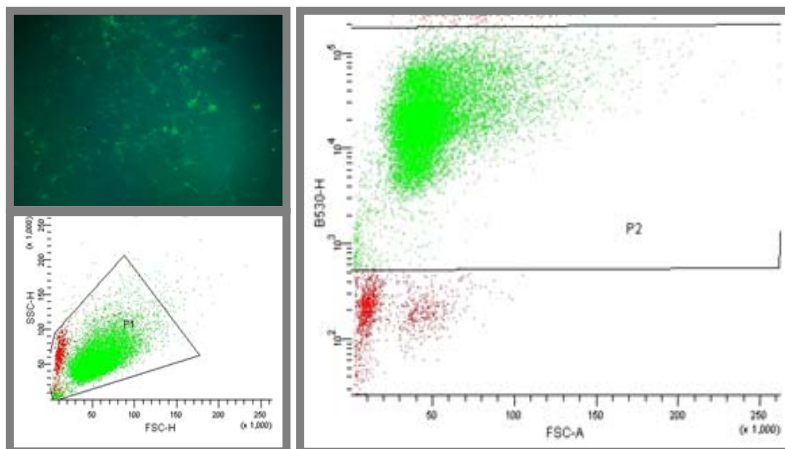


**Figure 55: Undiluted infected primary osteoblasts 90 hours after infection.** The GFP (+) cells account for 95% of the population. **Upper left panel:** Fluorescent picture of positive osteoblasts for GFP after infection. **Lower left panel:** Whole population in side (Y) and forward (X) scatter. **Upper right panel:** Whole population in red with fluorescent levels at 530 nm (green). P2=95%.

**Table 4.16.1: Titration experiments with primary osteoblasts** showing a GFP fluorescence intensity that matches the concentration of the virus and shows that the integration is stable for at least 3 weeks and detectable up to at least 7 weeks.

Titration	90 hours	3 weeks	7 weeks
Control	0%	0.1%	0.1%
Undiluted virus	95%	91.7%	30%
10 <sup>-1</sup> virus	24%	20%	-
10 <sup>-2</sup> virus	8%	7%	-

4.16.4 Taqman results for *Rb1*<sup>+/ $\Delta$ 19</sup> cells after infection showed increase in *RB1* expression:

Differential *Rb1*/*RB1* probes for mouse and human cDNA were used since we infected mouse cells with human *RB1*. cDNA was synthesised using conventionally extracted RNA and revealed that *Rb1* transcription remained constant both in control and infected cells whilst *RB1* transcripts of the infected cells, increased when compared to uninfected controls, demonstrating the expression of *RB1*. Cycle thresholds (Cts) for both *Rb1* and *RB1* genes were quantified (using  $\Delta\Delta$ Ct method for taqman quantification) 72 hours after infection and 3 weeks after infection, as shown in the table below (table 4.16.2).

**Table 4.16.2: Shows the levels of *RB1* messenger increased after infection with LV-*RB1*.** 72 hours after infection levels were very high and subsequently reduced 3 weeks after infection as seen in both last columns. The first two rows show the data for mouse *Rb1* and the two last rows show the data for *RB1* Human, showing high expression of *RB1* in those cells infected with LV-*RB1*.

Genotype	Ct <i>Rb1</i>	Ct <i>TBP</i> mouse	Expression 72h	Expression 3 weeks
<i>Rb1</i> <sup>+/<math>\Delta</math>19</sup> control	28,69	25,49	1	1
<i>Rb1</i> <sup>+/<math>\Delta</math>19</sup> LV- <i>RB1</i>	29,08	25,86	0,986	1,1
	Ct <i>RB1</i>	Ct <i>TBP</i> mouse	Expression 72h	Expression 3 weeks
<i>RB1</i> <sup>+/<math>\Delta</math>19</sup> control	36,68	25,49	1	1
<i>RB1</i> <sup>+/<math>\Delta</math>19</sup> LV- <i>RB1</i>	21,8	25,86	38967,94	675,58

4.16.5 Protein levels show *RB1* expression

Three weeks after LV-*RB1* infection the total protein levels of *Rb1*/*RB1* proteins were increased to about 1.6 fold relative to untreated *Rb1*<sup>+/ $\Delta$ 19</sup> cells, as shown in figure 56.

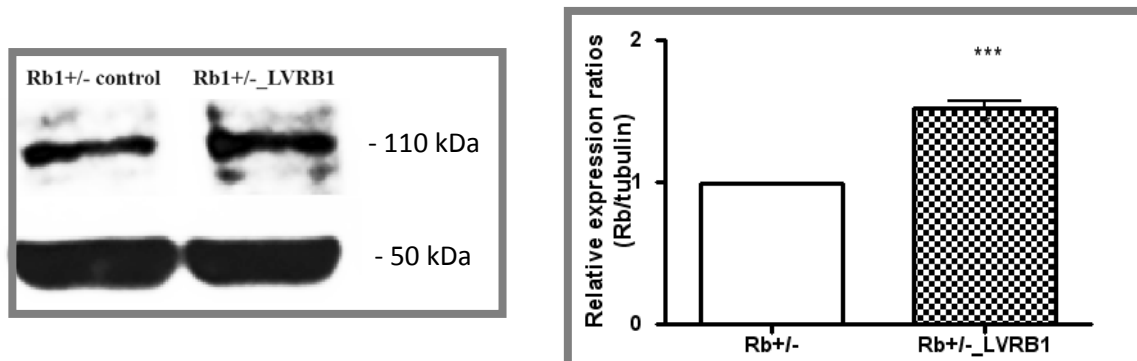


**Figure 56: Total retinoblastoma protein (*Rb1*/*RB1*) immunoreactivity and its quantification.** Left: Western blot for *Rb1*/*RB1* (110 kDa) 3 weeks after infection *RB1*-expressing Lentivirus using mAb that detects both human and mouse protein. G-tubulin (50 kDa) was detected as loading control. Right quantification (using ImageQuant) for 3 biological replicates with 2 technical replicates each (t-test \*\*\* ( $p \leq 0.0001$ )).

#### 4.17 Rescue of *Rb1*<sup>+/ $\Delta$ 19</sup> phenotype by *RB1* expression prevents loss of telomere length

Expression of *RB1* in primary osteoblasts showed a less severe telomere reduction when compared to the untreated *Rb1*<sup>+/ $\Delta$ 19</sup> cells.

Three biological replicates showed a better maintenance of the telomeres after recovering the phenotype inferred by the germline mutation in *Rb1* 3 and 6 passages after infection (as shown in figure 57). These data indicates maintenance of the telomeres rather than replenishment of such structures when recovering the *Rb1* phenotype caused by germline haploinsufficiency.

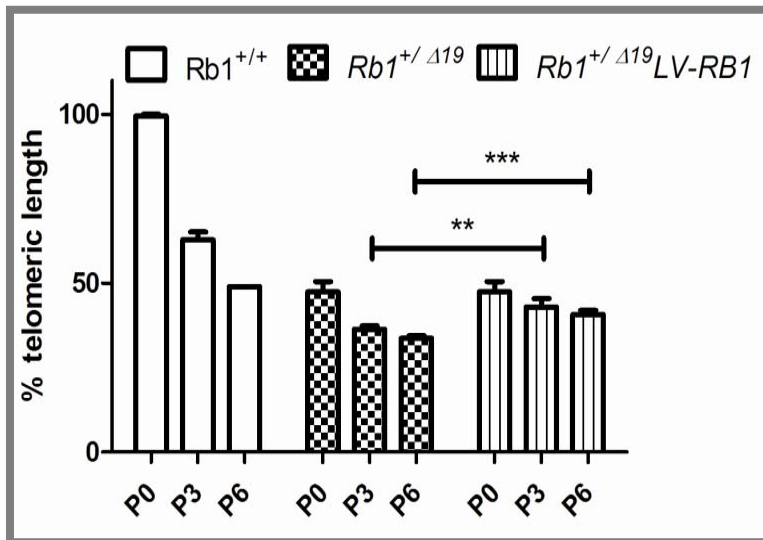


**Figure 57: Shows better telomere maintenance after partially replenishing *RB1* protein (LV-*RB1*).** Analysis performed by Flow-FISH. Shows the telomeric length differences between wt, mutant cells and those cultures infected with LV-*RB1*, 0, 3 and 6 passages after infection. Cells were at passage 8 when the experiment started (SD of 3 biological replicates, t-test for p3: \*\* $p \leq 0,01$  and for p6: \*\*\*  $p \leq 0,001$ ).

#### 4.18 Rescue of *Rb1* haploinsufficiency leads to a reduction of segregational defects

To assess whether the restoration of *Rb1* and hence telomere length led to the expected reduction in genomic instability we measured the sporadic rate of anaphase bridges. A reduction in segregational defects was evident at 6 passages after infecting cells with lentiviral *RB1* vector. As shown in figure 58, lane 2 showed increased defects in *Rb1*<sup>+/ $\Delta$ 19</sup> haploinsufficient cells, whilst lane 3 shows restoration of levels after expression of *RB1*.

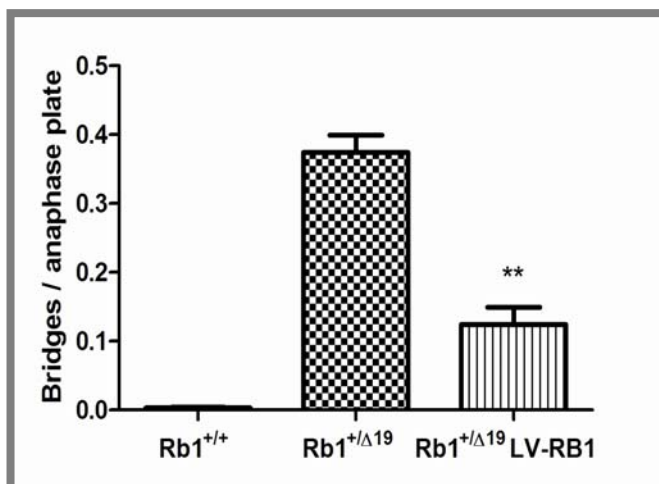


**Figure 58: Shows the reduction of segregational defects in *Rb1*<sup>+/ $\Delta$ 19</sup> cells when recovering its haploinsufficiency.** 50 anaphase plates of 2 biological replicates were assessed to check whether the better maintenance of the telomeres in LV-*RB1* infected cells led to a reduction of the segregation defects shown in the genomic instability sub-chapters. Indeed replenishment of the *Rb1* protein led to less segregational defects, both when compared to the uninfected *Rb1*<sup>+/ $\Delta$ 19</sup> cells as well as when compared to *Rb1*<sup>+/+</sup>. Note that the anaphase bridges are given here by anaphase plate. (SD of 2 biological replicates, t-test \*\*  $p \leq 0,01$ ).



#### 4.19 Telophase bridges present in *Rb1*<sup>+/ $\Delta$ 19</sup> as well as in osteosarcoma cell lines present several telomeric sequences along the bridge

The analysis of the telophase bridges present in *Rb1*<sup>+/ $\Delta$ 19</sup> cells, as well as in those present in mouse osteosarcoma (MOS) cell lines showed several telomeric signals along the bridges when using a telomeric specific PNA probe.

As shown in figure 59 b,c and d, MOS cell lines have several telomeric signals along the telophase bridges. In 59b and c, paired signals are visible, suggesting telomeric bridges arising from sister chromatids. Those cells presenting anaphase/telophase bridges populate the MOS cultures (in some cell lines up to 90% of the culture), showing that the defects are persistent over generations. In figure 59a, an example of bridges found in old *Rb1*<sup>+/ $\Delta$ 19</sup> osteoblasts (passage 15), presenting 2 telomeric signals along the bridge, feature not found in *Rb1*<sup>+/+</sup>.

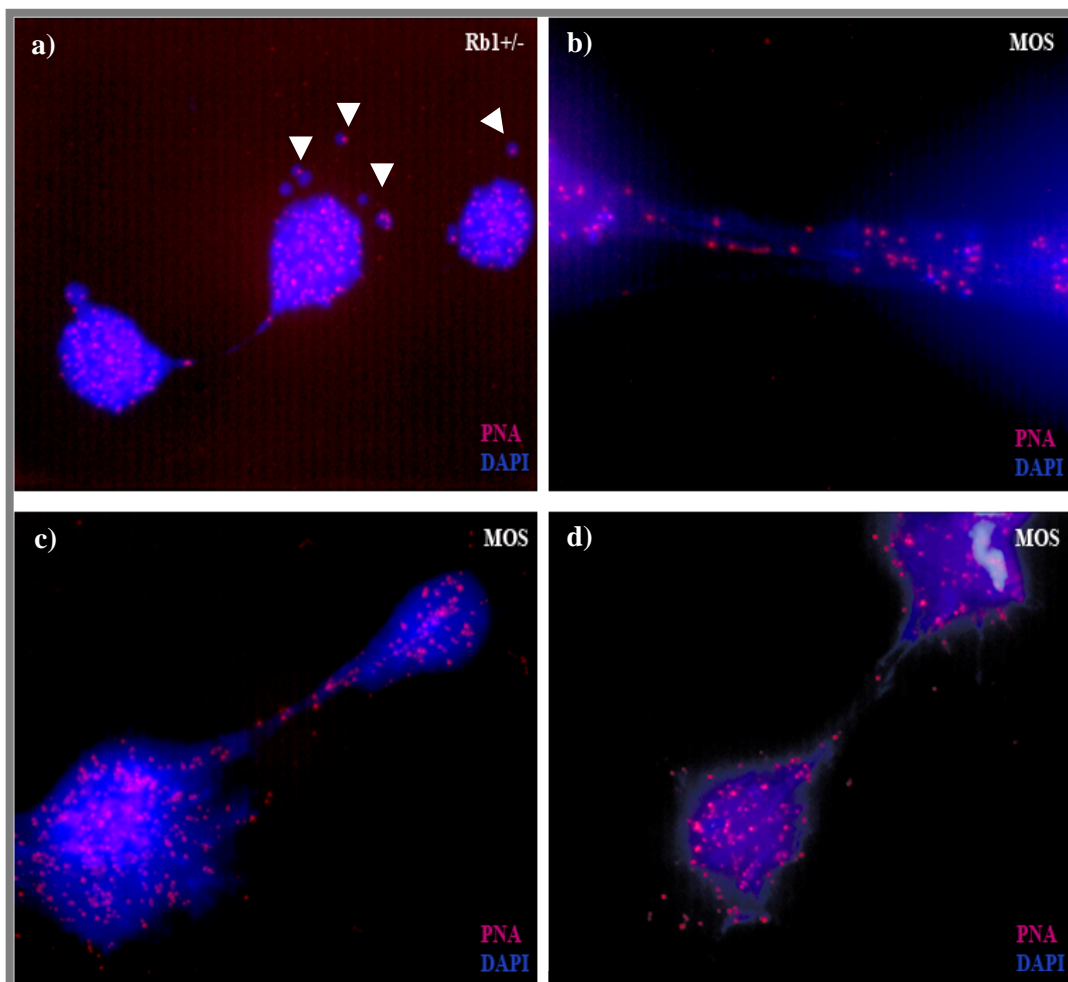


**Figure 59: Telophase bridges present in *Rb1*<sup>+/ $\Delta$ 19</sup> osteoblasts and MOS cell lines with several telomeric signals along the bridge.** a) Telophase bridge and MN (arrowheads) presenting telomeric sequences in old *Rb1*<sup>+/ $\Delta$ 19</sup> osteoblasts, passage 15, 48h after exposure to 2 Gy. 3 different MOS cell lines (figures b, c and d) show telophase bridges with several telomeric signals along the bridge (40x).



Note in figure 59a, the existence of several acentric fragments (MN) surrounding cell nuclei and that most of them carry telomeric sequences (arrowheads), suggesting the telomeric areas as a “hotspot” of damage in the *Rb1*<sup>+Δ19</sup> cells, which also points to BFB cycles that will lead to losses of DNA around the telomeres. When quantifying the amount of telomeric signals present in the acrocentric fragments (MN) of the *Rb1*<sup>+/+</sup> and *Rb1*<sup>+Δ19</sup> where up to 70% of the acentric fragments carried at least one telomeric signal. We discovered that more telomeric sequences and more frequently appear in the acentric fragments of the *Rb1*<sup>+Δ19</sup> osteoblasts (Figure 60).

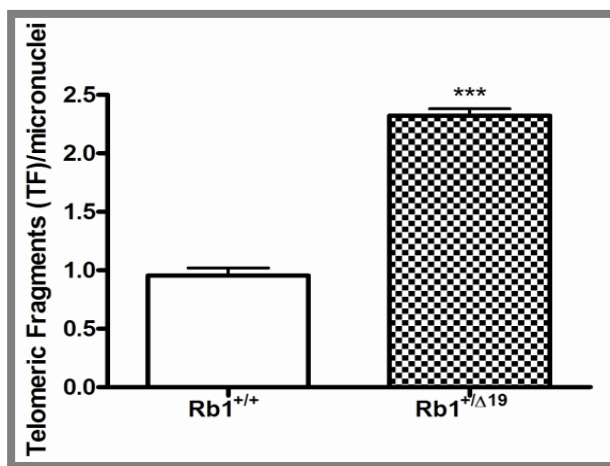


**Figure 60: Telomeric sequences present in MN in *Rb1*<sup>+/+</sup> and *Rb1*<sup>+Δ19</sup>.** Quantification of PNA signals (telomeres) present in 400 acentric fragments (MN) in osteoblasts from *Rb1*<sup>+/+</sup> and *Rb1*<sup>+Δ19</sup> at passage 11. Higher amount of telomeric signals have been recorded in *Rb1* haploinsufficient cells suggesting the telomeric areas as a “hotspot” of damage in the *Rb1*<sup>+Δ19</sup> cells.

#### 4.20 Telomere shortening in *Rb1*<sup>+Δ19</sup> cells and activation of ALT pathway

In the course of serial passaging *Rb1*<sup>+Δ19</sup> osteoblasts from two different biological cases showed the appearance of morphologically atypical cells. Beginning at late passages, these cells started to overgrow the mono-cell layer and formed colonies of more spindle like cells (Figure 61). After additional passages, such heterogeneous cultures were dominated by this new type, which grew faster with apparent loss of contact inhibition.



**Figure 61: Transformed *Rb*<sup>+Δ19</sup> cells in culture.** 2 examples of osteoblast cultures with regions of transforming cells. At late passages (in this example passage 15) cells started to lose their cell to cell adhesion and started growing in an uncontrolled manner. Arrows point to uncontrolled growth areas in the flask. **Left:** 3 days after passaging (passage 15). **Right:** 4 days after passaging (passage 15) showing a group of cells which lost contact inhibition (arrow).

This process coincided with the moment when the cells of the monolayer harboured potentially critical short telomeric length (short telomeres 5 passages before as shown in figure 62) and went into crisis (as seen by a drop of clonogenicity after plating and change in cell-morphology towards a flat shape with an increased area). These morphologically altered cells exhibit a sharp increase in their telomere length (Figure 62), which is not unusual for cells undergoing malignant transformation. Since osteosarcoma are a prototype of tumour activating the ALT mechanism instead of telomerase expression, we used then for comparison, to find out that the telomeric length of the *in vitro* transformed cells and the MOS cell lines were comparable. This findings show therefore that critically short telomeres in *Rb1*<sup>+/ $\Delta$ 19</sup> osteoblasts led to transformation and ALT activation.

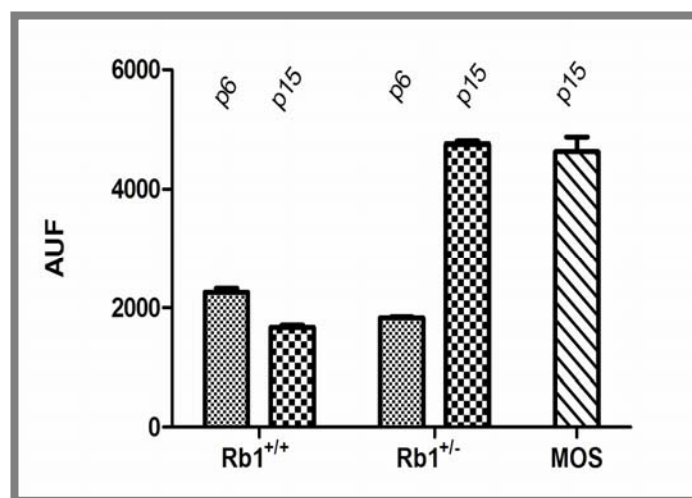


**Figure 62: Telomeric length is replenished by potentially activating ALT in *Rb1*<sup>+/ $\Delta$ 19</sup> cells undergoing spontaneous transformation.** Two biological replicates reached crisis during culture increasing telomeric length as revealed by Flow-FISH to levels of those reached by MOS cell lines, known to be ALT +, and above early passages of the same culture (SD for 2 biological replicates with 2 technical replicates each).

#### 4.21 ALT activated osteoblasts lost p53 via point mutation *in vitro* and induced fast tumourigenesis

To understand the molecular trigger responsible for the spontaneous *in-vitro* transformation of some *Rb1*<sup>+/ $\Delta$ 19</sup> osteoblasts they were analyzed for p53 mutations a known candidate gene to be mutated when cell cycle is disregulated. Aside the dramatic elongation of the telomeres, *in vitro* cultured cells acquired a p53 point mutation as found by sequencing genomic DNA (Figure 63). The point mutation was found to be a G for an A, in exon 8, changing an Arginin (AGA) for a Lysin (AAA) in FVB background. Cells presenting the mutation, overgrew in the culture, as seen in figure 61, early passages still show a mixture of the sequence (Figure 63b dashed arrow) and late passages show only the mutated sequence (Figure 63c).

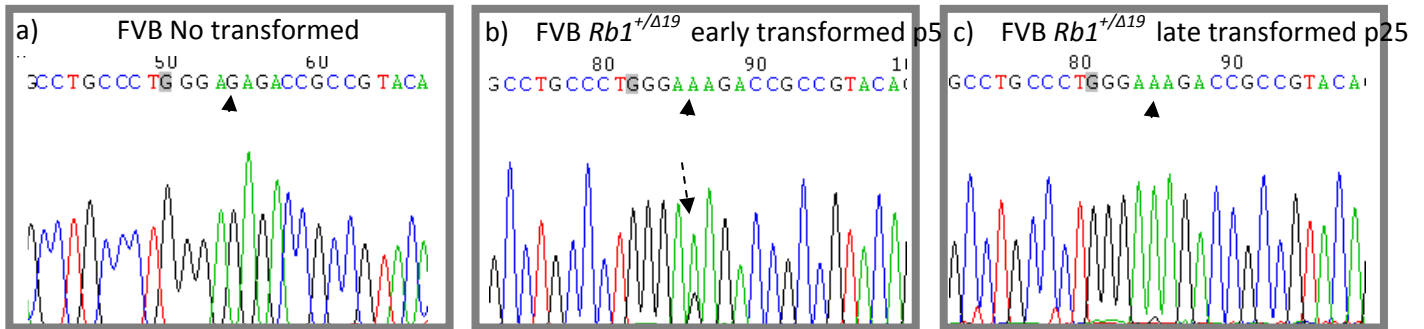


**Figure 63: *p53* spontaneous point mutation acquired during transformation:** *p53* was spontaneously mutated in *Rb1*<sup>+/ $\Delta$ 19</sup> osteoblasts during transformation. a) FVB control cell line (no transformed) carrying the sequence AGA for Arginin (arrowhead). b) Early transformed (passage 5) *Rb1*<sup>+/ $\Delta$ 19</sup> cell line showing a mixture of A and G in the sequence (dashed arrow), but mainly presenting A after transformation. c) Late transformed (passage 25) *Rb1*<sup>+/ $\Delta$ 19</sup> cell line showing the point mutation complete G to A.

Due to the carcinogenic potential of cells with a point mutation in *p53* paired to a mutation in *Rb1*, subcutaneous injections of these cells were performed in immuno competent mice to check for the incidence of tumours and the type of tumour developed.

When  $10^6$  transformed osteoblasts were subcutaneously injected in immuno-competent mice, Osteosarcoma-like tumours grew in 2 weeks after injection as seen in figure 64.



**Figure 64: Subcutaneous tumours arising from transformed cells.** Left: tumour protuberance two weeks after injection of transformed osteoblasts with  $10^6$  cells. Right: X-ray (arrow) showing little mineralisation of the tumour potentially due to the high proliferative state.

#### 4.22 PML-NBs numbers, a marker of ALT activation is elevated in *Rb1*<sup>+/ $\Delta$ 19</sup> cells, and is further increased after *in vitro* transformation

Using immunofluorescence (Figure 65b) PML-NBs were found increased in *Rb1*<sup>+/ $\Delta$ 19</sup> cells when compared to its *Rb1*<sup>+/+</sup> counterparts at the same passage number (passage 8) as seen in the first two bars of figure 65a. *In vitro* sporadically transforming cells (exhibiting elongated telomeres) showed an even greater increased in PML-NBs numbers (third bar in figure 65a), comparable with the numbers seen in a fully transformed osteosarcoma cell line (MOS), as seen in figure 65a, fourth bar. These data suggests that PML-NBs are involved in ALT activation, or telomere damage recognition towards ALT activation.

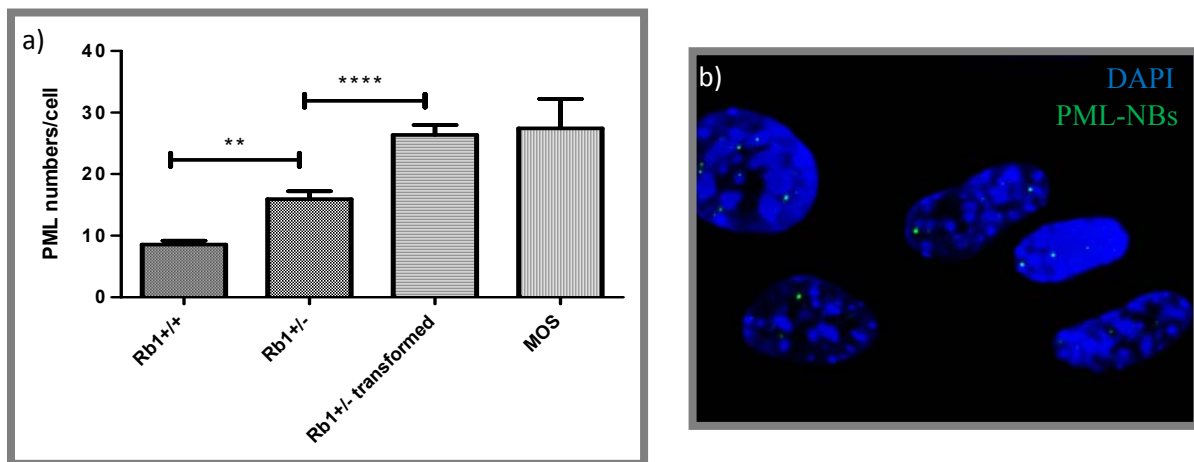


**Figure 65: PML-NBs numbers and *Rb1* genotype are linked.** **a)** *Rb1* haploinsufficient cells showed an increase in PML-NBs numbers, that were even greater increased in the spontaneously transformed cells. 2 biological replicates were used for this calculations following immunofluorescence (SD for 2 biological replicates with 2 technical replicates each). **b)** Immunofluorescence example of PML-NBs staining used for quantification.

Radiation exposure led to a further increase of PML-NBs numbers when comparing *Rb1*<sup>+/+</sup> and *Rb1*<sup>+/ $\Delta$ 19</sup>. As seen on figure 66, PML-NBs numbers increase after radiation exposure. The already increased baseline numbers in *Rb1*<sup>+/ $\Delta$ 19</sup> (Figure 66 at 0 Gy) are increased further after radiation, same effect found on *Rb1*<sup>+/+</sup> cells (Figure 66 at 4 Gy). These data suggests an amplification effect of damage and instability of these cells by radiation.

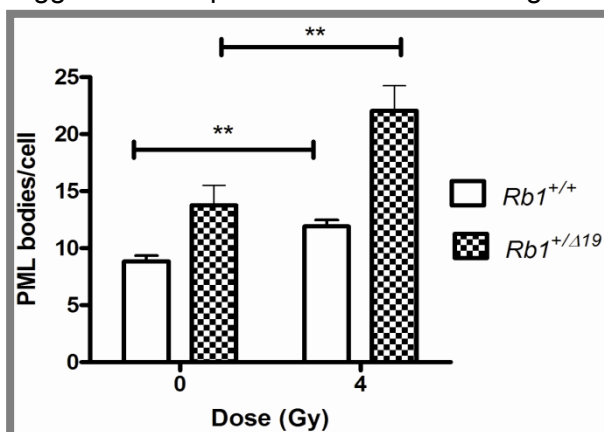


**Figure 66: PML-NBs numbers are increased after radiation exposure.** Quantification of PML-NBs in 200 cells for 2 biological replicates (SD) showed not only a baseline increase in PML-NBs numbers of *Rb1*<sup>+/ $\Delta$ 19</sup> cells (as seen in figure 62a) but also a further increase after 4 Gy of radiation exposure in both *Rb1*<sup>+/+</sup> and *Rb1*<sup>+/ $\Delta$ 19</sup> osteoblasts (SD for 2 biological replicates with 2 technical replicates each).

#### 4.23 PML-NBs numbers are not decreased by expression of *RB1* that rescues decline in telomere length, suggesting that *Rb1* replenishment is not enough to reverse ALT activation

Replenishment of *Rb1* via *LV-RB1* did not cause reduction on PML-NBs numbers. Quantification of PML-NBs numbers 3 passages after infection with *LV-RB1*, showed the same PML-NBs numbers as those present in *Rb1*<sup>+Δ19</sup> haploinsufficient cells used as control for the infection. PML-NBs numbers were elevated in both cultures, therefore, 3 passages after infection, where a telomeric maintenance was seen, does not seem to be enough to reduce PML-NBs numbers. As seen in figure 67, both, *Rb1*<sup>+Δ19</sup> as well as *Rb1*<sup>+Δ19</sup> *LV-RB1* cultures, showed an average of 19 PML-NBs per cell.

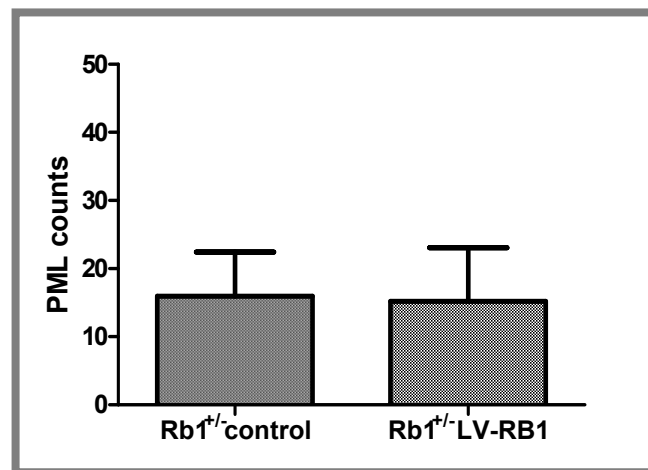


**Figure 67: PML-NBs counts after *Rb1* recovery.** The number of PML-NBs counts was the same for haploinsufficient cells as well as for those infected with *LV-RB1*. Quantification was performed 3 passages after infection. SD of 2 biological replicates.

#### 4.24 Epigenetic markers known to be crucial for telomere maintenance are reduced in $Rb1^{+/Δ19}$ osteoblasts and show a further decrease after irradiation

H4K20-3met levels, an established (Blasco 2007) epigenetic marker of the heterochromatin were reduced in  $Rb1^{+/Δ19}$  when compared to its  $Rb1^{+/+}$  counterparts. As seen in picture 68a and c, a co-culture of  $Rb1^{+/+}$  and  $Rb1^{+/Δ19}$  (stained with Dil for discrimination between genotypes) showed a decrease H4K20-3met fluorescence intensity in  $Rb1^{+/Δ19}$  when compared to  $Rb1^{+/+}$  counterparts, demonstrating a reduction of the methylation on lysine 20 of the Histone 4 in haploinsufficient cultures. Figure 68d shows same co-cultures where  $Rb1^{+/+}$  was Dil stained to ensure that the dye does not affect the immunofluorescence.

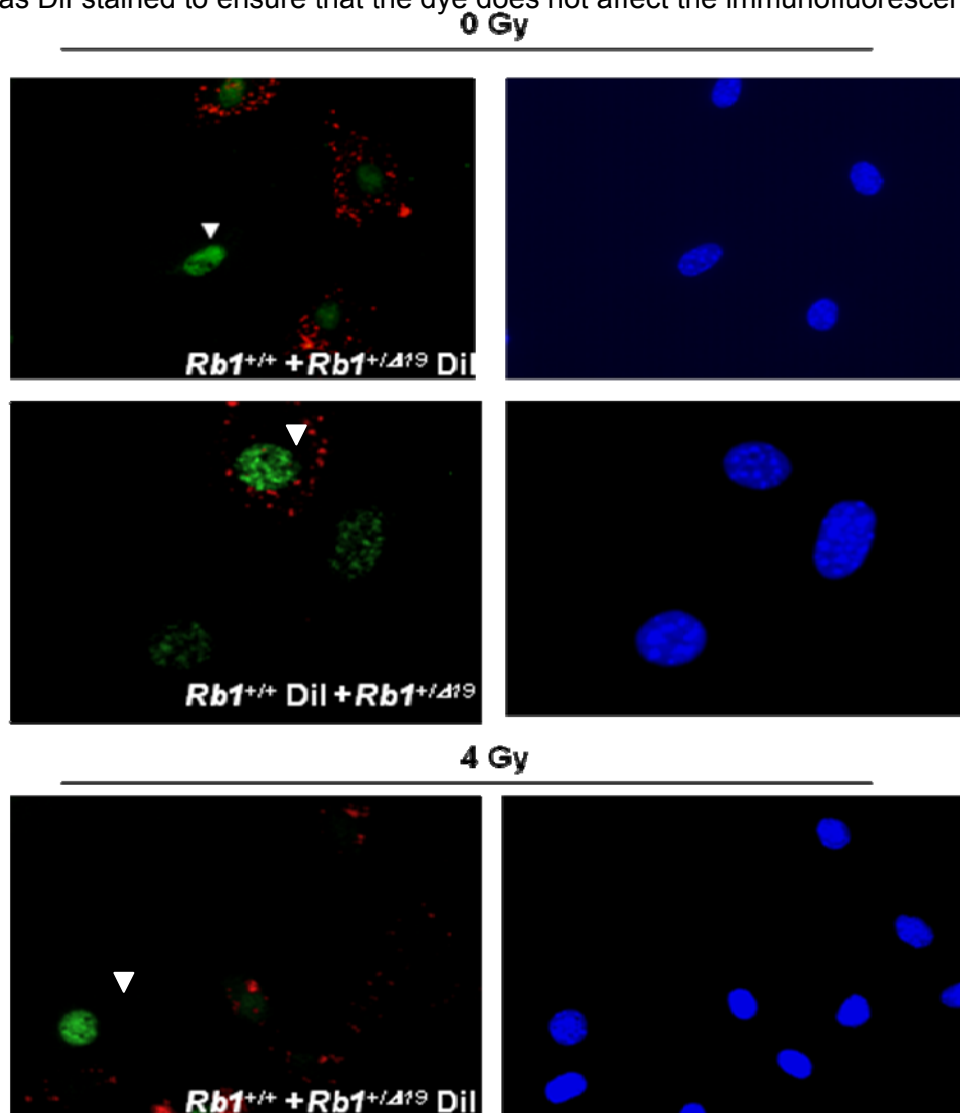


**Figure 68: Immunofluorescence of H4 K20 tri-met in primary osteoblasts.** a) Immunofluorescence detection of 3metK20H4 in primary osteoblasts (*Alexa Fluor 488(green)*). Right panels: Hoechst counterstaining of nuclei of the same image. Upper panel: To allow an accurate comparison of the histone immunolabelling the  $Rb1^{+/Δ19}$  19 cells were prelabelled with Dil (red dye) and mixed with unlabelled  $Rb1^{+/+}$  prior to immunolabelling. Middle panel: Dil-prelabelled  $Rb1^{+/+}$  cells (red dye) were mixed with unlabelled  $Rb1^{+/Δ19}$  cells prior to immunostaining. Arrowheads indicate  $Rb1^{+/+}$  cells. Lower panel: Dil-prelabelled  $Rb1^{+/Δ19}$  cells mixed with unlabelled  $Rb1^{+/+}$  after 4Gy radiation exposure. Immunofluorescence performed 48 hours after exposure.

Western blot analysis, using H4K20 tri-met antibody shows a reduction of the marker in *Rb1* haploinsufficient cells. *Rb1*<sup>+/ $\Delta$ 19</sup> cells showed a decreased signal when compared to the methylation levels of the *Rb1*<sup>+/+</sup> osteoblast, demonstrating a reduction of this marker in *Rb1* haploinsufficient cells (Figure 69).

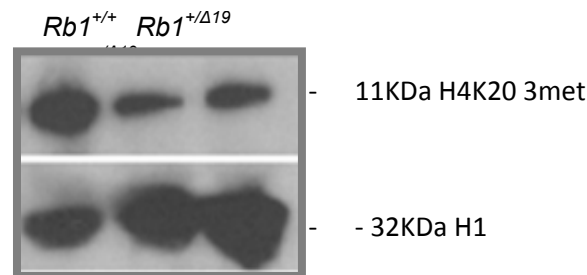


**Figure 69: Western blot of H4K20 tri-met in primary osteoblasts.** Acidic extraction of histones was performed followed by western blotting for H4 K20 tri-met. 2 biological replicates of haploinsufficient cultures are shown here with reduced methylation when compared to their wild-type counterpart. H1 (32KDa) served as loading control.

Average detectable fluorescence levels of H4K20 tri-met quantification showed a decrease in tri-methylation of *Rb1*<sup>+/ $\Delta$ 19</sup> cells when compared to *Rb1*<sup>+/+</sup> and a further reduction of the methylation after radiation for both genotypes, but more prominent for the *Rb1*<sup>+/ $\Delta$ 19</sup> osteoblasts. As seen in figure 70a (as well as in figures 68 and 69) the H4 K20 tri-met baseline levels are reduced in *Rb1*<sup>+/ $\Delta$ 19</sup> cells. A further reduction was observed after radiation exposure to 4 Gy (Figure 70b) where the detectable fluorescence was reduced, suggesting an implication of radiation towards a further loss of such specific methylation.

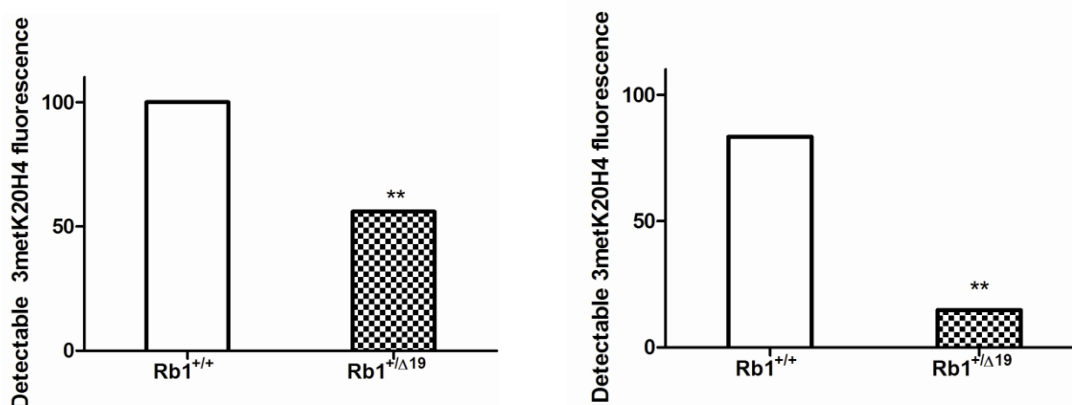


**Figure 70: Detectable levels of H4 K20 tri-met in our osteoblastic cultures.** Left panel: Loss of 3metK20H4 labelling in *Rb1*<sup>+/ $\Delta$ 19</sup> cells at passage 8. Right panel: Increased loss of 3metK20H4 labelling in *Rb1*<sup>+/ $\Delta$ 19</sup> cells at passage 8, 48h after exposure to a single acute dose of 4Gy. Data from two biological replicates. The analysis was performed by assessing fluorescence intensity of the cells from 0 (complete loss of fluorescence) to 4 (highest fluorescence intensity) in microscope slides assessing 250 cells. P value (0.0097) obtained by Gaussian approximation using Mann-Whitney test.

#### 4.25 *Rb1* influence on the H4K20 tri-met fluorescence intensity is not mediated by transcriptional regulation of the enzyme that catalysis H4 K20 tri-methylation

SUV4-20 is the enzyme that catalyses the specific methylation of Lys20 in H4K20 trimethylation (Blasco 2007), to the DNA. Being *Rb1* a transcription factor regulator, we hypothesised that *Rb1* mediated transcriptional regulation of the *SUV4-20h1* could lead to a change in H4 K20tri-met fluorescence. The expression levels of the *SUV4-20h1* protein were identical in *Rb1*<sup>+/+</sup> and *Rb1*<sup>+/ $\Delta$ 19</sup> osteoblasts (Figure 71), as well as sh*RB1* lentiviral infected cells showed the same levels of SUV4 protein being expressed (Figure 71). These results demonstrate that the interaction of *Rb1* with *SUV4-20h1* is not on a transcriptional level.

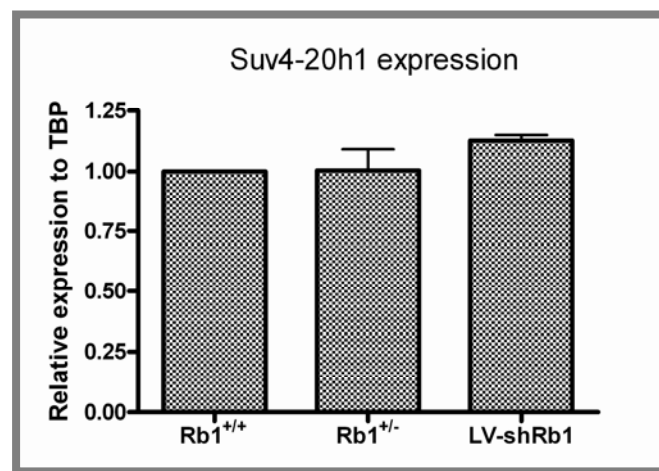


**Figure 71: Transcription levels of SUV4-20 methyl transferase.** The relative expression levels of this enzyme were the same in both *Rb1*<sup>+/+</sup> and *Rb1*<sup>+/ $\Delta$ 19</sup> cells as well as after knocking down *Rb1* with shRNA, when assaying with real time PCR. Analysis performed with 2 biological replicates.

These findings suggest that the regulation of the methylation by *Rb1* has to be via a mechanism other than transcriptional regulation of the SUV4-20h1 methylase by *Rb1*.



### V Evidence of increase tumourigenesis in FVB/N-*Rb1LoxP*: *CreCol* (+) mice after radiation

A cohort of 42 animals from the *Rb1-LoxP* x *col1a1-Cre* mating was established and irradiated using  $\text{Th}^{227}$  a bone seeking  $\alpha$ -emitter.

In such cohort, 18 were FVB/N-*Rb1LoxP*: *CreCol*(-) and therefore *Rb1*<sup>+/+</sup>. The other 24 animals were FVB/N-*Rb1LoxP*: *CreCol*(+) and therefore *Rb1*<sup>+/ $\Delta$ 19</sup>. Altogether in the cohort, 13 animals were diagnosed with osteosarcoma. 11 of the 24 mice that harbour a deletion of one copy of *Rb1* in normal bone developed osteosarcoma (median latency 402 days). Of the 18 mice without this pre-existing *Rb1* deletion in bone, only 2 were diagnosed with an osteosarcoma (median latency 392 days). As shown in figure 72, the latency period for osteosarcoma induction is similar for both genotypes, but the tumour incidence is significantly higher ( $p=4 \cdot 10^{-5}$  Fisher-Yates exact test) in those animals with *Rb1*<sup>+/ $\Delta$ 19</sup> genotype. Figure 72 shows the *Rb1*<sup>+/+</sup> line (full line) with 2 osteosarcoma (full squares) and the comparison to the osteosarcoma incidence in the *Rb1*<sup>+/ $\Delta$ 19</sup> cohort (dashed line) with 11 osteosarcomas (full diamonds). Results showed that the average latency time was not significantly different between genotypes but the tumour incidence was increased in the *Rb1*<sup>+/ $\Delta$ 19</sup> cohort, and the first tumours for each cohort developed with over 80 days difference (as shown below).

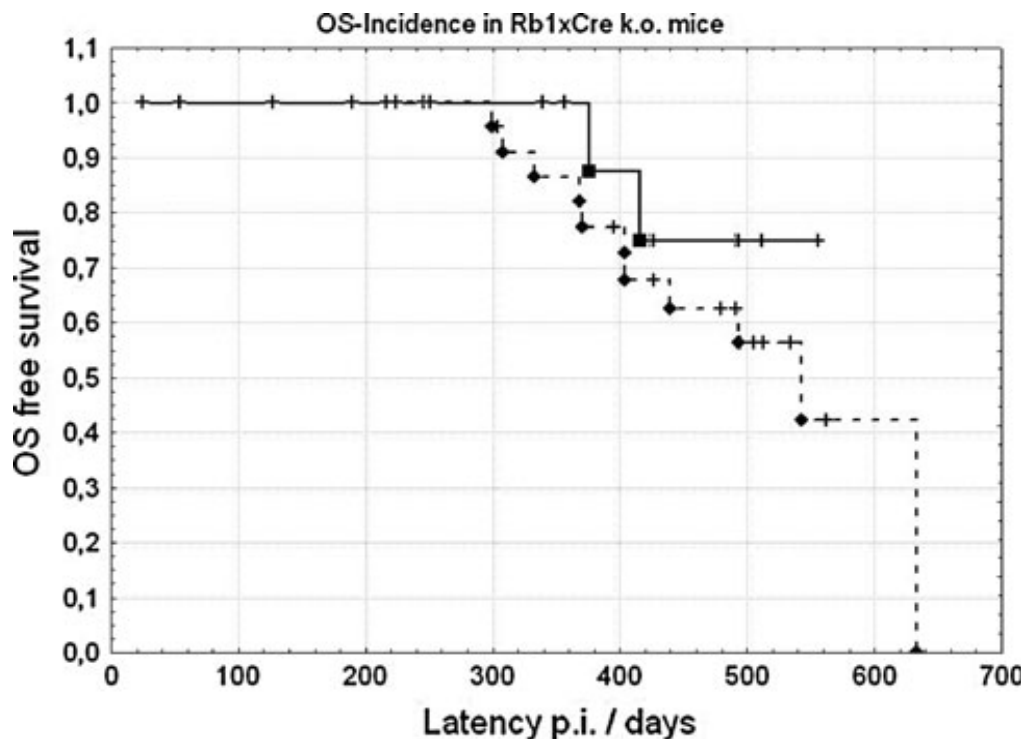


**Figure 72: Kaplan–Meier curve for development of osteosarcoma in female FVB/N-*Rb1LoxP* : *CreCol* mice after  $^{227}\text{Th}$  injection.** All mice carried heterozygote allele of the conditional *Rb1-LoxP* allele. *Full line*: Mice without expression of Cre recombinase. *Rb1-LoxP/CreCol*(-). *Dashed line*: Mice expressing Cre recombinase. *Rb1-LoxP/Cre Col* (+). Radiation derived non osteosarcoma tumours were leukaemias and linfomas. Vertical bars: censored data.

## VI *Rb1* LOH studies of the FVB *Rb1*<sup>+/ $\Delta$ 19</sup> osteosarcomas showed the further loss of the wild-type allele

Out of the 11 animals with osteosarcomas arising from the FVB *Rb1*<sup>+/ $\Delta$ 19</sup> cohort used for tumourigenesis studies after <sup>227</sup>Th incorporation (chapter 2 page 100), a total of 16 tumours (multifocal osteosarcomas) were analysed to investigate whether further loss of the wild-type allele of *Rb1* occurred during tumour development, enhancing the importance of the loss of the *Rb1* tumour suppressor gene during tumourigenesis.

For this analysis we opted for a genomic approach, quantifying allelic copy number using real time PCR of exon 19 (floxed exon, therefore targeting wild-type allele) and exon 17 (pan *Rb1* targeting both wild-type and mutant allele), comparing amplification and melting curves (Figure 73).

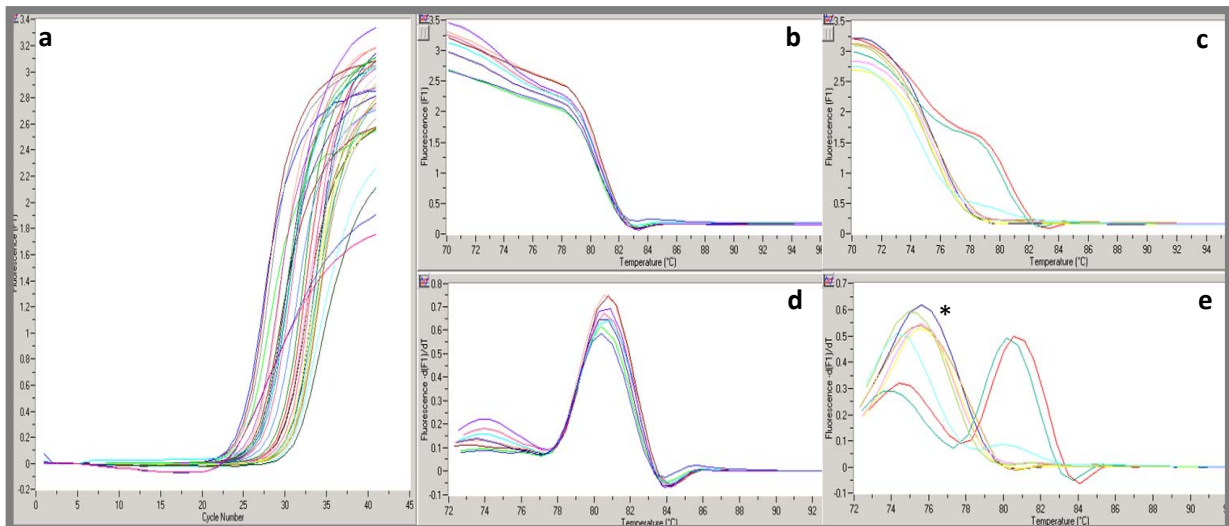


**Figure 73: Real time PCR results showing copy number changes of exon 19.** a) Amplification curves of both tumour and normal tissue samples. b) Melting curves of the normal tissue, c) Melting curves of the tumours showing the two cases that retained (at least partially) exon 19, c) melting peaks of the normal tissue. d) Melting peaks of the tumours showing (arrow head) the only two (in this set of tumours) that retained the wt allele and therefore one copy of exon 19. The other peak (\*) corresponds to the primer dimers peak increased by the lack of template.

Out of the 16 osteosarcomas, 5 arised from *Cre*(-) animals, and are therefore genetically wild type for the *Rb1* gene. Those tumours harvest segmental deletions for *Rb1* retaining about one copy of exon 17, and none of exon 19 (as seen in table 6.1 tumours 1,2,4 and 5) whilst tumour 3 seems to preserve *Rb1* length even though point mutations or other rearrangements can not be discarded.

Of the remaining 11 osteosarcomas arised from *Cre*(+) animals and were therefore genetically *Rb1*<sup>+/ $\Delta$ 19</sup>, 7 completely lost the wild-type allele as no copies of exon 19 were

detected, and only one copy of exon 17 (in table 6.1, tumours 8, 9, 10, 11, 13, 15 and 16) demonstrating LOH of the wild-type allele during osteosarcoma development.

The 4 remaining tumours arising from *Cre*(+) (in table below numbers: 6, 7, 12 and 14 (bold)) showed only partial loss of the remaining wild-type allele.

**Table 6.1: Table showing the 16 tumour cases arising from the <sup>227</sup>Th incorporation cohort.** In those tumours arising from *Cre*(-) only 1 case (osteosarcoma number 3\*) retained the *Rb1* gene completely. Tumours 1, 2, 4 and 5 carry segmental deletions of the *Rb1* alleles, retaining about one copy of exon 17, and none of exon 19. Of the remaining 11 osteosarcomas arising from *Cre*(+) animals, 7 of those tumours completely lost the wt allele as no copies of exon 19 were detected, and only one copy of exon 17 (in Table below, tumours 8, 9, 10, 11, 13, 15 and 16) and the 4 remaining tumours arising from *Cre*(+) (numbers: 6, 7, 12 and 14 (bold)) showed only partial loss of the remaining wt allele, and heterogeneity within the tumour.

Osteosarcoma	Cre status	Exon 17 (expression fold relative to D13mit 262)	Exon 19 (expression fold relative to D13mit 262)
1	-	0,57	≤0,01
2	-	0,68	≤0,01
3*	-	0,85	1
4	-	0,5	≤0,01
5	-	0,83	≤0,01
6	+	<b>0,58</b>	<b>0,44</b>
7	+	<b>0,44</b>	<b>0,33</b>
8	+	0,83	≤0,01
9	+	0,68	≤0,01
10	+	0,5	≤0,01
11	+	0,3	≤0,01
12	+	<b>0,11</b>	<b>0,65</b>
13	+	0,58	≤0,01
14	+	<b>0,30</b>	<b>0,41</b>
15	+	0,26	≤0,01
16	+	0,78	≤0,01

## VI DISCUSSION

Tumours are characterized by complex genetic alterations arising from DNA damage and genomic instability (Anderson et al 2001a, Bohgaki et al 2011, Boyle et al 1998). Genomic instability can be defined as the continuous formation of new structural and numerical chromosome aberrations (Lengauer et al 1998). It has been described as a common hallmark of cancer, where mutational gains and losses are the outcome of an unstable genome that drive the process of malignant transformation (Hanahan & Weinberg 2011). Genomic instability is a frequent feature of both epithelial (Alves Dos Santos et al 2011) and mesenchymal tumours (Deriano et al 2011). It can arise from the inappropriate segregation of chromosomes (Manning et al 2010), chromosomal recombination or unrepaired DNA damage (Bohgaki et al 2011). Genomic instability has been postulated to appear early during tumour progression (Anderson et al 2001b). In the case of familial cancer syndromes, genomic instability have been shown to result from inherited gene defects that lead to impaired DNA repair, failed damage recognition or loss of cell cycle checkpoints (Anderson et al 2001b). The complete list of genes whose mutation leads to the generation of genomic instability for each tumour type remains unknown.

Most leukaemia and also some solid tumours display complex chromosome alterations, including both non-balanced structural and numerical aberrations (Lengauer et al 1998). Rearrangements of the genome in these tumours result in the generation of chimaeric genes or TSG/oncogene deregulation resulting in changes to the gene dosage to the daughter cells (Jallepalli & Lengauer 2001).

Osteosarcoma are mesenchymal cell malignancies presenting high levels of genomic instability and ALT (alternative lengthening of the telomeres) activation, resulting in an exceptionally high level of both intra and inter tumour heterogeneity. The variability of the therapy response of osteosarcoma depends on the level of genetic instability present in the tumours (Letson & Muro-Cacho 2001) presumably allowing them to activate escape pathways to bypass therapy-induced cytotoxicity.

Osteosarcoma can arise with an approximately 1200 fold increased frequency in patients that have received localised radiotherapy to treat bilateral retinoblastoma. The majority of bilateral retinoblastoma patients carry a germline mutation in *Rb1* (Eng et al 1993, Wong et al 1997).

The direct involvement of the *Rb1* gene in the osteosarcoma development after irradiation was suggested by our previously reported findings. We showed that QTL mapping in *BALB/c* x *CBA/CA* backcrossed irradiated mice showed a strong susceptibility modifying effect due to an allelic variant of the *Rb1* locus (Rosemann et al 2006). An increase of *Rb1* gene expression from the *BALB/c* allele was found to be due to a promoter variant (unpublished

data). Tumour formation was seen to involve (in *BALB/c* x *CBA/CA*) the preferential loss of the *BALB/c* allele in the radiation-induced bone tumours (Rosemann et al 2006). This confirmed the link between *Rb1* and osteosarcomagenesis and demonstrates a synergistic interaction between a pre-existing germline mutation in the *Rb1* gene and the genotoxic stress administered by radiation.

Mutations inherited from parents or acquired *de novo* during embryogenesis can inactivate critical genes. Among them are those referred to as the "gatekeepers" and "caretakers" of the genome (Kinzler & Vogelstein 1997). Gatekeepers tumour suppressor genes are those involved in cellular signalling, growth regulation and cell cycle control, including cell cycle checkpoint genes (Kinzler & Vogelstein 1997). Caretakers are those that preserve the integrity of the genome and its accurate replication and segregation into the daughter cells. Whereas the function of a gatekeeper gene is restricted to the life-span of an individual cell, caretaker genes are important for maintaining the appropriate state and function of a cell and all of its progeny (Dominguez-Brauer et al 2010, Gao et al 2000, Hoeijmakers 2001).

Initially, the function of caretaker genes was considered to be restricted to DNA damage repair (Hoeijmakers 2001) involving genes such as *Blm* or *Fen1* (Nakayama 2002) and the cellular stress response *p53* (Gao et al 2000). Recently, genes with different functions aside from DNA repair or the cellular stress response have also been shown to act as caretakers of the genome, such as *TOP1* (Topoisomerase type I), *CDC6* (replication initiation), *LIG1* (ligase I), *POT1* (telomere capping), *H2AX* (chromatin decondensation) (Aguilera & Gomez-Gonzalez 2008). Among the known caretaker genes, those with an established tumour suppressor function, such as: *MCM4* (Shima et al 2007), *RPA70* (Wang et al 2005), *ATM* (Trenz et al 2006), *FANCA* (Lensch et al 2003), *BRCA1* (D'Andrea & Grompe 2003), *BRCA2* (Gochhait et al 2007) were found to have a function in maintaining chromosomal stability.

Recently, the *ARF* (alternative reading frame, p14) TSG, was postulated as a caretaker of the genome (Dominguez-Brauer et al 2010). The protein is transcribed from an mRNA from the alternate reading frame of the *INK4a/ARF* locus (*CDKN2A*) (Dominguez-Brauer et al 2010). Its biochemical function involves inhibition of cyclin/CDK complexes, and due to its association with cell cycle regulation it was intuitively classified as a gatekeeper TSG. In addition *INK4a/ARF* mutations lead to a loss of nucleotide excision repair (Dominguez-Brauer et al 2009). It was therefore proposed to be both a gatekeeper because of its ability to inhibit murine double minute 2 (*MDM2*) and a caretaker of the genome, due to its role in nucleotide excision repair.

To understand a possible caretaker function of *Rb1* tumour suppressor gene, the cellular functions affected by *Rb1* mutations were studied. In addition, the role of radiation exposure

and the synergistic effect of *Rb1* mutations with radiation were studied using *in vitro* assays on primary *Rb1*<sup>+/ $\Delta$ 19</sup> osteoblasts.

### 7.1 *Rb1* cell cycle and senescence regulation

*Rb1* is one of the major players in controlling the cell cycle checkpoint at G1/S transit. It is the main phosphorylation target of the cyclin E/D and CDK1/4 complexes (Bartkova et al 1996, Betticher et al 1997, Malumbres & Barbacid 2001). It has been previously reported that *Rb1* is a critical component of the cell cycle regulatory machinery (Riley et al 1994). The best understood molecular function is the ability of *Rb1* to sequester the E2F transcription factor (see scheme of interaction on page 7) and thereby switching off transcription of their target genes (Riley et al 1994). As the cyclin/cdks complex becomes activated during progress through G1 the level of phosphorylation of *Rb1* increases. Upon hyperphosphorylation by the Cyclin/CDK complexes the phospho*Rb1* (p*Rb1*) is no longer able to bind to E2F and consequently the inactive *Rb1*/E2F complex is dissociated. The released E2F is now able to transcriptionally activate a set of genes that allow the cell to enter S phase.

The G1/S checkpoint is known to be crucial to avoid the onset of DNA synthesis with in the presence of unrepaired DNA damage and subsequent fixation of mutations. It has been previously shown (Wilson et al 2010) how patients with hereditary retinoblastoma present chromatid-type aberrations in the G2 phase after irradiation in primary fibroblasts. This suggests that the correct repair of the DNA in G1 did not take place due to a failure to arrest the cell cycle in the G1/S checkpoint, leading to DNA aberrations later during the cell cycle adverting of the potential outcome of the inability of *Rb1*<sup>+/ $\Delta$ 19</sup> osteoblasts to block the cell cycle.

In accordance with this classical paradigm of the *Rb1* pathway it was shown that *Rb1*<sup>+/ $\Delta$ 19</sup> osteoblasts were unable to arrest the cell cycle in the G1/S checkpoint as efficiently as *Rb1*<sup>+/ $\Delta$ +</sup> cells after radiation exposure. Six hours after radiation exposure, *Rb1*<sup>+/ $\Delta$ 19</sup> cells failed to arrest the transition into S-phase as efficiently as *Rb1*<sup>+/ $\Delta$ +</sup> cells. This could result from the lower levels of *Rb1* protein caused by the *Rb1* haploinsufficiency being unable to recruit the free E2F in the nucleus.

The accurate regulation of the G1/S checkpoint is important for quiescence (reversible proliferation arrest), senescence (irreversible proliferation arrest) and differentiation (process by which an unspecialized cell becomes specialized into one cell type and loses proliferation capabilities (Narita et al 2003, Reimann et al 2011, Talluri et al 2010)). In particular the ability of irradiated cells to go into senescence after unrepaired radiation damage was found to be impaired in *Rb1*<sup>+/ $\Delta$ 19</sup> osteoblasts. Unirradiated *Rb1*<sup>+/ $\Delta$ 19</sup> primary cells showed a lower percentage of cells in senescence when compared to *Rb1*<sup>+/ $\Delta$ +</sup> cultures. After 2 and 4 Gy radiation exposure, *Rb1*<sup>+/ $\Delta$ 19</sup> failed to induce senescence to the same extent as

*Rb1*<sup>+/+</sup> osteoblasts which induced senescence in a dose dependent manner. Presumably, *Rb1*<sup>+/ $\Delta$ 19</sup> primary cells carried on into the S-phase with unrepaired damage. This could lead to the fixation of mutations in the DNA later during the cell cycle as seen in primary fibroblasts (Wilson et al 2010).

No pronounced radiation response was detectable for *Rb1*<sup>+/ $\Delta$ 19</sup> osteoblasts in senescence induction, and the levels of senescent cells were always lower when compared to the wild-type counterparts. This suggests that in the path towards tumourigenesis, *Rb1* mutations create on advantages towards senescence evasion. MOS cell lines established from murine osteosarcoma, were refractory to senescence induction even after radiation exposure. Those fully malignant osteosarcoma cells seem to have gained an “escape” capability of the G1/S check point control and therefore “learned” to avoid senescence. This is reiterated by the osteoblasts harbouring a haploinsufficient genotype.

Homozygous deletion of the *Rb1* gene causes polyploidy in MEFs, mouse embryonic fibroblasts (Gonzalo et al 2005) a feature that was also studied in human cancers (Hernando et al 2004). This effect has been suggested by Hernando et al to be due to uncoupling cell cycle progression and mitotic control, since the mitotic checkpoint protein Mad2 is a direct E2F target and, is aberrantly expressed in cells with *Rb1* pathway defects.

In the case of the haploinsufficient mouse osteoblasts, the polyploid fraction was increased when compared to their *Rb1*<sup>+/+</sup> counterparts as measured 24 hours agter 4 Gy of gamma irradiation. Whether the formation of polyploidy is linked to impaired cell cycle control at G1/S checkpoint, or if it is rather a sign of a defect of G2/M or spindle checkpoints remains to be investigated. Aneuploidy is a major outcome of unstable genomes, leading to cells with different DNA content (Hernando et al 2004, Sen 2000). Numeric aberrations in chromosomes arising from aneuploidy are commonly observed in human cancer (Sen 2000). This event is commonly associated with a escape from senescence (Sen 2000), demonstrating a complete deregulation of the cell cycle. It was previously shown (Berman et al 2008) that a complete *Rb1* knockout shows faster proliferation in osteoblasts in agreement with its tumour suppressor function. Here we show impaired capabilities already in the heterozygous osteoblasts, where *Rb1* haploinsufficiency in primary osteoblasts led to faster proliferation, and disregulated cell cycle control subsequent to radiation exposure. Both aneuploidy and escape from senescence were found as outcome of a paired effect between the haploinsufficient genotype after radiation exposure, demonstrating the complications arising from *Rb1* haploinsufficiency and indicating its gatekeeper function.

## 7.2 *Rb1* and CIN

The results in this work demonstrate that aging *Rb1*<sup>+/ $\Delta$ 19</sup> osteoblasts, without exposure to radiation have an increased tendency to become polyploid. The aging *Rb1*<sup>+/ $\Delta$ 19</sup> osteoblasts showed an increase in the polyploid fraction of up to 30% more than the *Rb1*<sup>+/+</sup> osteoblasts, indicating a more unstable genome. The difference was most pronounced at higher passage numbers demonstrating an accumulation of chromosomal instability in *Rb1*<sup>+/ $\Delta$ 19</sup> osteoblasts and its transmission from one cell to its progeny.

An increase in genomic instability in *Rb1* haploinsufficient cells was also indicated by the number of acentric fragments (micronuclei) and chromosome segregation defects seen before and after irradiation. Sporadic acentric fragments were present in unirradiated mononucleated *Rb1*<sup>+/ $\Delta$ 19</sup> osteoblasts. The acentric fragments in *Rb1*<sup>+/ $\Delta$ 19</sup> cells were up to 6 times more abundant than in *Rb1*<sup>+/+</sup> cells at the same late passages, although the difference in sporadic acentric fragments was already detectable at earlier passage numbers. This suggests an ongoing instability present in *Rb1* haploinsufficient cells that accumulates with aging.

After radiation exposure the incidence of acentric fragments increased in both *Rb1*<sup>+/+</sup> and *Rb1*<sup>+/ $\Delta$ 19</sup> osteoblasts, in agreement with data demonstrating the potential of radiation to induce double strand breaks (Acharya et al 2010, Jeggo et al 2011, Sak & Stuschke 2010, Somodi et al 2005, Stewart et al 2011). The difference in acentric fragment induction between the wild-type and haploinsufficient genotypes became even larger after 2 Gy of radiation exposure.

When assessing the fraction of cells with one or more micronuclei the total number of cells that were found to be affected (presenting acentric fragments) after 2 Gy of radiation was the same for both *Rb1*<sup>+/+</sup> and *Rb1*<sup>+/ $\Delta$ 19</sup> cell populations. This is in agreement with the assumption that acute chromosomal damage after radiation exposure is a deterministic effect (Edwards & Lloyd 1998). However, the average number of micronuclei per cell after 2 Gy was increased up to 1.7 fold in *Rb1*<sup>+/ $\Delta$ 19</sup> as compared to *Rb1*<sup>+/+</sup> cells, suggesting that *Rb1* haploinsufficiency leads to an accumulation of more chromosomal damage.

Segregational defects occur sporadically in the *Rb1*<sup>+/ $\Delta$ 19</sup> primary osteoblasts but not in *Rb1*<sup>+/+</sup> cells. Anaphase bridges, as well as persistent telophase bridges, were 1.8 fold increased in *Rb1*<sup>+/ $\Delta$ 19</sup> compared to their *Rb1*<sup>+/+</sup> counterparts. These types of bridges were both shown to be increased after exposure to 2 Gy of gamma irradiation in osteoblasts of both genotypes, but the increase was greater than that in the irradiated *Rb1*<sup>+/ $\Delta$ 19</sup> as compared to their *Rb1*<sup>+/+</sup> counterparts.



Segregational defects may arise from dysfunctional telomere since the unprotected chromosomal ends are highly recombinogenic (De Lange 2006, Stewenius et al 2007). The improper chromosomal fusions may lead to the generation of anaphase bridges (De Lange 2006). Anaphase bridges, are a manifestation of excessive telomere erosion and are 10 times more frequent in cells derived from a great variety of neoplasms and borderline malignant lesions than in normal tissue cells (Gisselsson et al 2000).

In high-grade glioblastoma it has been shown how telomere-dependent abnormal segregation of chromosomes is a common phenomenon generating instability as well as tumour diversity (Glanz et al 2007).

Segregational defects in *Rb1*<sup>+Δ19</sup> osteoblasts could be a result of the interaction between the two functions of *Rb1*: the inability to maintain genomic stability leading to acentric fragments and segregational defects (impaired caretaker function) coupled to a partial inhibition of cell cycle control functions leading to aneuploidy (impaired gatekeeper function)

The idea of genomic instability arising from mutations in DNA repair genes in some hereditary cancers (Negrini et al 2010) can be supplemented with findings from the current work, since we could show that heterozygous mutations in *Rb1*, a non DNA repair gene, whose mutations lead to hereditary forms of cancer and secondary cancer development, increases genomic instability.

These findings help understanding why mutations in *Rb1* both in human and mice predispose to radiation induced cancer which we postulate, arising from the results in this work, is due to an increased genomic instability possibly paired with an impaired G1/S checkpoint.

### 7.3 *Rb1* and telomeres

Telomeres cap the ends of eukaryotic chromosomes. Their main function is to protect the chromosome extremities from illegitimate recombination (Tusell et al 2010).

*Rb1*<sup>+Δ19</sup> cells presented a reduction of telomere length when compared to *Rb1*<sup>+/+</sup> cells of the same passage number. The dynamics of telomere shortening with aging were found to be faster in *Rb1*<sup>+Δ19</sup> cells when compared to wild-type osteoblasts. We speculate that such a defect leads to the formation of anaphase bridges in *Rb1*<sup>+Δ19</sup> cells due to fusion or recombination of dysfunctional telomeric ends.

The loss of telomeric DNA in many tumours generates karyotypic instability and associated amplification and deletion of chromosomal segments (Artandi & DePinho 2010) which arises from BFB (breakage-fusion-breakage) cycles. Several mechanisms for BFB have been proposed and include defects in the mitotic spindle (Elledge 1996, Nojima 1997) or defective NHEJ (Karanjawala et al 1999) that can occur in soft tissue sarcomas harbouring

chromosomal translocations (Karanjawala et al 2002, Lengauer 2001, Sharpless et al 2001). *In vitro* analysis of normal human cells in crisis, harboring short telomeres (Counter et al 1992), of human colorectal cancers in different stages (Hastie et al 1990), of engineered telomeric double strand breaks in mouse embryonic stem cells (Lo et al 2002a, Lo et al 2002b) and of tumours arising in mice with telomere dysfunction (Artandi et al 2000, Artandi & DePinho 2000a, Artandi & DePinho 2000b, Chin et al 1999) all supports the view that telomere dysfunction can serve as a potent driving force in the production of complex chromosomal rearrangements and aneuploidy. This is in concordance with conclusion from the current studies, suggesting recombinogenic processes at telomeres can disrupt their normal structure and that this process is more severe in cells with haploinsufficient *Rb1* mutations. This challenges the preconceived idea that telomere-based crisis does not appear to take place in mouse cancer cells (Prowse & Greider 1995). In this work we show that telomere crisis is a source of genomic instability. Accordingly, telomere-driven instability generates highly unstable genomes that could promote cell immortalization and the acquisition of a tumour phenotype through BFB (breakage, fusion, breakage) cycles (Tusell et al 2010).

When studying the potential for BFB mechanism being active in *Rb1*<sup>+Δ19</sup> cells, we used transformed mouse osteosarcoma cell lines as positive control. In these tumourigenic cells telophase bridges were found very frequently, and ALT was found to be activated as they harboured very long average telomeric length coupled with disparity in the signal intensity between telomere spots and high numbers of PML bodies. These cell lines showed several telomeric signals separated by non telomeric signals with the telophase bridges (suggesting ongoing rounds of BFB cycles). Having found the same feature of telomeric sequences along the length of the telophase bridges in *Rb1*<sup>+Δ19</sup> cells, we hypothesise that this could be the outcome of ongoing BFB cycles arising from the dysfunctional telomeres found in these cells. The cell cycle control impairment caused by the *Rb1* mutation (see above) would prevent an activation of the spindle checkpoint in cells that experience chromosome segregation defects, despite the presence of either radiation or BFB damaged cells. Since those damaged cells would continue to divide, the danger of passing chromosomal instability to the following cell generations increases. In addition, the G1/S checkpoint failure of this genotype prevents both the entrance into senescence (see above), as well as the cell cycle arrest after radiation exposure. These features could allow *Rb1*<sup>+Δ19</sup> cells to divide despite the presence of damages that might trigger BFB cycles, where chromosomal breaks are rejoined together or to another dysfunctional telomere by NHEJ (Murnane 2011). The subsequent breakage to a bridge happens at random along the chromatin fiber, most possible at fragile sites along the chromosome. These are chromosomal regions with a higher than average involvement in deletions, inversions and translocations, that where shown to be more prone to chromosome

breakage. Such breaks will potentially lead to acentric fragments, as shown before, a feature of *Rb1*<sup>+/ $\Delta$ 19</sup> osteoblasts.

In addition to deletions and translocations (Micci et al 2006), amplifications of the 6p21 region was shown by multicolor banding (mBAND) FISH in osteosarcoma (Lim et al 2005). The predicted intermediates associated with BFB, such as dicentric chromosomes, inverted duplications, and intra- and interchromosomal amplifications were identified in these cells (Lim et al 2005). This fragile sites frequently found in osteosarcoma (3p14, 13q14 or 6p23) were also found in retinoblastoma patients by investigation of the constitutional genetic instability by fragile site (FS) expression studies (Amare Kadam et al 2004).

Interchromosome end-to-end fusions occur before DNA synthesis and mainly results in dicentric chromosomes. *Rb1*<sup>+/ $\Delta$ 19</sup> cells exhibit dicentrics in metaphase spreads. Although dicentric chromosomes derived from fusions between chromatids always bridge at anaphase, they may only contribute to genomic instability if a twist between the two centromeres occurs during division (Tusell et al 2010). This means that the larger the intercentromeric distance, the greater the probability of twisting and of breaking apart (Tusell et al 2010). Although dicentrics are considered incompatible with cell division, in cases of check point defects they can also produce novel chromosomal variants with each cell division throughout the cell population, averting severe cellular consequences (Tusell et al 2010).

Upon breakage, non-reciprocal translocations and other non balanced rearrangements will occur. The balance between pre- and post-replicative end joining repair depends on the presence of other substrates competing for end-joining in the same cell (Tusell et al 2010). Therefore if other recombinogenic ends are available in the cell, as is the case for *Rb1*<sup>+/ $\Delta$ 19</sup> due to the shortened telomeres, new joining could occur, entering the BFB cycles and increasing instability in each round of replication. As several telomeric signals were found along the bridges found in *Rb1*<sup>+/ $\Delta$ 19</sup> osteoblasts this suggests ongoing BFB over multiple cell divisions. This would lead to rapid imbalances in gene dosage in the daughter cells, therefore leading to aneuploidy.

BFB cycles continue until the chromosome acquires a new telomere (Lo et al 2002a, Murnane 2006) most often by translocation of the end of another chromosome. Instability is not confined to a chromosome that loses its telomere, since the instability can also involved undamaged chromosomes if they are used as a recombination partner during DNA repair (Sabatier et al 2005). Amplified regions resulting from BFB cycles can also be unstable and form extrachromosomal DNA that can reintegrate at new locations (Lo et al 2002b).

As shown in this work, spontaneous extrachromosomal acentric fragments present in *Rb1*<sup>+/ $\Delta$ 19</sup> osteoblasts and carried more telomeric sequences than the *Rb1*<sup>+/+</sup> cells. Up to 70% of the acentric fragments carried telomeric sequences in *Rb1*<sup>+/ $\Delta$ 19</sup> cells, suggesting telomeric

and subtelomeric structures at the hotspots of DNA damage and enhance instability in *Rb1*<sup>+/ $\Delta$ 19</sup> osteoblasts.

Recovery of the *Rb1* haploinsufficiency, using a lentiviral system to introduce the *RB1* sequence into the *Rb1*<sup>+/ $\Delta$ 19</sup> primary mouse osteoblasts, led to a reduction in the rate of sporadic telomere losses when compared to the non infected *Rb1*<sup>+/ $\Delta$ 19</sup> osteoblasts. In this recovery system telomeres still lost length due to continuing cell divisions, but the shortening occurred less rapidly in the recovered than in the *Rb1* haploinsufficient cells.

*Rb1* recovery also led to a reduced incidence of sporadic segregational defects, with the incidence of anaphase bridges being reduced 3 passages after infection. This effect might be due to the combination restoration of Rb1's cell cycle control function preventing damaged cells from dividing, and restoration of caretaker function leading to a reduced erosion of the telomeres, therefore decreasing the source of telomere fusions.

These results of recovering the phenotype are in agreement with previous data that showed germline retinoblastoma mutation increase susceptibility to neuroendocrine cancer, whereas reintroduction of wild-type *Rb1* was able to suppress neoplastic phenotypes (Zheng & Lee 2001, Zheng & Lee 2002). Expression of a human *RB1* transgene in the *Rb1*<sup>+/ $\Delta$ 19</sup> mice suppressed carcinogenesis in all tissues studied, such as pituitary, thyroid, parathyroid glands and the adrenal medulla. Moreover the frequency of lung metastases of the neuroendocrine tumours were reduced in *Rb1*<sup>+/ $\Delta$ 19</sup> mice (Nikitin et al 1999) upon restoration of the Rb1 expression.

Telomere length reduction was found to be radiation independent, in both *Rb1*<sup>+/+</sup> and *Rb1*<sup>+/ $\Delta$ 19</sup> cells 48 hours after radiation exposure. This demonstrates that an acute radiation dose is not itself the main reason for telomere attrition. The effects of radiation are rather seen as the increase in chromosomal instability (by increasing the damage to the DNA) but not telomere erosion. One could speculate that an interaction of *Rb1*<sup>+/ $\Delta$ 19</sup> derived instability at telomeres with a genome wide level of random DNA breaks after radiation is the reason for the increased level of radiation-triggered chromosomal instability in these cells.

In the case of *Rb1* mutation carriers radiation would be expected to cause further detriment to an already unstably genome. This synergistic effect of radiation and a germline predisposition accelerates the process of transformation by increasing genomic instability.

It has recently been shown that Rb1 is also involved in the maintenance of centromere stability (Manning et al 2010). RB1 depletion compromised centromeric localization of CAP-D3/condensin II and reduced chromosome cohesion in Rb defective cells. This led to an increase in intercentromeric distance and deformation of centromeric structure and eventually to defects of chromosome segregation (anaphase bridges). In the same system it

was also shown that depletion of the retinoblastoma protein (pRB1) causes a rise of missegregation comparable with those seen in CIN tumour cells (Manning et al 2010).

#### 7.4 pRb1 and epigenetics

The close proximity of the phosphorylated form of Rb1 (pRb1) to the telomeres in metaphase spreads was demonstrated in this work. Mapping the pRb1 protein to the telomeres by immunofluorescence detection suggests a physical interaction of pRb1 with the DNA during cell division. Previous studies have shown the interaction of pRb1 with chromatin regulating enzymes such as histone deacetylases (HDACs), chromatin remodelers (SWI/SNF), and histone methyltransferases (HMTases) (Longworth & Dyson 2010), suggesting a possible regulation of these enzymes via pRb1.

The proteins shown to associate with pRb1 are chromatin-associated proteins with roles in transcriptional regulation, chromatin modification, and chromatin remodeling (Brehm et al 1998, Ferreira et al 1998, Litovchick et al 2007, Luo et al 1998, Narita et al 2003).

A reduction in a marker of heterochromatin H4K20 trimethylation with a proposed role in telomere and centromere maintenance (Gonzalo et al 2005) was detected in the *Rb1*<sup>+/ $\Delta$ 19</sup> cells. Such a reduction in H4K20 trimethylation status is believed to lead to a more open chromatin structure at the telomeres (Blasco 2007) since they tend to be more compact structures associated with telosomes, sheltering complexes and nucleosomes (de Lange et al 1990, Makarov et al 1993). Histone modifications are known to be characteristic of constitutive heterochromatin domains (Garcia-Cao et al 2002, Gonzalo et al 2006). These epigenetic marks are characteristic of compacted and transcriptionally silenced heterochromatin domains, and the level of methylation of the specific lysines may have important functional consequences for the assembly of (hetero)chromatin domains (Kourmouli et al 2004).

A misregulation of this epigenetic marker, as seen in *Rb1*<sup>+/ $\Delta$ 19</sup> cells could expose the telomeric repetitive DNA to either more radical-induced lesions but also to illegitimate intra- or interchromosomal recombinational processes. This could both explain why telomeres in *Rb1*<sup>+/ $\Delta$ 19</sup> osteoblasts are shorter than in their *Rb1* wild-type counterparts, and why these cells exhibit a higher frequency of anaphase bridges and polyploidy.

Rb1 recruits E2F, and this transcription factor is involved in *Rb1* mRNA transcription and Rb1 phosphorylation via a feedback loop (Burkhart et al 2010). However, it has been reported (Gonzalo et al 2005) that the ability of pRb1 family members to promote H4K20 trimethylation was unaffected by a dominant negative form of E2F. This suggests that pRb1 regulation of histone is likely to be distinct from its role in E2F regulation, supporting our theory of *Rb1* having both gatekeeper and caretaker functions.

The compaction of pericentric heterochromatin is thought to aid chromosome segregation, and abnormalities in pericentric heterochromatin were shown (Isaac et al 2006) to be one of the potential causes of the anaphase bridges that appeared in *Rb1*<sup>ALXCXE</sup> cells, lacking the enzyme binding domain (LXCXE) of *Rb1* (Isaac et al 2006). Our experiments reveal that the *Rb1*<sup>+/ $\Delta$ 19</sup> cells carry defects in heterochromatin markers, potentially favouring telomere dysfunction that leads to segregational defects, namely anaphase bridges, that will increase the CIN in those cells.

Haploinsufficiency of *Rb1* implies a reduction of the levels of pRb1 and this might lead to failure of recruitment of SUV4-20h1, an enzyme that catalyses the specific methylation of Lys20 in H4K20 trimethylation (Blasco 2007), to the DNA.

In this work, it was shown that the regulation by *Rb1* of the SUV4-20h1 is not on a transcriptional level. Expression levels of the SUV4-20h1 protein were identical for *Rb1*<sup>+/ $\Delta$ +</sup> and *Rb1*<sup>+/ $\Delta$ 19</sup> osteoblasts, as well as sh*RB1* lentiviral infected cells. It was previously suggested (Gonzalo et al 2005) that pRb1 mediates the stabilization of H4K20 trimethylation at heterochromatin instead of directing Suv420 HMTases to the region, since both, H4K20 trimethylation and SUV4-20h, remain at the pericentric heterochromatin when pRb is absent. Therefore, the complete picture of the mechanism of action still needs to be elucidated.

The epigenetic defect in *Rb1*<sup>+/ $\Delta$ 19</sup> was found to be amplified following radiation exposure, which suggests a more severe effect on genome stability again pointing to a genetic predisposition for *Rb1* mutation carriers.

### 7.5 *Rb1* and the ALT mechanism

ALT (alternative lengthening of the telomeres) is a telomerase-independent mechanism for replenishing the telomeres via recombination (Murray & Carr 2008). The telomere recombinogenic process is aided by the formation of PML rich nuclear bodies (Murray & Carr 2008).

PML-NBs (PML nuclear bodies) are mobile nuclear structures that have been implicated in numerous biological functions, such as gene transcription (both activation and repression), viral pathogenicity, tumour suppression, proteasomal degradation, cellular senescence, apoptosis and DNA repair (Dellaire & Bazett-Jones 2004, Strudwick & Borden 2002, Takahashi et al 2004, Zhong et al 2000a, Zhong et al 2000b). The DNA recombination and repair activities of the PML-NBs are regarded as essential for telomere lengthening via the ALT mechanism (Yeager et al 1999). Increased PML-NBs are a feature of ALT transformed cells (Stagno D'Alcontres et al 2007) where they appear to be bound to the telomeres forming APBs (associated PML bodies). The APBs are known to be sites of active recombination along the telomeres (Murray & Carr 2008, Yeager et al 1999).

In  $Rb1^{+\Delta19}$  cells the numbers of PML-NBs were increased when compared to their wild-type counterparts. They were further increased upon sporadic *in vitro* activation of ALT, as shown by the rapid telomere increase in  $Rb1^{+\Delta19}$  primary osteoblasts escaping cellular crisis. PML-NBs counts did not change after recovery of the  $Rb1^{+\Delta19}$  phenotype (by LV-*RB1* infection) which could imply that ALT activation is not directly related to *Rb1* expression, but is triggered by telomere shortening. Increased PML-NBs numbers in  $Rb1^{+\Delta19}$  could therefore suggest an increase in recombination and repair activities present due to decreased telomere length due to lack of *Rb1*. This could lead to the activation of ALT when reaching critical telomeric length, according to the data shown in this work.

### 7.6 *Rb1* haploinsufficiency in an *in-vivo* model

The predicted susceptibility to radiation osteosarcomagenesis arising from *Rb1* haploinsufficiency was studied *in-vivo* using a mouse model irradiated by injecting a bone-seeking alpha emitter  $^{227}\text{Th}$ .

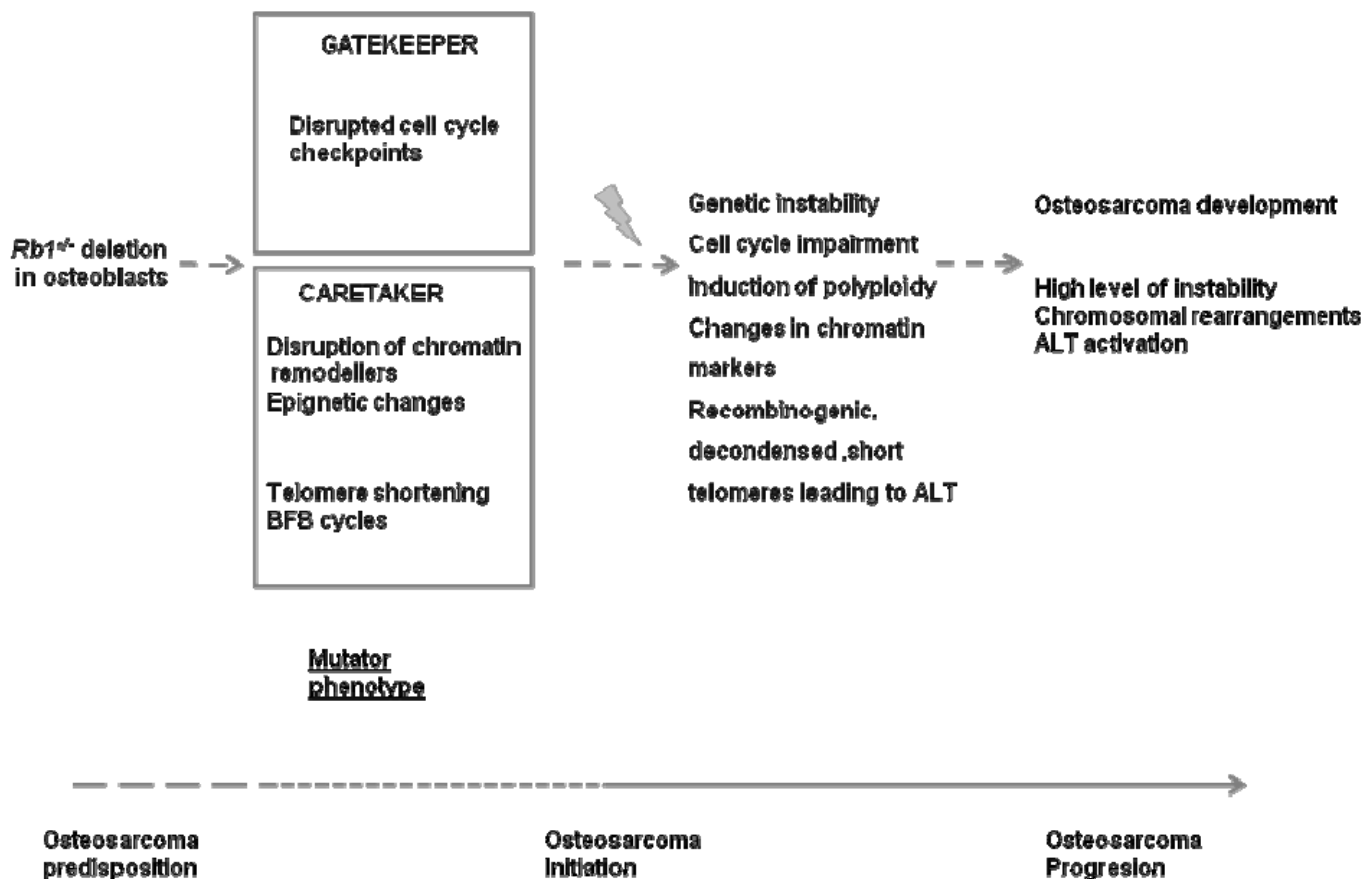
When mice lacking one copy of *Rb1* in the osteoblastic lineage (*Cre* driven recombination  $Rb1^{fl/+}$ ) was challenged with a bone tumour inducing radiation dose, 6 Gy to the skeleton (Rosemann et al 2006), osteosarcoma incidence was increased to 46% (CI 36%-68%) as compared to 11% (CI 4%-31%) in mice harbouring two copies of wild-type *Rb1* (Gonzalez-Vasconcellos et al 2011). Tumour latency after radiation exposure did not appear to be significantly different between genotypes, even though only 2 osteosarcomas developed in the wild-type cohort. The increased osteosarcoma induction in the  $Rb1^{+\Delta19}$  animals coupled with *in vitro* G1/S defects and telomere effects in *Rb1* haploinsufficient osteoblasts suggests that the increased susceptibility for radiation-induced osteosarcoma by *Rb1* germline mutations in man or a targeted heterozygote *Rb1* knock-out in mice is caused by an increase in genomic instability paired with a defective G1/S arrest.

LOH analysis of the radiation-induced osteosarcomas arising in irradiated  $Rb1^{+\Delta19}$  mice revealed that 7 out of the 11 osteosarcomas studied exhibited loss of the wild-type allele. Four tumours arising from the  $Rb1^{+\Delta19}$  cohort showed incomplete loss of the remaining wild-type allele. This could indicate that deletion of the remaining wild-type allele might not be essential for malignant transformation. Alternative loss of function due to mutations outside the studied exons 17 and 19 may occur and the imbalance may be present in a minority of the tumour cells or a contamination with normal cells.

### 7.7 *Rb1* mutator phenotype, a model of osteosarcoma development

From our *in vitro* data we are able to postulate that *Rb1* germline mutations inactivate the caretaker function of *Rb1*. This may lead to a mutator phenotype, a term originally coined by Loeb (Loeb 2001) promoting the accumulation of mutations above that predicted from the sporadic rate alone.

A model of osteosarcoma development based on these studies is shown in the scheme below:





## 7.8 Conclusions

In this work, it was demonstrated how haploinsufficient mutations in the retinoblastoma gene, aside an impaired cell cycle control and led to instability via defective telomeres. Such features infer a so called mutator phenotype to the cell population stressing the underlying mechanism of malignant transformation. Furthermore it was demonstrated how the underlying phenotype of *Rb1*<sup>+/ $\Delta$ 19</sup> mutations was amplified by radiation exposure triggering radiation induced osteosarcoma.

Our findings suggest a cumulative and transmissible instability occurs in *Rb1*<sup>+/ $\Delta$ 19</sup> cells, mainly because the defects are more pronounced during aging of the cells. The rise of defects in the *Rb1*<sup>+/ $\Delta$ 19</sup> cells, in particular after radiation exposure fixes a persistent enhancement in the rate at which mutations and chromosomal aberrations arise. Up to know the functions of *Rb1* were assumed to affect only cell cycle control, therefore showing a clear cell-autonomous effect. This cell autonomous action was assumed to be important for the life span of a single cell with non transmissible effects. Here we can show however that defects in the *Rb1* TSG affect the progeny. This non cell autonomous mechanism is more important for the multi-step carcinogenesis (Reimann et al 2011), since defects acquired in one cell can be fixed and transmitted to the next generation, allowing the accumulation of multiple lesions that drive the carcinogenic process.

Overall this study demonstrates the implications of the *Rb1 gene* in the maintenance of chromosomal stability via telomere regulation. Furthermore, it insights into the capabilities of germline mutations towards inferring tumour susceptibility. This works shows how the enhanced damage caused by the synergistic effect of radiation exposure coupled to *Rb1* haploinsufficient mutations to the osteoblasts can lead to osteosarcoma. These results are the first evidence of the *Rb1* caretaker function being directly implicated in tumourigenesis. Therefore after this study we can postulate that the loss of the caretaker function of the *Rb1* gene, triggers radiation induced cancer.

**VIII REFERENCES**

- Acharya MM, Lan ML, Kan VH, Patel NH, Giedzinski E, et al. 2010. Consequences of ionizing radiation-induced damage in human neural stem cells. *Free Radic Biol Med* 49: 1846-55
- Aguilera A, Gomez-Gonzalez B. 2008. Genome instability: a mechanistic view of its causes and consequences. *Nat Rev Genet* 9: 204-17
- Alves Dos Santos R, Teixeira AC, Mayorano MB, Carrara HH, Moreira de Andrade J, Takahashi CS. 2011. Variability in estrogen-metabolizing genes and their association with genomic instability in untreated breast cancer patients and healthy women. *J Biomed Biotechnol* 2011: 571784
- Amare Kadam PS, Ghule P, Jose J, Bamne M, Kurkure P, et al. 2004. Constitutional genomic instability, chromosome aberrations in tumor cells and retinoblastoma. *Cancer Genet Cytogenet* 150: 33-43
- Anastasov N, Klier M, Koch I, Angermeier D, Hofler H, et al. 2009. Efficient shRNA delivery into B and T lymphoma cells using lentiviral vector-mediated transfer. *J Hematop* 2: 9-19
- Anderson GR, Brenner BM, Swede H, Chen N, Henry WM, et al. 2001a. Intrachromosomal genomic instability in human sporadic colorectal cancer measured by genome-wide allelotyping and inter-(simple sequence repeat) PCR. *Cancer Res* 61: 8274-83
- Anderson GR, Stoler DL, Brenner BM. 2001b. Cancer: the evolved consequence of a destabilized genome. *Bioessays* 23: 1037-46
- Aragona M, Maisano R, Panetta S, Giudice A, Morelli M, et al. 2000. Telomere length maintenance in aging and carcinogenesis. *Int J Oncol* 17: 981-9
- Aranda-Anzaldo A, Dent MA. 2007. Reassessing the role of p53 in cancer and ageing from an evolutionary perspective. *Mech Ageing Dev* 128: 293-302
- Armitage P, Doll R. 1957. A two-stage theory of carcinogenesis in relation to the age distribution of human cancer. *Br J Cancer* 11: 161-9
- Arosarena OA, Del Carpio-Cano FE, Dela Cadena RA, Rico MC, Nwodim E, Safadi FF. 2011. Comparison of bone morphogenetic protein-2 and osteoactivin for mesenchymal cell differentiation: Effects of bolus and continuous administration. *J Cell Physiol*
- Artandi SE, Chang S, Lee SL, Alson S, Gottlieb GJ, et al. 2000. Telomere dysfunction promotes non-reciprocal translocations and epithelial cancers in mice. *Nature* 406: 641-5
- Artandi SE, DePinho RA. 2000a. A critical role for telomeres in suppressing and facilitating carcinogenesis. *Curr Opin Genet Dev* 10: 39-46
- Artandi SE, DePinho RA. 2000b. Mice without telomerase: what can they teach us about human cancer? *Nat Med* 6: 852-5
- Artandi SE, DePinho RA. 2010. Telomeres and telomerase in cancer. *Carcinogenesis* 31: 9-18

- Ascoli CA, Maul GG. 1991. Identification of a novel nuclear domain. *J Cell Biol* 112: 785-95
- Bartkova J, Lukas J, Gulberg P, Alsnér J, Kirkin AF, et al. 1996. The p16-cyclin D/Cdk4-pRb pathway as a functional unit frequently altered in melanoma pathogenesis. *Cancer Res* 56: 5475-83
- Baur JA, Zou Y, Shay JW, Wright WE. 2001. Telomere position effect in human cells. *Science* 292: 2075-7
- Beebe GW, Ishida M, Jablon S. 1962. Studies of the mortality of A-bomb survivors. I. Plan of study and mortality in the medical subsample (selection 1), 1950-1958. *Radiat Res* 16: 253-80
- Belchis DA, Meece CA, Benko FA, Rogan PK, Williams RA, Gocke CD. 1996. Loss of heterozygosity and microsatellite instability at the retinoblastoma locus in osteosarcomas. *Diagn Mol Pathol* 5: 214-9
- Belyakov OV, Prise KM, Trott KR, Michael BD. 1999. Delayed lethality, apoptosis and micronucleus formation in human fibroblasts irradiated with X-rays or alpha-particles. *Int J Radiat Biol* 75: 985-93
- Benetti R, Garcia-Cao M, Blasco MA. 2007. Telomere length regulates the epigenetic status of mammalian telomeres and subtelomeres. *Nat Genet* 39: 243-50
- Berman SD, Yuan TL, Miller ES, Lee EY, Caron A, Lees JA. 2008. The retinoblastoma protein tumor suppressor is important for appropriate osteoblast differentiation and bone development. *Mol Cancer Res* 6: 1440-51
- Bertuch AA, Buckley K, Lundblad V. 2003. The way to the end matters--the role of telomerase in tumor progression. *Cell Cycle* 2: 36-8
- Bertuch AA, Lundblad V. 2006. The maintenance and masking of chromosome termini. *Curr Opin Cell Biol* 18: 247-53
- Betticher DC, White GR, Vonlanthen S, Liu X, Kappeler A, et al. 1997. G1 control gene status is frequently altered in resectable non-small cell lung cancer. *Int J Cancer* 74: 556-62
- Bianchi A, Shore D. 2008. How telomerase reaches its end: mechanism of telomerase regulation by the telomeric complex. *Mol Cell* 31: 153-65
- Blasco MA. 2007. The epigenetic regulation of mammalian telomeres. *Nat Rev Genet* 8: 299-309
- Bohgaki T, Bohgaki M, Cardoso R, Panier S, Zeegers D, et al. 2011. Genomic instability, defective spermatogenesis, immunodeficiency, and cancer in a mouse model of the RIDDLE syndrome. *PLoS Genet* 7: e1001381
- Bois P, Jeffreys AJ. 1999. Minisatellite instability and germline mutation. *Cell Mol Life Sci* 55: 1636-48

- Boisvert FM, Kruhlak MJ, Box AK, Hendzel MJ, Bazett-Jones DP. 2001. The transcription coactivator CBP is a dynamic component of the promyelocytic leukemia nuclear body. *J Cell Biol* 152: 1099-106
- Boublikova L, Kalinova M, Ryan J, Quinn F, O'Marcaigh A, et al. 2006. Wilms' tumor gene 1 (WT1) expression in childhood acute lymphoblastic leukemia: a wide range of WT1 expression levels, its impact on prognosis and minimal residual disease monitoring. *Leukemia* 20: 254-63
- Bowden GT, Schneider B, Domann R, Kulesz-Martin M. 1994. Oncogene activation and tumor suppressor gene inactivation during multistage mouse skin carcinogenesis. *Cancer Res* 54: 1882s-85s
- Boyle JM, Mitchell EL, Greaves MJ, Roberts SA, Tricker K, et al. 1998. Chromosome instability is a predominant trait of fibroblasts from Li-Fraumeni families. *Br J Cancer* 77: 2181-92
- Brabletz T, Jung A, Spaderna S, Hlubek F, Kirchner T. 2005. Opinion: migrating cancer stem cells - an integrated concept of malignant tumour progression. *Nat Rev Cancer* 5: 744-9
- Brehm A, Miska EA, McCance DJ, Reid JL, Bannister AJ, Kouzarides T. 1998. Retinoblastoma protein recruits histone deacetylase to repress transcription. *Nature* 391: 597-601
- Brenton DP, Isenberg DA, Bertram J. 1980. Osteosarcoma complicating familial Paget's disease. *Postgrad Med J* 56: 238-43
- Brummelkamp TR, Bernards R, Agami R. 2002. A system for stable expression of short interfering RNAs in mammalian cells. *Science* 296: 550-3
- Bryan TM, Englezou A, Gupta J, Bacchetti S, Reddel RR. 1995. Telomere elongation in immortal human cells without detectable telomerase activity. *EMBO J* 14: 4240-8
- Burke JR, Deshong AJ, Pelton JG, Rubin SM. 2010. Phosphorylation-induced conformational changes in the retinoblastoma protein inhibit E2F transactivation domain binding. *J Biol Chem* 285: 16286-93
- Burkhart DL, Ngai LK, Roake CM, Viatour P, Thangavel C, et al. 2010. Regulation of RB transcription in vivo by RB family members. *Mol Cell Biol* 30: 1729-45
- Cao L, Peng B, Yao L, Zhang X, Sun K, et al. 2010. The ancient function of RB-E2F pathway: insights from its evolutionary history. *Biol Direct* 5: 55
- Castillero-Trejo Y, Eliazar S, Xiang L, Richardson JA, Ilaria RL, Jr. 2005. Expression of the EWS/FLI-1 oncogene in murine primary bone-derived cells Results in EWS/FLI-1-dependent, ewing sarcoma-like tumors. *Cancer Res* 65: 8698-705
- Chan SR, Blackburn EH. 2004. Telomeres and telomerase. *Philos Trans R Soc Lond B Biol Sci* 359: 109-21
- Chang IB, Cho BM, Moon SM, Park SH, Oh SM, Cho SJ. 2010. Loss of heterozygosity at 1p, 7q, 17p, and 22q in meningiomas. *J Korean Neurosurg Soc* 48: 14-9

- Chen Z, Wang ZY, Chen SJ. 1997. Acute promyelocytic leukemia: cellular and molecular basis of differentiation and apoptosis. *Pharmacol Ther* 76: 141-9
- Chin L, Artandi SE, Shen Q, Tam A, Lee SL, et al. 1999. p53 deficiency rescues the adverse effects of telomere loss and cooperates with telomere dysfunction to accelerate carcinogenesis. *Cell* 97: 527-38
- Clark-Knowles KV, Senterman MK, Collins O, Vanderhyden BC. 2009. Conditional inactivation of Brca1, p53 and Rb in mouse ovaries results in the development of leiomyosarcomas. *PLoS One* 4: e8534
- Cong YS, Wright WE, Shay JW. 2002. Human telomerase and its regulation. *Microbiol Mol Biol Rev* 66: 407-25, table of contents
- Counter CM, Avilion AA, LeFeuvre CE, Stewart NG, Greider CW, et al. 1992. Telomere shortening associated with chromosome instability is arrested in immortal cells which express telomerase activity. *EMBO J* 11: 1921-9
- D'Andrea AD, Grompe M. 2003. The Fanconi anaemia/BRCA pathway. *Nat Rev Cancer* 3: 23-34
- Dacquin R, Starbuck M, Schinke T, Karsenty G. 2002. Mouse alpha1(I)-collagen promoter is the best known promoter to drive efficient Cre recombinase expression in osteoblast. *Dev Dyn* 224: 245-51
- Dai X, Huang C, Bhusari A, Sampathi S, Schubert K, Chai W. 2010. Molecular steps of G-overhang generation at human telomeres and its function in chromosome end protection. *EMBO J* 29: 2788-801
- De Lange T. 2005. Telomere-related genome instability in cancer. *Cold Spring Harb Symp Quant Biol* 70: 197-204
- De Lange T. 2006. *Telomeres*. Cold Spring hrbour laboratory press.
- de Lange T, Shiue L, Myers RM, Cox DR, Naylor SL, et al. 1990. Structure and variability of human chromosome ends. *Mol Cell Biol* 10: 518-27
- Dellaire G, Bazett-Jones DP. 2004. PML nuclear bodies: dynamic sensors of DNA damage and cellular stress. *Bioessays* 26: 963-77
- Deng CX, Scott F. 2000. Role of the tumor suppressor gene Brca1 in genetic stability and mammary gland tumor formation. *Oncogene* 19: 1059-64
- Deriano L, Chaumeil J, Coussens M, Multani A, Chou Y, et al. 2011. The RAG2 C terminus suppresses genomic instability and lymphomagenesis. *Nature* 471: 119-23
- Dionne I, Wellinger RJ. 1996. Cell cycle-regulated generation of single-stranded G-rich DNA in the absence of telomerase. *Proc Natl Acad Sci U S A* 93: 13902-7
- Dominguez-Brauer C, Brauer PM, Chen YJ, Pimkina J, Raychaudhuri P. 2010. Tumor suppression by ARF: gatekeeper and caretaker. *Cell Cycle* 9: 86-9

- Dominguez-Brauer C, Chen YJ, Brauer PM, Pimkina J, Raychaudhuri P. 2009. ARF stimulates XPC to trigger nucleotide excision repair by regulating the repressor complex of E2F4. *EMBO Rep* 10: 1036-42
- Edwards AA, Lloyd DC. 1998. Risks from ionising radiation: deterministic effects. *J Radiol Prot* 18: 175-83
- Eilber FC, Rosen G, Nelson SD, Selch M, Dorey F, et al. 2003. High-grade extremity soft tissue sarcomas: factors predictive of local recurrence and its effect on morbidity and mortality. *Ann Surg* 237: 218-26
- Eisenberg MB, Woloschak M, Sen C, Wolfe D. 1997. Loss of heterozygosity in the retinoblastoma tumor suppressor gene in skull base chordomas and chondrosarcomas. *Surg Neurol* 47: 156-60; discussion 60-1
- Elledge SJ. 1996. Cell cycle checkpoints: preventing an identity crisis. *Science* 274: 1664-72
- Eng C, Li FP, Abramson DH, Ellsworth RM, Wong FL, et al. 1993. Mortality from second tumors among long-term survivors of retinoblastoma. *J Natl Cancer Inst* 85: 1121-8
- Erfle V, Schulte-Overberg S, Marquart KH, Adler ID, Luz A. 1979. Establishment and characterization of C-type RNA virus-producing cell lines from radiation-induced murine osteosarcomas. *J Cancer Res Clin Oncol* 94: 149-62
- Eskiw CH, Bazett-Jones DP. 2002. The promyelocytic leukemia nuclear body: sites of activity? *Biochem Cell Biol* 80: 301-10
- Eskiw CH, Dellaire G, Bazett-Jones DP. 2004. Chromatin contributes to structural integrity of promyelocytic leukemia bodies through a SUMO-1-independent mechanism. *J Biol Chem* 279: 9577-85
- Eskiw CH, Dellaire G, Mymryk JS, Bazett-Jones DP. 2003. Size, position and dynamic behavior of PML nuclear bodies following cell stress as a paradigm for supramolecular trafficking and assembly. *J Cell Sci* 116: 4455-66
- Fearon ER. 1997. Human cancer syndromes: clues to the origin and nature of cancer. *Science* 278: 1043-50
- Fenech M, Chang WP, Kirsch-Volders M, Holland N, Bonassi S, Zeiger E. 2003. HUMN project: detailed description of the scoring criteria for the cytokinesis-block micronucleus assay using isolated human lymphocyte cultures. *Mutat Res* 534: 65-75
- Fenech M, Morley A. 1985. Solutions to the kinetic problem in the micronucleus assay. *Cytobios* 43: 233-46
- Fenech M, Morley AA. 1986. Cytokinesis-block micronucleus method in human lymphocytes: effect of in vivo ageing and low dose X-irradiation. *Mutat Res* 161: 193-8
- Ferbeyre G, de Stanchina E, Querido E, Baptiste N, Prives C, Lowe SW. 2000. PML is induced by oncogenic ras and promotes premature senescence. *Genes Dev* 14: 2015-27

- Ferreira R, Magnaghi-Jaulin L, Robin P, Harel-Bellan A, Trouche D. 1998. The three members of the pocket proteins family share the ability to repress E2F activity through recruitment of a histone deacetylase. *Proc Natl Acad Sci U S A* 95: 10493-8
- Feugeas O, Guriec N, Babin-Boilletot A, Marcellin L, Simon P, et al. 1996. Loss of heterozygosity of the RB gene is a poor prognostic factor in patients with osteosarcoma. *J Clin Oncol* 14: 467-72
- Fodde R, Smits R. 2002. Cancer biology. A matter of dosage. *Science* 298: 761-3
- Gambacorta M, Flenghi L, Fagioli M, Pileri S, Leoncini L, et al. 1996. Heterogeneous nuclear expression of the promyelocytic leukemia (PML) protein in normal and neoplastic human tissues. *Am J Pathol* 149: 2023-35
- Gao Y, Ferguson DO, Xie W, Manis JP, Sekiguchi J, et al. 2000. Interplay of p53 and DNA-repair protein XRCC4 in tumorigenesis, genomic stability and development. *Nature* 404: 897-900
- Garcia-Cao M, Gonzalo S, Dean D, Blasco MA. 2002. A role for the Rb family of proteins in controlling telomere length. *Nat Genet* 32: 415-9
- Geng Y, Eaton EN, Picon M, Roberts JM, Lundberg AS, et al. 1996. Regulation of cyclin E transcription by E2Fs and retinoblastoma protein. *Oncogene* 12: 1173-80
- Ghule P, Kadam PA, Jambhekar N, Bamne M, Pai S, et al. 2006. p53 gene gets altered by various mechanisms: studies in childhood sarcomas and retinoblastoma. *Med Sci Monit* 12: BR385-96
- Gisselsson D, Pettersson L, Hoglund M, Heidenblad M, Gorunova L, et al. 2000. Chromosomal breakage-fusion-bridge events cause genetic intratumor heterogeneity. *Proc Natl Acad Sci U S A* 97: 5357-62
- Glanz C, Rebetz J, Stewenius Y, Persson A, Englund E, et al. 2007. Genetic intratumour heterogeneity in high-grade brain tumours is associated with telomere-dependent mitotic instability. *Neuropathol Appl Neurobiol* 33: 440-54
- Gochhait S, Bukhari SI, Bairwa N, Vadhera S, Darvishi K, et al. 2007. Implication of BRCA2 -26G>A 5' untranslated region polymorphism in susceptibility to sporadic breast cancer and its modulation by p53 codon 72 Arg>Pro polymorphism. *Breast Cancer Res* 9: R71
- Goel A, Nagasaka T, Spiegel J, Meyer R, Lichliter WE, Boland CR. 2010. Low frequency of Lynch syndrome among young patients with non-familial colorectal cancer. *Clin Gastroenterol Hepatol* 8: 966-71
- Golubnitschaja O. 2007. Cell cycle checkpoints: the role and evaluation for early diagnosis of senescence, cardiovascular, cancer, and neurodegenerative diseases. *Amino Acids* 32: 359-71
- Gonzalez-Vasconcellos I, Domke T, Kuosaite V, Esposito I, Sanli-Bonazzi B, et al. 2011. Differential effects of genes of the Rb1 signalling pathway on osteosarcoma incidence and latency in alpha-particle irradiated mice. *Radiat Environ Biophys* 50: 135-41

- Gonzalo S, Garcia-Cao M, Fraga MF, Schotta G, Peters AH, et al. 2005. Role of the RB1 family in stabilizing histone methylation at constitutive heterochromatin. *Nat Cell Biol* 7: 420-8
- Gonzalo S, Jaco I, Fraga MF, Chen T, Li E, et al. 2006. DNA methyltransferases control telomere length and telomere recombination in mammalian cells. *Nat Cell Biol* 8: 416-24
- Gorgojo L, Little JB. 1989. Expression of lethal mutations in progeny of irradiated mammalian cells. *Int J Radiat Biol* 55: 619-30
- Gossner W, Luz A. 1994. Tumours of the jaws. *IARC Sci Publ*: 141-65
- Grant EJ, Neriishi K, Cologne J, Eguchi H, Hayashi T, et al. 2011. Associations of Ionizing Radiation and Breast Cancer-Related Serum Hormone and Growth Factor Levels in Cancer-Free Female A-Bomb Survivors. *Radiat Res*
- Griffith JD, Comeau L, Rosenfield S, Stansel RM, Bianchi A, et al. 1999. Mammalian telomeres end in a large duplex loop. *Cell* 97: 503-14
- Guo A, Salomoni P, Luo J, Shih A, Zhong S, et al. 2000. The function of PML in p53-dependent apoptosis. *Nat Cell Biol* 2: 730-6
- Haber D, Harlow E. 1997. Tumour-suppressor genes: evolving definitions in the genomic age. *Nat Genet* 16: 320-2
- Hagemann G, Kreczik A, Treichel M. 1996. [The demonstration of heritable lethal mutations in the progeny of x-ray-irradiated CHO cells by micronucleus count in clone cells]. *Strahlenther Onkol* 172: 320-5
- Hanahan D, Weinberg RA. 2000. The hallmarks of cancer. *Cell* 100: 57-70
- Hanahan D, Weinberg RA. 2011. Hallmarks of cancer: the next generation. *Cell* 144: 646-74
- Harland M, Goldstein AM, Kukulizch K, Taylor C, Hogg D, et al. 2008. A comparison of CDKN2A mutation detection within the Melanoma Genetics Consortium (GenoMEL). *Eur J Cancer* 44: 1269-74
- Hartwell LH, Weinert TA. 1989. Checkpoints: controls that ensure the order of cell cycle events. *Science* 246: 629-34
- Hastie ND, Dempster M, Dunlop MG, Thompson AM, Green DK, Allshire RC. 1990. Telomere reduction in human colorectal carcinoma and with ageing. *Nature* 346: 866-8
- Hatakeyama M, Weinberg RA. 1995. The role of RB in cell cycle control. *Prog Cell Cycle Res* 1: 9-19
- Hayakawa T, Haraguchi T, Masumoto H, Hiraoka Y. 2003. Cell cycle behavior of human HP1 subtypes: distinct molecular domains of HP1 are required for their centromeric localization during interphase and metaphase. *J Cell Sci* 116: 3327-38



- Hayflick L, Moorhead PS. 1961. The serial cultivation of human diploid cell strains. *Exp Cell Res* 25: 585-621
- He H, Multani AS, Cosme-Blanco W, Tahara H, Ma J, et al. 2006. POT1b protects telomeres from end-to-end chromosomal fusions and aberrant homologous recombination. *EMBO J* 25: 5180-90
- Henson JD, Hannay JA, McCarthy SW, Royds JA, Yeager TR, et al. 2005. A robust assay for alternative lengthening of telomeres in tumors shows the significance of alternative lengthening of telomeres in sarcomas and astrocytomas. *Clin Cancer Res* 11: 217-25
- Hernando E, Nahle Z, Juan G, Diaz-Rodriguez E, Alaminos M, et al. 2004. Rb inactivation promotes genomic instability by uncoupling cell cycle progression from mitotic control. *Nature* 430: 797-802
- Hoeijmakers JH. 2001. Genome maintenance mechanisms for preventing cancer. *Nature* 411: 366-74
- Huvos AG, Woodard HQ. 1988. Postradiation sarcomas of bone. *Health Phys* 55: 631-6
- Huvos AG, Woodard HQ, Cahan WG, Higinbotham NL, Stewart FW, et al. 1985. Postradiation osteogenic sarcoma of bone and soft tissues. A clinicopathologic study of 66 patients. *Cancer* 55: 1244-55
- Isaac CE, Francis SM, Martens AL, Julian LM, Seifried LA, et al. 2006. The retinoblastoma protein regulates pericentric heterochromatin. *Mol Cell Biol* 26: 3659-71
- Jallepalli PV, Lengauer C. 2001. Chromosome segregation and cancer: cutting through the mystery. *Nat Rev Cancer* 1: 109-17
- Jamali M, Trott KR. 1996. Persistent increase in the rates of apoptosis and dicentric chromosomes in surviving V79 cells after X-irradiation. *Int J Radiat Biol* 70: 705-9
- Jeggo PA, Geuting V, Loblrich M. 2011. The role of homologous recombination in radiation-induced double-strand break repair. *Radiother Oncol*
- Karanjawala ZE, Grawunder U, Hsieh CL, Lieber MR. 1999. The nonhomologous DNA end joining pathway is important for chromosome stability in primary fibroblasts. *Curr Biol* 9: 1501-4
- Karanjawala ZE, Murphy N, Hinton DR, Hsieh CL, Lieber MR. 2002. Oxygen metabolism causes chromosome breaks and is associated with the neuronal apoptosis observed in DNA double-strand break repair mutants. *Curr Biol* 12: 397-402
- Kaste SC, Ahn H, Liu T, Liu W, Krasin MJ, et al. 2008. Bone mineral density deficits in pediatric patients treated for sarcoma. *Pediatr Blood Cancer* 50: 1032-8
- Kim NW, Piatyszek MA, Prowse KR, Harley CB, West MD, et al. 1994. Specific association of human telomerase activity with immortal cells and cancer. *Science* 266: 2011-5
- Kinzler KW, Vogelstein B. 1997. Cancer-susceptibility genes. Gatekeepers and caretakers. *Nature* 386: 761, 63

- Kiyono T, Foster SA, Koop JI, McDougall JK, Galloway DA, Klingelutz AJ. 1998. Both Rb/p16INK4a inactivation and telomerase activity are required to immortalize human epithelial cells. *Nature* 396: 84-8
- Knudsen ES, Wang JY. 1996. Differential regulation of retinoblastoma protein function by specific Cdk phosphorylation sites. *J Biol Chem* 271: 8313-20
- Knudsen ES, Wang JY. 1997. Dual mechanisms for the inhibition of E2F binding to RB by cyclin-dependent kinase-mediated RB phosphorylation. *Mol Cell Biol* 17: 5771-83
- Knudson AG, Jr. 1971. Mutation and cancer: statistical study of retinoblastoma. *Proc Natl Acad Sci U S A* 68: 820-3
- Knudson AG, Jr. 1986. Genetics of human cancer. *J Cell Physiol Suppl* 4: 7-11
- Kornberg RD, Thomas JO. 1974. Chromatin structure; oligomers of the histones. *Science* 184: 865-8
- Koshurnikova NA, Gilbert ES, Sokolnikov M, Khokhryakov VF, Miller S, et al. 2000. Bone cancers in Mayak workers. *Radiat Res* 154: 237-45
- Kourmouli N, Jeppesen P, Mahadevhaiah S, Burgoyne P, Wu R, et al. 2004. Heterochromatin and trimethylated lysine 20 of histone H4 in animals. *J Cell Sci* 117: 2491-501
- Lengauer C. 2001. How do tumors make ends meet? *Proc Natl Acad Sci U S A* 98: 12331-3
- Lengauer C, Kinzler KW, Vogelstein B. 1998. Genetic instabilities in human cancers. *Nature* 396: 643-9
- Lensch MW, Tischkowitz M, Christianson TA, Reifsteck CA, Speckhart SA, et al. 2003. Acquired FANCA dysfunction and cytogenetic instability in adult acute myelogenous leukemia. *Blood* 102: 7-16
- Letson GD, Muro-Cacho CA. 2001. Genetic and molecular abnormalities in tumors of the bone and soft tissues. *Cancer Control* 8: 239-51
- Levine AJ, Burger MM. 1993. UICC Study Group on Basic and Clinical Cancer Research: genotypes and phenotypes of tumor suppressors. Meeting held at Woods Hole, MA, October 1-4, 1992. *Int J Cancer* 53: 883-5
- Lim G, Karaskova J, Beheshti B, Vukovic B, Bayani J, et al. 2005. An integrated mBAND and submegabase resolution tiling set (SMRT) CGH array analysis of focal amplification, microdeletions, and ladder structures consistent with breakage-fusion-bridge cycle events in osteosarcoma. *Genes Chromosomes Cancer* 42: 392-403
- Lin SC, Skapek SX, Lee EY. 1996. Genes in the RB pathway and their knockout in mice. *Semin Cancer Biol* 7: 279-89
- Litovchick L, Sadasivam S, Florens L, Zhu X, Swanson SK, et al. 2007. Evolutionarily conserved multisubunit RBL2/p130 and E2F4 protein complex represses human cell cycle-dependent genes in quiescence. *Mol Cell* 26: 539-51

- Little JB. 2003. Genomic instability and radiation. *J Radiol Prot* 23: 173-81
- Little MP. 1997. Comments on the article "Studies of the mortality of atomic bomb survivors. Report 12, part I. Cancer: 1950-1990" by D. A. Pierce, Y. Shimizu, D. L. Preston, M. Vaeth and K. Mabuchi (*Radiat. Res.* 146, 1-27, 1996). *Radiat Res* 148: 399-401
- Lo AW, Sabatier L, Fouladi B, Pottier G, Ricoul M, Murnane JP. 2002a. DNA amplification by breakage/fusion/bridge cycles initiated by spontaneous telomere loss in a human cancer cell line. *Neoplasia* 4: 531-8
- Lo AW, Sprung CN, Fouladi B, Pedram M, Sabatier L, et al. 2002b. Chromosome instability as a result of double-strand breaks near telomeres in mouse embryonic stem cells. *Mol Cell Biol* 22: 4836-50
- Loeb LA. 2001. A mutator phenotype in cancer. *Cancer Res* 61: 3230-9
- Lois C, Hong EJ, Pease S, Brown EJ, Baltimore D. 2002. Germline transmission and tissue-specific expression of transgenes delivered by lentiviral vectors. *Science* 295: 868-72
- Longworth MS, Dyson NJ. 2010. pRb, a local chromatin organizer with global possibilities. *Chromosoma* 119: 1-11
- Lorimore SA, Coates PJ, Wright EG. 2003. Radiation-induced genomic instability and bystander effects: inter-related nontargeted effects of exposure to ionizing radiation. *Oncogene* 22: 7058-69
- Luciani JJ, Depetris D, Usson Y, Metzler-Guillemain C, Mignon-Ravix C, et al. 2006. PML nuclear bodies are highly organised DNA-protein structures with a function in heterochromatin remodelling at the G2 phase. *J Cell Sci* 119: 2518-31
- Luo RX, Postigo AA, Dean DC. 1998. Rb interacts with histone deacetylase to repress transcription. *Cell* 92: 463-73
- Luz A, Muller WA, Linzner U, Strauss PG, Schmidt J, et al. 1991. Bone tumor induction after incorporation of short-lived radionuclides. *Radiat Environ Biophys* 30: 225-7
- Ma D, Zhou P, Harbour JW. 2003. Distinct mechanisms for regulating the tumor suppressor and antiapoptotic functions of Rb. *J Biol Chem* 278: 19358-66
- Mabuchi K, Soda M, Ron E, Tokunaga M, Ochikubo S, et al. 1994. Cancer incidence in atomic bomb survivors. Part I: Use of the tumor registries in Hiroshima and Nagasaki for incidence studies. *Radiat Res* 137: S1-16
- Maire G, Yoshimoto M, Chilton-MacNeill S, Thorne PS, Zielenska M, Squire JA. 2009. Recurrent RECQL4 imbalance and increased gene expression levels are associated with structural chromosomal instability in sporadic osteosarcoma. *Neoplasia* 11: 260-8, 3p following 68
- Makarov VL, Lejnine S, Bedoyan J, Langmore JP. 1993. Nucleosomal organization of telomere-specific chromatin in rat. *Cell* 73: 775-87

- Malumbres M, Barbacid M. 2001. To cycle or not to cycle: a critical decision in cancer. *Nat Rev Cancer* 1: 222-31
- Manning AL, Longworth MS, Dyson NJ. 2010. Loss of pRB causes centromere dysfunction and chromosomal instability. *Genes Dev* 24: 1364-76
- Manolagas SC. 2000. Birth and death of bone cells: basic regulatory mechanisms and implications for the pathogenesis and treatment of osteoporosis. *Endocr Rev* 21: 115-37
- Marder BA, Morgan WF. 1993. Delayed chromosomal instability induced by DNA damage. *Mol Cell Biol* 13: 6667-77
- Marino S, Vooijs M, van Der Gulden H, Jonkers J, Berns A. 2000. Induction of medulloblastomas in p53-null mutant mice by somatic inactivation of Rb in the external granular layer cells of the cerebellum. *Genes Dev* 14: 994-1004
- Martinez P, Blasco MA. 2011. Telomeric and extra-telomeric roles for telomerase and the telomere-binding proteins. *Nat Rev Cancer* 11: 161-76
- Martinez P, Thanasoula M, Carlos AR, Gomez-Lopez G, Tejera AM, et al. 2010. Mammalian Rap1 controls telomere function and gene expression through binding to telomeric and extratelomeric sites. *Nat Cell Biol* 12: 768-80
- Martinez P, Thanasoula M, Munoz P, Liao C, Tejera A, et al. 2009. Increased telomere fragility and fusions resulting from TRF1 deficiency lead to degenerative pathologies and increased cancer in mice. *Genes Dev* 23: 2060-75
- Matsunaga E. 1980. Hereditary retinoblastoma: host resistance and second primary tumors. *J Natl Cancer Inst* 65: 47-51
- Mays CW, Spiess H. 1979. Bone tumors in thorotrast patients. *Environ Res* 18: 88-93
- Mc CB. 1951. Chromosome organization and genic expression. *Cold Spring Harb Symp Quant Biol* 16: 13-47
- Meadows AT, Strong LC, Li FP, D'Angio GJ, Schweisguth O, et al. 1980. Bone sarcoma as a second malignant neoplasm in children: influence of radiation and genetic predisposition for the Late Effects Study Group. *Cancer* 46: 2603-6
- Medema RH, Herrera RE, Lam F, Weinberg RA. 1995. Growth suppression by p16ink4 requires functional retinoblastoma protein. *Proc Natl Acad Sci U S A* 92: 6289-93
- Mertens WC, Bramwell V. 1994. Osteosarcoma and other tumors of bone. *Curr Opin Oncol* 6: 384-90
- Micci F, Panagopoulos I, Bjerkehagen B, Heim S. 2006. Consistent rearrangement of chromosomal band 6p21 with generation of fusion genes JAZF1/PHF1 and EPC1/PHF1 in endometrial stromal sarcoma. *Cancer Res* 66: 107-12
- Miller CW, Aslo A, Campbell MJ, Kawamata N, Lampkin BC, Koeffler HP. 1996. Alterations of the p15, p16, and p18 genes in osteosarcoma. *Cancer Genet Cytogenet* 86: 136-42

- Muntoni A, Reddel RR. 2005. The first molecular details of ALT in human tumor cells. *Hum Mol Genet* 14 Spec No. 2: R191-6
- Muratani M, Gerlich D, Janicki SM, Gebhard M, Eils R, Spector DL. 2002. Metabolic-energy-dependent movement of PML bodies within the mammalian cell nucleus. *Nat Cell Biol* 4: 106-10
- Murnane JP. 2006. Telomeres and chromosome instability. *DNA Repair (Amst)* 5: 1082-92
- Murnane JP. 2011. Telomere dysfunction and chromosome instability. *Mutat Res*
- Murray JM, Carr AM. 2008. Smc5/6: a link between DNA repair and unidirectional replication? *Nat Rev Mol Cell Biol* 9: 177-82
- Nabetani A, Yokoyama O, Ishikawa F. 2004. Localization of hRad9, hHus1, hRad1, and hRad17 and caffeine-sensitive DNA replication at the alternative lengthening of telomeres-associated promyelocytic leukemia body. *J Biol Chem* 279: 25849-57
- Nakayama H. 2002. RecQ family helicases: roles as tumor suppressor proteins. *Oncogene* 21: 9008-21
- Narita M, Nunez S, Heard E, Narita M, Lin AW, et al. 2003. Rb-mediated heterochromatin formation and silencing of E2F target genes during cellular senescence. *Cell* 113: 703-16
- Navid F, Willert JR, McCarville MB, Furman W, Watkins A, et al. 2008. Combination of gemcitabine and docetaxel in the treatment of children and young adults with refractory bone sarcoma. *Cancer* 113: 419-25
- Negrini S, Gorgoulis VG, Halazonetis TD. 2010. Genomic instability--an evolving hallmark of cancer. *Nat Rev Mol Cell Biol* 11: 220-8
- Nikitin AY, Juarez-Perez MI, Li S, Huang L, Lee WH. 1999. RB-mediated suppression of spontaneous multiple neuroendocrine neoplasia and lung metastases in Rb+/Δ19 mice. *Proc Natl Acad Sci U S A* 96: 3916-21
- Nojima H. 1997. Cell cycle checkpoints, chromosome stability and the progression of cancer. *Hum Cell* 10: 221-30
- Nusse M, Beisker W, Kramer J, Miller BM, Schreiber GA, et al. 1994. Measurement of micronuclei by flow cytometry. *Methods Cell Biol* 42 Pt B: 149-58
- Ottaviani G, Jaffe N. 2009a. The epidemiology of osteosarcoma. *Cancer Treat Res* 152: 3-13
- Ottaviani G, Jaffe N. 2009b. The etiology of osteosarcoma. *Cancer Treat Res* 152: 15-32
- Ozasa K, Shimizu Y, Sakata R, Sugiyama H, Grant EJ, et al. 2011. Risk of cancer and non-cancer diseases in the atomic bomb survivors. *Radiat Prot Dosimetry* 146: 272-5

- Peters AH, O'Carroll D, Scherthan H, Mechtler K, Sauer S, et al. 2001. Loss of the Suv39h histone methyltransferases impairs mammalian heterochromatin and genome stability. *Cell* 107: 323-37
- Pierce DA, Shimizu Y, Preston DL, Vaeth M, Mabuchi K. 1996. Studies of the mortality of atomic bomb survivors. Report 12, Part I. Cancer: 1950-1990. *Radiat Res* 146: 1-27
- Pitcher ME, Davidson TI, Fisher C, Thomas JM. 1994. Post irradiation sarcoma of soft tissue and bone. *Eur J Surg Oncol* 20: 53-6
- Polednak AP. 1978a. Bone cancer among female radium dial workers. Latency periods and incidence rates by time after exposure: brief communication. *J Natl Cancer Inst* 60: 77-82
- Polednak AP. 1978b. Long-term effects of radium exposure in female dial workers: differential white blood cell count. *Environ Res* 15: 252-61
- Polednak AP, Stehney AF, Rowland RE. 1978. Mortality among women first employed before 1930 in the U.S. radium dial-painting industry. A group ascertained from employment lists. *Am J Epidemiol* 107: 179-95
- Prowse KR, Greider CW. 1995. Developmental and tissue-specific regulation of mouse telomerase and telomere length. *Proc Natl Acad Sci U S A* 92: 4818-22
- Reddel RR. 2003. Alternative lengthening of telomeres, telomerase, and cancer. *Cancer Lett* 194: 155-62
- Reddel RR, Bryan TM. 2003. Alternative lengthening of telomeres: dangerous road less travelled. *Lancet* 361: 1840-1
- Reimann M, Schmitt CA, Lee S. 2011. Non-cell-autonomous tumor suppression: oncogene-provoked apoptosis promotes tumor cell senescence via stromal crosstalk. *J Mol Med*
- Riley DJ, Lee EY, Lee WH. 1994. The retinoblastoma protein: more than a tumor suppressor. *Annu Rev Cell Biol* 10: 1-29
- Rosemann M, Kuosaite V, Kremer M, Favor J, Quintanilla-Martinez L, Atkinson MJ. 2006. Multilocus inheritance determines predisposition to alpha-radiation induced bone tumorigenesis in mice. *Int J Cancer* 118: 2132-8
- Rosemann M, Kuosaite V, Nathrath M, Atkinson MJ. 2002. The genetics of radiation-induced osteosarcoma. *Radiat Prot Dosimetry* 99: 257-9
- Rosemann M, Kuosaite V, Nathrath M, Strom TM, Quintanilla-Martinez L, et al. 2003. Allelic imbalance at intragenic markers of Tbx18 is a hallmark of murine osteosarcoma. *Carcinogenesis* 24: 371-6
- Rosenthal J, Bolotin E, Shakhnovits M, Pawlowska A, Falk P, et al. 2008. High-dose therapy with hematopoietic stem cell rescue in patients with poor prognosis Ewing family tumors. *Bone Marrow Transplant* 42: 311-8

- Sabatier L, Ricoul M, Pottier G, Murnane JP. 2005. The loss of a single telomere can result in instability of multiple chromosomes in a human tumor cell line. *Mol Cancer Res* 3: 139-50
- Saiki RK, Gelfand DH, Stoffel S, Scharf SJ, Higuchi R, et al. 1988. Primer-directed enzymatic amplification of DNA with a thermostable DNA polymerase. *Science* 239: 487-91
- Saito T, Oda Y, Kawaguchi K, Takahira T, Yamamoto H, et al. 2004. PTEN and other tumor suppressor gene mutations as secondary genetic alterations in synovial sarcoma. *Oncol Rep* 11: 1011-5
- Sak A, Stuschke M. 2010. Use of gammaH2AX and other biomarkers of double-strand breaks during radiotherapy. *Semin Radiat Oncol* 20: 223-31
- Salomoni P, Pandolfi PP. 2002. The role of PML in tumor suppression. *Cell* 108: 165-70
- Schotta G, Lachner M, Sarma K, Ebert A, Sengupta R, et al. 2004. A silencing pathway to induce H3-K9 and H4-K20 trimethylation at constitutive heterochromatin. *Genes Dev* 18: 1251-62
- Schroeder TM, Jensen ED, Westendorf JJ. 2005. Runx2: a master organizer of gene transcription in developing and maturing osteoblasts. *Birth Defects Res C Embryo Today* 75: 213-25
- Schvartzman JM, Sotillo R, Benezra R. 2010. Mitotic chromosomal instability and cancer: mouse modelling of the human disease. *Nat Rev Cancer* 10: 102-15
- Seger YR, Garcia-Cao M, Piccinin S, Cunsolo CL, Doglioni C, et al. 2002. Transformation of normal human cells in the absence of telomerase activation. *Cancer Cell* 2: 401-13
- Sen S. 2000. Aneuploidy and cancer. *Curr Opin Oncol* 12: 82-8
- Sharpless NE, Ferguson DO, O'Hagan RC, Castrillon DH, Lee C, et al. 2001. Impaired nonhomologous end-joining provokes soft tissue sarcomas harboring chromosomal translocations, amplifications, and deletions. *Mol Cell* 8: 1187-96
- Shima N, Alcaraz A, Liachko I, Buske TR, Andrews CA, et al. 2007. A viable allele of Mcm4 causes chromosome instability and mammary adenocarcinomas in mice. *Nat Genet* 39: 93-8
- Smogorzewska A, de Lange T. 2002. Different telomere damage signaling pathways in human and mouse cells. *EMBO J* 21: 4338-48
- Somodi Z, Zyuzikov NA, Kashino G, Trott KR, Prise KM. 2005. Radiation-induced genomic instability in repair deficient mutants of Chinese hamster cells. *Int J Radiat Biol* 81: 929-36
- Soriano P. 1999. Generalized lacZ expression with the ROSA26 Cre reporter strain. *Nat Genet* 21: 70-1
- Sowby D. 2008. Some recollections of UNSCEAR. *J Radiol Prot* 28: 271-6
- Spieß H. 2002. Peteosthor - a medical disaster due to Radium-224A personal recollection. *Radiat Environ Biophys* 41: 163-72

- Spiess H, Gerspach A. 1978. Soft-tissue effects following <sup>224</sup>Ra injections into humans. *Health Phys* 35: 61-81
- Stagno D'Alcontres M, Mendez-Bermudez A, Foxon JL, Royle NJ, Salomoni P. 2007. Lack of TRF2 in ALT cells causes PML-dependent p53 activation and loss of telomeric DNA. *J Cell Biol* 179: 855-67
- Stewart GD, Nanda J, Katz E, Bowman KJ, Christie JG, et al. 2011. DNA strand breaks and hypoxia response inhibition mediate the radiosensitisation effect of nitric oxide donors on prostate cancer under varying oxygen conditions. *Biochem Pharmacol* 81: 203-10
- Stewenius Y, Jin Y, Ora I, de Kraker J, Bras J, et al. 2007. Defective chromosome segregation and telomere dysfunction in aggressive Wilms' tumors. *Clin Cancer Res* 13: 6593-602
- Strong LC, Williams WR, Ferrell RE, Tainsky MA. 1989. Genetic analysis of childhood sarcoma. *Princess Takamatsu Symp* 20: 151-7
- Strudwick S, Borden KL. 2002. Finding a role for PML in APL pathogenesis: a critical assessment of potential PML activities. *Leukemia* 16: 1906-17
- Sunters A, McCluskey J, Grigoriadis AE. 1998. Control of cell cycle gene expression in bone development and during c-Fos-induced osteosarcoma formation. *Dev Genet* 22: 386-97
- Sztan M, Papai Z, Szendroi M, Looij M, Olah E. 1997. Allelic Losses from Chromosome 17 in Human Osteosarcomas. *Pathol Oncol Res* 3: 115-20
- Takahashi Y, Lallemand-Breitenbach V, Zhu J, de The H. 2004. PML nuclear bodies and apoptosis. *Oncogene* 23: 2819-24
- Talluri S, Isaac CE, Ahmad M, Henley SA, Francis SM, et al. 2010. A G1 checkpoint mediated by the retinoblastoma protein that is dispensable in terminal differentiation but essential for senescence. *Mol Cell Biol* 30: 948-60
- Tang DJ, Hu L, Xie D, Wu QL, Fang Y, et al. 2005. Oncogenic transformation by SEI-1 is associated with chromosomal instability. *Cancer Res* 65: 6504-8
- Tessema M, Lehmann U, Kreipe H. 2004. Cell cycle and no end. *Virchows Arch* 444: 313-23
- Thompson DE, Mabuchi K, Ron E, Soda M, Tokunaga M, et al. 1994. Cancer incidence in atomic bomb survivors. Part II: Solid tumors, 1958-1987. *Radiat Res* 137: S17-67
- Trenz K, Smith E, Smith S, Costanzo V. 2006. ATM and ATR promote Mre11 dependent restart of collapsed replication forks and prevent accumulation of DNA breaks. *EMBO J* 25: 1764-74
- Trott KR, Jamali M, Manti L, Teibe A. 1998. Manifestations and mechanisms of radiation-induced genomic instability in V-79 Chinese hamster cells. *Int J Radiat Biol* 74: 787-91
- Tusell L, Pampalona J, Soler D, Frias C, Genesca A. 2010. Different outcomes of telomere-dependent anaphase bridges. *Biochem Soc Trans* 38: 1698-703



- Ulaner GA, Hoffman AR, Otero J, Huang HY, Zhao Z, et al. 2004. Divergent patterns of telomere maintenance mechanisms among human sarcomas: sharply contrasting prevalence of the alternative lengthening of telomeres mechanism in Ewing's sarcomas and osteosarcomas. *Genes Chromosomes Cancer* 41: 155-62
- Ulaner GA, Huang HY, Otero J, Zhao Z, Ben-Porat L, et al. 2003. Absence of a telomere maintenance mechanism as a favorable prognostic factor in patients with osteosarcoma. *Cancer Res* 63: 1759-63
- Unni KK. 1998. Osteosarcoma of bone. *J Orthop Sci* 3: 287-94
- Wadayama B, Toguchida J, Shimizu T, Ishizaki K, Sasaki MS, et al. 1994. Mutation spectrum of the retinoblastoma gene in osteosarcomas. *Cancer Res* 54: 3042-8
- Wang Y, Putnam CD, Kane MF, Zhang W, Edelmann L, et al. 2005. Mutation in Rpa1 results in defective DNA double-strand break repair, chromosomal instability and cancer in mice. *Nat Genet* 37: 750-5
- Wang ZG, Delva L, Gaboli M, Rivi R, Giorgio M, et al. 1998. Role of PML in cell growth and the retinoic acid pathway. *Science* 279: 1547-51
- Weichselbaum RR, Beckett M, Diamond A. 1988. Some retinoblastomas, osteosarcomas, and soft tissue sarcomas may share a common etiology. *Proc Natl Acad Sci U S A* 85: 2106-9
- Weichselbaum RR, Beckett MA, Diamond AA. 1989. An important step in radiation carcinogenesis may be inactivation of cellular genes. *Int J Radiat Oncol Biol Phys* 16: 277-82
- Weidtkamp-Peters S, Lenser T, Negorev D, Gerstner N, Hofmann TG, et al. 2008. Dynamics of component exchange at PML nuclear bodies. *J Cell Sci* 121: 2731-43
- Weinstein IB. 1988. The origins of human cancer: molecular mechanisms of carcinogenesis and their implications for cancer prevention and treatment--twenty-seventh G.H.A. Clowes memorial award lecture. *Cancer Res* 48: 4135-43
- Wilson PF, Nagasawa H, Fitzek MM, Little JB, Bedford JS. 2010. G2-phase chromosomal radiosensitivity of primary fibroblasts from hereditary retinoblastoma family members and some apparently normal controls. *Radiat Res* 173: 62-70
- Wilson PF, Nagasawa H, Warner CL, Fitzek MM, Little JB, Bedford JS. 2008. Radiation sensitivity of primary fibroblasts from hereditary retinoblastoma family members and some apparently normal controls: colony formation ability during continuous low-dose-rate gamma irradiation. *Radiat Res* 169: 483-94
- Wong FL, Boice JD, Jr., Abramson DH, Tarone RE, Kleinerman RA, et al. 1997. Cancer incidence after retinoblastoma. Radiation dose and sarcoma risk. *JAMA* 278: 1262-7
- Wu G, Lee WH, Chen PL. 2000. NBS1 and TRF1 colocalize at promyelocytic leukemia bodies during late S/G2 phases in immortalized telomerase-negative cells. Implication of NBS1 in alternative lengthening of telomeres. *J Biol Chem* 275: 30618-22

- Wu WS, Xu ZX, Hittelman WN, Salomoni P, Pandolfi PP, Chang KS. 2003. Promyelocytic leukemia protein sensitizes tumor necrosis factor alpha-induced apoptosis by inhibiting the NF-kappaB survival pathway. *J Biol Chem* 278: 12294-304
- Yeager TR, Neumann AA, Englezou A, Huschtscha LI, Noble JR, Reddel RR. 1999. Telomerase-negative immortalized human cells contain a novel type of promyelocytic leukemia (PML) body. *Cancer Res* 59: 4175-9
- Yin Y, Shen WH. 2008. PTEN: a new guardian of the genome. *Oncogene* 27: 5443-53
- Yuan K, Chung LW, Siegal GP, Zayzafoon M. 2007. alpha-CaMKII controls the growth of human osteosarcoma by regulating cell cycle progression. *Lab Invest* 87: 938-50
- Zhang Y, Cao H, Wang M, Zhao WY, Shen ZY, et al. 2010. Loss of chromosome 9p21 and decreased p16 expression correlate with malignant gastrointestinal stromal tumor. *World J Gastroenterol* 16: 4716-24
- Zheng L, Lee WH. 2001. The retinoblastoma gene: a prototypic and multifunctional tumor suppressor. *Exp Cell Res* 264: 2-18
- Zheng L, Lee WH. 2002. Retinoblastoma tumor suppressor and genome stability. *Adv Cancer Res* 85: 13-50
- Zhong S, Salomoni P, Pandolfi PP. 2000a. The transcriptional role of PML and the nuclear body. *Nat Cell Biol* 2: E85-90
- Zhong S, Salomoni P, Ronchetti S, Guo A, Ruggero D, Pandolfi PP. 2000b. Promyelocytic leukemia protein (PML) and Daxx participate in a novel nuclear pathway for apoptosis. *J Exp Med* 191: 631-40
- Zou D, Han W, You S, Ye D, Wang L, et al. 2011. In vitro study of enhanced osteogenesis induced by HIF-1alpha-transduced bone marrow stem cells. *Cell Prolif* 44: 234-43

## IX ANNEX I

➤ RB1 cloning sequences:

cDNA fw 1	cDNA rev1
cDNA fw2	IRAT forward
cDNA rev2	IRAT rev1
cDNA fw3	

Table showing the sequencing primers (see materials for sequence) and the format of the sequencing regions performed by each primer in *RB1* sequence show below.

Complete *RB1* sequence of positive *Rb1* clone checked with the pool of primers shown above (match to the sequence in ENSEMBL):

```
CGGGGGAGGGCGCGTCCGGTTTTCTCAGGGGACGTTGAAATTATTTTTGTAACGGGA
GTCGGGAGAGGACGGGGCGTGCCCCGACGTGCGCGCGCGTCGTCTCCCCGGCGCT
CCTCCACAGCTCGCTGGCTCCCGCCGCGGAAAGGCGTCATGCCGCCAAAACCCCC
GAAAACGGCCGCCACCGCCGCGCTGCCGCCGCGGAACCCCCGGCACCGCCGCCG
CCGCCCTCCTGAGGAGGACCCAGAGCAGGACAGCGGCCCGGAGGACCTGCCTCTC
GTCAGGCTTGAGTTTGAAGAAACAGAAGAACCTGATTTTACTGCATTATGTCAGAAATTA
AAGATACCAGATCATGTCAGAGAGAGAGCTTGGTTAACTTGGGAGAAAGTTTCATCTGT
GGATGGAGTATTGGGAGGTTATATTCAAAAGAAAAGGAACTGTGGGGAATCTGTATCT
TTATTGCAGCAGTTGACCTAGATGAGATGTCGTTCACTTTTACTGAGCTACAGAAAAACA
TAGAAATCAGTGTCCATAAATCTTAACTTACTAAAAGAAATTGATACCAGTACCAAAGT
TGATAATGCTATGTCAAGACTGTTGAAGAAGTATGATGTATTGTTTGAAGTCTTTCAGCAA
ATTGGAAAGGACATGTGAACTTATATATTTGACACAACCCAGCAGTTCGATATCTACTGA
AATAAATTCTGCATTGGTGCTAAAAGTTTCTTGGATCACATTTTTATTAGCTAAAGGGGAA
GTATTACAAATGGAAGATGATCTGGTGATTTCACTTTCAGTTAATGCTATGTGTCCTTGACT
ATTTTATTAACCTCTCACCTCCCATGTTGCTCAAAGAACCATATAAACAGCTGTTATACC
CATTAATGGTTCACCTCGAACACCCAGGCGAGGTCAGAACAGGAGTGCACGGATAGCA
AAACAAGTAAAGATGATACAAGAATTATTGAAGTTCTCTGTAAAGAACATGAATGTAATA
TAGATGAGGTGAAAAATGTTTATTTCAAAAATTTTATACCTTTTATGAATTCTCTTGGACTT
GTAACATCTAATGGACTTCCAGAGGTTGAAAATCTTTCTAAACGATACGAAGAAATTTAT
CTTAAAAATAAAGATCTAGATGCAAGATTATTTTTGGATCATGATAAACTCTTCAGACTG
ATTCTATAGACAGTTTTGAAACACAGAGAACACCACGAAAAAGTAACCTTGATGAAGAGG
TGAATGTAATTCCTCCACACACTCCAGTTAGGACTGTTATGAACACTATCCAACAATTA
TGATGATTTTAAATTCAGCAAGTGATCAACCTTCAGAAAATCTGATTTCTATTTTAAACA
CTGCACAGTGAATCCAAAAGAAAGTATACTGAAAAGAGTGAAGGATATAGGATACATCTT
TAAAGAGAAATTTGCTAAAGCTGTGGGACAGGGTGTGTCGAAATTGGATCACAGCGAT
ACAACTTGGAGTTCGCTTGTATTACCGAGTAATGGAATCCATGCTTAAATCAGAAGAAG
AACGATTATCCATTCAAATTTTAGCAAACCTTCTGAATGACAACATTTTTTCATATGTCTTTA
TTGGCGTGCGCTCTTGAGGTTGTAATGGCCACATATAGCAGAAGTACATCTCAGAATCT
```

TGATTCTGGAACAGATTTGTCTTTCCCATGGATTCTGAATGTGCTTAATTTAAAAGCCTTT  
 GATTTTTACAAAGTGATCGAAAGTTTTATCAAAGCAGAAGGCAACTTGACAAGAGAAATG  
 AATAAACATTTAGAACGATGTGAACATCGAATCATGGAATCCCTTGCAATGGCTCTCAGAT  
 TCACCTTTATTTGATCTTATTAACAATCAAAGGACCGAGAAGGACCAACTGATCACCTT  
 GAATCTGCTTGTCTCTTAATCTTCTCTCCAGAATAATCACACTGCAGCAGATATGTAT  
 CTTTCTCCTGTAAGATCTCCAAAGAAAAAGGTTCAACTACGCGTGTAATTCTACTGCA  
 AATGCAGAGACACAAGCAACCTCAGCCTTCAGACCCAGAAGCCATTGAAATCTACCTC  
 TCTTCACTGTTTTATAAAAAAGTGTATCGGCTAGCCTATCTCCGGCTAAATACACTTTGT  
 GAACGCCTTCTGTCTGAGCACCCAGAATTAGAACATATCATCTGGACCCTTTTCCAGCA  
 CACCCTGCAGAATGAGTATGAACTCATGAGAGACAGGCATTTGGACCAAATTATGATGT  
 GTTCCATGTATGGCATATGCAAAGTGAAGAATATAGACCTTAAATTCAAATCATTGTAA  
 CAGCATAACAAGGATCTTCCATGCTGTTTCCAGGAGACATTCAAACGTGTTTTGATCAAAG  
 AAGAGGAGTATGATTCTATTATAGTATTCTATAACTCGGTCTTCATGCAGAGACTGAAAA  
 CAAATATTTTGCAGTATGCTTCCACCAGGCCCTACCTTGTCCACCAATACCTCACATTC  
 CTCGAAGCCCTTACAAGTTTCTAGTTCACCCTTACGGATTCTGGAGGGAACATCTATA  
 TTTCACCCCTGAAGAGTCCATATAAAATTTGAGAAGGTCTGCCAACACCAACAAAAATGA  
 CTCCAAGATCAAGAATCTTAGTATCAATTGGTGAATCATTGGGACTTCTGAGAAGTTCC  
 AGAAAATAAATCAGATGGTATGTAACAGCGACCGTGTGCTCAAAGAAGTGTGAAGGA  
 AGCAACCCTCCTAAACCACTGAAAAACTACGCTTTGATATTGAAGGATCAGATGAAGCA  
 GATGGAAGTAAACATCTCCAGGAGAGTCAAATTTGAGCAGAACTGGCAGAAATGAC  
 TTCTACTCGAACACGAATGCAAAGCAGAAAATGAATGATAGCATGGATACCTCAAACAA  
 GGAAGAGAAATGAGGATCTCAGGACCTTGGTGGACACTGTGTACACCTCTGGATTCAAT  
 GTCTCTCACAGATGTGACTGTATAACTTTCCAGGTTCTGTTTTATGGCCA.

- Sequencing of the construct with primer Rev1. into the 5' end of the expression vector

CCGCCTGTGGTGCCTCCTGAACTGCGTCCGCCGTCTAGGTAAGTTTAAAGCTCAGGTC  
 GAGACCGGGCCTTTGTCCGGCGCTCCCTTGAGCCTACCTAGACTCAGCCGGCTCTCC  
ACGCTTTGCCTGACCCTGCTTGCTCAACTCTACGTCTTTGTTTCGTTTTCTGTTCTGCGC  
 CGTTACAGATCCAAGCTGTGACCGGCGCCTACTCTAGAGCTAGCGAATTCGAATTTAA  
**TCGGATCC**TTATTTTTGTAACGGGAGTCGGGAGAGGACGGGGCGTGCCCCGACGTGCG  
 CGCGCGTCGTCTCCCGGCGCTCCTCCACAGCTCGCTGGCTCCCGCCGCGGAAAGG  
 CGTCATGCCGCCAAAACCCCCGAAAAACGGCCGCCACCGCCGCGCTGCCGCCG  
 GGAACCCCCGGCACCGCCGCCGCCGCCCTCCTGAGGAGGACCCAGAGCAGGACA

GATCC	<i>Bam</i> HI site
TTCGAATTTAAATCG	pCDH-EF1-T2A-GFP vector starts
CTCCACGCTTTGCCTGACCCTGCTT	EF1 primer
TTATT	Beginning of <i>RB1</i> sequence (5' end)

- Sequence with primer fw3 into the 3' end of the expression vector showing the replenished recognition site for the restriction enzyme and the following T2A sequence of the expression vector (Figure 19)

AGATGAAGCAGATGGAAGTAAACATCTCCCAGGAGAGTCCAAATTTMGMGAAACTG  
GCAGAAATGACTTCTACTCGAACACGAATGCAAAGCAGAAAATGAATGATAGCATGGA  
TACCTCAAACAAGGAAGAGAAATGAGGATCTCAGGACCTTGGTGGACACTGTGTACACC  
TCTGGATTCAATTGTCTCTCACAGATGTGACTGTATAACTTTCCCAGGTTCTGTTTATGGC  
CACGCGGCCGCTGAGGGCAGAGGAAGTCTTCTAACATGCGGTGACGTGGAGGAGAAT  
CCCGGCCCTTCCGGAATGGAGAGCGACGAGAGCGGCCTGCCCGCCATGGAGATCGAG  
TGCCGCATCACCGGCACCCTGAACGGCGTGGAGTTCGAGCTGGTGGCGGCGGAGAGG  
GCACCCCAAGCAGGGCCGCATGACCAACAAGATGAAGAGCACCAAAGGCGCCCTGA  
CCTTCAGCCCCTACCTGCTGAGCCACGTGATGGGCTACGGCTTCTACCACTTCGGCAC  
CTACCCAGCGGCTACGAGAACCCTTCCTGCACGCCATCAACAACGGCGGCTACACC  
AACACCCGCATCGAGAAGTACGAGGACGGCGGCGTGTGACGTGAGCTTCAGCTACC  
GCTACGAGGCCGGC

<b>TGTTTATGGCCAC:</b>	<b>End of <i>RB1</i> sequence (3' end) without poli-A signal</b>
<b><u>GCGGCC;</u></b>	Not I site
<b><u>GAGGGCAGAGGAAGTCTTCTAACATGCGGTGACGTGGAGGAGAATCCC</u></b> <b><u>GGCCCT:</u></b>	T2A sequence

- Another example of H4K20 3met (page 98):

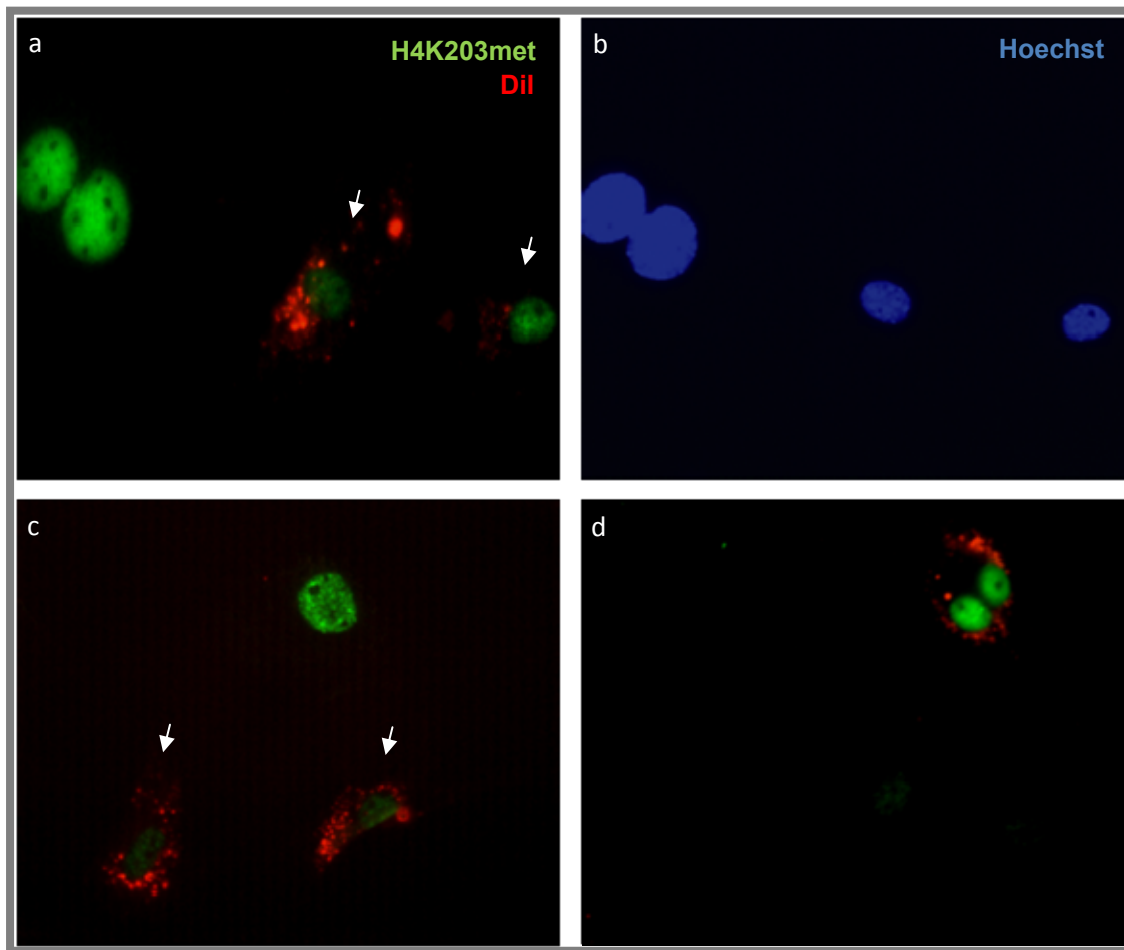


**Figure 68: Immunofluorescence of H4 K20 tri-met in primary osteoblasts.** a) A mixed population of  $Rb1^{+/+}$  and  $Rb1^{+/\Delta 19}$  (Dil stained) was co-cultured using Dil, a lipophilic dye, to distinguish the genotypes to later be stained with anti-H4 K20 tri-met. b) Hoechst counter staining corresponding to figure a. c) Another picture of a mixed population of  $Rb1^{+/+}$  and  $Rb1^{+/\Delta 19}$  (with Dil) showing the reduced fluorescence intensity of the haploinsufficient cells. d) A mixed population of  $Rb1^{+/+}$  (contrary to the other pictures, now is this genotype stained with Dil) and  $Rb1^{+/\Delta 19}$  to ensure that Dil is not affecting the immunofluorescence. Arrowheads point to  $Rb1^{+/\Delta 19}$  cells.

**X ACKNOWLEDGEMENTS**

I would like to thank first of all Prof Michael Atkinson, for giving me the chance to do my PhD in his lab, for his support, for promoting my work and myself as a scientist, but above all, for believing in me.

I would like to extend those thanks to Dr Michael Rosemann. He supported me and taught me lots in the lab, as well as great, interesting and helpful discussions along the way. Danke!

I would also like to express my gratitude to Prof. Graw for all the support with the University matters as being my “Doktorvater”, as well as to Prof Trott, for his continuous support and encouragement since we met in the fall of 2006.

To Bahar Sanli-Bonazzi, for all the help in the lab, as well as for her continuous support during the last 4 years, the chats, the laughs and for her friendship. It was awesome having met you and a pleasure to work with you during this time. Thanks so much for everything! Teşekkürler!!!

To Natasa Anastasov, for teaching me the work of an S2 lab, cloning and developing a lentiviral system, as well as for the “coffee chats”, it was great fun!

Zarko Barjaktarovic and Omid Azimzadeh for being there for all the problems related to proteomics, office *balances and imbalances* and for being great friends!

To my friends Patricia e Ilaria, the Sardinia team was simply the best and I will never forget any of our Munich stories! Eskerrik asko and Grazie mille!

A mi familia y amigos, por estar ahí en los momentos más complicados de mi vida, por no dejarme sola, por estar desde la distancia ahí para mi.

A mi madre, que cual ave fenix ha vuelto a mi vida y ha estado ahí para mí durante estos años complicados.

A mis abuelos, Conchita y Mario, por creer en mi desde que era pequeña...por saber que podía, y apoyarme siempre. Gracias!

To my “three countries”, Spain, England and Germany...I am what I am, because of you, and I am so thankful for all the experiences!

A ti, por todo, especialmente por hacerme tan feliz! Por devolverme la esperanza y la sonrisa perfecta...pero sobre todo, porque no puedo esperar al futuro contigo! TQPpp.

*To my mice, the real heroes of all scientific projects. My deepest thanks to the Rb1 tumour suppressor gene, for all the things it taught me, and because among a bunch of deseperating evenings, some amazing ones were hidden, and those taught me the joy of a new discovery, making up for any frustration and teaching me the beauty of science.*

## IX CURRICULUM VITAE

### Personal Details

**Address:** Kathi-Kobus-str 9, 4OG  
80797 München

**Telephone:** +491774266421

**E-mail:** [iria.gonzalez@helmholtz-muenchen.de](mailto:iria.gonzalez@helmholtz-muenchen.de) **Date of Birth:** 28<sup>th</sup> January 1981  
[iriagonzalez@gmail.com](mailto:iriagonzalez@gmail.com)

**Status:** Single

**Nationality:** Spanish

---

### Employment & Work Experiences

- ◆ PhD at the Helmholtz Center Munich. *Function of Rb1 in radiation induced cancer.*
- ◆ May 2007-September 2007: MSc project at Helmholtz Center in Munich. Rb1 deletion in murine osteoblasts and its implications in the cell cycle after radiation exposure.
- ◆ Summer 2005: (Undergraduate Summer Placement) University Of Kent, Canterbury, England with Professor Mick Tuite.
- ◆ Spring 2005: Biochemistry department at the USC (University of Santiago de Compostela), on Prot- $\alpha$  and its interaction with other proteins.
- ◆ Summer 2004: Desy summer program (Hamburg, Germany), I worked at the EMBL, with the aim to clone and express a human protein, hZiPD. I returned in November-December 2004 to continue working on the same project.  
During my stay at Desy I also worked for two weeks in the accelerator, Doris, with a project in XAFS spectroscopy.
- ◆ Spring 2004: Microbiological laboratory in Santiago, Spain on bacterial and toxin disease.
- ◆ Summer 2003: GSI laboratory (Darmstadt, Germany) working on DNA damage caused by X-ray radiation. This role involved the use of particle accelerators and its application in cancer research.

### Education

Since November 2007- Present: **Technical university (TU) München, Germany.** PhD work. Radiation Biology Institute (ISB), **Helmholtz Zentrum München.**  
September 2006- September 2007 : **UCL London** MSc Radibiology and Oncology.  
2000-October 2005: **Santiago de Compostela's University.** BSc Molecular Biology  
1995-2000: **Instituto Público de Nigran,** High School.

### Languages

Native tongue – Spanish and Galician  
Fluent written and spoken English  
Basic level of German and Italian

### Scientific societies:

Association of Radiation Research (ARR) UK (since 2010)  
American Association of Cancer Research (AACR) USA (since 2011)

### Fellowships, Awards and Honours

Stipendium award from GSI for summer program (2003)  
Stipendium award from the EMBL for summer program in DESY (2004)  
Stipendium award from the University of Canterbury for summer program at Mick Tuite's lab (2005)  
Fellowship from Cancer Research UK and Risc Rad European project for the MSc (2006-2007)  
Travel award from CSHL for Telomere meeting attendance (2009)  
Poster prize Helmholtz Munich annual science day (2009)



**Posters and talks:**

XX International Congress of Genetics, Berlin 2008: Poster  
Women in Radiation Sciences, Helmholtz meeting, 2009: Poster and co-chairing.  
Telomere meeting at Cold Spring Harbour, Long Island, NY, 2009: poster  
NCI Radiation conference, George Town University, Washington, 2009: poster  
Association of Radiation Research meeting, Oxford, UK, 2010: talk  
EMBO telomere biology and DNA damage, Marseille, France, 2010: poster  
AACR annual meeting, Orlando, USA, 2011: poster  
DoReMi –1<sup>st</sup> Periodic Meeting, Royal Academie of Sciences and Arts of Belgium: Talk

**Publication List:**

- 1) Gonzalez-Vasconcellos I, Domke T, Kuosaitte V, Esposito I, Sanli-Bonazzi B, et al. 2011. **Differential effects of genes of the Rb1 signalling pathway on osteosarcoma incidence and latency in alpha-particle irradiated mice.** *Radiat Environ Biophys* 50: 135-41
- 2) Ludyga N, Anastasov N, Gonzalez-Vasconcellos I, Ram M, Hofler H, Aubele M. 2011. **Impact of protein tyrosine kinase 6 (PTK6) on human epidermal growth factor receptor (HER) signalling in breast cancer.** *Mol Biosyst* 7: 1603-12
- 3) C. Rumenapp, J. Smida, I. Gonzalez-Vasconcellos, D. Baumhoer, B. Malfoy, N.S. Hadj-Hamou, B. Sanli-Bonazzi, M. Nathrath, M.J. Atkinson, M. Rosemann: **Secondary radiation-induced bone tumors demonstrate a high degree of genetic instability predictive of a poor prognosis** (Accepted in July 2011).
- 4) M. Rosemann, I. Gonzalez-Vasconcellos, T. Domke, M. Nathrath and M.J. Atkinson: NATO science for peace and security series C: Environmental security: **“Radiation, Environmental Mutagenesis and Evolution”** Radiobiology and environmental security, Springer 2011)
- 5) O. Klymenko, K. J. Heiliger, I. Gonzalez-Vasconcellos, C. Dalke, M.J. Atkinson, M. Rosemann: NATO science for peace and security series C: Environmental security: **“Molecular changes in radiation induced thyroid carcinomas in mice”** Radiobiology and environmental security, Springer 2011)
- 6) M. Rosemann, I. Gonzalez-Vasconcellos, Kuosaitte V., Schneider R., Kremer M, Nadri L., M.J. Atkinson: **Reduced Rb1 expression by a promoter variant increases susceptibility for radiation induced osteosarcoma in mice** (Submitted in August 2011).

***“Owing to this struggle for life, any variation, however slight and from whatever cause proceeding, if it be in any degree profitable to an individual of any species, in its infinitely complex relationship to other organic beings and to external nature, will tend to the preservation of that individual, and will generally be inherited by its offspring.***

*Chapter III: struggle for existence. The origin of Species. Charles Darwin 1809-1882*

***„Science is but a perversion of itself unless it has as its ultimate goal the betterment of humanity“***

*Nikola Tesla 1853-1943*

***The important thing in science is not so much to obtain new facts as to discover new ways of thinking about them.***

*William Lawrence Bragg 1890-1971*

***A fact is a simple statement that everyone believes. It is innocent, unless found guilty. A hypothesis is a novel suggestion that no one wants to believe. It is guilty, until found effective.***

*Edward Teller 1908-2003*

***Science and everyday life cannot and should not be separated. Science, for me, gives a partial explanation for life. In so far as it goes, it is based on fact, experience and experiment.***

*Rosalind Franklin 1920-1958*

***Today, the theory of evolution is an accepted fact for everyone but a fundamentalist minority, whose objections are based not on reasoning but on doctrinaire adherence to religious principles.***

*James D Watson 1928-*

***The way to do research is to attack the facts at the point of greatest astonishment.***

*Celia Green, 1972*

***To know the history of science is to recognize the mortality of any claim to universal truth.***

*Evelyn Fox Keller, Reflections on Gender and Science, 1995*